2017

The Viscosity and Thermal Conductivity of Heavy Oils and Solvents

Ramos-Pallares, Ramon Francisco

UNIVERSITY OF CALGARY

The Viscosity and Thermal Conductivity of Heavy Oils and Solvents

by

Ramon Francisco Ramos-Pallares

THESIS

SUBMITTED TO THE FACULTY OF GRADUATE STUDIES

IN PARTIAL FULFILMENT OF THE REQUIREMENTS FOR THE

DEGREE OF DOCTOR OF PHILOSOPHY

GRADUATE PROGRAM IN CHEMICAL AND PETROLEUM ENGINEERING

CALGARY, ALBERTA

AUGUST, 2017

Abstract

Viscosity and thermal conductivity are related properties and models for both are required for reservoir and process simulation. In most heavy oil processes, the viscosity must be reduced by heating and/or dilution with solvents. To design and optimize these processes, accurate viscosity models are required for both reservoir and process simulation. Current models are challenging to apply to heavy oils. Thermal conductivity is required for the simulation of heat exchange operations in refineries. Current models are either intended for liquid phases or computationally intensive.

This thesis presents the development of predictive viscosity and thermal conductivity models for reservoir and process simulation. The models were developed based on an experimental dataset collected in this thesis that includes the viscosity and thermal conductivity of whole and diluted heavy oils, partially deasphalted oils, asphaltenes, distillation cuts and pure hydrocarbons. The Expanded Fluid (EF) and the Generalized Walther (GW) viscosity models were updated to predict the viscosity of whole and diluted crude oils and their fractions (such as deasphalted oils). The EF model is suitable for process simulation and is applicable across the whole phase diagram. The required inputs are a distillation assay, the oil specific gravity, experimental or predicted fluid density at the process conditions, and pressure. The GW model is suitable for reservoir simulation and is only applicable to liquids well below their critical point. The inputs are a distillation assay, the oil specific gravity, temperature, and pressure. The EF concept was also used to develop a thermal conductivity model suitable for process simulation using the same inputs as the EF viscosity model.

The updated EF and GW viscosity models and the EF thermal conductvity model are applicable to crude oils over a wide range of API gravities, temperatures and pressures. They have fewer parameters than other models, the parameters have physical significance, and they are easily correlated to fluid properties. The predicted viscosities and thermal conductivities are within 50% and 3% of the experimental values, respectively. The

deviations are less than obtained with other available methods. A straightforward tuning procedure allows the models to fit data to within the experimental error.

Acknowledgements

The culmination of this thesis has been thanks to the work of a lot of people to whom I owe all my gratitude. Firstly, I would like to thank my supervisor, Dr. Harvey W. Yarranton, for his commitment to this work, guidance, support, patience and the infinite number of hours he invested on editing my writing, presentations and reports. Dr. Yarranton always encouraged me to produce the best, to be accurate, and to learn how to be clear and coherent, despite my horrid English. Being part of his research group was a privilege. Thanks for the opportunity of working on this project, it was really fun.

I also want to thank my co-supervisor, Dr. Shawn D. Taylor, for the fruitful discussions we had along this project and for the uncounted challenging questions he always formulated to me. He taught me that the most rewarding part of being a graduate student is to invest time in understanding the fundamentals. He also taught me the value, and responsibility, behind saying "I do not know".

I want to extend my gratitude to Dr. Marco A. Satyro. He was a big contributor to the viscosity part of this thesis and the one who put in our heads the crazy idea of measuring thermal conductivity of heavy oils. I thank him for his valuable advice and for his super ingenious approaches to solve modelling and mathematical problems. Despite the complexity of the problem, his advice always led to the simplest solution.

There were numerous methodological, experimental and paperwork challenges along this project. However, my two lab managers, Elaine Baydak and Florian Schoeggl, were always eager to help with insightful discussions and advice. I want to express my gratitude especially to Mr. Schoeggl for his constant help during the 14 dark months that took us to figure out what was wrong with the apparatus and the methodology to measure liquid thermal conductivity.

To E. Cervera, in Boston, Massachusetts

And,

To T. Uprichard, in Calgary, Alberta

Table of Contents

List of Tables

List of Figures and Illustrations

The definition of symbols is context dependent

Uppercase Symbols

A : fluid-specific parameter [kg m^{-3} mPa^{-1}] in Eq. 2.10

: Mason and Saxena (1958) parameter, Eq. 2.73
: Walther model fluid-specific parameter
: fluid-specific coefficient in Yaws (2008), Eq 4.6
: area [m^2], Eq. 3.4, 3.5

B : fitting parameter in Yaws (1995) correlation, Eq. 8.3
: Walther model fluid-specific parameter
: fluid-specific coefficient in Yaws (2008), Eq 4.6
: Tait-COSTALD fluid-specific parameter, Eq. 6.6

B_μ : fluid specififc parameter [mPa^{-1}] in Eq. 2.11

C : C$_1$[mW m^{-1}K^{-1}] and C$_2$ [mW m^{-1} K^{-2}] parameters Eq. 2.65
: Tait-COSTALD fluid-specific parameter, Eq. 6.4
: fluid-specific coefficient in Yaws (2008), Eq 4.6
: fitting parameter in Yaws (1995) correlation, Eq. 8.3

C_v : constant volume heat capacity [kJ kmol^{-1} K^{-1}]

C_p : constant pressure heat capacity [kJ kmol^{-1} K^{-1}]

D : diameter [m]
: fluid-specific coefficient in Yaws (2008), Eq 4.6

F : empirical correction factor in Eq. 2.5

G_{ij} : Grunberg-Nissan interaction parameter, Eq. 2.55

H/C : atomic hydrogen-to-carbon ratio

I : blending index, Eq. 2.56, 2.60, 2.61

K	: Watson characterization factor
	: fluid-specific parameter in Eq. 2.67
	: thermal conductivity factor, Eq. 3.19
	: fitting and fluid-specific parameter in Eq. 8.2
L	: Grunberg-Nissan interaction parameter, Eq. 2.55
M	: molecular weight [mol g^{-1}]
M_d	: torque [N m]
P	: pressure [kPa]
R	: universal gas constant (=8.314 kJ kmol^{-1} K^{-1})
	: thermal resistance [m^2 K mW^{-1}]
	: electrical resistance [ohm], Eq. 3.15
V_o	: molar volume [m3 kmol^{-1}] at the liq-sol phase transition
T	: temperature [K, °R or °C]
T_g	: glass transition temperature [K]
T_g^W	: proxy glass transition temperature [K], Eq. 7.1
V	: linear velocity [m s^{-1}] in Eq. 2.1
	: molar volume [m^3 kmol^{-1}]
	: voltage [V], Eq. 3.18
Z	: compressibility factor
	: modified compressibility factor in Eq. 2.6
Z_{RA}	: Rackett compressibility factor, Eq. 6.8

Lowercase Symbols

c_2	: Expanded Fluid model parameter, dimensionless
c_3	: Expanded Fluid model parameter [kPa^{-1}]
d	: adjustable parameter in Eq. 2.64

$f(x,y)$	: denotes a function of variables x and y
q	: heat flux [W m^{-2}]
r_o	: radius [m], Eq. 3.17
t	: time [s]
v	: molar volume [m^3 kmol^{-1}] : specific volume [m^3 kg^{-1}]in Eq. 2.10
v_s	: saturated liquid molar volume [kmol m^{-3}]
v_o	: specific volume [m3 kg^{-1}] at the liq-sol phase transition
w	: mass fraction
x	: mole fraction
ΔX	: change of property X with respect to a reference value

Greek Letters

α	: Chung *et al.* (1984, 1988) correlation parameter, Eq. 2.6 : reduced boiling point temperature in Eq. 2.23 : Shu (1984) association parameter, Eq. 2.57 : thermal diffusivity [m^2 s^{-1}], Eq. 3.17
α_{ij}	: EF model viscosity binary interaction parameter
α_{ij}^{*}	: Walther model viscosity binary interaction parameter
β_{ij}	: density binary interaction parameter
γ	: fluid-specific parameter [m K mW^{-1}] in Eq. 2.13 : Euler constant (= 0.5772156649), dimensionless, Eq. 3.17
δ	: viscosibility [kPa^{-1}], Eq. 4.15
$\delta*$	: shear rate [s^{-1}]
θ_{ij}	: EF thermal conductivity model interaction parameter

λ	: thermal conductivity [mW m^{-1} K^{-1}]
λ'	: translational thermal conductivity [mW m^{-1} K^{-1}]
λ''	: internal degrees of freedom thermal conductivity
λ_o	: fluid-specific parameter [mW m^{-1} K^{-1}] in Eq. 2.13
μ	: viscosity [mPa·s]
v	: kinematic viscosity [cSt]
ρ	: density [kg m^{-3}]
ρ_s^o	: compressed state density [kg m^{-3}]
σ	: diameter of the hard sphere [A°]
Σ	: summation
τ_{yx}	: shear stress [Pa]
ϕ	: volume fraction
ϕ_{ij}	: Wilke's equation parameter, Eq. 4.11
ψ	: temperature coefficient thermal conductivity [mWm^{-1}K^{-2}]
ω	: angular velocity [rad s^{-1}] : acentric factor
Ω_v	: collision integral

Subscripts

b	: property at the normal boiling point
c	: property at the critical point : indicates the cone in a cone and plate rheometer, Eq. 3.7
F	: dilute gas friction contribution in Eq. 2.16

G	: dilute gas property
i,j	: "*i* th" and "*j* th" mixture components
o	: property at the reference state
	: property of the reference component in Eq. 2.15
r	: reduced property
asph	: asphaltenes
cal	: calculated variable
malt	: maltenes
meas	: measured variable
mix	: mixture
norm	: normalized variable
pred	: predicted value
Ref	: property of *n*-alkane reference component
rep	: value reported in the literature

Superscripts

o	: property of a reference component

Abbreviations

AARD	: average absolute relative deviation [%]
API	: American Petroleum Institute
BPR	: back pressure regulator
CapVis	: capillary viscometer
DAO	: deasphalted crude oil
EF	: Expanded Fluid

GC   : gas chromatography
Gr   : Grashof number

GW   : Generalized Walther model

MARD   : maximun absolute relative deviation [%]

NBP   : normal boiling point [°C, °R, K]

NIST   : National Institute of Standards and Technology

Nu   : Nusselt number

OF   : objective function

PIONA   : paraffins, isoparaffins, oleofins, naphthenics, aromatics

Pr   : Prandtl number

PRT   : platinum resistivity thermometer

Re   : Reynolds number

SARA   : Saturates, aromatics, resins, asphaltenes

SG   : specific gravity at 15.6°C

TBP   : true boiling point [°C, °R, K]

CHAPTER ONE: INTRODUCTION

1.1 Overview

The worldwide reserves of heavy oil and bitumen are estimated at 4,700 billion barrels oil-in-place, which is almost five times higher than the estimated reserves of conventional oils (Total, 2007). In Western Canada, particularly in Alberta, the reserves of heavy oil and bitumen are estimated at 2000 billion barrels oil-in-place (Total, 2007). Heavy oil and bitumen could potentially to extend the world's energy reserves by 15 years (SER, 2010) and are likely to play a significant role in future oil production.

Compared to conventional oils, heavy oils and bitumen have higher viscosities, as high as a million mPa·s at room conditions, and much lower API gravities, Figure. 1.1. Therefore, the high viscosity of these fluids must be reduced by heating or dilution for their recovery, transport, and processing. For example, steam and solvent assisted processes are commonly implemented in Western Canada to recover heavy oil (AEUB, 2006). Heavy oil and bitumen are diluted with condensates or other solvents for transport by rail or pipeline. Mined bitumen is heated and diluted with either naphtha or a paraffinic solvent in the froth treatment stage of the bitumen extraction process (Masliyah *et al*., 2011).

To model these processes, the phase behavior, physical properties, and transport properties of the bitumen and solvent mixtures must be determined. This thesis focuses on transport properties. The fundamental similarity between momentum, heat, and mass transfer has been noted previously (Bird *et al*., 2000; Chhabra *et al*., 1980). Diffusivity is considered elsewhere (Richardson, 2016) and the aim here is to develop self-consistent models for viscosity and thermal conductivity.
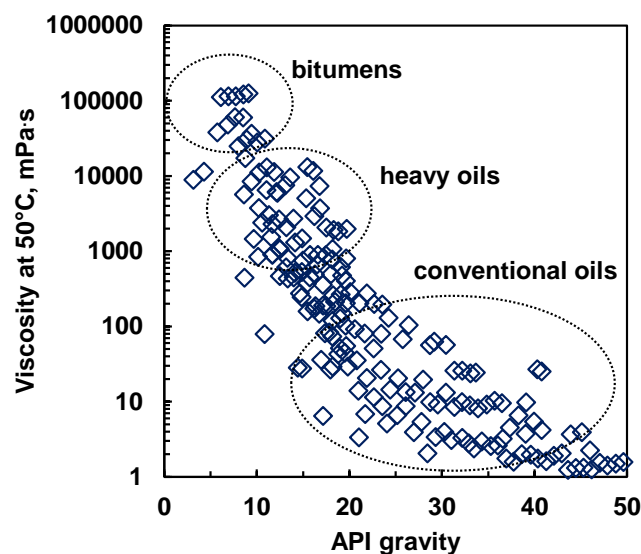
Figure 1.1. Viscosity at 50°C and 0.1 MPa for different crude oils (data from Boduszynski *et al.*, 1998).

1.1.1 Viscosity

A considerable amount of effort has been aimed at collecting viscosity data of heavy oils and bitumen in the last thirty years (AOSTRA, 1984; Boduszynski *et al.*, 1998). The development of solvent assisted recovery processes, such as VAPEX, motivated the collection of diluted heavy oil viscosity data. The available data include Western Canada bitumen saturated with methane, ethane, nitrogen, carbon dioxide (Mehrotra and Svrcek, 1988); diluted with toluene and xylenes (Mehrotra, 1990; Guan *et al.*, 2013); and, diluted with low and high molecular weight alkanes (Motahhari, 2013; Kariznovi *et al.*, 2013). Note that no data for heavy oils diluted with cyclic or high molecular weight aromatic solvents have not yet been reported. Additionally, only a few heavy oil distillation cut viscosity datasets have been reported (Mehrotra *et al.*, 1989). Distillation cut viscosity data is useful for developing a predictive model for pseudo-component characterized oils. Therefore, there is a need for viscosity data for heavy oil with a greater variety of solvents and for heavy oil distillation cuts in order to develop and test predictive models for whole and diluted heavy oils and their fractions.

2

Dozens of viscosity models have been developed but most are only applicable to the liquid or gas phase and there are only a few full-phase models applicable across the entire fluid phase diagram. Most of these models have been developed for pure hydrocarbons and light oils and are not capable of describing the viscosity of mixtures of heavy oil or bitumen and solvents with enough accuracy for reservoir and process simulation.

The Corresponding States model (CS), the Friction Theory (*f*-theory) model, and the Expanded Fluid (EF) model are full-phase viscosity models that have been tested on crude oils and used in reservoir simulators. These models are briefly reviewed below:

- *Corresponding States (CS)* relates the reduced viscosity of a fluid to the reduced viscosity of a reference fluid at the same set of reduced conditions (Hanley, 1976; Pedersen *et al.* 1984). Correction factors have been included into the model in order to correct the non-correspondence of most fluids to the reference fluid. The application of CS model to heavy oils is challenging as these fluids correspond to the reference fluid (methane or propane) at temperatures below its freezing point and therefore relevant reference viscosities do not exist (Lindeloff, *et al*., 2004). In addition, this model is computationally intensive requiring iterative procedures for the calculation of the reference fluid properties and correction factors.

- *Friction Theory (f-Theory)* (Quiñones-Cisneros *et al*,. 2000) relates the viscosity of a fluid to the friction forces between the fluid layers that arise from the attractive and repulsive contributions to the thermodynamic pressure. Repulsive and attractive pressure terms are calculated with a cubic equations of state (EoS) with critical properties tuned to match phase behavior data. Three adjustable parameters have been introduced to improve the accuracy of the predictions for heavy hydrocarbons (Quiñones-Cisneros *et al.*, 2001a) and crude oils characterized into pseudo-components defined from GC analysis (Quiñones-Cisneros *et al.*, 2001b). The adjustable parameters are determined by tuning the model against experimental viscosity data.The *f*-theory has been tested in crude oils with molecular weights up to 400 g/mol and

3

viscosities up to 10,000 mPa·s at pressures below and above the saturation value (Quinonez-Cisneros *et al.*, 2005).

- *The Expanded Fluid (EF) model* correlates viscosity to density (Yarranton and Satyro, 2009). The EF concept states that properties that depend on the spacing between molecules can be modelled across the phase diagram as a function of fluid expansion (density). This concept is at the heart of several viscosity models including the corresponding states model. However, Yarranton and Satyro used the compressed state density (the density at which the viscosity approaches infinity) rather than the critical point as the reference point for their model. This choice of reference point is better suited for heavy oils.

Although the Expanded Fluid (EF) viscosity model has been successfully tested on conventional oils, heavy oils and diluted bitumen, its predictive capabilities are limited. A predictive EF model for use in reservoir and process simulators requires the following: 1) a systematic approach to predict the viscosity of mixtures; 2) the ability to predict viscosity for an oil characterized into pseudo-components; 3) an accurate input density. To date, the EF model treats a mixture as a single component fluid with model parameters calculated from those of the mixture components assuming ideal viscosity mixing. However, the viscosity mixing process is not ideal and deviations as high as 80% have been observed for bitumen/solvent blends. In addition, the version of the EF model for characterized oils is based on GC assay data. Although this approach produces good results for conventional oils, the results for heavy oils and bitumen are not satisfactory. The issue is that up to 70 wt% of heavy oils and bitumen is lumped into a C30+ fraction (Yarranton *et al.*, 2013) and this fraction contains heavy components that contribute the most to the fluid viscosity. Therefore, the EF model becomes highly sensitive to the uncertainties related to the characterization of the C30+ fraction. Finally, the fluid density used as input for the EF model is predicted from cubic equations of state (CEoS). It has been well documented that cubic EoS do not provide accurate predictions of liquid densities (Motahhari *et al.*, 2013). Hence, the

accuracy of the EF model is limited by the accuracy of the density data predicted from the CEoS.

Most heavy oil and bitumen *in-situ* processes operate at liquid conditions far from the critical point. For these applications, a single phase liquid model is sufficient. Liquid viscosity models are based on the empirical observation that liquid viscosity decreases with temperature and do not require an input density. Arguably, the most successful of these models is the Walther correlation which forms the basis of most refinery blending rules. The Walther model is briefly described below:

- *The Walther model* (Walther, 1931) correlates the double log of viscosity to the log of temperature for liquids far from their critical point. While limited to the liquid phase, the accuracy of the Walther model is not constrained by the physical state of a reference fluid, an equation of state, the tuning of critical properties, or accurate density data. The only inputs of the Walther model are the absolute temperature and two fluid-specific parameters (Walther parameters) calculated by fitting the correlation to experimental viscosity data, usually at atmospheric pressure.

  Yarranton *et al*. (2013) developed a generalized version of the Walther model to predict the viscosity of liquid crude oils at any temperature and pressure as a departure from the viscosity calculated at atmospheric pressure. They also extended the Walther model to predict the viscosity of crude oils characterized into pseudo-components based on an extrapolated GC assay. The method was tested on Western Canada heavy oils with molecular weights and viscosities up to 550 g/mol and 1×10^6 mPa·s, respectively. The model parameters were correlated to molecular weight. This approach is easy to implement in simulators and rapid to solve. However, its accuracy for heavy oils is limited by the large extrapolation required to define the pseudo-components. The characterization was based on C30 assays where approximately 70 wt% of the oil was characterized as single carbon number fractions. In the authors' experience, measurement errors in the C30+ mass fraction and small differences in the extrapolation procedure can significantly shift the predicted viscosity.

1.1.2 Thermal Conductivity

The thermal conductivity of crude oils plays an important role in the design and simulation of heat transfer and non-isothermal mass transfer processes in refinery operations (Aboul-Seoud *et al.*, 1999). However, unlike viscosity, experimental data on the thermal conductivity of crude oils are scarce. This lack of data leads to unverified design assumptions; for example, AOSTRA (1984) recommends a value of 151 mW m^{-1} K^{-1} as the average thermal conductivity of heavy oils and bitumen, presuming that the effect of crude oil composition, temperature, and pressure can be neglected. Figure 1.2 shows that there is some deviation in the thermal conductivity data of heavy oils even at 25°C. Little is known about the effect of temperature, pressure, and solvent dilution on the thermal conductivity of heavy oils.
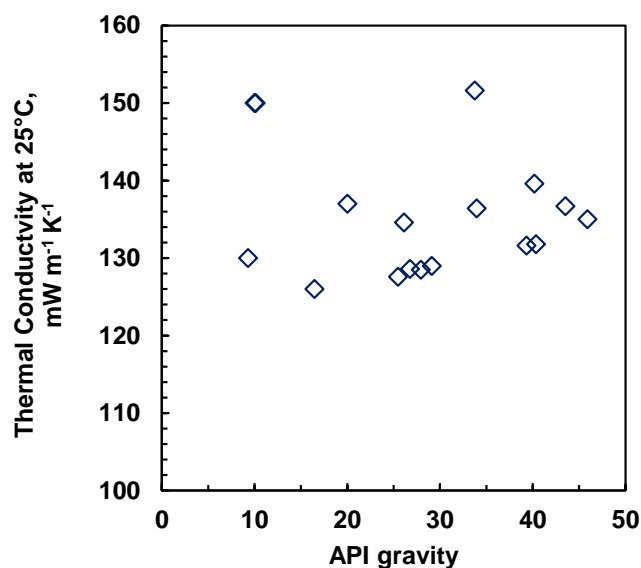
Figure 1.2. Thermal conductivity at 25°C and 0.1 MPa of crude oils (data from AOSTRA, 1984; Rastorguev and Grigor'ev, 1968; Guzman *et al.*, 1989 and Elam *et al.*, 1989).

The Corresponding States (CS) thermal conductivity model is the only full-phase model that has been applied to pure hydrocarbon, distillation cuts, and crude oils. The great majority of thermal conductivity models are totally empirical and mostly constrained to the liquid phase. These models are briefly described below:

- *Corresponding States (CS) model* relates the translational thermal conductivity of a fluid to the reduced translational thermal conductivity of a reference fluid at the same set of reduced coordinates (Hanley, 1976; Christensen and Fredenslund, 1980). The total thermal conductivity of a fluid is estimated by adding an internal degrees of freedom contribution, calculated from a separate set of correlations, to the translational contribution. Corrections factors have been incorporated into the model to account for the non-correspondence of most fluids to the reference substance. The implementation of this model in process simulators is challenging as it demands complex iterative algorithms for the calculation of correction factors and reference fluid properties.

- *Liquid Phase Correlations* describe the linear decrease in thermal conductivity of liquid hydrocarbon and distillation cuts with temperature at conditions far away from the critical point. The great majority of those correlations have only two parameters: one representing the slope and the other intercept of the linear temperature dependence. The two parameters are fluid and pressure specific and must be determined by fitting to data.

The thermal conductivity models described here were developed for conventional oils and most only apply in the liquid phase. The only full phase model, the Corresponding States model, is expected to have the same difficulties with heavy oil thermal conductivity as it does with viscosity. The Expanded Fluid concept is an attractive option for predicting the thermal conductivity of heavy oils because it is anchored at the compressed state density and extends naturally to the critical point.

1.2 Objectives

The main objective of this study is to develop a predictive methodology for the viscosity and thermal conductivity of heavy oils and bitumen for process and reservoir simulation applications. For process simulation, the Expanded Fluid viscosity model will be extended to characterized oils and a new thermal conductivity model will be developed based on the

Expanded Fluid concept. For reservoir simulation, the Walther viscosity correlation will be updated to for oils characterized based on a distillation assay. The thermal conductivity of crude oils is not a significant property in reservoir applications and the EF model results, even with less accurate density inputs, were considered to be sufficient. Therefore, an independent model was not developed.

The specific objectives of this thesis are to:

1. develop a consistent approach to predict the viscosity of dilute heavy oils using the Expanded Fluid (EF) model based on pure hydrocarbon binaries and bitumen/solvent pseudo binaries viscosity data.
2. propose and validate an experimental method to collect viscosity data of heavy oil distillations cuts, whole, deasphalted and partially deasphalted oils and C5-asphaltenes using a cone and plate rheometer.
3. develop a new characterization approach for crude oils based on a distillation assay and suitable for viscosity and thermal conductivity modelling
4. extend the EF viscosity model to predict the fluid viscosity of crude oils characterized from a distillation assay. Correlations for the model parameters will be developed using the data collected for Objective 2.
5. propose and test a methodology to predict the liquid density of crude oils characterized from a distillation assay.
6. extend the Walther correlation to predict the liquid viscosity of crude oils characterized from a distillation assay. Correlations for the model parameters will be developed using the data collected for Objective 2.
7. validate an experimental approach for the measuring of thermal conductivity of whole and diluted crude oils at temperatures up to 200°C and 10 MPa. This experimental method will be based on the hot wire technique that has been widely used to determine the thermal conductivity of liquids.
8. develop a full-phase thermal conductivity model based on the Expanded Fluid concept suitable for pure hydrocarbons, crude oils, and their mixtures.

9. extend the thermal conductivity model to predict the thermal conductivity of crude oils characterized from a distillation assay.

1.3 Thesis Structure

This thesis is divided into nine chapters, not including the introduction:

Chapter Two briefly reviews petroleum chemistry, classification, composition, and characterization methods. Then, the relationship between viscosity, thermal conductivity, and fluid expansion is described. Finally, a summary of different single phase and full phase models for viscosity and thermal conductivity of crude oils, distillation cuts, and their mixtures with pure hydrocarbons is provided.

Chapter Three describes the apparatuses and procedures used to measure the density, viscosity, and thermal conductivity of the samples used in this thesis. Other techniques such as determination of water content and asphaltene precipitation are presented. The chemicals and materials used to prepare diluted oil samples are also described.

Chapter Four presents and compares the Expanded Fluid (EF) and Walther viscosity models. Previously developments, such as extension to GC characterized oils, are discussed.

Chapter Five presents a methodology to predict the viscosity of pure hydrocarbon mixtures and diluted crude oils using the EF viscosity model. This methodology was developed using pure hydrocarbon binaries data and data from bitumen/solvent pseudo-binaries collected at temperatures and pressures up to 175°C and 10 MPa, respectively. The methodology was tested not only on data collected in this study but also on data collected from the literature.

Chapter Six describes an approach to predict the viscosity of distillation assay characterized heavy oils, bitumen and conventional oils based on the Expanded Fluid (EF) viscosity model. This chapter also presents correlations for the prediction of liquid density of distillation characterized oils at any temperature and pressure. The developed predictive approach is tested on viscosity data collected in this thesis for distillation cuts, deasphalted

oils, partially deasphalted oils, and whole crude oils. The method is also tested on an independent dataset collected from the literature. A tuning scheme is also proposed for use when at least a viscosity data point is available.

Chapter Seven presents a methodology to predict the viscosity of oils characterized from a distillation assay using the Walther model. A methodology to predict the viscosity of pure hydrocarbon mixtures and diluted crude oils is also presented. The range of conditions at which the model is applicable was determined. Correlations for the model parameters were developed based on the data collected in this thesis. The model is tested on viscosity data collected in this study and from the literature. A tuning methodology is also developed and described in this chapter.

Chapter Eight presents the development of a thermal conductivity model based on the Expanded Fluid concept. The model is developed from pure hydrocarbon data and tested on whole crude oils modelled as single components. Mixing rules with correlated interaction parameters are also developed for pure hydrocarbon mixtures and diluted crude oils applications. Finally, the model is extended to predict the thermal conductivity of oils characterized from a distillation assay. The proposed approach was tested on data for distillation cuts from the literature and crude oils from this thesis.

Chapter nine presents the conclusions from this thesis and provides recommendations for future studies.

NOTE 1:
The EF and the Walther viscosity models are intended to be applicable only to Newtonian fluids. Newtonian fluids are those for which viscosity is independent of the applied shear rate. All the viscosity data collected in this thesis correspond to a range of temperatures and pressures for which the fluids are Newtonian. The description of non-Newtonian fluids is beyond the scope of this study.

NOTE 2:

The experimental viscosity, density and thermal conductivity data used in this thesis were divided into two groups: 1) data collected in this study, according to the techniques summarized in Chapter 3, and; 2) data collected from the literature. A detailed description of each group is included in Chapters 5 to 8 under the title "Data Collected and Organization of Datasets".

CHAPTER TWO: LITERATURE REVIEW

This chapter presents a review of the fundamental concepts used in this work to develop a consistent methodology to predict the viscosity and thermal conductivity of crude oils based on fluid expansion. The first section reviews the general definition, composition, and classification of petroleum as well as crude oil characterization methods with an emphasis on distillation. The second section addresses the concepts of viscosity and thermal conductivity as well as the relation of these transport properties to volume expansion. Finally, in the third section, methodologies to predict the viscosity and thermal conductivity of crude oils and petroleum fluids are summarized.

2.1 Petroleum Definition and Composition

Petroleum is a naturally occurring mixture of hydrocarbons and other compounds containing variable amounts of sulfur, nitrogen and oxygen as well as trace amounts of metallic constituents including vanadium, nickel, and iron (Speight, 2007). This definition includes petroleum in the form of gas (natural gas), liquid (crude oil), semi-solids (bitumen) or solids (wax or asphaltite) (Riazi, 2005). This thesis focuses on crude oil.

Crude oils are dark viscous fluids usually containing dissolved volatile components such as light alkanes (carbon numbers from C1 to C4) and non-hydrocarbons such as nitrogen (N_2), carbon dioxide (CO_2), hydrogen sulfide (H_2S), helium (He), and traces of water (Kidnay, 2011). Crude oils containing dissolved gases are known as *live oils*. Dissolved gases are released from solution when the pressure is reduced below the saturation value. Crude oils which have lost all dissolved gases are known as *dead oils*. In this thesis, the term crude oil, or simply oil, refers to dead oil.

Crude oil composition covers a great variety of hydrocarbons in a wide range of organic functionality, size, and molecular weight. This composition varies with location, age of the field, and reservoir depth (Speight, 2007). A brief description of the different chemical

12

families that have been identified in crude oils is provided below (Altgelt and Boduszynsky 1994).

Paraffins are saturated hydrocarbons with straight or branched chains (normal and isoparaffins, respectively). The carbon atoms in these compounds are bonded with single covalent bonds. Paraffinic oils are light oils.

Naphthenes are cycloparaffins; that is molecules containing a saturated ring structure. The saturated ring might have five, six or occasionally seven carbon atoms (cyclopentanes, cyclohexanes, and cycloheptanes, respectively). Most naphthenes in crude oils have paraffinic side chains and may have more than one ring in the molecule; for instance, mono-naphthenes, di-naphthenes and tri-naphthenes. The rings can also be non-fused or fused if they share more than one carbon atom.

Aromatics are hydrocarbon compounds with at least one benzene ring. Aromatics are classified by the number of aromatic rings in the molecule; for instance, mono, di or tri aromatics. Aromatics in crude oil usually have paraffinic side chains and may include naphthenic rings. The aromatic and naphthenic rings in this class of compounds can be fused or non-fused. The complexity of aromatic compounds increases greatly as the number of rings increases due to large number of possible arrangements of naphthenic and aromatic rings and side chains.

Heterocompounds are hydrocarbons from the above groups in which one or more heteroatoms (N, S, O, V, Ni, Fe) form part of the molecule. The presence of the heteroatoms and their functionality adds to the complexity of the structural arrangements of the hydrocarbon compounds. Heterocompounds are commonly part of the high molecular weight fractions of petroleum fluids.

2.2 Crude Oil Classification

Several classification approaches have been proposed for crude oils mainly related to production and refining process selection (AOSTRA, 1984). The UNITAR classification sorts dead oils according to their viscosity and specific gravity at reservoir conditions, Figure 2.1. Oils can also be classified as conventional or unconventional according to the recovery method employed. Conventional oils are light to intermediate oils (Figure 2.1) produced by traditional recovery methods such as primary production and water flooding. Unconventional oils are heavy oils and bitumen (Figure 2.1) usually produced using thermal recovery methods or mining. However, in some cases, light oils are classified as unconventional oils because they must be recovered using unconventional methods due to the low permeability of their reservoir rock.
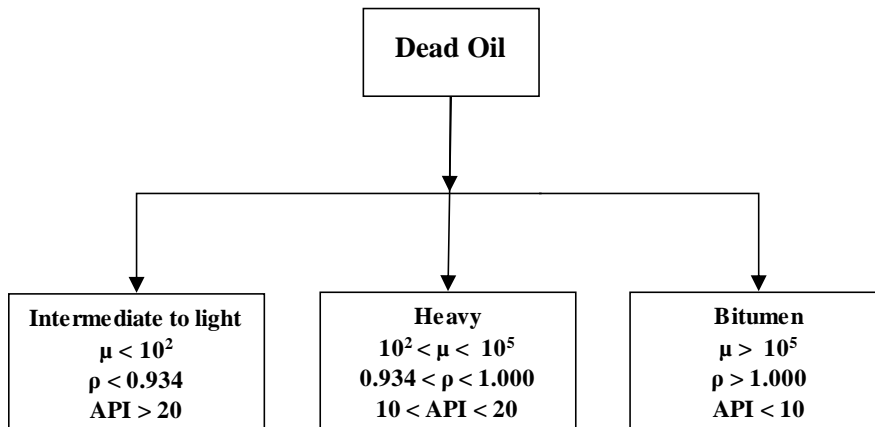
Figure 2.1. Schematic representation of the UNITAR classification of crude oils. Symbols μ and ρ stand for viscosity, in mPa·s, and density, in g/cm^3, respectively. Adapted from AOSTRA (1984).

A classification based on composition represents a crude oil as a mixture of three fractions as shown in the triangular diagram in Figure 2.2. The type of oil and its physical properties are determined by the chemical species most prominent in the fluid (McCain, 1990). In general, paraffinic oils have relatively lower density, viscosity and boiling point than naphthenic oils. The highest density, viscosity and boiling point is found in oils with high

contents of aromatic and heterocompounds. This classification led to the conclusion that conventional oils are mostly paraffinic and naphthenic fluids whereas heavy oils and bitumen have a high content of aromatic hydrocarbons and polar heterocompounds.
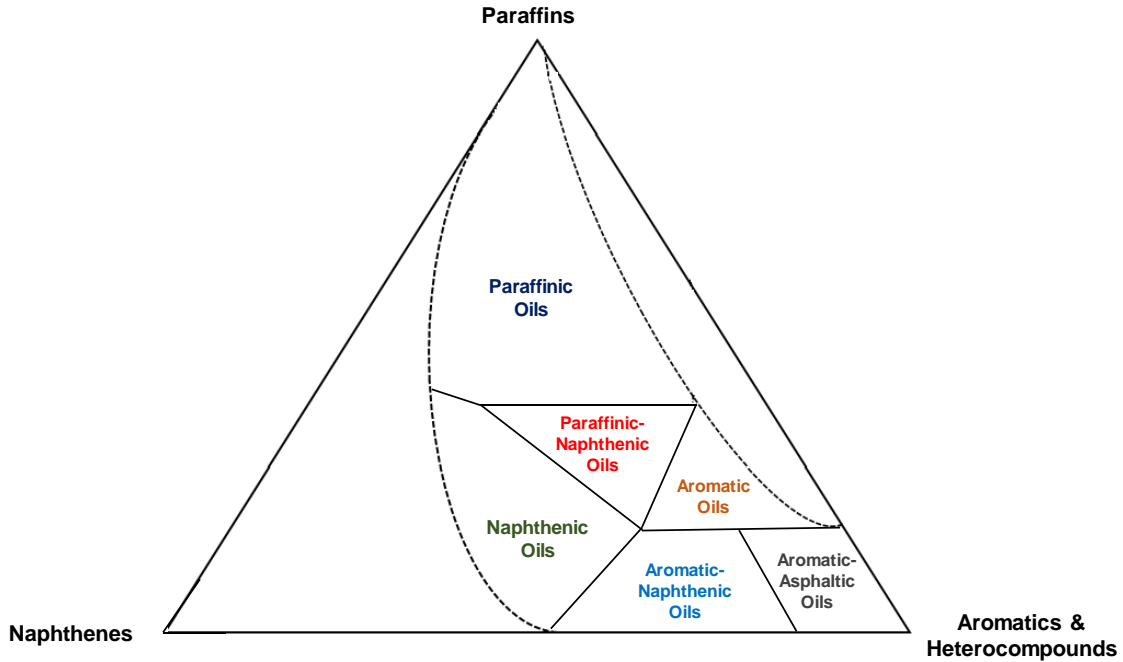
Figure 2.2. Ternary composition diagram separating paraffins, naphthenes and aromatics and heterocompounds. Crude oil types are shown in the different regions in the diagram. Adapted from Cornelius (1987).

2.3 Crude Oil Characterization

Characterizing crude oils in terms of composition is the first step for calculations of their properties and prediction of their thermodynamical behavior in both upstream (reservoir) and downstream (surface facility and refinery) processes. For instance, the nature of the products obtained in refinery operations depends greatly on the characteristics of the crude oil used as feedstock (Speight, 2007). The objective of crude oil characterization is to separate the oil into a finite number of fractions that represent the distribution of properties within the oil.

According to the continuum concept introduced by Boduszynski (1987), properties of crude oil components are continuously distributed across a wide range of molecular weights which extends from smallest to largest components. Note that the molecular weight range of the fractions broadens with boiling point due to the increase in the variety of chemical species. As the molecular weight and boiling point increase other properties such as aromaticity, heteroatom content increase as shown in Figure 2.3.
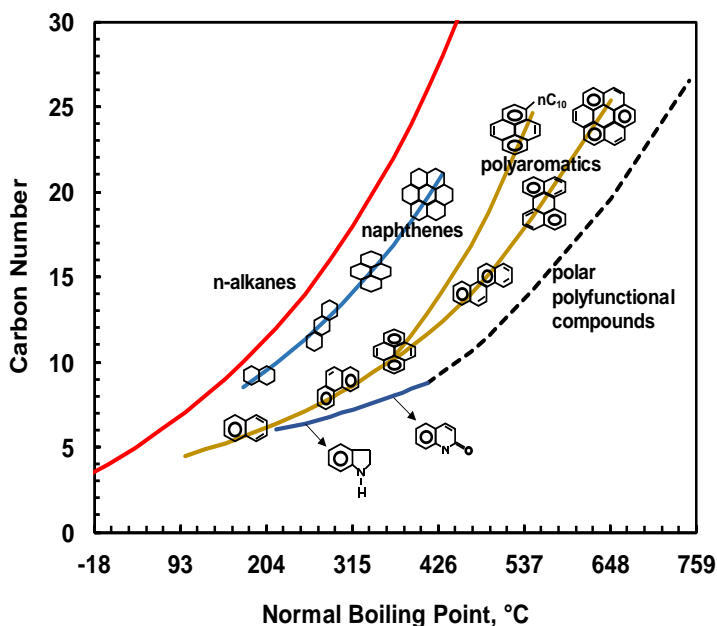
Figure 2.3. Effect of the boiling point on the variety of chemical components found in distillation fractions. Adapted from Altgelt and Boduszynsky, (1994). Boiling points are approximated.

Figure 2.4 shows that transport properties, such as viscosity, also vary systematically with boiling point. The viscosity of boiling cuts from the light oil is close to that of *n*-alkanes; however, the viscosity of the medium and heavy oil cuts deviate to higher viscosities. The deviation arises from an increase in the naphthenic and aromatic of the oils. The exponential increment in the viscosity of the heaviest cuts is a consequence of the presence of a great variety polynuclear aromatics and polar heterocompounds (Altgelt and Boduszynsky, 1994).
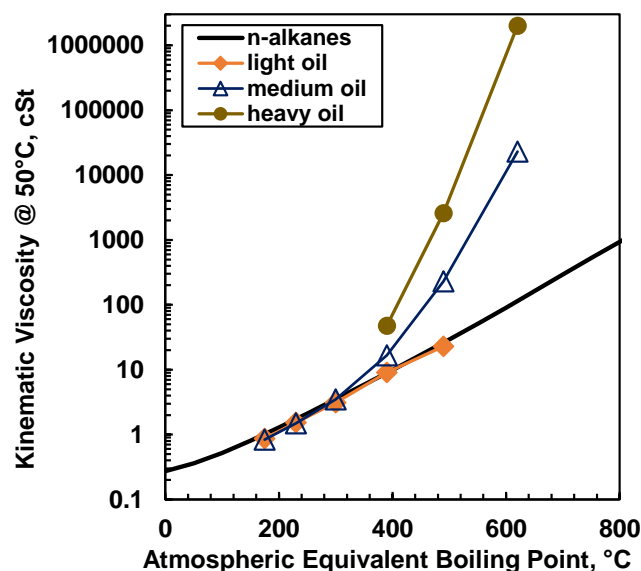
Figure 2.4. Atmospheric kinematic viscosity at 50°C versus boiling of *n*-alkanes and distillation cuts of a light (Altamont, °API= 42.2), a medium (Alaska North Slope, °API=27.6), and a heavy oil (Kern River, °API=13.6). Data from Altgelt and Boduszynsky, (1994).

An assay is required as a starting point to characterize this wide distribution of properties. Several types of crude oil assay have been developed based on the separation of oil components according to solubility, carbon number, and volatility. Each method provides valuable information regarding the nature of crude oils; however, not all methods provide the same kind of information and hence the choice of characterization depends on the information required to analyze a given process. For instance, distillation is the method chosen to characterize crude oils in refineries because it provides information about products such as gasoline, lube oils, and base stocks (Altgelt and Boduszynsky. 1994). In contrast, solubility based characterization is chosen in flow assurance because solubility data provide more information about the components which can precipitate under certain conditions. A variety of crude oil characterization techniques are described in detail elsewhere (Altgelt and Boduszynsky, 1994; Riazi, 2005; Speight, 2007;). Distillation was the characterization technique chosen for this thesis and a brief summary is provided

below. SARA analysis is often used to characterize dead heavy oil and is also summarized below.

2.3.1 Distillation

Distillation separates a crude oil into a number of fractions or "cuts" by boiling point range (Whitson and Brule, 2000). The basis of this separation is the difference in volatility of components which decreases with molecular weight. Each fraction, or "cut", contains chemical species within a narrow range of molecular weight and consequently limiting their chemical size and structural diversity (Altgelt and Boduszynsky, 1994). This characteristic makes petroleum boiling fractions suitable candidates to represent "pseudo-components" which are not real components of the crude oil, but can nonetheless be used to model its properties (Riazi, 2005). Another important advantage of distillation is that cut properties such as average molecular weight, specific gravity, atomic hydrogen-to-carbon ratio, viscosity, and thermal conductivity can be measured and used to develop correlations. These properties are often correlated to boiling point and can therefore be estimated once a distillation assay is obtained (Riazi, 2005).

Several distillation techniques have been developed for crude oils and are summarized elsewhere (Riazi, 2005; Speight, 2007; Castellanos-Diaz, 2012; Powers, 2014). The range of distillable material decreases as the specififc gravity of the oil increases; hence, reduced pressure techniques have been developed in order to extend the range of distillation and consequently obtain a better characterization of heavy fractions. For heavy oils, conventional distillation techniques at atmospheric pressure can distill up to 5 wt% of the oil whereas commercially available low pressure laboratory techniques can distill up to 35 wt% of the oil. A deep vacuum apparatus recently developed by Castellanos-Diaz *et al.* (2014) is capable of distilling up to 50 wt% of a heavy oil using pressures as low as $1x10^{-6}$ Pa. The collected low pressure boiling points are interconverted to their atmospheric equivalent by extrapolation of the vapor pressure of the different distillation cuts (Sanchez-Lemus *et al.*, 2014). The apparatus also allows the collection of up to six distillation cuts, which can be used for the direct measurement of their physical and transport properties.

2.3.2 SARA Fractionation

SARA fractionation, Figure 2.5, divides the oil into solubility and adsorption classes: saturates, aromatics, resins, and asphaltenes. Note, the non-asphaltene fractions are collectively referred to as maltenes. Each one of the fractions obtained contains a great variety of compounds from the distinct groups of chemical families. Hence, the properties of each fraction vary relatively little between different dead heavy oils. A description of each one of the SARA fractions is provided below.

```
                        ┌──────────────┐
                        │  Crude Oil   │
                        └──────────────┘
                     n-pentane or n-heptane
            ┌────────────────────┴────────────────────┐
    ┌──────────────┐                         ┌──────────────────┐
    │  Asphaltenes │                         │ Deasphalted Oil  │
    └──────────────┘                         └──────────────────┘
                                                    Clay
                                    ┌─────────────────┴─────────────────┐
                              ┌──────────────┐               ┌──────────────┐
                              │    Resins    │               │     Oils     │
                              └──────────────┘               └──────────────┘
                                                                Silica Gel
                                                   ┌──────────────┴──────────────┐
                                            ┌──────────────┐           ┌──────────────┐
                                            │   Aromatics  │           │   Saturates  │
                                            └──────────────┘           └──────────────┘
```
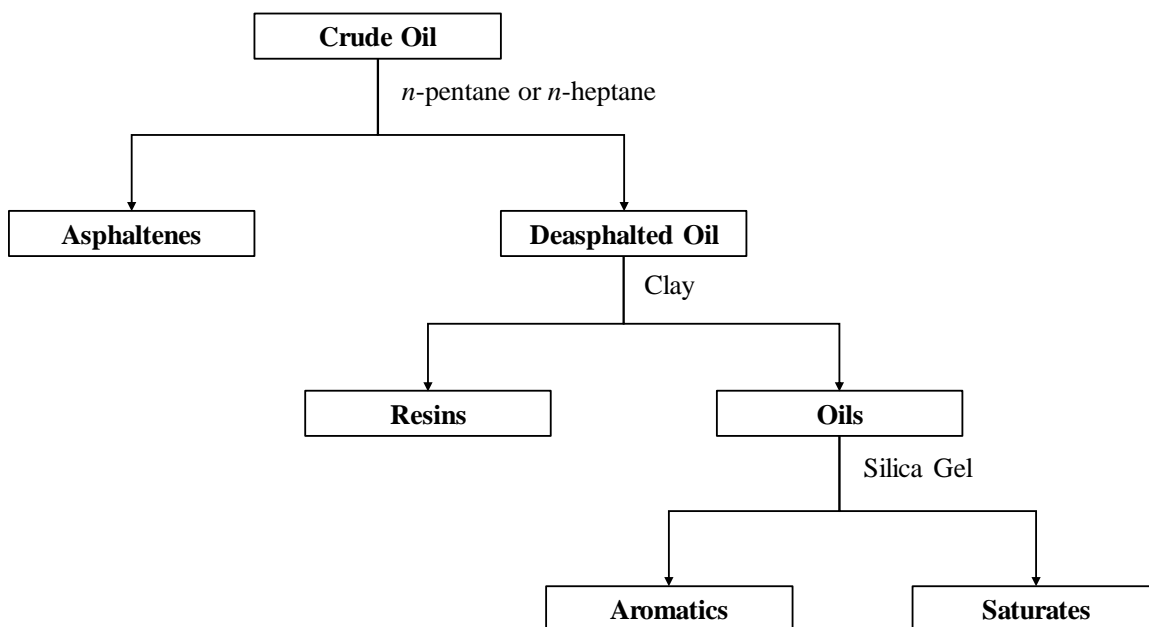
Figure 2.5. Solvent fractionation procedure for crude oils. Adapted from Speight (2007) and Riazi (2005).

Saturates consist of paraffins and cycloparaffins (Speight, 2007) with molecular weight and density between 300 and 600 g/mol and 0.869 and 0.880 g/cm^3, respectively (Powers, 2014). These are the least polar components of the oil.

Aromatics consist of small aromatic components containing few aromatic rings with some alkyl chains or naphthenic rings attached to the aromatic rings (Speight, 2007). Their molecular weight ranges from 300 and 800 g/mol and their density from 0.990 and 0.999 g/cm^3 (Powers, 2014).

19

Resins consist of molecules with larger aromatic cores, alkyl side chains, and naphthenic rings. Resins have higher polarity and lower atomic hydrogen-to-carbon ratio than aromatics (Speight, 2007). Their molecular weight ranges from 700 to 1300 g/mol and their density from 1.044 and 1.049 g/cm^3 (Powers, 2014).

Asphaltenes are the most polar, aromatic, and heaviest fraction of a crude oil. The asphaltenes are dark brown solid powders which precipitate from the crude oil in an excess of *n*-alkane solvents such as *n*-pentane or *n*-heptane but remain soluble in solvents such as benzene, toluene, chloroform, and carbon tetrachloride (AOSTRA, 1984). Asphaltenes are a solubility class component and their quantity and composition depend on the precipitant and the procedure used to recover them. Their composition has not yet been defined (Yarranton *et al*., 2000) but it has been accepted that asphaltenes are composed of hundreds of thousands of different structures containing aromatic rings with attached alkyl chains, naphthenic rings, and heteroatoms (McKenna *et al*., 2013).

At least some of the asphaltenes self-associate into nano-aggregates (Yarranton and Masliyah, 1996) and their apparent molecular weight depends on concentration, solvent type, and temperature. Their "monomer" molecular weight varies between 500 and 2000 g/mol (Yarranton *et al*., 2007; Mullins, 2007). The apparent molecular weight of nanoaggregates can range up to 100000+ g/mol. The density of asphaltenes, determined from asphaltene/toluene mixtures assuming they form regular solutions, ranges from 1078 to 1189 kg/m^3 (Barrera, *et al*., 2013)

2.4 Viscosity and Thermal Conductivity

Viscosity and thermal conductivity are transport properties required for the design of a variety of processes and process units in the petroleum industry including *in situ* oil recovery processes, pipelines, and heat exchangers. Momentum and heat are transferred by means of either molecular movement (conduction) or bulk fluid movement (convection); or a combination of both. Heat is also transferred by radiation, but it is out of the scope of this work and not discussed here.

Viscosity is the proportionality factor between the momentum transferred by conduction and a driving force, in this case the velocity gradient. For one dimensional flow, this relationship is given by (Bird *et al*., 2002):

$$\tau_{yx} = -\mu \frac{\partial V_x}{\partial y}$$
(2.1)

where τ_{yx} is the shear stress which causes transfer of momentum, μ is the viscosity, V_x is the velocity in the x-coordinate, and y is the distance in the y- coordinate. Equation 2.1 is known as Newton's law of viscosity. Viscosity can be considered as the resistance of a fluid to shear stress. Fluids with a higher viscosity require more mechanical energy to flow at the same rate. Viscosity, μ, as given in Equation 2.1 is known as dynamic viscosity and when divided by the density of the fluid is known as kinematic viscosity. In this work the word viscosity denotes dynamic viscosity. The unit for viscosity used along this work, unless otherwise stated, is mPa·s.

Similarly, thermal conductivity is the proportionality factor between heat transfer and a thermal gradient, and the one dimensional relationship is given by:

$$q = -\lambda \frac{\partial T}{\partial y}$$
(2.2)

where q is the heat flux, λ is the thermal conductivity, and T is temperature. Equation 2.2 is known as Fourier's law of conduction. Thermal conductivity can be considered as the resistance of a fluid to transfer heat. Fluids with low thermal conductivity are poor heat conductors. The unit for thermal conductivity used in this work, unless otherwise stated, is $mWm^{-1}K^{-1}$.

Viscosity and thermal conductivity are fluid properties that depend on temperature and pressure. In the case of dilute gases, viscosity and thermal conductivity are independent of pressure and only increase with temperature. For gases at higher pressures, both properties increase with temperature and pressure; however, the effect of pressure on thermal conductivity is not as strong as that on viscosity. In the case of liquids, both properties decrease with temperature and increase with pressure. The viscosity of liquids decreases

21

rapidly and non-linearly with temperature whereas their thermal conductivity decreases slowly and almost linearly (except for water, multi-hydroxy and multi-amine molecules for which thermal conductivity increases with temperature). There is little effect of pressure on the thermal conductivity of liquids, except at very high pressures (Poling *et al*., 2001).

2.4.1 Viscosity and Thermal Conductivity of Dilute Gases

Viscosity and thermal conductivity of dilute gases can be predicted using models derived from elementary kinetic theory under the assumption that the gas was composed of non-attractive rigid spheres (hard-spheres theory) (Poling *et al*., 2001):

$$\mu_G = 26.69 \times 10^{-4} \frac{(MT)^{0.5}}{\sigma^2} \tag{2.3}$$

$$\lambda_G = 26.3 \times 10^{-21} \frac{(MT)^{0.5}}{\sigma^2} \tag{2.4}$$

where the subscript "*G*" indicates a dilute gas property, M is molecular weight, T is the absolute temperature, and σ is the diameter of the hard sphere in Å.

The Chapman-Enskog theory (Chapman and Cowling, 1939) has been used in order to b account for interaction (repulsion and attraction) between gas molecules. The postulates of the theory are the same as those of the elemental kinetic theory but the hard sphere diameter, σ, is modified by a dimensionless parameter which captures the deviation from the hard sphere due to intermolecular interactions. This parameter is the collision integral, Ω_v, and depends on the potential energy of interactions and temperature. The final Chapman-Enskog expressions for viscosity and thermal conductivity of dilute gases are the same as Equations. 2.3 and 2.4 but are divided by Ω_v ($\Omega_v = 1$ for hard sphere fluids). Details of estimation of Ω_v are given elsewhere (Poling *et al*., 2001).

The use of the Chapman-Enskog expressions is challenging because it requires parameters that are difficult to estimate: the potential energy of interactions, used in the calculation of Ω_v, and the hard sphere diameter. Chung *et al* (1984, 1988) proposed empirical correlations that relate those two parameters to the critical temperature and critical volume,

respectively. They also proposed an empirical factor which corrects for molecular shape and polarity. The Chung *et al.* correlation for dilute gas viscosity is given by:

$$\mu_G = 4.0785 \times 10^{-3} \frac{F_c \left(MWT \right)^{0.5}}{v_c^{2/3} \Omega_v} \tag{2.5}$$

where v_c is the critical volume and F_c is the empirical correction factor calculated as a function of the acentric factor, critical volume and dipolar moment. A similar modification of the original Chapman-Enskog expression for thermal conductivity was not possible. Equation 2.4 is only applicable to monoatomic molecules for which thermal conductivity only depends on changes of translational energy during collisions (Poling *et al.*, 2001). For polyatomic molecules, thermal conductivity is strongly affected by changes in translational, rotational and vibrational during a collision (Chung *et al.*, 1984). Hence, thermal conductivity is more dependent on molecular structure than viscosity.

Chung *et al.* (1984, 1988) proposed a correlation for the thermal conductivity of dilute gases considering the contributions from translational and internal molecular energies. The final expression is given as follows:

$$\frac{\lambda_G M}{\mu_G C_v} = \frac{3.7}{C_v / R} \left[1 + \alpha \frac{0.215 + 0.28288\alpha - 1.061\beta + 0.26665Z}{0.6366 + \beta Z + 1.061\alpha Z} \right] \tag{2.6}$$

$$\beta = 0.7862 - 0.7109\omega + 1.3168\omega^2 \tag{2.7}$$

$$Z = 2.0 + 10.5 T_r^2 \tag{2.8}$$

$$\alpha = \left(C_v / R \right) - 1.5 \tag{2.9}$$

where C_v is the isochoric heat capacity in J/mol.K, R is the gas constant and T_r is the reduced temperature. Poling *et al.* (2001) recommends Chung *et al* (1984, 1988) correlations for the predictions of pure hydrocarbon dilute gas viscosity and thermal conductivity.

The hard-sphere theory (also known as Enskog theory) has been extended to predict the viscosity and thermal conductivity of dense fluids. According to this theory, the only difference between a dilute and a dense system composed by hard spheres is that the rate

of collision in the latter is higher than that in the former (McLaughlin, 1964; Alder, 1966). The viscosity and thermal conductivity of a dense fluid are calculated as a departure from the dilute gas value. The departure expression, which is representative of the collision rate, is a function of the density of the fluid and the hard-sphere second virial coefficient (this second virial coefficient is only a function of molecular diameter). However, the application of the Enskog theory to real fluid produces less than satisfactory results. Sengers (1965) proposed a modification of the Enskog theory in order to account for attractive intermolecular forces. This modification extended the range of application of the Enskog theory to higher densities. Hanley and McCarty (1972) further modified the Enskog theory by assuming that the main difference between hard sphere and real fluids is the temperature dependence of the collision rate. That temperature effect is captured by introducing a temperature dependent hard-sphere second virial coefficient estimated by fitting the hard-sphere equation of state to actual PVT data. The authors found that the modified theory gave satisfactory predictions for the viscosity and thermal conductivity of fluids at densities up to twice the critical density. However, the range of application decreases as temperature increases.

2.4.2 Viscosity and Thermal Conductivity of Liquids

To date, there has not been a unified approach to predict the viscosity and thermal conductivity of liquids due to the lack of a theoretical model that allows a consistent description of the liquid phase. For instance, the application of the Enskog theory, or any modified version, to liquids does not give satisfactory results. According to this theory the mechanism of transfer of momentum and heat is only due to collision between molecules; however, in liquids, the molecules vibrate in a reduced space rather than wandering freely as a consequence of high intermolecular forces; therefore, collisions play a negligible role in momentum and heat transfer (Poling *et al.*, 2001). McLaughlin, (1964) points out that the higher value of the transport properties in liquids compared to gases is because the transfer of momentum and heat is facilitated by the higher density of the liquids. However, little is known about the transfer mechanism in liquids.

The great majority of viscosity and thermal conductivity models proposed for liquids are based on empirical or semi-empirical ideas. Comprehensive summaries were provided by Poling *et al.* (2001) and Latini *et al.* (2006). In this thesis, the focus is on the models based on the idea proposed by Hildebrand (1971) that the transport properties of a liquid are a function of the change in the fluid molar volume. This principle has been used to develop models for viscosity and thermal conductivity.

2.4.3 Relation of Viscosity and Thermal Conductivity to Fluid Expansion

Batschinski (1913) empirically found that the fluidity (inverse of viscosity) of non-associated liquids was almost independent of temperature at constant volume. He proposed that viscosity is not a direct function of temperature but closely connected to the free volume. Based on empirical evidence, he formulated a linear relation between fluidity and free volume:

$$\frac{1}{\mu} = A(v - v_o)$$

(2.10)

where A is a constant, v is the specific volume and v_o is the Van der Waals specific covolume. Later, Hildebrand (1971) found that Equation 2.10 is not appropriate for liquids at temperatures close to the melting point and proposed the following improved correlation:

$$\frac{1}{\mu} = B_\mu \left(\frac{V - V_o}{V_o} \right)$$

(2.11)

where V is the molar volume and B_μ and V_o are fluid-specific parameters. The ratio on the the right hand side of Equation 2.11 is known as the specific unoccupied molar volume. Note that V_o is the molar volume at which the fluidity is equal to zero. Hildebrand (1971) also noted that a small increase in the molar volume corresponds to a small increment in the intermolecular separation but a large decrease in the viscosity.

Equation 2.11 has been extensively used to model the viscosity of liquid hydrocarbons and their mixtures. Przezdziecki and Sridhar (1985) tested the correlation on alkanes, alkyl halides, aromatics, aryl halides, acetone and acetic acid. They also developed correlations for the parameters B_μ and V_o as a function of the liquid critical pressure and temperature,

acentric factor, molecular weight and freezing point temperature. Diller and Van Poolen (1985) proposed a temperature dependence on the parameters B and V_o in order to improve the fitting for n-butane and isobutane at high temperatures and pressures. Cullinan and Kosanovich (1975) found that Equation 2.11 is also applicable to binary mixtures of hydrocarbons.

Hildebrand and Lamoreaux (1972) studied the variation of viscosity of fluids from the dense liquid to the dilute gas state. Using experimental data of n-propane and carbon dioxide they found a linear relation between fluidity and molar volume independent of temperature and pressure when the molar volume is less than 0.5 times the corresponding critical molar value (V_c). At molar volumes beyond $0.5V_c$, the straight line separates into isotherms which become horizontal tending toward the value of the dilute gas fluidity. Recall that the value of dilute gas viscosity is only a function of the temperature. Two different n-propane isotherms are shown in Figure 2.6.
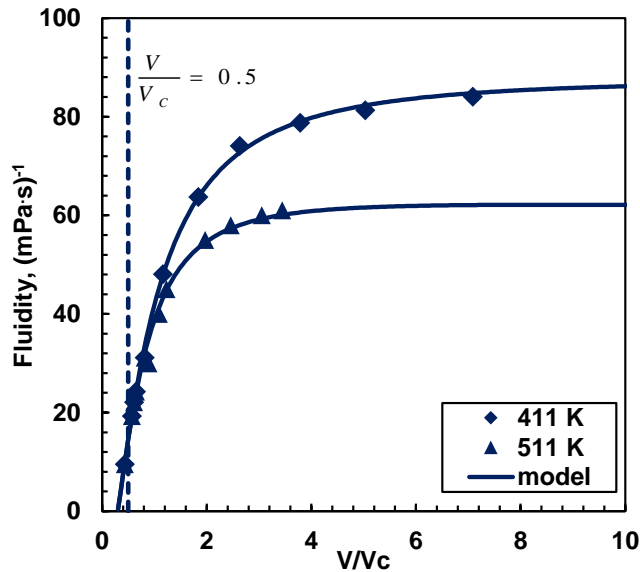
Figure 2.6. Variation of n-propane fluidity with the ratio of molar volume to critical volume. Data taken from Hildebrand and Lamoreaux (1972, 1974).

Hildebrand and Lamoreaux (1974) proposed that the change in the linear behavior of fluidity versus molar volume beyond $0.5V_c$ is a consequence of different mechanisms of

momentum transfer in the liquid and gas phases. They formulated a generalized viscosity model applicable to fluids from the dense liquid to the dilute gas states considering that the viscosity in the liquid phase is only a function of the specific unoccupied volume, independent of pressure and temperature. In the gas phase it is a function of a random thermal momentum transfer which is dependent on temperature (this thermal momentum is related to the collision rate). The viscosity of a fluid is given by:

$$\mu = \frac{1}{B_\mu \left(\dfrac{V - V_o}{V_o} \right)} + \mu_G \left[1 - \left(\frac{0.5 V_c}{V} \right)^{2/3} \right] \qquad (2.12)$$

where μ_G is the dilute gas viscosity. The first term on the right hand side corresponds to the original viscosity model for liquids proposed by Hildebrand (1971). Equation 2.12 was fit to the experimental data presented in Figure 2.6.

The volume expansion concept proposed by Hildebrand (1971) has been used by other researchers to model the thermal conductivity of fluids. Chhabra *et al*. (1980) proposed a correlation for the thermal conductivity of liquid hydrocarbons based on volume expansion:

$$\frac{1}{\lambda} = \frac{1}{\lambda_o} + \gamma \left(\frac{V - V_o}{V_o} \right) \qquad (2.13)$$

where λ_o and γ are fluid-specific parameters independent of temperature. The modelling of thermal conductivity has not received as much attention as that of viscosity because there are few data available in the literature.

Despite of the success of the Hildebrand (1971) approach for modelling viscosity of hydrocarbons, some problems have been reported. Eicher and Zwolinsky (1972) found that the model does not fit the data of some hydrocarbons including *n*-hexane, *n*-decane, *n*-heptadecane over a wide range of temperatures. The authors state that viscosity is not only a function of volume expansion but also dependent on other thermodynamic variables.

2.4.4 Viscosity and Thermal Conductivity in the Critical Region

Large density changes in the vicinity of the critical point cause a sudden increment in the value of viscosity and thermal conductivity (Lee, 1987; Perkins and Sengers, 2013;). This anomalous behavior known as critical enhancement has been reported for many hydrocarbons and non-hydrocarbons (Lee, 1987; Neindre *et al*., 1991; Poling *et al*., 2001). Figure 2.7 shows the critical enhancement of viscosity and thermal conductivity of carbon dioxide.
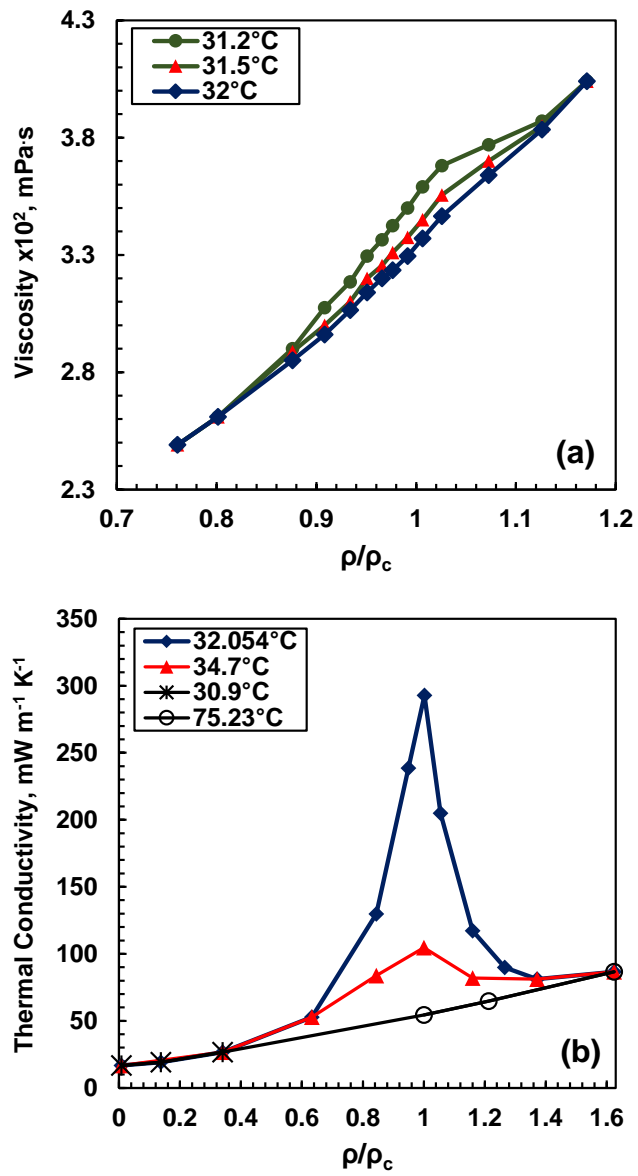
Figure 2.7. Transport properties of carbon dioxide near the critical point (T_c= 31°C, ρ_c= 468 kg/m^3): a) viscosity (data from Naldrett and Maass, 1940), b) thermal conductivity (data from Guildner, 1958).

The critical enhancement of viscosity is observed over a narrow range of densities and temperatures around the critical point. The critical enhancement of thermal conductivity is larger and occurs over a broader region (Figure 2.7). These trends have been observed for several hydrocarbons (Poling *et al*., 2001). The effect of critical enhancement on viscosity is so small that it is neglected for many engineering applications (Sengers and Watson, 1986). An accurate mathematical description of the critical enhancement of thermal conductivity has not been yet developed; however, statistical mechanics and corresponding states have been used to model the critical enhancement for carbon dioxide, nitrogen, and water (Sengers, 1985).

2.5 Viscosity and Thermal Conductivity Models for Crude Oils

A summary of different viscosity and thermal conductivity models proposed for crude oils and petroleum fluids is presented in this section, beginning with a description of viscosity models used in reservoir simulators followed by a summary of different viscosity models for distillation cuts and mixing rules for diluted oils and cuts. Viscosity models for pure hydrocarbons and their mixtures are not presented here. Detailed summaries of those models were provided by Mehrotra *et al*. (1996) , Poling *et al*. (2001) and Motahhari (2013). Finally, a summary of different thermal conductivity models for pure hydrocarbons and petroleum fluids is presented.

2.5.1 Crude Oil Viscosity Models

There are three full-phase viscosity models suitable for use in crude oil reservoir simulators: Corresponding States (CS), Friction Theory (*f*-theory), and the Expanded Fluid (EF) models. The former two are presented here while the EF model is reviewed in detail in Chapter 4 because it is used in this thesis. These models are semi-theoretical approaches that encompass the viscosity of crude oils in the gas, liquid, and supercritical phases. They have also been extended to predict the viscosity of crude oils characterized based on distillation or gas chromatographic (GC) assays.

2.5.1.1 Corresponding States

The Corresponding States (CS) principle is that the reduced properties of all fluids map similarly with respect to the reduced temperature and pressure (Pedersen *et al*., 1984). A reduced property is the value of the property at a given temperature and pressure divided by the value of the property at the critical point. If the reduced properties of fluids correspond to another, a reference model can be created that maps out the reduced property relationships. The properties of any fluid can be determined from the reference model if the fluid critical properties are known.

In this case, the reduced viscosity can be expressed as function of reduced density and temperature:

$$\mu_r(T,P) = f(T_r, \rho_r) \qquad (2.14)$$

where the subscript "*r*" refers to the reduced property. The function "*f*" is determined for only one of the substances in the group known as reference substance for which viscosity data are available. The viscosity of another member of the group is calculated as follows:

$$\mu_i(\rho,T) = \mu_o \left[\rho\left(\frac{\rho_{C,o}}{\rho_{C,i}}\right), T\left(\frac{T_{C,o}}{T_{C,i}}\right) \right] \left(\frac{M_i}{M_o}\right)^{1/2} \left(\frac{\rho_{C,i}}{\rho_{C,o}}\right)^{2/3} \left(\frac{T_{C,i}}{T_{C,o}}\right)^{1/2} \qquad (2.15)$$

where subscripts "*i*" and "*o*" refer to any substance in the group and the reference substance, respectively. Subscript "*c*" refers to the property evaluated at the critical point.

The fundamental idea behind CS is that the intermolecular potential energy of all the substances is described by a unique function of the intermolecular separation (Hanley, 1976). However, this assumption is only obeyed by monoatomic non-polar molecules and its application to complex hydrocarbon molecules is not possible. Hanley (1976) modified the original formulation of CS (Equation 2.14) in order to predict the viscosity of pure hydrocarbons and mixtures. Two correction terms, called shape factors, were introduced to account for the non-correspondence of hydrocarbons. The shape factors are a function of the acentric factor, density, and temperature. Using this modified version of CS, the

viscosity of ethane, propane, butane, carbon dioxide and nitrogen were predicted using methane as reference fluid; however, large deviations were observed at high densities.

Ely and Hanley (1981) used CS to predict the viscosity of pure hydrocarbons including alkanes, alkenes, aromatics and naphthenes, and their binary mixtures. The pure components ranged from carbon numbers C1 to C20. Methane was selected as the reference fluid and shape factors as a function of acentric factor and reduced temperature and volume were included. The calculation scheme included an iterative process for the calculation of the shape factors that depends on the reduced volume, which itself is found by the CS model. To extend the model to mixtures, the authors assumed that a mixture behaves as a hypothetical pure fluid, which follows the CS principle. A set of mixing rules was reported to calculate the mixture parameters from those of the pure components. The mixing rules include binary interaction parameters, but they were set to zero. The proposed method predicted the viscosity of pure hydrocarbons and binary mixtures within 8%. Baltatu (1982) extended the model to heavier hydrocarbons and distillation cuts by introducing aromaticity corrections or mass shape factors.

Pedersen *et al.* (1984) extended the CS model to predict the viscosity of crude oils characterized into pseudo-components defined from GC assay data. The method uses reduced pressure as one of the coordinates rather than reduced density. A rotational coupling coefficient was introduced to correct the deviations from the CS principle rather than shape factors. This rotational coupling coefficient has the advantage of being easy to correlate to the reduced density. Methane was used as the reference fluid. A set of mixing rules for the mixture critical temperature and pressure, molecular weight and rotational coupling coefficient were reported. The method was tested not only in crude oils but also on pure hydrocarbons and binary mixtures. The advantage of this approach compared to that of Ely and Hanley (1981) is that the calculation of the rotational coupling coefficient does not demand a complex iterative process as that to estimate shape factors. This method predicted the viscosity of the fluids in the test dataset within 10%; however, its predictive capabilities are low for heavy oil systems.

Pedersen and Fredenslund (1987) proposed a modification to the original Pedersen model to improve its performance for heavy oils. The reason for the poor performance of the model for heavy oil systems is that methane, which is used as reference fluid, is often solid at the corresponding reduced temperature and pressure. New expressions for the rotational coupling coefficient and the average molecular weight were proposed in order to extend the range of applicability of the model to reduced temperatures below 0.4 (freezing point of methane). The new expressions were developed using heavy oil distillation cut viscosity data. The viscosity of several pure hydrocarbons and heavy distillation cuts was predicted within 15% at reduced temperatures below 0.4. Deviations can be reduced by tuning the fluid molecular weight and rotational parameter. This model has been implemented in most commercial simulators (Schumberger, 2010; CMG, 2011).

The CS model has been extensively used to predict the viscosity of whole and diluted heavy oils and bitumen in a wide range of temperatures and pressures. Mehrotra and Svrcek (1987) used the Ely and Hanley (1981) version to predict the viscosity of four different Western Canada bitumen characterized into pseudo-components. The authors used 1,2,3,4,5,6,7,8-octahydrophenantrene as the reference fluid and the modified shape factors proposed by Johnson *et al.* (1987). However, although the results are considerably better than those estimated when methane was used as reference fluid, the model predictions are not accurate for viscosities below 200 mPa·s. Lindeloff *et al.* (2004) developed a reference function based on crude oil viscosity data in order to improve the Pedersen and Fredenslund (1987) version. The objective of this new reference function was to switch back to methane as the reference fluid at low reduced temperatures in order to improve the accuracy of predictions for heavy oils. The modified model was tested on a data base of 8 different heavy oils with API gravities below 10. The results show that the modified version performs better than the original one; however, tuning seems necessary in order to capture the actual behavior of viscosity versus pressure of the tested fluids.

2.5.1.2 Friction Theory

The underlying idea of the Friction Theory (*f*-Theory) model is that the viscosity of a fluid can be expressed as a dilute gas viscosity contribution and a residual viscosity contribution which arises from the friction between fluid layers (Quiñones-Cisneros *et al*., 2000):

$$\mu = \mu_G + \mu_F \tag{2.16}$$

where μ is the dynamic viscosity and subscripts "*G*" and "*F*" indicate the dilute gas and friction contributions, respectively. The dilute gas viscosity is easily calculated from the Chung *et al*. (1988) correlation whereas the residual viscosity is assumed to be a function of the repulsive and attractive van der Waals pressure terms:

$$\mu_F = \kappa_r P_r + \kappa_a P_a + \kappa_{rr} P_r^2 \tag{2.17}$$

Where P_r and P_a are the repulsive and attractive pressure terms, respectively, κ_r and κ_a are the linear repulsive and attractive friction coefficients, respectively, and κ_{rr} is the quadratic repulsive friction coefficient. The attractive and repulsive pressure terms can be calculated from a cubic equation of state (EoS) such as Peng-Robinson (PR) or Soave-Redich-Kwong (SRK). The three friction coefficients are fluid-specific and temperature dependent and are determined by fitting the model to experimental data. The temperature dependency of the parameters is captured by an exponential series requiring at least seven adjustable parameters. Note that value of the adjustable parameters depends on the EoS used to calculate the pressure terms. The model was also extended to mixtures by means of mass-based mixing rules for the three friction coefficients along with the customary mixing rules for the EoS parameters. The results show that the model fits viscosity data of alkanes from methane to decane within 10% and predicts the viscosity of binary mixtures within 10%. The model can be tuned for mixtures by adjusting its average molecular weight.

Due to the high number of parameters required for the calculation of the three friction coefficients, a version of the *f*-Theory with only one adjustable parameter has been proposed (Quiñones-Cisneros *et al*., 2001a). This version was developed by coupling the *f*-Theory with the Corresponding States principle in order to produce generalized correlations for the three model parameters. Each parameter is calculated as a departure from a critical coefficient. The critical coefficients as well as the generalized departure

functions were determined by fitting the model to data of *n*-alkanes from methane to *n*-octadecane. The only input of this version is a characteristic critical viscosity value. This version of the *f*-theory was tested on *n*-alkanes, isoparaffins, aromatics, cyclics, nitrogen and carbon dioxide.

The one-parameter *f*-Theory was extended to predict the viscosity of crude oils characterized into pseudo-components. The pseudo-components were defined from GC assay data with a chi-squared (χ^2) probability distribution applied to the C11+ heavy fraction (Quiñones-Cisneros *et al.*, 2003). The critical viscosity values of the pseudo-components were found to be proportional to the molecular weight and critical pressure and temperature. The proportionality factor was determined by tuning the model to viscosity data. This version of the model has been successfully tested on natural gas (Zéberg-Mikkelsen *et al.*, 2002) and on dead and live crude oils with molecular weight lower than 200 g/mol (Quiñones-Cisneros *et al.*, 2001b). An additional tuning parameter is required for crude oils with molecular weights higher than 200 g/mol in order to correct the repulsive and attractive pressure terms calculated from the EoS (Quiñones-Cisneros *et al.*, 2004). This two-parameter version of the *f*-Theory successfully fitted the viscosity data above the saturation pressure of heavy oils with molecular weights up to 443 g/mol within experimental error and provided predictions of gas and liquid viscosity at pressures below saturation (Quinonez-Cisneros *et al.*, 2005).

2.5.2 Viscosity Models for Crude Oil Distillation Cuts

This group includes empirical and semi-theoretical models to predict viscosity at atmospheric pressure of distillation cuts either at reference temperatures or over a range of temperatures. The accepted reference temperatures in the petroleum industry are 37.7°C (100°F) and 98.8°C (210°F) (Twu, 1985). When viscosity is predicted at those two temperatures, interpolation is necessary for estimation at different temperatures. Twu, (1985) and Altgelt and Boduszynski (1994) recommend the ASTM interpolation method based on linear relation between the double natural logarithm of viscosity and the natural logarithm of the absolute temperature developed by Wright (1969). Since these methods

are only applicable to atmospheric pressure, another procedure would be required to determine the viscosity at higher pressures.

2.5.2.1 The Watson Charts

Watson and co-workers (1935) obtained several distillation cuts from different American conventional oils. The kinematic viscosity of the cuts at 37.7°C (100°F), 50°C (122°F) and 98.8°C (210°F) were measured at atmospheric pressure. Other properties of the cuts such as boiling point, API gravity were also measured. The data was used to create charts representing the kinematic viscosity as function of normal boiling point, API gravity and a characterization factor defined as:

$$K = \frac{\sqrt[3]{1.8T_b}}{SG} \tag{2.18}$$

where K is the known as the Watson characterization factor, T_b and SG are the normal boiling point in K and specific gravity at 15.6°C, respectively. The API Technical Data Book (1978) replotted the Watson charts as a nomographs. The Watson charts are accepted as industry standards for estimating viscosity of distillation cuts obtained from light to moderate heavy crude oils (Twu, 1986); however, they are not useful for computer applications because the method is entirely graphic.

2.5.2.2 The Abbott Correlations

Abbott *et al*. (1971) developed analytical expressions of the API nomograph for the prediction of kinematic viscosities of distillation cuts at 37.7°C and 98.8°C. The correlations use the Watson characterization factor and API gravity as inputs and agree with the Watson charts quite well except at high viscosities (Twu, 1986). The Abbott correlations are given by:

$$\log(v_{37.7°C}) = 4.3971 - 1.94733K + 0.127690K^2 + 3.26290 \times 10^{-4}(API)^2 - 1.18248 \times 10^{-2}K(API)$$
$$+ \frac{0.171617K^2 + 10.9943(API) + 9.50633 \times 10^{-2}(API)^2 - 0.860218K(API)}{(API) + 50.3642 - 4.78231K}$$

$$\tag{2.19}$$

$$\log(\nu_{98.8°C}) = -0.463634 - 0.166532(API) + 5.13447 \times 10^{-4}(API)^2 - 8.48995 \times 10^{-3}K(API) +$$
$$\frac{8.03250 \times 10^{-2}K + 1.24899(API) + 0.197680(API)^2}{(API) + 26.786 - 2.6296K}$$

<div align="right">(2.20)</div>

where ν is the kinematic viscosity in cSt (mm^2/s). The authors recommend that the correlations not be used for $K \leq 10$ and $API \leq 0$ where scarcity of the data is reflected in occasional erratic behavior of the correlations. Riazi (2005) points out that the Abbott correlations cannot be applied to heavy oils and should be used with special care when $K > 12.5$ and $API > 80$. Twu (1985) found singularities in Equations 2.19 and 2.20 for some combinations of API and K. The average error of the Abbott correlations is in the range of 15 to 20% when applied to distillation cuts with kinematic viscosities in the range of 0.5 to 20 cSt (Riazi, 2005).

2.5.2.3 The Twu Correlations

Twu (1985) developed analytical expressions to predict the kinematic viscosity of distillation cuts at two temperatures, 37.7°C and 98.8°C, from their normal boiling point and specific gravity using a departure function from n-alkane reference fluids. The kinematic viscosity of the reference fluids is calculated according to:

$$\ln(\nu_{98.8°C} + 1.5) = 4.73227 - 27.0975\alpha + 49.4491\alpha^2 - 50.4706\alpha^4 \qquad (2.21)$$

$$\ln(\nu^o_{37.7°C}) = 0.801621 + 1.37179\ln(\nu^o_{98.8°C}) \qquad (2.22)$$

where

$$\alpha = 1 - \frac{T_b}{T_c^o} \qquad (2.23)$$

and

$$T_c^o = T_b\left(0.533272 + 0.191017 \times 10^{-3}T_b + 0.779681 \times 10^{-7}T_b^2 - 0.284376 \times 10^{-10}T_b^3 + \frac{0.959468 \times 10^{28}}{T_b^{13}}\right)^{-1}$$

<div align="right">(2.24)</div>

where T_b is the normal boiling point in °R and the superscript 'o' denotes the value of the property for the n-alkane reference fluids.

The correlations for kinematic viscosities at 98.8°C and 37.7°C are given by:

$$\ln\left(v_{98.8°C}+\frac{450}{T_b}\right)=\ln\left(v_{98.8°C}^o+\frac{450}{T_b}\right)\left(\frac{1+2f_2}{1-2f_2}\right)^2 \tag{2.25}$$

$$f_2=|x|\Delta SG-21.1141\frac{\Delta SG^2}{T_b^{0.5}} \tag{2.26}$$

$$|x|=\left|1.99873-\frac{56.7394}{T_b^{0.5}}\right| \tag{2.27}$$

$$\ln\left(v_{37.7°C}+\frac{450}{T_b}\right)=\ln\left(v_{37.7°C}^o+\frac{450}{T_b}\right)\left(\frac{1+2f_1}{1-2f_1}\right)^2 \tag{2.28}$$

$$f_1=1.33932|x|\Delta SG+21.1141\frac{\Delta SG^2}{T_b^{0.5}} \tag{2.29}$$

where ΔSG is the difference in specific gravity between the component or distillation cut and the reference n-alkane. For distillation cuts, ΔSG is defined as:

$$\Delta SG=SG-SG^o \tag{2.30}$$

for pure components, ΔSG is defined as:

$$\Delta SG=\gamma\left(\frac{1+2h}{1-2h}\right)^2 \tag{2.31}$$

$$h=\left(-21.6364+\frac{844.687}{T_b^{0.5}}\right)\gamma-\left(458.199-\frac{7573.00}{T_b^{0.5}}\right)\gamma^2 \tag{2.32}$$

$$\gamma=(SG-SG^o)(1.49546-SG) \tag{2.33}$$

The specific gravity of the reference n-alkane is calculated as:

$$SG^o=0.843593-0.128624\alpha-3.36159\alpha^3-13749.5\alpha^{12} \tag{2.34}$$

Twu tested his correlations on a dataset containing several distillation cuts and pure hydrocarbons with specific gravity ranging from 0.63 to 1.11 for boiling points ranging from 50°C to 714°C, and kinematic viscosity (at 37.7°C) ranging from 0.33 to 1750 cSt. The calculated average deviations for distillation cuts and pure hydrocarbons were 6.8% and 8.5%, respectively. Altgelt and Boduszynski (1994) used the Twu correlations to predict the kinematic viscosity at 37.7°C and 98.8°C of 20 distillation cuts obtained from

3 American, 1 Mexican, and 1 Arabian heavy oils. The viscosities of the cuts were predicted within ±100% except for kinematic viscosities higher than 200 cSt for which deviations were high.

2.5.2.4 API Correlations

The American Petroleum Institute (API) developed a set of correlations to predict the kinematic viscosity of distillation cuts and liquid coals at 37.7°C and 98.8°C (API, 1997) using normal boiling point and Watson factor as inputs. The kinematic viscosity in cSt at 37.7°C is calculated as follows:

$$\nu_{37.7°C} = \nu_1 + \nu_2 \tag{2.35}$$

$$\log(\nu_1) = -1.35579 + 8.16059 \times 10^{-4} T_b + 8.38505 \times 10^{-7} T_b^2 \tag{2.36}$$

$$\log(\nu_2) + A_1 + A_2 K \tag{2.37}$$

$$A_1 = 34.9310 - 8.84387 \times 10^{-2} T_b + 6.73513 \times 10^{-5} T_b^2 - 1.01394 \times 10^{-8} T_b^3 \tag{2.38}$$

$$A_2 = -2.92649 + 6.98405 \times 10^{-3} T_b - 5.09947 \times 10^{-6} T_b^2 + 7.49378 \times 10^{-10} T_b^3 \tag{2.39}$$

The kinematic viscosity in cSt at 98.8°C is given by:

$$\log(\nu_{98.8°C}) = -1.92353 + 2.41071 \times 10^{-4} T_b + 0.511300 \log(T_b \nu_{37.7°C}) \tag{2.40}$$

where the normal boiling point is in °R. The API correlations are only valid for fluids with boiling points between 65°C and 650°C and API gravities between 0 and 75. Equations 2.35 to 2.40 predicted the viscosity of over 7000 data points with an average error of 14% with better results for light to intermediate cuts than for heavy cuts. The lowest deviations were found for distillation cuts with API gravity higher than 30 (API, 1997).

2.5.2.5 The Beg Correlation

Beg *et al.* (1988) developed a correlation for the prediction of kinematic viscosity versus temperature for distillation cuts. A database of 12 distillation cuts obtained from 4 different Arabian oils were used as a development dataset. The API gravity of the oils ranged between 28 and 36 and the cut API gravity ranged between 25 and 56. The kinematic viscosity is calculated as:

$$v = \left[-0.0339(API)^{0.188} + 0.241\left(\frac{T_b}{B}\right)\right]\exp\left(\frac{B}{T}\right) \tag{2.41}$$

$$B = \exp(5.471 + 0.00342T_b) \tag{2.42}$$

where the normal boiling point, T_b, and the temperature, T, are in K. The correlation predicted the viscosity of 34 distillation cuts from 13 different oils with an average deviation of 7.4%. The API gravity of these cuts was between 30 and 60.

2.5.2.6 The Dutt Correlation

Dutt (1990) used an "Antoine-type" equation to correlate the viscosity versus temperature of distillation cuts at atmospheric pressure. The only input of the correlation is the boiling point temperature in °C. The kinematic viscosity of the cut is given by:

$$\ln(v) = -3.0171 + \frac{44278 + 1.6452T_b}{T + (239 - 0.19T_b)} \tag{2.43}$$

where T and T_b are in °C. Equation 2.43 predictions were tested against 250 viscosity data points from distillation cuts covering a boiling point range from 90 to 400°C and a kinematic viscosity range from 0.4 to 6 cSt. The average absolute deviation was 6%.

2.5.2.7 The Miadonye Correlation

Miadonye *et al.* (1993) developed a correlation to predict the kinematic viscosity of distillation cuts obtained from American conventional oils in a wide range of temperatures at atmospheric pressure. It requires a single measured viscosity data point at 37.7°C at atmospheric pressure as input. The kinematic viscosity in cSt is calculated as follows:

$$\log(v) = \frac{b}{\left(1 + \dfrac{T - 37.78}{310.93}\right)^s} + C \tag{2.44}$$

where

$$b = \left[\log(v_{37.7°C})\right] - C \tag{2.45}$$

$$s = 0.28008b + 1.6180 \tag{2.46}$$

$$C = -0.86960 \tag{2.47}$$

where $V_{37.7°C}$ and T are the measured kinematic viscosity data point and the temperature in °C. The authors found that kinematic viscosities are predicted within 1% for distillation cuts with viscosities below 3 cSt.

2.5.3 Mixing Rules for Crude Oils Blends

Different mixing rules have been proposed to predict the liquid viscosity of diluted crude oils and crude oil blends. The general form of viscosity mixing rules can be written as:

$$f(\mu_{mix}) = \sum W_i f(\mu_i) \qquad (2.48)$$

where the subscripts "*mix*" and "*i*" indicate the mixture and component "*i*" respectively; $f(\mu_{mix})$ and $f(\mu_i)$ are functions of the dynamic or kinematic viscosity, and *W* is a weight factor. The weight factor can be simply the molar, mass or volume fraction of the component or a more elaborate function of the composition. Detailed summaries of viscosity mixing rules for pure hydrocarbons and petroleum fluids are provided by Poling *et al*. (2001), Viswanath *et al.* (2007), Centeno *et al*. (2011) and Sutton and Bergman (2012). A summary of different mixing rules used in petroleum applications is presented in Table 2.1.

Table 2.1. Different mixing rules used in petroleum applications. The symbol *I* stands for viscosity blending index.

Method	Mixing Rule	Eq.
Arrhenius (1887)	$\ln \mu_{mix} = \sum X_i \ln(\mu_i),$ X can be volume, molar or mass fraction	2.49
Bingham, (1914)	$\mu_{mix}^{-1} = \sum \phi_i \mu_i^{-1}$	2.50
Kendall and Monroe (1917)	$\mu_{mix}^{1/3} = \sum x_i \mu_i^{1/3}$	2.51
Double-Log (Centeno, 2011)	$\log[\log(\mu_{mix}+1)] = \sum w_i \log[\log(\mu_i+1)]$	2.52
Power Law (Barrufet, 2003)	$\mu^n = \sum w_i \mu_i^n$ *n* is an empirical exponent	2.53
Linear (Centeno, 2011)	$\mu_{mix} = \sum x_i \mu_i$	2.54

Table 2.1 Cont'd. Different mixing rules used in petroleum applications. The symbol I stands for viscosity blending index.

Method	Mixing Rule	Eq.
Grunberg-Nissan (1949)	$\ln \mu_{mix} = \sum_i x_i \ln \mu_i + 0.5 \sum_i \sum_j x_i x_j G_{ij}$ G_{ij} is a binary interaction parameter	2.55
Cragoe (1933)	$I_{cr,mix} = \sum w_i I_{cr,i}$, where $I_{cr} = \dfrac{1000\ln(20)}{\ln\left(\dfrac{\mu}{0.0005}\right)}$	2.56
Shu (1984)	$\ln \mu_{mix} = a_1 \ln(\mu_1) + a_2 \ln(\mu_2)$ $a_1 = \dfrac{\alpha\phi_1}{\alpha\phi_1 + \phi_2}$, $a_2 = 1 - a_1$ $\alpha = \dfrac{17.04(\rho_1 - \rho_2)^{0.5237}\rho^{3.2745}\rho^{1.6316}}{\ln\left(\dfrac{\mu_1}{\mu_2}\right)}$, where $\rho_1 > \rho_2$	2.57
Barrufet (2003)	This method updates Shu as follows: $\alpha = 0.35242695 x_{light}^{-0.71154}$ x_{light} is the mole fraction of the lighter component	2.58
(A. K. Mehrotra, 1990)	$\log(\mu_{mix} + 0.7) = \sum\left[x_i\left(\dfrac{M_i}{M_{mix}}\right)^{0.5}\right]\log(\mu_i + 0.7)$	2.59
Refutas (Al-Besharah,1987)	$I_{R,mix} = \sum w_i I_{R,i}$ where $I_R = 14.534\ln[\ln(\nu_i + 0.8)] + 10.975$	2.60
Chevron (Baird, 1989)	$I_C = \sum \phi_i I_{C,i}$ where $I_C = \dfrac{\ln(\nu_i)}{\ln(1000\nu_i)}$	2.61

The lack of a generalized theoretical foundation that allow the prediction of viscosity of mixtures has led to the development of numerous mixing rules entirely based on empirical observations. Different mixing rules have been developed for different types of mixtures.

The simplest mixing rules (Equations 2.49 to 2.54) are intended for mixtures of components of similar molecular weight from the same chemical family (symmetric mixtures). As differences between mixture components grow higher (asymmetric mixtures), the prediction of mixture viscosity becomes challenging and consequently more complex mixing rules must be used (Equations 2.55 to 2.61). Equations 2.56 to 2.61 have been developed specifically to model the viscosity of diluted and blended crude oils. However, those mixing rules do not produce accurate results when used to predict the viscosity of diluted heavy oils and bitumen and their blends (Centeno *et al*., 2011; Shu, 1984).

Several researchers have evaluated and compared the performance of different mixing rules for whole and diluted heavy oils. Argillier *et al*. (2005) recommends the Shu mixing rule (Equation 2.57) to predict the viscosity of Venezuelan heavy oils diluted with naphtha. Barrufet *et al*. (2003) developed a new expression for the parameter *α* in the Shu mixing rule (Equation 2.58) to improve its performance when used to predict the viscosity of heavy oil diluted with high molecular weight alkanes. Nourozieh *et al*. (2013), Kariznovi *et al*. (2013) and Guan *et al*. (2013) tested the Power Law (Equation 2.53), Arrhenius (Equation 2.49), Cragoe (Equation 2.56) and Shu (Equation 2.57) mixing rules to predict the viscosity of Athabasca bitumen diluted with high molecular weight alkanes and aromatic solvents. The authors recommended the Arrhenius mixing rule for prediction purposes; however, the best results are found when the Power Law mixing rule is fitted to the data (note that the parameter *n* is a tuning parameter). Wen and Kantzas (2004) reported that the Shu mixing rule (Equation 2.57) produced more accurate results than the Cragoe mixing rule (Equation 2.56) when tested on four different Western Canada bitumen diluted with paraffinic and aromatic solvents. Mago *et al*. (2005) tested the Arrhenius and Power law mixing rule to predict the viscosity of a pseudo-component characterized Venezuelan heavy oil. The viscosity of the fluid was used as input for simulation of a cyclic steam stimulation process. This study concluded that both mixing rules do not describe the change of oil viscosity with temperature appropriately, which impacts the accuracy of simulation results. Finally,

Yarranton *et al*. (2013) and Centeno *et al*. (2011) recommend to use the double log mixing rule (Equation 2.52) for diluted heavy oils.

An additional term has been added to some mixing rules in order to capture the non-ideality of the mixing process. This term is usually a function of the composition and a viscosity binary interaction parameter which can be adjusted to match the prediction to the measured data as in the case of the Grunberg-Nissan mixing rule (Equation 2.55). The value of viscosity binary interaction parameters depends on the mixing rule, temperature, and pressure, but is independent of composition (Viswanath *et al*., 2007). However, in order to make the mixing rule totally predictive, correlations for the interaction parameters must be developed. Poling *et al.*(2001) presented an approach to predict Grunberg-Nissan interaction parameters based on group contribution. The method has been tested on pure hydrocarbon binaries but not on crude oil systems. Mehrotra (1990) introduced a non-ideal term in Equation 2.59 and correlated interaction parameters for Cold Lake bitumen distillation cuts. The mixing rules as well as the correlated parameters were tested on the viscosity of Cold Lake bitumen diluted with toluene. The bitumen was represented with five pseudo-components. The viscosity of the mixtures was predicted with average deviation of 5%.

2.5.4 Thermal Conductivity Models for Petroleum Fluids

The great majority of thermal conductivity models proposed for petroleum fluids are only intended for the liquid phase. Only the corresponding states model is suitable for gas and liquid phases.

2.5.4.1 Corresponding States

The corresponding states (CS) principle has also been extended to predict the thermal conductivity of pure hydrocarbons, distillation cuts, and crude oils characterized into pseudo-components. According to CS, the thermal conductivity of a substance "i" is related to that of a reference substance as follows (Hanley, 1976):

$$\lambda_i(\rho, T) = \lambda_o \left[\rho \left(\frac{\rho_{C,o}}{\rho_{C,i}} \right), T \left(\frac{T_{C,o}}{T_{C,i}} \right) \right] \left(\frac{M_i}{M_o} \right)^{1/2} \left(\frac{\rho_{C,i}}{\rho_{C,o}} \right)^{2/3} \left(\frac{T_{C,i}}{T_{C,o}} \right)^{1/2} \qquad (2.62)$$

where subscripts "*i*" and "*o*" indicate the substance under study and the reference substance, respectively. The similarity between the expressions for the viscosity and thermal conductivity (Equations 2.15 and 2.62, respectively) is not surprising considering that according the CS principle both properties vary consistently in relation to the critical point.

Hanley (1976) predicted the thermal conductivity of ethane, propane, butane, nitrogen, and carbon dioxide using methane as the reference fluid. Shape factors were introduced to correct the deviations from the CS principle. The author points out that the results are preliminary because the CS principle does not take into account the contribution of the internal degrees of freedom to the thermal conductivity (recall that thermal conductivity is the result of a translational and internal degrees of freedom contributions). Ely and Hanley (1983) proposed that the translational contribution to the thermal conductivity can be calculated from the CS model whereas the degrees of freedom contribution can be calculated from the Eucken correlation for polyatomic gases:

$$\frac{\lambda'' M}{\mu_G} = 1.32 \left(C_{pG} - 2.5R \right) \qquad (2.63)$$

where λ'' is the internal degrees of freedom contribution to thermal conductivity and C_{pG} is the ideal gas isobaric heat capacity. A density and temperature dependent correction factor was introduced to take into account possible deviations of the translational thermal conductivity from the CS principle. This version of the model also uses the original shape factors proposed by Hanley (1976). The model was tested on a dataset containing alkanes, branched alkanes, alkenes, and aromatics. The model predicted the thermal conductivity within 15%; however, higher deviations were observed for heavy fluids and at conditions near the freezing point where the effect of density over the internal degrees of freedom might be important (Ely and Hanley, 1983). This version of the model was also extended to mixtures by means of mixing rules for the model parameters and for the internal degrees of freedom contribution to the thermal conductivity. Baltatu *et al*. (1985) successfully

45

tested this version of the CS model to predict the thermal conductivity of coal derived liquids and distillation cuts.

Christensen and Fredenslund (1980) proposed another calculation approach for the translational contribution to the thermal conductivity based on the CS states principle using methane as reference fluid. This approach uses pressure and a fluid-specific rotational coupling coefficient rather than density and shape factors used by Ely and Hanley (1983). The thermal conductivity contribution that arises from internal degrees of freedom is calculated as follows:

$$\lambda'' = d\frac{\mu_G C_v}{M}\left(1 + 0.053432\rho_r - 0.030182\rho_r^2 - 0.029725\rho_r^3\right) \qquad (2.64)$$

where C_v is the ideal gas isochoric heat capacity and ρ_r is the reduced density. The parameter d is an adjustable value found equal to 1.18653 after fitting the model to pure hydrocarbon data. The model predicts the thermal conductivity of methane, ethane, propane, butane, pentane, nitrogen, and carbon dioxide within 5% of experimental values. The authors state that the main source of error comes from Equation 2.64. Pedersen and Fredenslund (1987) propose a generalized correlation for the prediction of the rotational coupling coefficient using reduced density and molecular weight as inputs. They also report that the model predicts heavy oil distillation cuts thermal conductivity to within 20 %. Of experimental values.

2.5.4.2 The Linear Model

It has been shown experimentally that the thermal conductivity of liquid hydrocarbons is a linear function of temperature:

$$\lambda = C_1 - C_2 T \qquad (2.65)$$

where C_1 and C_2 are fluid-specific pressure dependent constants determined by fitting Equation 2.65 to experimental data. Riazi (2005) recommends Equation 2.65 for the modelling of the thermal conductivity of liquid hydrocarbons between the freezing and boiling point. The constants in Equation 2.65 can be calculated using the thermal conductivity at the freezing and boiling points reported for several hydrocarbons in the API

Technical Databook (1997). In the case of uncharacterized petroleum fractions, the API Technical Databook (1997) recommends to use C_1 and C_2 equal to 164 mW/m.°K and 0.1277 mW/m.K^2, respectively. For characterized fractions, C_1 and C_2 are calculated as a function of the normal boiling point in K, T_b, as $25.51T_b^{0.2904}$ mW/m.K and $0.01982\,T_b^{0.2904}$ mW/m.K^2, respectively. The Standard for Tubular Exchanger Manufacturer Association (TEMA, 1968) suggests C_1 and C_2 values of 140 mW/m.°C and 0.075 mW/m.(°C)^2 to predict the thermal conductivity of petroleum fluids at atmospheric pressure and temperatures from 20 to 525°C.

Other linear models analogous to Equation 2.65 have been proposed for the prediction of thermal conductivity of crude oils. Rastorguev and Grigor'ev (1968) proposed the following empirical relation based on experimental thermal conductivity data at atmospheric pressure obtained from 13 different Russian crude oils:

$$\lambda = \lambda_{To}\left[1 - \psi(T - T_o)\right] \tag{2.66}$$

where λ_{To} is the thermal conductivity at the reference temperature T_o and T is the temperature in °C. ψ is the temperature coefficient of thermal conductivity. The authors chose 30°C as the reference temperature and developed a correlation for $\lambda_{30°C}$ as a function of the paraffin content in the crude oil and another correlation for ψ as function of the density at 20°C. Grigor'ev and Svidchenko (1979) proposed generalized correlations for λ_{To} as a function of the freezing point of the crude oil and ψ as function the density at 20°C. The correlations are applicable to crude oils and petroleum liquids with molecular weights up to 400 g/mol. Jamieson *et al*. (1975), using a reference temperature of 60°C, developed two charts for the prediction of λ_{To} and ψ as a function of molecular weight and ring content, defined as the combined content of naphthenics and aromatics in the petroleum sample. Another chart was supplied for the prediction of the ring content as a function of molecular weight and aniline point.

2.5.4.3 Density Based Thermal Conductivity Correlations

In general, the thermal conductivity of liquid hydrocarbons, distillation cuts and crude oils decreases with density at constant pressure. This empirical observation has been used in

several studies in order to propose correlations relating both properties. Vargaftik (1949) proposed the following correlation applicable to pure hydrocarbons:

$$\lambda = K\rho^{4/3} \qquad (2.67)$$

where K is a fluid-specific constant. Efendiev (1973) used Equation 2.67 to predict the thermal conductivity of crude oils and petroleum fluids. The constant K was estimated using measured density and thermal conductivity at a reference temperature and the density was estimated from a linear relation to temperature.

Bland and Davidson (1967) showed that experimental thermal conductivity of pure hydrocarbon mixtures, crude oils and distillation cuts can be correlated as:

$$\lambda = \frac{117}{SG}(1.000 - 0.00054T) \qquad (2.68)$$

where SG is the specific gravity and T is in °C. The authors also present a chart to predict the thermal conductivity of petroleum fluids as a function of temperature and API gravity. Another correlation that uses SG to predict thermal conductivity of petroleum fluids was proposed by Aboul-Seoud and Moharam (1999):

$$\lambda = 2540.312\left(\frac{SG}{T}\right)^{0.5} + 14.4485 \qquad (2.69)$$

where T is in K. This correlation predicts the thermal conductivity of distillation cuts with SG ranging between 0.731 and 1.00 with an average deviation of 3%.

2.5.5 Thermal Conductivity of Liquids at High Pressure

The effect of pressure on liquid thermal conductivity is negligible below 3.5 MPa (Poling *et al.*, 2001). The following expression is recommended by the API Technical Databook (1997) for higher pressures and reduce temperatures between 0.4 and 0.8:

$$\lambda_P = \lambda_{Po}\left(\frac{C_P}{C_{Po}}\right) \qquad (2.70)$$

where subscripts P and P_o indicates the property at pressure P and at a reference pressure, respectively. The constant C is calculated at P and P_o according to:

$$C = 17.77 + 0.065 P_r - 7.764 T_r - \frac{2.054 T_r^2}{\exp(0.2 P_r)} \tag{2.71}$$

Other expressions to account for the effect of pressure on thermal conductivity of liquids have been proposed and are presented elsewhere (Grigor'ev and Svidchenko, 1980).

2.5.6 Thermal Conductivity of Mixtures

2.5.6.1 Dilute Gas Mixtures

The kinetic theory of gases can be used to formulate mixing rules for the thermal conductivity of mixtures of mono-atomic gases at low density. However, the use of these mixing rules for mixtures of polyatomic gases leads to large deviations (Poling *et al*., 2001). Empirical mixing rules have been proposed for the prediction of the thermal conductivity of dilute gas mixtures. For mixtures of non-polar gases, the following empirical mixing rule has been proposed (Wassiljewa, 1904):

$$\lambda_{G,mix} = \sum_i^n \frac{y_i \lambda_{G,i}}{\sum_j^n A_{ij} y_i} \tag{2.72}$$

where the parameter A_{ij} is given by (Mason and Saxena, 1958):

$$A_{ij} = \frac{\left[1 + \left(\mu_{G,i}/\mu_{G,j} \right)^{1/2} \left(M_i/M_j \right)^{1/4} \right]^2}{\left[8 \left(1 + M_i/M_j \right) \right]^{1/2}} \tag{2.73}$$

A more complex expression for the calculation of the parameter A_{ij} has been proposed by Lindsay and Bromley (1950); however, the results obtained do not differ significantly from those obtained from Equation 2.73 (Poling *et al*., 2001). This mixing rule has been widely used to predict the thermal conductivity of dilute gas mixtures of pure hydrocarbons with pure component dilute gas viscosities and thermal conductivities calculated from Equations 2.5 and 2.6, respectively (Poling *et al*., 2001; Riazi, 2005). This mixing rule is recommended by the API Technical Databook (1997) with *Aij* calculated from the Lindsay and Bromley (1950) approach.

2.5.6.2 Liquid Mixtures

Several empirical mixing rules have been proposed in order to predict the thermal conductivity of mixtures of liquid hydrocarbons. The simplest is a linear mixing rule proposed by Wada *et al*. (1985) for mixtures of *n*-alkanes:

$$\lambda_{mix} = \sum w_i \lambda_i \qquad (2.74)$$

Equation 2.74 predicted the thermal conductivity of binary and ternary mixtures of *n*-heptane, *n*-undecane and *n*-hexadecane within 1.5% when experimental thermal conductivities of the mixture components were used.

A power law mixing rule has also been proposed for thermal conductivity of liquid mixtures in which the ratio of pure component thermal conductivities does not exceed two (Poling *et al*., 2001):

$$\lambda_{mix} = \left(\sum_i w_i \lambda^{-2} \right)^{-1/2} \qquad (2.75)$$

This mixing rule has been applied successfully to binary and ternary mixtures of hydrocarbons (Poling *et al*., 2001; Rowley *et al*., 1988).

Li (1976) developed the following mixing rule for liquid hydrocarbons at conditions far away from the critical point:

$$\lambda_{mix} = \sum_i \sum_j \phi_i \phi_j \lambda_{ij} \qquad (2.76)$$

$$\lambda_{ij} = 2 \left(\frac{1}{\lambda_i} + \frac{1}{\lambda_j} \right)^{-1} \qquad (2.77)$$

where ϕ is the volume fraction of the mixture components. This method is recommended by the API Technical Databook (1997) for mixtures of pure component liquid hydrocarbons and distillation cuts. The average error is approximately 5%. This method fails to predict any maximum or minimum thermal conductivity of a mixture as a function of composition (Li, 1976).

2.6 Summary

The fundamental similarity between the transfer of momentum and heat suggests that the same physical mechanism controls the change of viscosity and thermal conductivity of fluids across the phase diagram. However, the lack of a unified theory of transport properties has led to the development of dozens of different correlations for the modelling of transport properties of pure hydrocarbons, crude oils and distillation cuts. In this section, the discussion was focused on the modelling of viscosity and thermal conductivity of petroleum fluids in the single gas and liquid phases and across the phase diagram. The only approaches that incorporate unified methodology for the calculation of both transport properties are the Hildebrand (1971) molar volume expansion correlation and the Corresponding States (CS) model. However, the application of both approaches in reservoir and process simulators is challenging as the former is only applicable to low molecular weight liquid hydrocarbons and the latter produces poor results for heavy oils. Furthermore, for some applications that only require viscosity in the liquid phase far away from the critical point, the application of the CS model is computationally intensive.

CHAPTER THREE: EXPERIMENTAL METHODS

This chapter presents a description of the different experimental methods used in this thesis. A summary of the chemicals and crude oils samples is presented and the sample preparation techniques are explained. Then, the apparatus and techniques to measure density, viscosity, and thermal conductivity are presented. The development of reliable methodologies for the measurement of viscosity and thermal conductivity was a major component of this thesis.

3.1 Chemicals and Crude Oil Samples

A total of twelve dead oil samples were used in this study: WC-B-B1, WC-B-B2, WC-B-B3, WC-B-A1, WC-B-A2, WC-B-A3, US-HO-A1, MX-HO-A1, CO-B-B1, CO-B-A1, EU-HO-A1 and ME-CV-A1. WC, US, MX, CO, EU and ME correspond to the oil producing regions of Western Canada (WC), United States (US), Mexico (MX), Colombia (CO), Europe (EU) and Middle East (ME), respectively. B, HO and CV indicate bitumen, heavy oil or conventional oil, respectively; and the third term indicates the source reservoir and sample number.

Selected physical properties of the crude oil samples are summarized in Table 3.1. Spinning band distillation assays were available for all of the above oils except WC-B-B2 and WC-B-B3 (Sanchez-Lemus *et al*., 2014). The WC-B-B2 and WC-B-B3 samples were recovered from the same reservoir as WC-B-B1 but had different density, viscosity and asphaltene content. The distillation curve and other properties such as atomic hydrogen-to-carbon (H/C) ratio and molecular weight were assumed to be the same as the WC-B-B1 sample.

Deep vacuum distillation cuts from the oils WC-B-B1, WC-B-A1, US-HO-A1, MX-HO-A1, CO-B-B1 and CO-B-A1 were provided by Sanchez-Lemus *et al.* (2014) and details of the procedures used to obtain these cuts are provided in the same reference. Asphaltene samples were prepared in this study as described later.

Table 3.1. Specific gravity (SG), atomic hydrogen-to-carbon (H/C) ratio, molecular weight (M), viscosity at 20°C and atmospheric pressure, asphaltene content, and toluene insoluble (TI) content of samples measured in this study.

Sample	SG	H/C	M g/mol	Viscosity at 20°C, mPa·s	C5-Asph. wt%	TI wt%
WC-B-B1	1.012	1.473	558	89,200	17	0.63
WC-B-B2	1.018	1.473	558	437,000	21	1.27
WC-B-B3	1.020	1.473	558	150000	22	0.68
WC-B-A1	0.996	1.577	585	33,737	16	0.51
WC-B-A2	1.026	1.476	598	7,500,000	22	0.72
WC-B-A3	1.101	1.453	550	33,737	18	0.55
US-HO-A1	0.961	1.587	548	5,627	14	0.62
MX-HO-A1	0.976	1.624	652	831,600	21	0.81
CO-B-B1	0.992	1.473	577	106,500	22	0.74
CO-B-A1	1.106	1.440	603	2,800,000	27	1.00
EU-HO-A1	0.968	1.596	475	5,036	7	0.31
ME-CV-A1	0.872	1.756	475	18.1	3.8	0.03

The solvents used for the preparation of the diluted bitumen samples were ethane (purity of 99%), propane (purity of 99.5%), *n*-butane (purity of 99.5%), *n*-pentane (purity of 99.5%), *n*-heptane (purity of 99.5%), *n*-dodecane (purity of 99.5%), *n*-eicosane (purity of 99.5%), toluene (purity of 99.5%), cyclohexane (purity of 99%), and 1-methylnaphthalene (purity of 99%). Pressurized ethane, liquid propane, and liquid *n*-butane were purchased from Praxair Canada Inc. Liquid atmospheric *n*-pentane, *n*-heptane, *n*-dodecane, toluene and cyclohexane were obtained from VWR. Solid *n*-eicosane and liquid 1-methylnaphthalene were obtained from Sigma-Aldrich.

Certified viscosity standards S20, S30000 and N450000, purchased from Cannon Instruments, were used for the calibration of the cone and plate rheometer. High purity

n-pentane (purity of 99.5%), *n*-heptane (purity of 99.5%) and *n*-tetradecane (purity of 99.5%), toluene (purity of 99.5%) and deionized ultra-filtered water (obtained from Fisher Scientific Chemicals) were used for the calibration and accuracy check of the thermal conductivity apparatus. Technical grade acetone and toluene purchased from VWR were used for cleaning. Technical grade *n*-pentane (purity of 98%), also bought from VWR, was used for asphaltene precipitation. ACS grade 2-propanol and toluene purchased from VWR were used in the Karl Fischer apparatus.

3.2 Sample Preparation

3.2.1 *Water Content Determination*

When the water content in a crude oil sample was higher than 1 wt%, the sample had to be dewatered prior to any analysis. If water is not removed, the distillation assay, density, viscosity and thermal conductivity of the sample will be incorrect. The water content was determined using a Karl Fischer titrator (Metrohm 787KF Titrino). The titrant was Aqualine Complete^{TM} 5 from Fisher Scientific. The electrolyte solution was a mixture of 26 vol% 2-propanol and 74 vol% toluene (both dried using molecular sieves). Crude oil samples were diluted by mass with the electrolyte solution and shaken until dissolved. The water mass content in the sample was determined from a calibration curve of volume of titrant used versus water content. All of the samples had a water content below 1% except for CO-B-A1, US-HO-A1 and EU-HO-A1.

3.2.2 *Dewatering*

To remove the water from a bitumen, the sample was continuously sonicated in a bath set at 50°C for at least 48 hours in order to promote the coalescence of water droplets. Then, the sample was transferred into a separatory funnel also maintained at 50°C and left to settle until the water settled to the bottom of the funnel where it could be removed. Typically, one week was required for complete settling; that is, until no more water was observed at the bottom of the funnel. The temperature of the separatory funnel was controlled with a heating tape. The temperature was kept at 50°C in order to maximize the settling rate without a significant loss of volatile components. The final water content of

the sample was determined by Karl Fischer titration. All the samples had less than 1 wt% of water content after the dewatering process.

3.2.3 *Deasphalting Oil and Determination of Asphaltene and Solid Content*

Asphaltenes were precipitated from bitumen using a 40:1 ratio (mL/g) of *n*-pentane: bitumen. The mixture was sonicated in an ultrasonic bath for 60 min at room temperature and left to settle for 24 h. The supernatant was filtered through a 24 cm Whatman #2 filter paper (pore size 8μm) until approximately 20% of the solution remained in the beaker. A total of 10% of the original volume of solvent was added to the remaining asphaltenes in the beaker, and then the mixture was sonicated for 60 min and left to settle overnight for 8 h. The remaining mixture was filtered through the same filter paper. The filter cake was washed using 25 mL aliquots of *n*-pentane at least three times a day until the effluent from the filter was almost colorless and then dried for 8 days. All of the filtrate was placed in a rotary evaporator and the solvent was evaporated to recover the residual oil. The evaporation process was performed until the mass of the residue no longer changed with time. The final product of this process is termed maltenes. Note, if only some of the C5-asphaltenes were removed in the first step, the product is termed a (partially) deasphalted oil (DAO). The filter cake contains the asphaltenes and any co-precipitated material and is here termed asphaltene-solids. The asphaltene-solids content is the mass of the filter cake divided by the mass of the bitumen.

Material referred to as solids corresponds to mineral material, such as sand, clay, ash, and adsorbed organics that precipitates along with the asphaltenes (Mitchell and Speight, 1973). Solids were removed from the asphaltenes by dissolving the asphaltene-solids in toluene and centrifuging the mixture to separate out the solids, here termed toluene insolubles. A solution of asphaltenes-solids in toluene was prepared at 10 kg/m³ at room temperature. The mixture was sonicated in an ultrasonic bath for 20 minutes or until all of the material was dispersed. After 1 hour, the mixture was divided into centrifuge tubes and centrifuged at 4000 rpm for 6 minutes. The supernatant (solid-free asphaltene solution) was decanted into a beaker and allowed to evaporate until the mass no longer changed. The

residue in the centrifuge tubes was dried and weighed. The toluene insoluble content is the mass of residue divided by the original asphaltene-solid mass. The asphaltenes extracted with *n*-pentane and treated with toluene are termed here C5-asphaltenes. The C5-asphaltene and toluene insoluble (TI) content of the samples used in this study are summarized in Table 3.1.

3.2.4 *Preparation of Dilute Crude Oil Samples*

Mixtures of the dead bitumen and liquid solvents (*n*-pentane, *n*-heptane, toluene, cyclohexane and 1-methylnaphthalene) were prepared at ambient temperature and atmospheric pressure. A known mass of dead oil and solvent (between 20 and 350 g depending on the method for viscosity measurements and 200 g for thermal conductivity determinations) were placed in a beaker equipped with a lid and mixed continuously in a rotary mixer at 6 rpm until a homogenous mixture was observed. Aliquots were collected after every hour of mixing in order to measure the density of the mixture. The mixture was considered homogeneous when its density was no longer changing with mixing time, typically after 12 hours. Mixtures of *n*-eicosane, which is solid at room temperature, and dead bitumen were prepared at 50°C where the *n*-eicosane was a liquid. Once the mixture was homogeneous, its final mass was determined in order to recalculate the solvent concentration to take into account any evaporation (usually less than 1 wt%) which was assumed to be only from solvent losses.

Mixtures of the dead oil and gaseous solvents (ethane, propane and *n*-butane) were prepared using an in-house mixing apparatus (only viscosity and density was determined for these samples). Details of the apparatus and procedure are provided elsewhere (Motahhari *et al.*, 2011b). Briefly, this apparatus consists of a horizontal cylindrical vessel with two moving pistons on either sides of a perforated disk fixed in the middle of the vessel. To prepare each mixture, a known mass of the pressurized solvent (determined by direct measurement) was filled into the pre-evacuated volume of the cylinder. Then, the required mass of the bitumen to reach the intended composition of the mixture was injected into the cylinder. The bitumen and solvent were mixed by displacing the pistons back and forth forcing the sample to flow through the perforated plate for 2 to 3 days at 10 MPa and

50°C. A Quizix SP-5200 pump system with hydraulic oil as the working fluid was used to move the pistons. Temperature was controlled to within ±0.5 °C using heating tapes. The mixture was assumed to be completely mixed and equilibrated when there was no longer any pressure and volume change. The mixture was then displaced to the transfer vessel for the density and viscosity measurements.

3.2.5 *Density and Viscosity Measurements*

Viscosity was measured in two apparatuses: 1) a capillary viscometer with an in-line density meter; 2) a cone and plate rheometer. A second Anton Paar DMA 4500M oscillating U-tube density meter was used to determine the density of the samples tested with the cone and plate apparatus. At least 350 mL of sample are required to measure viscosity and density in the capillary viscometer and about 8 mL of sample are required for the cone and plate rheometer and the U-tube density meter. The amount of sample available was the determining factor in selecting the device to measure viscosity and density.

3.2.6 *Capillary Viscometer (CapVis)*

The capillary viscometer (CapVis) apparatus used in this thesis was designed, constructed and calibrated by Motahhari (2013). He also developed and validated a systematic procedure for the measurement of liquid viscosities. This device consists of two transfer vessels and two capillary tubes in a temperature controlled oven, Figure 3.1. The apparatus is also equipped with an Anton Paar DMA HPM density meter with an external Anton Paar mPDS 2000V3 evaluation unit. Hydraulic oil is used as the displacement fluid and pressure in the apparatus is controlled using a back pressure regulator (BPR) on the return line of the hydraulic oil. The set pressure of the regulator is maintained using compressed air and is monitored with a Bourdon pressure gauge with a precision of 0.05 MPa. The temperature of the air bath is controlled within ±0.05°C of the intended measurement temperature, except for the room temperature experiments. The room temperature varied within a range of ±0.25°C.

The inside diameter and approximate length of the capillary tubes are: 6.35 mm and 1 m, respectively, for Tube 1 and 3.1 mm and 12 m, respectively, for Tube 2. Each capillary

tube was calibrated over a temperature range of 20 to 175°C using Cannon Instruments certified viscosity standards. The density meter was calibrated using pure nitrogen and distilled water at temperature range of 20 to 175°C and pressures up to 10 MPa. The measured viscosity and density reproduced the calibration data, as well as *n*-heptane and toluene data from the literature, to within ±3% and ±0.5 kg/m³, respectively.

Density and viscosity measurements were taken simultaneously for each fluid at each test pressure and temperature. Prior to the measurements, the fluid was flowed back and forth through the apparatus to ensure homogeneity, which was confirmed when the density and pressure drop through capillary tubes were consistent for the entire displacement. To collect the required data for the viscosity measurement, the fluid was flowed from one vessel to other though one of the installed capillary tubes at 5 different fixed flow rates. Once the flow reached a steady state condition at each flow rate, the pressure difference between its inlet and outlet was recorded. The viscosity of the fluid was then calculated from the slope of the differential pressures versus flow rate and the calibration constant of the capillary tube. All of the data in this thesis followed linear trends consistent with Newtonian laminar flow.

To measure density, the flow rate through the capillary tube was set at 0.001 cm³/min to maintain the test pressure set by BPR throughout the apparatus. Once the flow reached a steady state condition, the density was measured. Measurements on the diluted bitumen samples were undertaken from room temperature up to 175°C in steps of 25°C. At each temperature, the data were collected at pressures well above the bubble point pressure of the fluid up to 10 MPa in steps of 2.5 MPa.
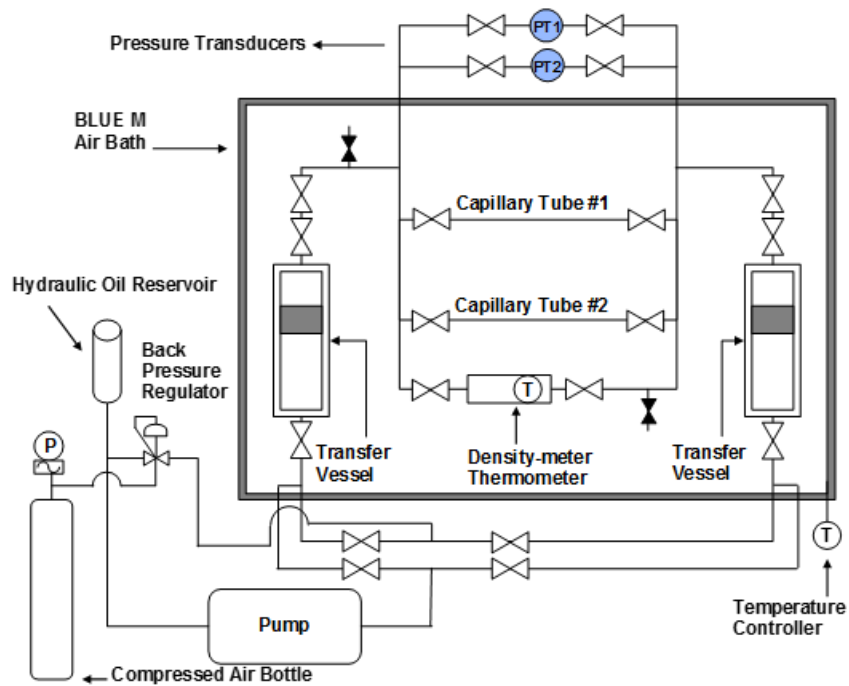
Figure 3.1. Schematic of the capillary viscometer and in-line density-meter apparatus.

3.2.7 *Cone and Plate Rheometer*

Two cone and plate rheometers were used in this study. The first one was a HAAKE Rotovisco 1 equipped with an external circulator for temperature control. The second was an Anton Paar MCR-52 cone and plate rheometer equipped with an Anton Paar Peltier P-PTD 200 mechanism for temperature control. Both apparatuses are only designed for liquids at atmospheric pressure with a temperature range between -10°C and 200°C and an upper viscosity limit of 400,000 mPa·s. The key elements of these devices are a stationary horizontal plate and a truncated cone vertically positioned on top of the plate as shown in Figure 3.2. The plate works as a sample holder and as a heating/cooling mechanism. The plate of the HAAKE Rotovisco 1 rheometer is in direct contact with the thermal fluid whereas that of the Anton Paar MCR-52 rheometer is equipped with aforementioned Peltier mechanism. Each rheometer is provided with a sensor and controller that maintains the temperature of the plate within ± 0.1°C. The cone works as the measurement element. Three different titanium cones with radius of 3, 2 and 1 cm and angle of 1° were used for

the HAAKE Rotovisco 1. A single stainless-steel cone with a radius of 2.5 cm and an angle of 1° was used for the Anton Paar MCR-52. The cone rotates at a constant angular velocity controlled by an electric motor. The vertical separation between the plate and the cone, known as the gap, is set in such a way that the imaginary tip of the cone just touches the plate (Figure 3.2).
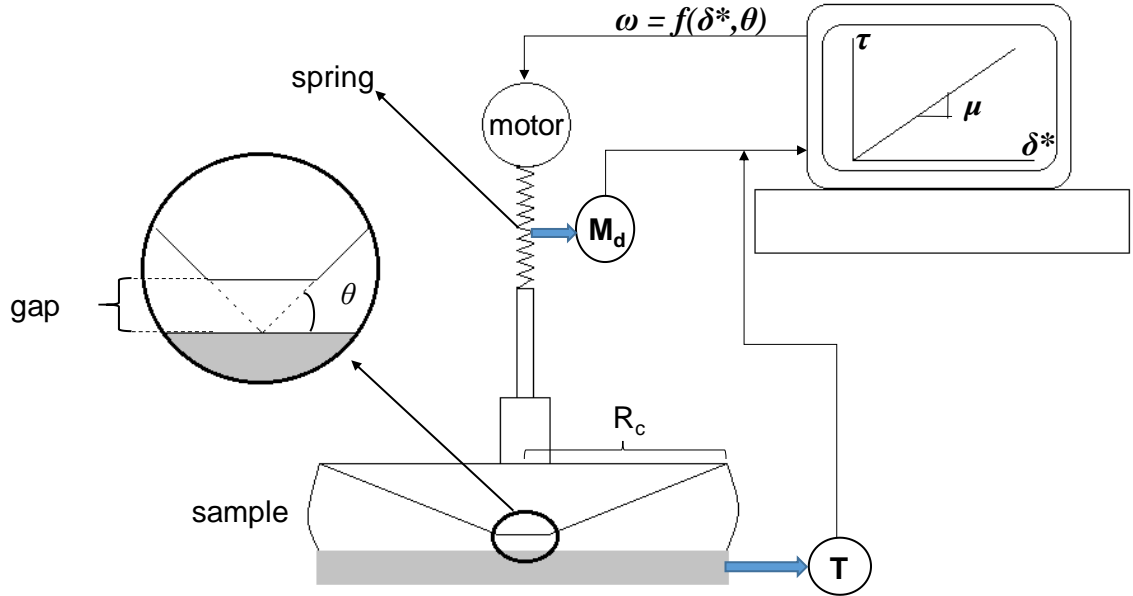
Figure 3.2. Schematics of the cone and plate rheometer used in this study.

The viscosity of a sample at a given temperature is not directly measured but determined from a shear stress versus shear rate curve. For Newtonian fluids, the relation between the two variables is linear and the viscosity is determined as the slope of a straight line which passes through the origin. The shear stress is proportional to the torque applied over the cone in order to maintain a constant angular velocity. The torque is measured as a function of the deformation (torsion) of a calibrated spring. The angular velocity is determined from the input value of shear rate and the angle of the cone according to (Schramm, 2000):

$$\omega = \theta \overset{*}{\delta} \tag{3.1}$$

where $\overset{*}{\delta}$ is the shear rate, ω is the angular velocity and θ is the cone angle.

60

Finally, the shear stress is calculated as (Schramm, 2000):

$$\tau_{z\theta} = \left(\frac{3}{2\pi R_c^3}\right) M_d \tag{3.2}$$

where $\tau_{z\theta}$ is the shear stress, R_c is the radius of the cone, M_d is the torque.

3.2.7.1 Viscosity Measurement

Viscosity at a given temperature at atmospheric pressure was determined from five different measurements of shear stress versus shear rate. Prior to any measurement, the apparatus was leveled by adjusting the screw feet. Then, the surfaces of the plate and the cone were cleaned using toluene. Next, the cone was attached to the apparatus and the gap was automatically adjusted to 0.1±0.001 mm by the rheometer. The temperature of the plate was then set to the desired value and left to stabilize. Once the temperature has reached the steady state value, the gap was re-adjusted in order to account for any thermal expansion of the cone. Note that the temperature is controlled only in the plate but some heat is transferred to the cone by radiation and convection. Then the cone was automatically lifted by the apparatus and the sample was placed on the plate. The cone was returned to the measurement position after visual confirmation that all air bubbles trapped in the sample were released. To ensure maximum accuracy, the space between the plate and the cone must be completely filled with sample. Any excess of sample that comes out of the edges of the cone must be trimmed using a spatula. Finally, the system was left to sit until the temperature reached a steady state.

Once the temperature of the system was stable for 10 min, the temperatures of the plate and the cone were recorded. The temperature of the plate is provided by the apparatus whereas the temperature of the cone was measured using a type K thermocouple calibrated against a platinum resistance thermometer (PRT). Then, the cone was set to rotate at a constant angular velocity corresponding to a determined value of shear rate (see Equation 3.1) until a stable value of shear stress was observed, typically after 30 s. This procedure was repeated at five different shear rates. The viscosity was calculated from the shear stress versus shear rate straight line. The temperature of the sample was estimated according to

the procedure presented in the following section. All the samples tested in this study were Newtonian.

3.2.7.2 Apparatus Calibration

The calibration of the two cone and plate rheometers used in this thesis is described in this section. The following metrics are used to assess the errors of the calibration process:

$$AARD(\%) = \frac{100}{N} \sum_{1}^{n} \left| \frac{X_{meas} - X_{rep}}{X_{rep}} \right| \qquad (3.3)$$

$$MARD(\%) = 100 \max \left| \frac{X_{meas} - X_{rep}}{X_{rep}} \right| \qquad (3.4)$$

$$bias(\%) = \frac{100}{N} \sum_{1}^{N} \frac{X_{meas} - X_{rep}}{X_{rep}} \qquad (3.5)$$

where AARD and MARD are the average absolute relative deviation and maximum absolute relative deviation, respectively, N is the number of data points, X is the variable under study and the subscripts *meas* and *rep* indicate the experimentally measured and reported variable, respectively. The same error metrics will be used in this thesis to judge the quality of the developed model predictions compared to the experimental data in the subsequent chapters.

Calibration of the two cone and plate rheometers was necessary in order to determine if the temperature reported by the apparatus corresponds to the actual temperature of the sample. Recall that the device does not measure the temperature of the sample directly but assumes that it is the same as that of the plate. Two different certified viscosity standards, S20 and S30000, obtained from Cannon Instruments were used as calibration fluids. The data is reported at atmospheric pressure. After calibration, it was found that the temperature reported by the Anton Paar MCR-52 corresponded to that of the sample; however, there were serious discrepancies between the temperature reported by the HAAKE Rotovisco 1 rheometer and that of the sample. The discussion below focuses on the results obtained from the latter.

Figure 3.3 compares measured versus reported viscosities of standards S20 and S30000. The Walther viscosity model was fit to the reported data in order to make the comparison easier. The Walther model is given by:

$$\log[\log(\mu+1)] = A - B\log(T) \tag{3.6}$$

where A and B are fitting constants and T is the absolute temperature in K. Equation 3.6 fits the data of standards S20 with AARD, MARD and bias of 0.7, 1 and 0.001%, respectively, and that of and S30000 with AARD, MARD and bias of 2, 3 and 0.05%, respectively.
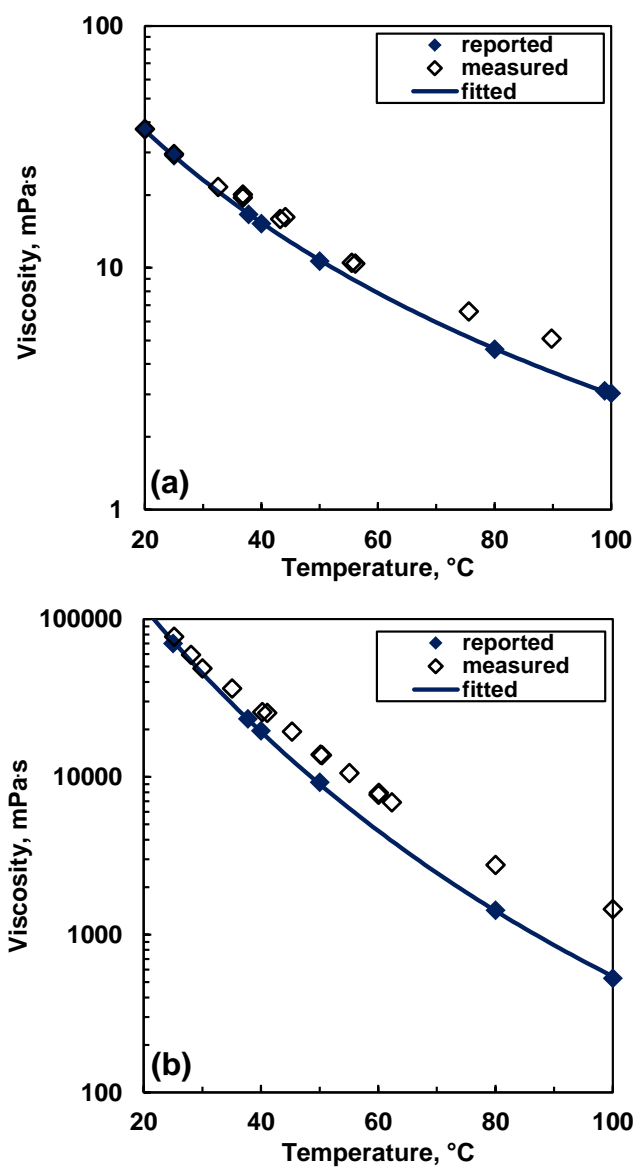
Figure 3.3. Measured (with no temperature correction) and reported viscosities of Cannon Instruments viscosity standards at atmospheric pressure: a) S20, b) S30000. Viscosities were measured in the HAAKE Rotovisco 1 apparatus.

The measured data in Figure 3.3 was plotted using the temperature reported by the HAAKE Rotovisco 1 apparatus which corresponds to that of the plate. The data shows a systematic deviation from the reported data as the temperature increases which suggest that the temperature of the plate does not corresponds to the actual temperature of the sample.

Therefore, a temperature correction methodology based on heat transfer principles was developed in order to predict the actual temperature of the sample.

3.2.7.3 Temperature Correction Model

The heat transfer through the cone and plate system was modeled as two cylindrical slabs in series representing the sample and the cone as shown in Figure 3.4. A third hypothetical slab was inserted to represent the thermal contact resistance between the plate and the sample. At steady state, it was assumed that the heat is transferred only in the vertical direction from the plate to the sample, from the sample to the cone and finally from the cone to the surrounding air. Heat is transferred between the slabs by conduction and from the cone to the air by natural convection. The temperature of the slab representing the sample was assumed to be uniform and constant. This assumption is justified by the small thickness (0.1 mm) of the sample slab.
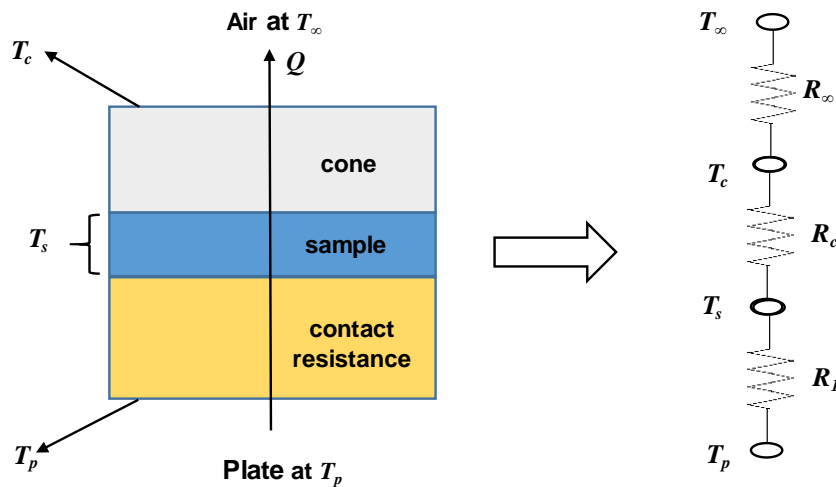
Figure 3.4. Slab model of the cone and plate rheometer and its electrical resistance analogy. T and R are the temperature and thermal resistance, respectively. Subscripts c, s, p and ∞ refer to cone, sample, plate and air, respectively.

The heat transfer through the slabs was represented using an electrical resistance analogy, Figure 3.4. The only unknown variables are the temperature of the sample, T_s, and the

thermal contact resistance, R_1. The temperature of the cone, the plate and the surrounding air are measured. The thermal resistances of the cone, R_c, and the air, R_∞, are calculated as:

$$R_c = \frac{z}{A_c \lambda_c} \tag{3.7}$$

$$R_\infty = \frac{1}{A_c h_\infty} \tag{3.8}$$

where z, A_c and λ_c are the thickness (3 mm), transversal area (calculated using the cone radius) and thermal conductivity of the cone (19.04 $\mathrm{Wm^{-1}K^{-1}}$, reported by the manufacturer), respectively. The natural convection heat transfer coefficient, h_∞, was calculated from the Churchill and Chu (1975) correlation. This correlation has been used to simulate the convective heat transfer from parallel plate and cone and plate rheometers to the surrounding air (Barker and Wilson, 2006):

$$Nu^{0.5} = 0.56^{0.5} + \left\{ \frac{Gr\,Pr/300}{\left[1 + \left(0.5/Pr\right)^{9/16}\right]^{16/9}} \right\}^{1/6} \tag{3.9}$$

where Nu, Gr and Pr are the Nusselt, Grashof and Prandtl numbers, respectively, defined as:

$$Nu = \frac{h_\infty L^*}{\lambda_\infty} \tag{3.10}$$

$$Gr = \frac{g\beta(T_c - T_\infty)(L^*)^3}{v_\infty^2} \tag{3.11}$$

$$Pr = \frac{v_\infty}{\alpha_\infty} \tag{3.12}$$

$$L^* = \frac{9D_c}{11} \tag{3.13}$$

where λ_∞, v_∞, α_∞ and β_∞ are the thermal conductivity, kinematic viscosity, thermal diffusivity and thermal expansion coefficient of the air, respectively, and D_c is the cone diameter. The physical properties of the air were taken from the NIST database (2008) at atmospheric pressure and at film temperature defined as the arithmetic average between the cone and air temperature.

The unknown contact thermal resistance and the temperature of the sample are calculated as:

$$R_1 = R_\infty \frac{T_p - T_c}{T_c - T_\infty} - R_c \qquad (3.14)$$

$$T_s = T_p - R_1 \frac{T_p - T_\infty}{\left(R_1 + R_c + R_\infty\right)} \qquad (3.15)$$

Note that the above expressions are completely predictive and functions only of the physical properties and geometrical parameters of the system. Figure 3.5 shows the results after applying the temperature correction to the data from standards S20 and S30000. The AARD, MARD and bias were of 2, 6, -2%, respectively, for standard S20 and 4, 8 and -4%, respectively, for standard S30000. The viscosity of another viscosity standard, S45000, was subsequently measured at temperatures up to 135°C and compared to reported values. The reported viscosity of this standard ranges between 2,556 and 1.6×10^6 mPa·s. After temperature correction, the AARD, MARD and bias were of 5, 8 and 3, respectively. The repeatability of the viscosity measurement for the three standards was assessed as $\pm 3\%$.
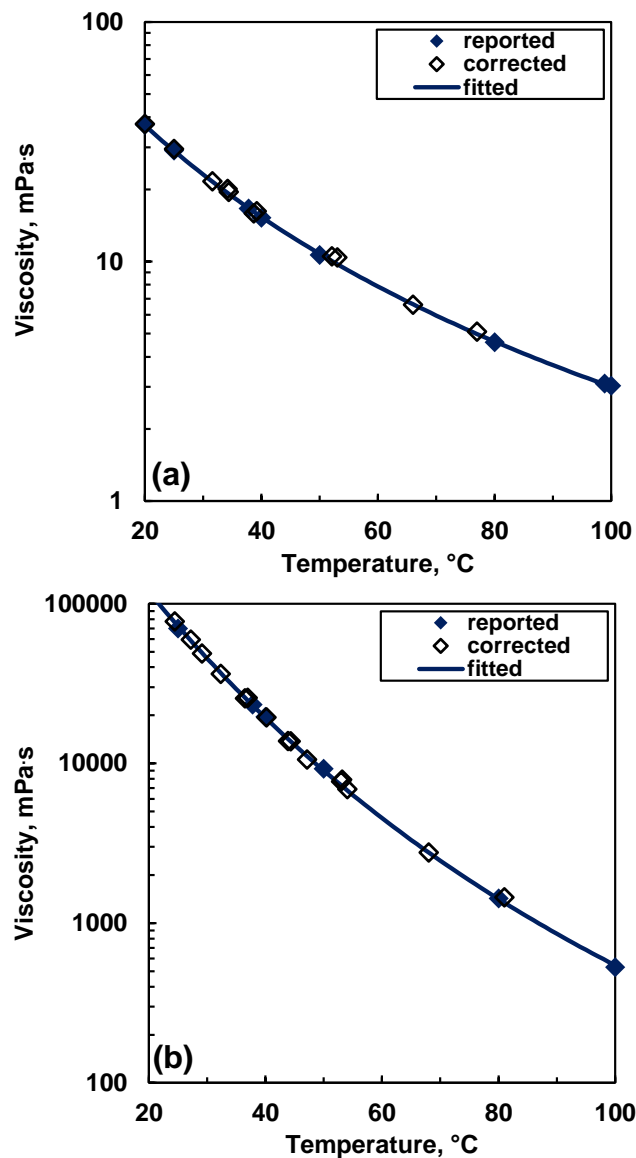
Figure 3.5. Measured (after temperature correction) and reported viscosities of Cannon Instruments viscosity standards at atmospheric pressure: a) S20, b) S30000. Viscosities were measured in the HAAKE Rotovisco 1 apparatus.

3.2.7.4 Measuring the Viscosity of Petroleum Fluids

The viscosity of some whole and diluted crude oils and distillation cuts was measured using the cone and plate rheometer according to the procedure described in Section 3.2.7.1. The temperatures at which the viscosities were reported were corrected when the HAAKE

Rotovisco 1 was used according to the method introduced in the previous section. Recall that no temperature correction is required when using the Anton Paar MCR-52 apparatus. All measurements in the cone and plate rheometer were taken at atmospheric pressure. The temperature of the sample was kept well below the bubble point to avoid losing volatile components. The loss of volatile components was detected as an increment in the viscosity of the fluid at constant temperature. In general, the measurements were performed at a maximum temperature of 75°C for oils with repeatability of ±5%, 50°C for diluted oils with repeatability of ±5%, 100°C for maltenes with repeatability of ±4%. For distillation cuts the measurements were consistent below the boiling point with repeatability of ±3%.

3.2.8 *Oscillating U-Tube Density Meter*

The densities of the samples tested in the cone and plate rheometer were determined using an Anton Paar DMA 4500M oscillating U-tube density meter at atmospheric pressure and temperatures up to 75°C. Temperature of the sample cell was controlled to within ±0.01°C by a Peltier mechanism enabling measurements from 0°C to 90°C. Pure component samples were injected directly into the apparatus and their density was measured once thermal equilibrium was reached at a set temperature. For the mixtures of bitumen and solvent, the sample was first sonicated at 20°C until homogeneous. The mixture was considered homogeneous when its density was no longer changing with mixing time, typically after 12 hours. The instrument was calibrated using reverse-osmosis water and nitrogen. The precision and repeatability of the density measurements were ±0.01 kg/m³ and ± 0.05 kg/m³ respectively.

The density of C5-asphaltenes was indirectly calculated from the densities of asphaltene/toluene mixtures at temperatures up to 90°C and at atmospheric pressure. The densities of a series of mixtures with different asphaltene concentrations were measured at each temperature using the Anton Paar DMA 4500M density meter described above. It was assumed that the asphaltenes formed regular solutions (Barrera *et al*., 2013) with toluene as follows:

$$\rho_{mix} = \left(\sum \frac{w_i}{\rho_i} \right)^{-1} \qquad\qquad (3.16)$$

where ρ is density and subscripts *mix* and *i* denote the mixture and component *i*, respectively. The densities were determined at each temperature from a least squares fit of the mixing rule to the mixture data. The repeatability of the indirectly determined densities was found to be ± 0.9 kg/m³.

3.2.9 *The Hot Wire Apparatus*

The hot wire apparatus is a transient technique originally proposed by Stâlhane and Pyk in 1931 to measure the thermal conductivity of fine powders and liquids. This technique has become very popular in the last 50 years due to its accuracy, reproducibility and especially because it is possible to practically eliminate the effects of natural convection and radiation (De Groot *et al*., 1974; Assael *et al*., 2010). To date, the hot wire technique has been used to measure the thermal conductivity of gases, liquids, suspensions, melts and even conventional crude oils, distillation cuts and coal liquids (Baltau *et al*., 1985; Elam *et al*., 1989; Assael *et al*., 2010).

3.2.9.1 Physical Principle and Ideal Model

The physical principle behind the hot wire technique is the transfer of a constant heat flux during a short period of time from a thin platinum wire to an infinite-acting medium of constant physical properties. The wire, which serves as heating element and thermometer, is immersed into the medium in a cylindrical configuration that gives a radial heat flux. The rate at which the temperature of the wire changes is a function of the thermal conductivity of the medium. van Der Held *et al*. (1949, 1953) obtained an analytical solution for the temperature of the wire by solving the transient one-dimensional Fourier equation subjected to the following assumptions:

1) The wire has infinitesimal diameter and infinite length.
2) The wire has zero heat capacity and heat generation is constant along the full length of the wire.
3) The wire has infinite thermal conductivity.

4) The fluid surrounding the wire is isotropic, infinite in extent, and in local thermodynamic equilibrium.

5) The fluid is dense and at constant pressure.

6) Energy is transferred by pure one-dimensional radial conduction only.

7) The wire and the surrounding fluid are initially at uniform temperature and there is no temperature discontinuity at the interface between the wire and the fluid.

The solution to the Fourier equation with assumptions is given by:

$$\Delta T_w = \frac{q}{4\pi\lambda}\left[\ln\left(\frac{4\alpha t}{r_o^2}\right) - \gamma\right] \tag{3.17}$$

where ΔT_w is the temperature change of the wire, λ and α are the thermal conductivity and thermal diffusivity of the medium, respectively, q is the heat per unit length, r_o is the radius of the wire, t is the time, and γ is the Euler constant ($\gamma = 0.5772...$). Equation 3.17, known as the ideal solution, shows a linear relation between the change of the wire temperature and the logarithm of time. Hence, the thermal conductivity of the medium can be estimated from the slope of the straight line on a plot of temperature difference versus log time.

3.2.9.2 Deviations from the Ideal Model

Actual hot wire devices do not satisfy all the assumptions taken to derive Equation 3.17 and deviations from the ideal straight line behavior have been observed and widely documented in the literature (Horrocks and McLaughlin, 1963; Harman, 1969; Mani, 1971; De Groot *et al.*, 1974; Healy *et al.*, 1976;). A typical temperature rise versus time diagram can be divided into three different regions as shown in Figure 3.6. Each region is described below.

Region 1: the deviation from the straight line behavior at early times is caused by thermal gradients inside the wire (thermal conductivity of the wire is finite) and also by the accumulation of heat within the wire due to the non-zero heat capacity. This phenomenon is known as wire capacitance (Harman, 1969; De Groot *et al.*, 1974).

Region 2: the temperature rise in the wire follows the straight line behavior because the system satisfies all the assumptions taken to derive Equation 3.17, at least during the timeframe of the measurement. Deviations from the straight line behavior in this region are observed for two cases: 1) when the properties of the fluid such as density, thermal conductivity and heat capacity are highly affected by temperature changes and, 2) when heat is also transferred by radiation. The effect of the variable fluid properties on the accuracy of the measured thermal conductivity has been found to be negligible at conditions far away from the critical point (Harman, 1969; De Groot *et al*., 1974 and Healy *et al*., 1976). The effect of radiation has been found to be negligible even for fluids absorbing in the infrared region, such as toluene (Mani, 1971; Nieto de Castro *et al*., 1983; Perkins and Nieto de Castro, 1991).

Region 3: the temperature rise in the wire deviates from the straight line behavior at late times due to the development of convective currents in the fluid that cool down the wire faster than when heat is transferred only by conduction. These currents are the result of density variations in the fluid layers adjacent to the wire that are at a higher temperature than the bulk fluid (Mani, 1971). The time at which the effect of those currents starts affecting the straight line behavior is known as the onset of convection. The onset of convection depends on fluid density and geometric variables such as wire length and cell diameter. In general, the onset of convection occurs earlier for less dense fluids, shorter wires, and smaller cell diameters (De Groot *et al*., 1974).
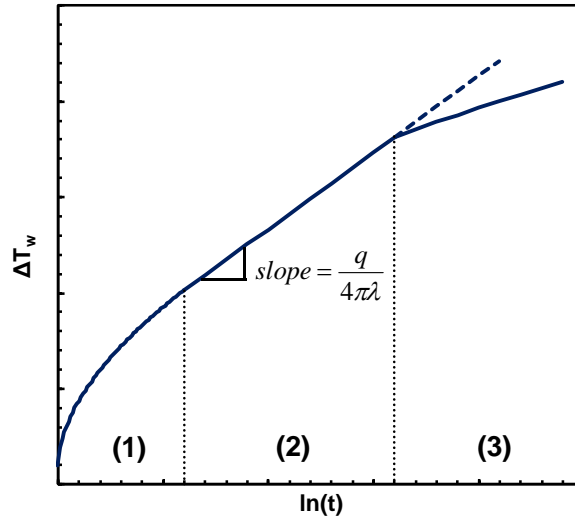
Figure 3.6. Diagram of temperature rise versus time for a typical hot wire apparatus. Adapted from De Groot *et al*. (1974).

3.2.9.3 Description of the Apparatus

An apparatus was commissioned to measure the thermal conductivity of liquid samples using the transient hot wire principle, Figure 3.7. This device was designed for temperatures from ambient to 200°C and pressures up to 10 MPa and requires 150 mL of sample. The apparatus consists of a thermal conductivity sensor fixed along the axis of the cylindrical high pressure measurement cell, an air bath, a cylindrical transfer vessel equipped with a piston, and a pump. The sensor is welded to the top cap of the pressure cell.

The entire cell is placed in a temperature controlled air bath which maintains temperature within ±0.1°C of the intended measurement temperature. The air bath is insulated with a 3 cm layer of glass wool in order to minimize the heat losses to the surroundings. The transfer vessel is used to control the pressure of the system and is equipped with a piston connected to a Quizix SP-5200 pump which uses hydraulic oil as displacement fluid. The pump controls pressure within ±0.005 MPa of the measurement value.
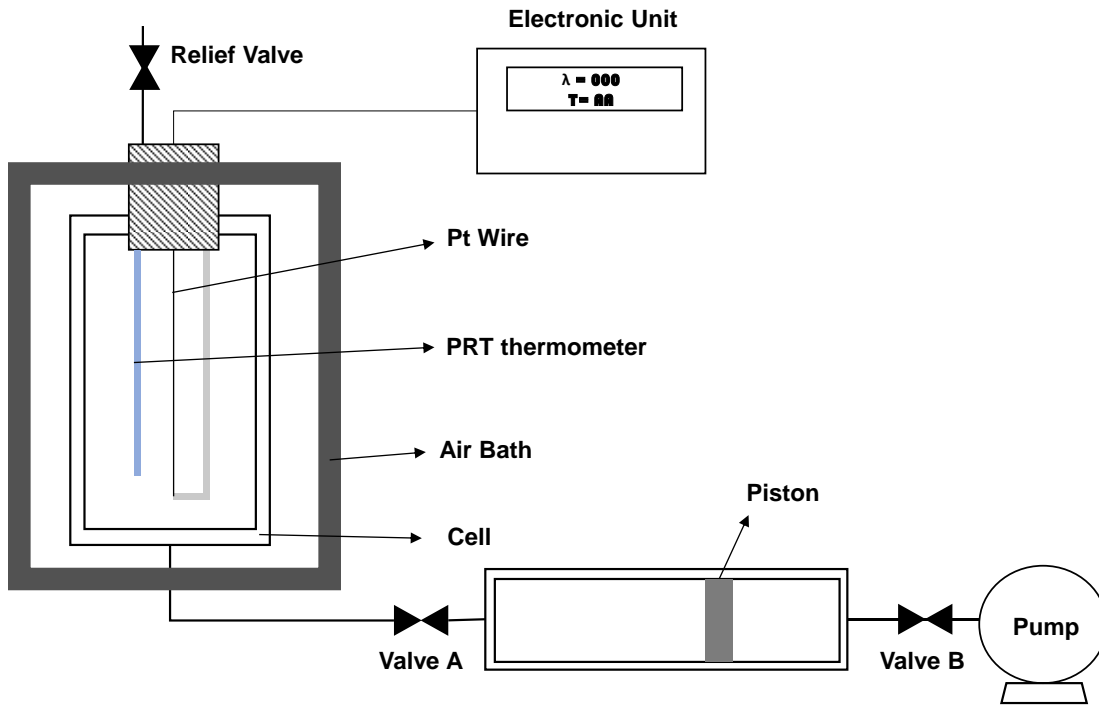
Figure 3.7. Schematics of the Transient Hot Wire apparatus used designed in this study.

The heart of the apparatus is the thermal conductivity sensor and control unit purchased from ThermTest Instruments Inc. The sensor consists of a thin platinum wire (diameter 0.1 mm, length 3.5 cm) in a radially symmetric configuration and a platinum resistance thermometer (PRT) that allows the direct measurement of the sample temperature. The control unit automatically controls the voltage applied to the wire, measures its electrical resistance, and calculates the thermal conductivity of the sample. The control unit and the sensor are capable of measuring thermal conductivities in the range of 10 to 200 $mWm^{-1}K^{-1}$.

The control unit operates as follows. A step voltage is applied to the wire ends for a period of 0.8 s. During this period of time, the electrical resistance of the wire is measured 50 times using an automatic and calibrated Wheatstone bridge. The wire is directly connected to one of the bridge legs. The heat dissipated by the wire per unit length is calculated as:

$$q = \frac{V^2}{RL} \tag{3.18}$$

74

where *V*, *R* and *L* are the voltage, electrical resistance, and wire length, respectively. The temperature of the wire is calculated from its resistance using a calibration function defined by the manufacturer. The wire length and diameter were also estimated from calibration by the manufacturer. Finally, the unit fits Equation 3.17 to the data in order to determine the thermal conductivity of the sample. The thermal conductivity is reported at the temperature measured by the PRT thermometer. Note that the voltage applied by the unit cannot be controlled by the user.

3.2.9.4 Procedure for Thermal Conductivity Measurement

Apparatus Preparation. Prior to any measurement, the measurement cell, transfer vessel, and their connection line were cleaned using toluene and rebuilt. All of the O-rings and copper gaskets were replaced before each new fluid was introduced to ensure leak-free cells. Both vessels were pressure tested using compressed air up to 10 MPa to ensure no leakage.

To begin an experiment, the sample was placed in the transfer vessel and left to sit to release any trapped air bubbles. This cell was then connected to the pump and hydraulic oil was injected to displace the piston in order to force all the air out. The transfer vessel was connected to the measurement cell while keeping the transfer vessel isolated (Valve A in Figure. 3.7 closed). Then, the measurement cell was evacuated overnight using a vacuum pump. Finally, the fluid was injected from the transfer vessel into the measurement cell by pumping hydraulic oil into the transfer vessel.

Measurement. The thermal conductivity of a sample was measured at constant temperature and pressures from 0.1 to 10 MPa, using increments of 2.5 MPa. Note, the pressure of the system was always set above the saturation pressure of the sample to avoid the separation of volatiles. Prior to any measurement, the temperature of the bath was adjusted until the sample reached the desired temperature. The pressure was set at the desired value and the sample was then left to reach a stable temperature, usually for 10 hours. The thermal conductivity at constant pressure was measured at least 10 times with an interval of 3

minutes between measurements. This interval allowed the system to regain a stable temperature. The thermal conductivity was reported as the average of the ten measurements. During the measurement, the temperature was kept within ± 0.01°C. The same procedure was followed at each pressure and temperature of interest.

3.2.9.5 Validation of Method

The fluids chosen to test the thermal conductivity measurements were *n*-pentane, *n*-heptane, *n*-tetradecane, and deionized water because literature data were available for these fluids over a range of temperatures. The measured thermal conductivity of those fluids is reported in Appendix A. Note, liquid thermal conductivity data are scarce and mostly reported at atmospheric pressure. The literature data for the thermal conductivities as well as the value of other properties such as viscosity and density were taken from NIST database (2008). As an example, Figure. 3.8 shows the literature data for toluene and *n*-tetradecane at 0.1 MPa. The reported liquid thermal conductivity data are linear versus temperature, as expected at conditions far from the critical point (Poling *et al*., 2001). In order to compare the measured data with the literature values, the literature data were fit with a straight line.
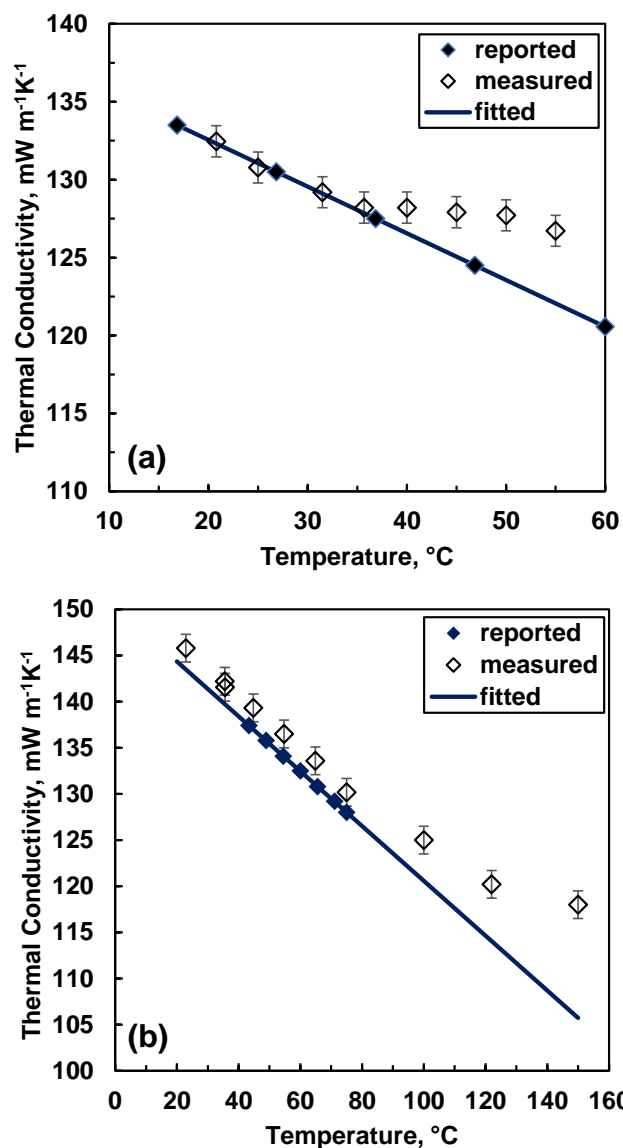
Figure 3.8. Reported and measured thermal conductivity at 0.1MPa of toluene (a) and *n*-tetradecane (b). Reported data were taken from the NIST database (2008).

Figure 3.8 also shows the data measured in this thesis for the same test fluids. At lower temperatures, the measured data follows a straight line with the same slope as the measured data. However, at higher temperatures the measured thermal conductivity data is higher than expected, deviating from the straight line trend. The deviations found in the straight line zone between reported and measured data are consistent with the uncertainty related

to the estimation of the electrical resistance of the wire; which is determined within ± 0.08 Ohm. The average relative error of measured values is 0.5% for toluene, at temperatures below 35°C, and 1.5% for n-tetradecane, at temperatures below 70°C. The departure from the straight line behavior might be a consequence of natural convection.

The deviation from the straight line occurred at lower temperatures for toluene than for n-tetradecane indicating that fluid properties might have an effect on the departure from the trend. The deviations can be expressed as a conductivity factor defined as follows:

$$K = \frac{\lambda_{rep}}{\lambda_{meas}} \tag{3.19}$$

where K is the thermal conductivity factor and subscripts rep and $meas$ stand for reported and measured, respectively. A value of $K=1$ indicates that the measured value has not been affected by natural convection. Recall that natural convection causes a smaller change in the wire temperature than when only conduction is present which in turn is translates into a higher thermal conductivity (see Section 3.2.9.1). Hence, $K<1$ indicates that convection cannot be neglected.

To determine if the deviations were the result of natural convection, the Grashof number for each experiment was determined. The Grashof number, defined in Equation 3.11, is the ratio between the buoyancy and viscous forces of a fluid, and is a governing dimensionless number for heat transfer due to natural convection (Bird *et al*., 2002). The higher the Grashof number, the more likely that convection dominates. In this case, the characteristic length, L^*, for the Grashof number is the length of the platinum wire.

Figure 3.9 shows the conductivity factor versus the Grashof number for all four test fluids. The conductivity factor is equal to one for Grashof numbers below 10,000 but decreases at higher Grashof numbers. Hence, it was concluded that the effects of natural convection on the determination of thermal conductivity can be neglected for Grashof numbers below 10,000. Table 3.2 shows the errors in the measured thermal conductivity of the test fluids for Grashof numbers below 10,000. The measured data were within 5% of reported values.

The repeatability of the measurements was ±3%. All of the data reported in this thesis were collected at Grashof numbers below 10,000.
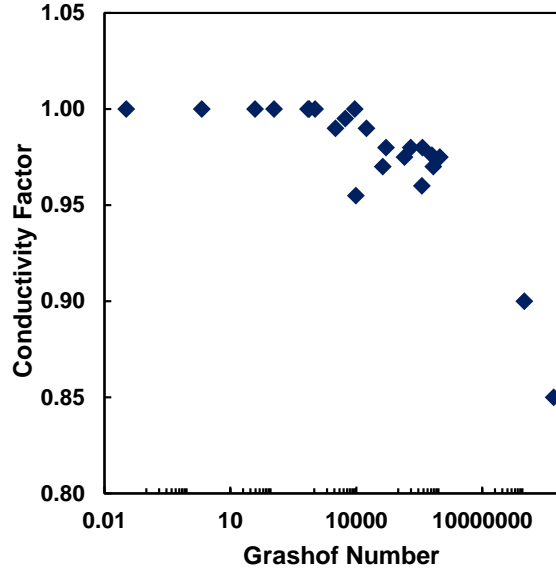
Figure 3.9. Conductivity factor versus Grashof number.

Table 3.2. Summary of the deviations of the measured versus literature thermal conductivity for the test fluids.

Calibration Test Fluid	Range of Conditions		AARD %	MARD %	Bias %
	Temperature °C	Pressure MPa			
n-Pentane	20 - 30	0.1 - 10	5	12	-5
n-Heptane	20 - 30	0.1 - 10	4	5	1
n-Tetradecane	20 - 80	0.1 - 10	2	4	-2
Toluene	20 - 30	0.1 - 10	5	8	4
Water	20 - 90	0.1	1	2	1

CHAPTER FOUR: MODELING THE VISCOSITY OF CRUDE OILS USING THE EXPANDED FLUID AND GENERALIZED WALTHER VISCOSITY MODELS

One of the objectives of this thesis is to develop a consistent methodology to predict the viscosity of distillation characterized crude oils using the Expanded Fluid (EF) and generalized Walther (GW) viscosity models. Both models were previously developed to model the viscosity of pure hydrocarbons, crude oils, and mixtures over a wide range of temperatures and pressures. The EF model is a full phase model but requires accurate input densities. The Walther model is only valid in the liquid region, but does not require density data. This chapter presents the EF and GW models that are used to develop the methodology for characterized oils in subsequent chapters. The previous application of these models to fluids characterized based on GC assays is also presented.

4.1 The Expanded Fluid (EF) Viscosity Model

The Expanded Fluid (EF) model (Yarranton and Satyro, 2009) relates the departure of a fluid's viscosity from its viscosity in the dilute gas state, both at the same temperature, as a function of fluid expansion as follows:

$$\mu - \mu_G = c_1 \left(\exp(c_2 \beta) - 1 \right) \tag{4.1}$$

where μ and μ_G are the viscosity of the fluid and the dilute gas, respectively, in mPa·s, c_1 and c_2 are fitted constants, and β is the fluid expansion parameter given by:

$$\beta = \frac{1}{\exp\left\{ \left(\dfrac{\rho_s^*}{\rho} \right)^n - 1 \right\} - 1} \tag{4.2}$$

where ρ is the density in kg/m^3 of the fluid, ρ_s^* is the density in kg/m^3 at which the viscosity of the fluid tends to infinity and the exponent n is an empirical parameter used to improve the fit near the critical point. This exponential function of density is constrained to approach infinity as the viscosity of the fluid approaches infinity and to approach zero as the viscosity of the fluid approaches the dilute gas state value.

Equation 4.1 was fitted to a dataset composed by pure hydrocarbons collected from the literature. The exponent n (dimensionless) and the parameter c_1 (in mPa·s) were fixed for all hydrocarbons:

$$n = 0.65 \tag{4.3}$$

$$c_1 = 0.165 \tag{4.4}$$

The other parameters, c_2 (dimensionless) and ρ_s^* were found to be fluid-specific. Yarranton and Satyro (2009) introduced a pressure dependence on the parameter ρ_s^* to improve the performance of the model at high pressure:

$$\rho_s^* = \frac{\rho_s^o}{\exp(-c_3 P)} \tag{4.5}$$

where ρ_s^o is the compressed state density in a vacuum, c_3 is a fitting parameter in kPa^{-1} and P is the pressure in kPa. The EF model is only valid for Newtonian fluids and is applicable across the entire phase diagram.

The inputs are the fluid density, pressure, the dilute gas viscosity, and three fluid-specific parameters: c_2, c_3 and ρ_s^o. The pressure is specified and the density must be measured or calculated independently. The dilute gas viscosity of pure hydrocarbons is calculated using the following empirical correlation (Yaws, 2008):

$$\mu_G = A_o + B_o T + C_o T^2 + D_o T^3 \tag{4.6}$$

where A_o, B_o, C_o and D_o are constants specific for each pure component and T is the absolute temperature in K. The constants are obtained from the Yaws' handbook (2008). The three fluid-specific parameters must be determined by fitting the EF model to experimental data.

The EF model has been successfully fitted on many pure hydrocarbons included n-alkanes, branched alkanes, aromatics, cyclics, and certified viscosity standards. The fitted viscosities were, on average, within 5% of the measured values when measured densities are used as the input. However, the model is sensitive to the accuracy of the input density. In practice, measured densities of pure components are not available at all conditions across the phase diagram and therefore must be predicted. Satyro and Yarranton (2010) proposed

an alternative version of the EF model specially adjusted to use densities calculated from the Peng Robinson equation of state with volume translation. In this version of the model, n and c_1 were set to 0.4872 and 0.4214 mPa·s, respectively. The authors also report a new set of fluid-specific parameters for different pure hydrocarbons which are different from those estimated when experimental densities were used as input. The version of the EF model used in this thesis is that developed using experimental density as input.

4.1.1 *Mixing Rules*

The EF model treats a mixture as a single component fluid with fluid-specific parameters calculated from those of the mixture components using the following mixing rules (Motahhari *et al.*, 2011a):

$$\rho_{s,mix}^{o} = \left(\sum_{i}^{nc} \sum_{j}^{nc} \frac{w_i w_j}{2} \left(\frac{1}{\rho_{s,i}^{o}} + \frac{1}{\rho_{s,j}^{o}} \right) \left(1 - \alpha_{ij}\right) \right)^{-1} \tag{4.7}$$

$$\frac{c_{2,mix}}{\rho_{s,mix}^{o}} = \sum_{i}^{nc} \sum_{j}^{nc} \frac{w_i w_j}{2} \left(\frac{c_{2,i}}{\rho_{s,i}^{o}} + \frac{c_{2,j}}{\rho_{s,j}^{o}} \right) \left(1 - \alpha_{ij}\right) \tag{4.8}$$

$$c_{3,mix} = \left(\sum_{i}^{nc} \frac{w_i}{c_{3,i}} \right)^{-1} \tag{4.9}$$

where nc is the number of components in the mixture and w_i is the mass fraction of the component i in the mixture. α_{ij} is the EF viscosity binary interaction parameter with a default value of zero.

The dilute gas viscosity of the mixture ($\mu_{G,mix}$) is calculated using Wilke's method (1950) as follows:

$$\mu_{G,mix} = \sum_{i}^{nc} \frac{x_i \mu_{G,i}}{\sum_{j}^{nc} x_j \phi_{ij}} \tag{4.10}$$

where:

$$\phi_{ij} = \frac{\left[1 + \left(\mu_{G,i}/\mu_{G,j}\right)^{0.5} \left(M_j/M_i\right)^{0.25}\right]^{2}}{\left\{8\left[1 + \left(M_i/M_j\right)\right]\right\}^{0.5}} \tag{4.11}$$

and where x_i, $\mu_{o,i}$ and M are the mole fraction, dilute gas viscosity and molecular weight of the component i of the mixture. To date, the EF model and the mixing rules with interaction parameter set to zero have been successfully tested on over 40 pure hydrocarbon binaries. The pure hydrocarbon mixtures include binaries alkane/alkane, alkane/aromatic, alkane/cyclic, aromatic/aromatic, and aromatic/cyclic. The AARD, MARD for the pure hydrocarbon mixtures were of 3 and 33%, respectively (Motahhari *et al*., 2011a).

4.1.2 *Modeling of Crude Oil Viscosity Using the EF Model*

The EF model has also been used to model the viscosity of dead and live crude oils (Yarranton and Satyro, 2009; Motahhari *et al*., 2011b). Dead crude oils are modeled as a single component fluid with EF model parameters calculated by fitting the model to measured viscosity data using measured density as the input. The dilute gas viscosity of the crude oil is determined from Equation 4.6 (Motahhari *et al*., 2013). The EF model is fitted to the viscosity data by adjusting the parameters c_2, c_3 and ρ_s^o using a non-linear least-squares method to minimize the following objective function:

$$OF = \sum \left[\ln\left(\frac{\mu_{pred}}{\mu_{meas}}\right) \right]^2 \tag{4.12}$$

where subscripts *pred* and *meas* indicate the predicted value from the model and measure value, respectively.

If only viscosity data at atmospheric pressure is available, only the parameters c_2 and ρ_s^o can be determined. In this case, the parameter c_3 can be predicted using the empirical correlation proposed by Motahhari *et al* (2013):

$$c_3 = \frac{2.8 \times 10^{-7}}{1 + 3.23 \exp\left(-1.54 \times 10^{-2} M\right)} \tag{4.13}$$

where c_3 is in kPa^{-1} and M is the molecular weight. Equation 4.13 was developed using high pressure viscosity data of pure hydrocarbons and tested on high pressure viscosity data of crude oils.

Live crude oils are modelled as a mixture of a gaseous solvent(s) and dead crude oil (Motahhari *et al.*, 2011b). The EF parameters of the gaseous solvents are calculated by fitting the correlation to pure component data and those of the dead oil are calculated as described above. The estimated EF parameters of the mixture components, the mixture mass composition, and its density are use to predict its viscosity at a given condition. First, the EF mixture parameters are calculated using the mass-based mixing rules with the binary interaction parameters set equal to zero. Then, the experimental density and the calculated EF parameters are used to predict the mixture viscosity. However, interaction parameters set to zero do not usually produce accurate viscosity values (Motahhari *et al.*, 2011b). In this case, the EF predictions can be improved by tuning the binary interaction parameters to match the experimental data. The objective function defined in Equation 4.12 is used for this purpose. The same approach is used to model the viscosity of dead oils diluted with liquid solvents. The EF model with interaction parameters set to zero predicted the viscosity of 6 pseudo-pairs Western Canada bitumen/solvent with AARD and MARD of 23 and 65%, respectively. By tuning interaction parameters, the AARD and MARD were reduced to 6 and 25%, respectively (Motahhari *et al.*, 2011b; Motahhari, 2013). The solvents used to prepared the blends were ethane, propane, butane, pentane, heptane and a condensate.

4.2 The Generalized Walther (GW) Model

The viscosity of a liquid at a given temperature and pressure can be calculated as a departure from the viscosity at the same temperature at atmospheric pressure as follows (Yarranton *et al.*, 2012) :

$$\mu = \mu_o\left[1 + \delta(P - P_o)\right] \qquad (4.14)$$

where μ is the liquid viscosity in mPa·s, P is pressure in kPa, δ is the viscosibility in kPa^{-1}, and the subscript o indicates a property at atmospheric pressure. The viscosibility accounts for the change in the liquid viscosity with pressure and is related to temperature as follows:

$$\delta = \delta_1 - \delta_2 T \qquad (4.15)$$

where δ_1 in kPa^{-1} and δ_2 in kPa^{-1}K^{-1} are fluid specific parameters and T is the absolute temperature in K. The viscosity of the liquid at atmospheric pressure is determined using the Walther correlation (Walther, 1931):

$$\log[\log(\mu_o + 1)] = A - B\log(T)$$ (4.16)

where T is the absolute temperature and A and B are two fluid-specific parameters calculated by fitting the correlation to experimental viscosity data at atmospheric pressure. The Walther correlation is based on the empirical observation that the double log of the Newtonian viscosity at atmospheric pressure is a straight line when plotted against the log of the absolute temperature. This linear relation is followed by liquid pure hydrocarbons and crude oils at conditions far from the critical point. The Walther correlation is recommended by the American Petroleum Institute, API (1997), for modelling the viscosity of liquid hydrocarbons, petroleum fluids, and crude oils at atmospheric pressure. It has also been used as criteria to check the consistency of viscosity data (Butler, 1997). The Generalized Walther model fits the data of over 18 pure hydrocarbons, including alkanes, cyclics, aromatics and carbon dioxide, with AARD and MARD of 6 and 20%, respectively (Yarranton *et al.*, 2013).

4.2.1 *Mixing Rules*

The generalized Walther model treats a mixture as one single fluid with fluid-specific parameters calculated from those of the pure components of the mixture as follows (Yarranton *et al.*, 2013):

$$A_{mix} = \sum_i^{nc} \frac{w_i w_j}{2}(A_i + A_j)(1 - \alpha_{ij}^*)$$ (4.17)

$$B_{mix} = \sum_i^{nc} \frac{w_i w_j}{2}(B_i + B_j)(1 + \alpha_{ij}^*)$$ (4.18)

$$\ln[\ln(\delta_{1,mix} + 1)] = \sum_i^{nc} w_i \ln[\ln(\delta_{1,i} + 1)]$$ (4.19)

where i and j indicate a component, nc is the number of components in the mixture, w is mass fraction, and α_{ij}^* is the Walther viscosity binary interaction parameter between components i and j with a default value of zero. The Generalized Walther model has been

tested on over 35 pure hydrocarbon mixtures, including alkane/alkane, aromatic/alkane, cyclic/alkane, cyclic/aromatic and aromatic/aromatic binaries. The AARD and MARD were of 6 and 21%, respectively (Yarranton *et al*., 2013).

4.2.2 *Modelling of Crude Oil Viscosity Using the Generalized Walther Model*

The generalized Walther model has been used to model the liquid viscosity of dead and diluted crude oils. Although Yarranton *et al*. (2013) proposed a method to predict the Walther parameters *A* and *B* in Equation 4.16 for GC characterized crude oils, the discussion here focusses on crude oils characterized as a single component. First, the parameters *A* and *B* are determined by fitting Equation 4.16 to viscosity data at atmospheric pressure using the objective function defined in Equation 4.12. Then the viscosibility parameters, δ_1 and δ_2, are determined by fitting the model to data at higher pressures. For cases where high pressure data are not available, Yarranton *et al*. (2013) proposed the following correlations for the viscosibility parameters based on high pressure viscosity data for alkanes, aromatics, cyclics, and Western Canada heavy oils:

$$\delta_1 = 0.008 + 0.00006M \tag{4.20}$$

$$\delta_2 = 0.0033\delta_1 \tag{4.21}$$

The model can also be used to model the viscosity of live and diluted crude oils modeled as a mixture of dead oil and solvent. The solvent can be a single component or a mixture, but must be homogeneous and in the liquid state so that the model can be applied. The mixture parameters are determined by combining those of the dead oil and solvent using the mass-based mixing rules given in Equations 4.17 to 4.19.

Yarranton *et al*. (2013) reported that the mass-based mixing rules with the binary interaction parameters set to zero are appropiate to predict the viscosity of heavy oils diluted with solvents with molecular weight higher than that of *n*-pentane. Non-zero binary interaction parameters are required for low molecular weight hydrocarbon solvents and carbon dioxide. The model, with interaction parameters set to zero, predicts the viscosity of bitumen/solvent pseudo-binaries with AARD and MARD of 15 and 20%, respectively.

4.3 Comparison of the EF and Generalized Walther Models

The main difference between the two models is their range of applicability. Figures 4.1 and 4.2 show the EF and GW models fit to viscosity data of saturated *n*-hexane and of cyclohexane in the high pressure region, respectively. Note how the EF model is continuous along the entire phase envelope including the critical zone whereas the GW model is only applicable for the liquid phase. The GW model systematically deviates from the data as approaching the critical point. .
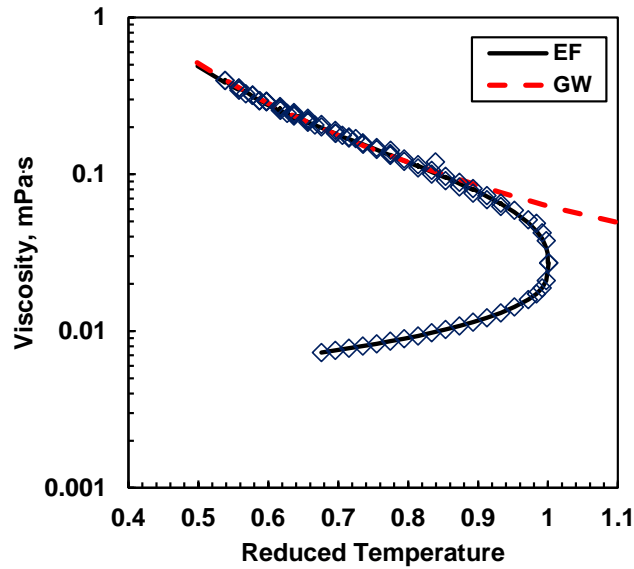
Figure 4.1. Viscosity of *n*-hexane in the phase envelope and (data from NIST, 2008).
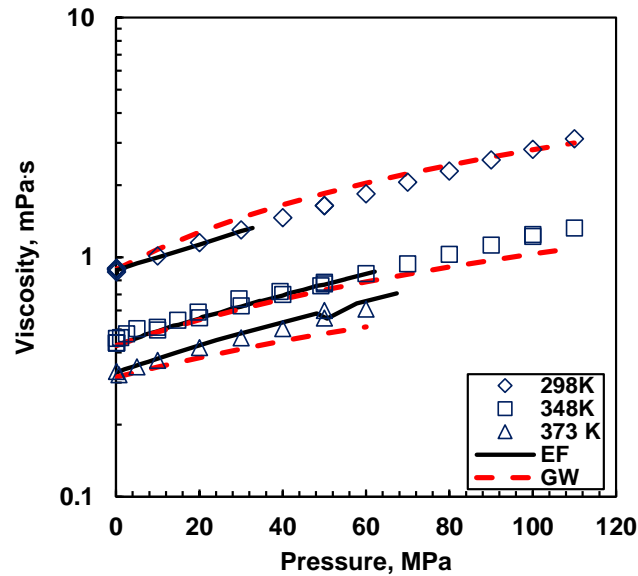
Figure 4.2. Viscosity of cyclohexane in the high pressure region (data from NIST, 2008). Note that the jumps in the correlated viscosities results from the scatter in the density data, which was not smoothed prior to applying.

Both models are simple to apply, require minimal computational time, and have simple tuning procedures. The advantage of the EF model is that it is applicable over the entire phase diagram. It has potential applications in the simulation of multi-phase downstream and upstream operations. Its principal disadvantage is that the accuracy of the calculated viscosity depends strongly on the accuracy of the density used as input. Therefore, one of the challenges is to predict density data accurately enough for EF model calculations.

The advantage of the GW model is that it does not require density data. Since most reservoir processes operate in the liquid region far from the critical point, the GW model has potential application in the simulation of those processes. The principal disadvantage of the GW model is that it is only applicable to liquids far from the critical point. To date, there is not a clear criterion to determine the temperature and pressure at which the GW model is no longer applicable.

4.4 The Extension of the EF and GW Models to Characterized Oils

The EF and GW models have been extended to predict the viscosity of crude oils characterized as a mixture of defined components and pseudo-components that represent property distribution in the fluid. The pseudo-component approach is required to predict phase viscosities when phase separations occur and components partition between the phases; for example, in solvent based *in situ* processes and partial deasphalting processes. To develop a pseudo-component based viscosity model, correlations for the pseudo-component viscosity parameters are required.

EF Model Pseudo-Component Correlations

Motahhari *et al.* (2013) developed an approach to predict the EF fluid-specific parameters c_2, and ρ_s^o for pseudo-components as a departure from *n*-alkane reference values, as follows:

$$c_2 = c_{2,REF} + \Delta c_2 \tag{4.22}$$

$$\rho_s^o = \rho_{s,REF}^o + \Delta \rho_s^o \tag{4.23}$$

where subscript "*REF*" indicate the reference property and Δc_2 and $\Delta \rho_s^o$ are the departure functions for c_2, and ρ_s^o, respectively. The reference functions are defined as:

$$c_{2,REF} = \left(9.353 \times 10^{-2} + 4.42 \times 10^{-4} M\right) \exp\left(\frac{-333.4}{M} - 1.660 \times 10^{-4} M\right) + 4.77 \times 10^{-2} \ln(M) \tag{4.24}$$

$$\rho_{s,REF}^o = \left(\frac{-4775}{M} + 3.984 M^{0.4}\right) \exp\left(-1.298 \times 10^{-3} M\right) + \frac{938.3}{1 + 8.419 \times 10^{-2} \exp\left(-1.060 \times 10^{-3} M\right)} \tag{4.25}$$

The departure functions are given by:

$$\Delta c_2 = \left(0.4925 - \frac{191900}{M^{2.67}}\right) \Delta SG^2 + \left(-0.371 + \frac{83930}{M^{2.67}}\right) \Delta SG \tag{4.26}$$

$$\Delta \rho_s^o = \frac{14640}{M^{0.67}} \Delta SG^2 + 739 \Delta SG \tag{4.27}$$

where ΔSG is defined as:

$$\Delta SG = SG - SG_{REF} \tag{4.28}$$

and:

$$SG_{REF} = 0.843593 + \frac{0.1419}{M^{0.5}} - \frac{16.60}{M} - \frac{41.27}{M^2} + \frac{2535}{M^3} \tag{4.29}$$

Note that only molecular weight and specific gravity are required to determine c_2, and ρ_s^o for each pseudo-component. The parameter c_3 for each pseudo-component is calculated from Equation 4.13. The dilute gas viscosity of each pseudo-component is calculated from Equation 4.6 using the coefficients of the n-alkane with the same molecular weight of the pseudo-component.

Finally, the EF fluid-specific parameters for the crude oil are calculated by combining those of the pseudo-components using the mass-based mixing rules. Although the viscosity mixing of pseudo-components might not be ideal, the binary interaction parameters are set to zero because no consistent method was found to predict them. The dilute gas viscosity of the mixture of pseudo-components is calculated from Equation 4.10 as recommended by Motahhari (2013). This version of the EF model predicted the viscosity of eight different dead and live Western Canada heavy oils with and average deviation of 70% (Motahhari *et al.*, 2013). Experimental density was used as input.

Walther Model Pseudo-Component Correlations

Yarranton *et al.* (2013) developed the following correlations for the Walther model parameters A and B of pseudo-components:

$$A = 9.77[1 - \exp(-0.01M)] + 0.00028M \tag{4.30}$$

$$B = 3.71[1 - \exp(-0.015M)] \tag{4.31}$$

Note that only the molecular weight is required to determine A and B for each pseudo-component. The GW fluid-specific parameters for the crude oil are calculated by combining those of the pseudo-components using the mass-based mixing rules. The binary interaction parameters are set to zero as with the EF model. The viscosibility parameters

δ_1 and δ_2 are not determined for each pseudo-component but rather for the whole crude oil. They are calculated from Equations 4.20 and 4.21 using the molecular weight of the oil as input. The GW model predicted the viscosity of four Western Canada heavy oils within 70% (Yarranton *et al*., 2013).

Issues with Characterized Oil Methodology

In the above studies, the pseudo-components were defined from GC assay data (Motahhari *et al*., 2013; Yarranton *et al*., 2013). An extrapolation is required in order to fully define the heaviest fraction which constitutes up to 70 wt% of the oil (Yarranton *et al*., 2013). This fraction contains heavy components that contribute the most to the fluid viscosity; therefore, any uncertainties in the molecular weight can cause high deviations. Typically, an exponential distribution is recommended for the extrapolation of the heaviest fraction (Whitson and Brule, 2000). The molecular weight of the heaviest fraction is then adjusted so that there is a smooth transition of the molar distribution from low to high carbon numbers. However, in most cases, the predicted molecular weight of the oil does not agree with the experimental value. In this case, both the mass fraction and the molecular weight of the heaviest fraction must be adjusted to match the molecular weight of the oil and maintain a smooth molar distribution. However, this process also introduces a great deal of uncertainty on the predicted viscosity.

To illustrate the effect of adjusting heavy fraction parameters, the viscosity of a Western Canada heavy oil WC-HO5 was modeled first by adjusting only the molecular weight and then after adjusting the heavy mass fraction and molecular weight to match the molecular weight of the oil. Viscosity, density, and GC assay data for this fluid were reported by Motahhari (2013). The heaviest fraction of the heavy oil, C30+, constitutes 70 wt% of the fluid and was extrapolated using an exponential distribution. Once fully characterized, it was divided into 5 pseudo-components. The number of pseudo-components was chosen equal to that minimum recommended by Yarranton *et al*. (2013).

Figure 4.3a shows the measured and modeled viscosity calculated after adjusting only the molecular weight of the heavy fraction (M=809 g/mol). In this case, the calculated molecular weight of the oil is 483 g/mol whereas the experimental value is 556 g/mol. The EF and GW models predict the viscosity of the fluid with an average deviation of 54% and 65%, respectively. Figure 4.3b shows the EF and GW predictions after adjusting the molecular weight and mass fraction of the heaviest fraction to match the measured molecular weight of the heavy oil. In this case, the molecular weight of the heaviest fraction was adjusted from 809 g/mol to 908 g/mol and the mass fraction was slightly increased to ensure smooth transition in the molecular weight distribution. After adjusting the heaviest fraction parameters, the average deviation of the EF model was reduced from 54 to 15% and that of the GW model increased from 65 to 84%. The results show that the predictions are highly sensitive to changes in the molecular weight of the heaviest fraction. Note that while in this example the adjustments to the heavy fraction improved the EF model prediction, in other cases the prediction becomes worse.

The above analysis highlights two issues in the previous characterization methodologies: 1) no predictive method for the binary interaction parameters between pseudo-components; 2) high uncertainty in the heavy fraction characterization. The two issues are addressed in Chapters 5 and 6, respectively, for the EF model and then in Chapter 7 for the GW model.
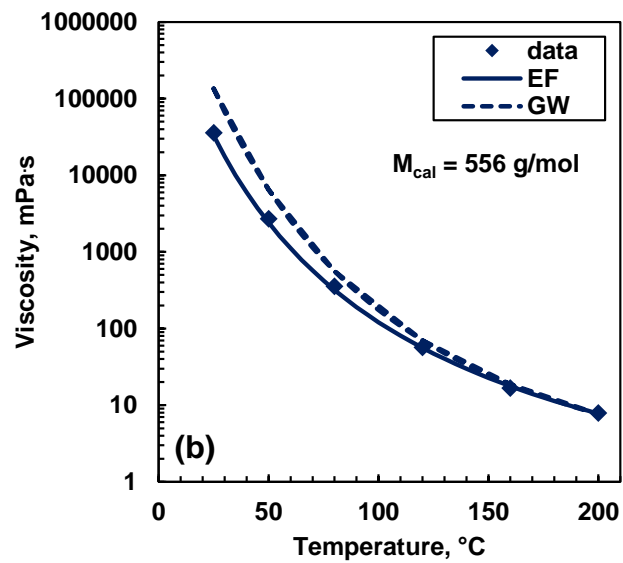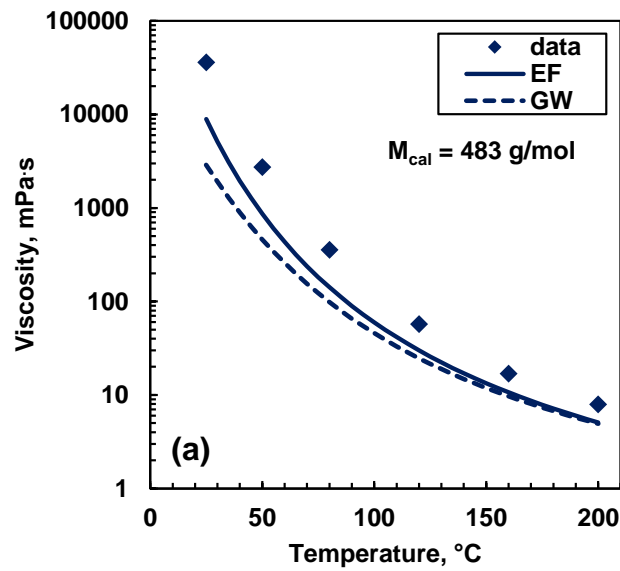
Figure 4.3. Measured and modeled viscosity of the Western Canada heavy oil WC-HO5 at 0.1 MPa (data from Motahhari, 2013): a) modeled using adjusted molecular weight of heavy fraction; b) modeled with adjusted heavy fraction molecular weight and mass fraction. M_{cal} refers to the molecular weight of the oil calculated after the extrapolation. The experimental molecular weight of the fluid is 556 g/mol.

CHAPTER FIVE: PREDICTING THE VISCOSITY OF HYDROCARBON MIXTURES AND DILUTED CRUDE OILS USING THE EXPANDED FLUID MODEL[1]

This chapter presents the development of a generalized correlation to predict the EF model viscosity binary interaction parameters. The interaction parameters are required to capture the non-ideal viscosity mixing between pairs of pure hydrocarbons and oil pseudo-components. They are also required for modeling pseudo-binaries of crude oil and solvent when the crude oil is modeled as a single component. Correlated interaction parameters are a step towards making the EF model predictive for mixtures.

A development density and viscosity dataset was compiled from the literature which included pure hydrocarbon binaries with components from different chemical families including *n*-alkanes, branched alkanes, cyclics and aromatics. In addition, experimental viscosity and density data for the pseudo-binaries of heavy oil with different types of solvents (*n*-alkanes, cyclohexane, toluene and 1-methylnaphthalene) were collected at temperatures, pressures and solvent content up to 175°C, 10 MPa and 50 wt%, respectively. The EF model parameters for each component fluid were determined by fitting the viscosity data for that fluid. The viscosity interaction parameters were calculated for each pair of components by fitting the EF model to the binary and pseudo-binary mixture data. The calculated viscosity binary interaction parameters, α_{ij}, were then correlated to specific gravity and the hydrogen-to-carbon ratio of the component fluids. Finally, the proposed correlation was assessed against a test dataset (other pure hydrocarbon mixtures from the literature, diluted crude oils, and diluted deasphalted oil from this study) and an independent dataset (diluted crude oils from the literature).

---

[1] The contents of this chapter were published in *Energy & Fuels*, 30(5), **2016**, 3575–3595.

5.1 Data Collected and Organization of Datasets

5.1.1 *Data Collected in This Study*

Viscosity and density data for the WC-B-B1 bitumen (B1 in legends) and its pseudo-binaries with ethane, propane, *n*-butane, *n*-pentane and *n*-heptane were measured in the capillary viscometer (CapVis) at temperatures from 21 to 175°C and pressures up to 10 MPa. The same device was used to measure the viscosity and density of bitumen WC-B-B2 (B2 in legends), its pseudo-binaries with *n*-eicosane, toluene, and cyclohexane, and its pseudo-ternary with heptol (a mixture of 50 wt% *n*-heptane and 50 wt% toluene).

The viscosity of CO-B-A1 (B3), ME-CV-A1 (CV1) and an oil blend, called here Blend1, were measured in the cone and plate rheometer (C&P) at temperatures up to 100°C and atmospheric pressure. Blend1 was prepared by mixing ME-CV-A1 with deasphalted WC-B-B2 (WC-B-B2-DAO) in a 30 to 70 mass ratio. The cone and plate rheometer was also used to measure the viscosity of the pseudo-binaries CO-B-A1/toluene, ME-CV-A1/toluene, ME-CV-A1/1-methylnaphthalene (MN), WC-B-B2/1-methylnaphthalene, and the pseudo-ternaries of Blend1 (ME-CV-A1/WC-B-B2-DAO) with *n*-tetradecane and with 1-methylnaphthalene. These viscosities were measured at temperatures up to 50°C and atmospheric pressure. The temperature was kept below 50°C to avoid evaporation of solvent. Density was determined in the U-tube oscillating density meter at temperatures up to 50°C and atmospheric pressure. Viscosity and density of the pseudo-binary ME-CV-A2/*n*-pentane were measured in the capillary viscometer. The cone and plate rheometer was used in cases where only a small amount of sample was available. This device requires only 2 mL of sample whereas the CapVis demands 350 mL of sample. A summary of selected physical properties of the crude oils used in this study is presented in Table 5.1.

The maximum solvent content considered in this study was 50 wt%. Higher solvent contents were not examined because most of the viscosity reduction was observed to occur at solvent contents below 50 wt%. For some solvents, such as ethane, the maximum solvent content was set lower in order to avoid the onset of asphaltene precipitation.

Density and viscosity data for one multi-component hydrocarbon mixture (10 wt% *n*-pentane, 20 wt% *n*-heptane, 5 wt% *n*-octane, 6 wt% *n*-pentadecane, 29 wt% cyclohexane, and 30 wt% toluene) were also measured using the capillary viscometer. All of the experimental data are tabulated in Appendix B.

Table 5.1. Pentane-precipitated (C5) asphaltene and toluene insoluble (TI) contents, hydrogen-to-carbon atomic ratio, specific gravity (SG) at 15.6°C, and viscosity at 20°C of the oil samples used in this study.

Sample	Legend	C5 Asphaltene Content wt%	TI Content wt%	H/C Ratio	SG @15.6°C	Viscosity @20°C mPa·s
WC-B-B1	B1	17	0.63	1.473	1.012	89,200
WC-B-B2	B2	21	1.27	1.470	1.020	437,000
CO-B-A1	B3	27	1.00	1.440	1.106	2,800,000
ME-CV-A1	CV1	3.8	0.03	1.756	0.872	18.1
Blend1	Blend1	1.4	0.009	1.624	0.953	1,085
WC-B-B2-DAO	DAO	0	0	1.568	0.989	3,050

5.1.2 *Datasets*

The samples in this study were divided into two groups: a development dataset from which the viscosity binary interaction parameter correlation was developed and a test dataset that was used to evaluate the proposed correlation. An additional dataset collected from the literature provided an independent test of the proposed correlation. Each dataset is described in detail below.

Development Dataset

This dataset includes viscosity and density data of the Western Canadian bitumens WC-B-B1 and WC-B-B2 diluted with a variety of solvents and over a wide range of conditions, Table 5.2. The bitumens B1 and B2 proceed from the same source reservoir, but with different physical properties, Table 5.1.

Viscosity and density data for 67 different pure hydrocarbon binaries (3850 data points) from the literature reported at 25°C and 0.1 MPa (Chevalier *et al*., 1990; Queimada *et al*., 2003; Al-Gherwi *et al*., 2006), were also included in the development dataset. These mixtures consisted of components from different chemical families including *n*-alkanes, branched alkanes, cyclic and aromatics, and spanned the entire range of composition.

Table 5.2. Samples, measurement method and conditions for the data measured in this study for the development dataset. MN stands for 1-methylnaphthalene. NP is number of data points.

Mixture	Method	NP	Range of Conditions		
			Temp. °C	Pressure MPa	Solvent Content wt%
B1/ethane	CapVis	18	20-175	0.1-10	5.2
B1/ propane	CapVis	39	20-175	0.1-10	7-16
B1/*n*-butane	CapVis	61	20-175	0.1-10	7-15
B1/*n*-pentane	CapVis	53	20-175	0.1-10	15-30
B1/*n*-heptane	CapVis	53	20-175	0.1-10	15-30
B1/toluene	CapVis	95	20-175	0.1-10	5-50
B2/*n*-eicosane	CapVis	54	20-175	0.1-10	5.8-25
B2/cyclohexane	CapVis	62	20-175	0.1-10	5-40
B2/MN	C&P	15	10-50	0.1	5-50

Test Dataset

The samples and conditions from this study that were included in the test dataset are presented in Table 5.3. This dataset included pseudo-binary mixtures of solvent with oils from two different geographic regions; a Colombian bitumen, CO-B-A1 (B3), and a Middle Eastern conventional oil, ME-CV-A1 (CV1). Three pseudo-ternary mixtures were also included, one with a single oil and two solvents and the others with a blended oil and one solvent. Finally, three pseudo-binary mixtures prepared with the deasphalted oil (DAO) from WC-B-B2 (B2) were added to the dataset. The sample properties and asphaltene content of the original oils were provided in Table 5.1.

97

Table 5.3. Samples, measurement method and conditions for the data measured in this study for the test dataset. MN stands for 1-methylnaphthalene and NP is the number of data points.

Mixture	Method	NP	Range of Conditions		
			Temp. °C	Pressure MPa	Solvent Content wt%
Binary – Whole Oil					
B3/toluene	C&P	18	20-35	0.1	5-10
B3/MN	C&P	12	25-50	0.1	14.3
CV2/*n*-pentane	CapVis	25	21-150	0.1-10	10
CV1/toluene	C&P	32	0-15	0.1	6-10
CV1/MN	C&P	40	10-25	0.1	2-8
Ternary - Whole Oil					
B2/heptol	CapVis	94	20-175	0.1-10	5-39
Blend1/*n*-tetradecane	C&P	28	0-50	0.1	1.8-5
Blend1/MN	C&P	28	0-50	0.1	5-8
Binary - DAO					
B2-DAO/*n*-octane	C&P	15	20-40	0.1	12
B2-DAO/*n*-dodecane	C&P	16	25-50	0.1	5-18
B2-DAO/toluene	C&P	30	20-50	0.1	2-10.2

Viscosity and density data from the literature were also included in the test dataset. The literature data included 772 data points for 8 binaries and 8 multi-component hydrocarbon mixtures (with the number of components ranging between 3 and 6)(Baylaucq *et al*., 1997a, 1997b; Dauge *et al*., 1999 ; Canet *et al.*, 2001; Boned *et al*., 2003; Queimada *et al*., 2003; Iloukhani and Rezaei-Sameti, 2005; Nhaesi and Asfour, 2005; Al-Gherwi *et al*., 2006; Wang *et al*., 2007; Silva *et al.*, 2009). These mixtures featured asymmetric components and included data at temperatures from 20 to 80°C and pressures up to 100 MPa. The six component hydrocarbon mixture measured in this study was added to this dataset.

Independent Dataset

Viscosity and density data (a total of over 1500 data points) were compiled from the literature for 5 different diluted Western Canada bitumens (4 from the Athabasca region and 1 from the Cold Lake region) and one diluted Canadian heavy oil (MacKay River), Table 5.4. The diluents included pure hydrocarbons such as *n*-pentane, *n*-hexane, *n*-decane,

n-tetradecane, toluene and xylene. The Independent Dataset includes 9 pseudo-binaries and 2 pseudo-ternaries at temperatures from 20 to 200°C, pressures up to 10 MPa, and solvent contents up to 50 wt%. The pseudo-ternaries were prepared from McKay River bitumen diluted with two different *n*-hexane/toluene mixtures: Mixture1 (75 wt% *n*-hexane) and Mixture2 (25 wt% *n*-hexane).

Table 5.4. Samples and conditions for the Independent Dataset.

Mixture	NP	Range of Conditions			Ref.
		Temp. °C	Pressure MPa	Comp. %wt	
Athabasca 1/toluene	300	25-71	0.1-10	5-50	Guan, 2013
Athabasca 1/xylene	300	25-71	0.1-10	5-50	Guan, 2013
Athabasca 2/pentane	28	50-200	1	5-10	Argüelles, 2012
Athabasca 3/decane	300	25-71	0.1-10	5-50	Nourozieh, 2013
Athabasca 4/tetradecane	300	25-71	0.1-10	5-50	Kariznovi, 2013
Cold Lake /toluene	30	25-100	0.1	1-10	Mehrotra, 1990
McKay River/hexane	140	25-71	1-10	5-35	Khan, 2014
McKay River/decane	145	25-71	1-10	35-50	Khan, 2014
McKay River/toluene	145	25-71	1-10	5-50	Khan, 2014
McKay River/Mixture1	67	25-71	1-10	5-50	Khan, 2014
McKay River/Mixture2	70	25-71	1-10	5-50	Khan, 2014

5.2 Single Component EF Fluid-Specific Parameters

The fluid specific parameters of the EF model for pure solvents used in this work were taken from Yarranton and Satyro (2009), Motahhari *et al*., (2011a) and Motahhari (2013), and are provided in Appendix B. The crude oils used here were characterized as single components for the purpose of viscosity modeling. The fluid-specific parameters of the EF model for the bitumens were determined as described in Section 4.1.2 using measured density as an input. Briefly, the EF fluid-specific parameters ρ_s^o, c_2 and c_3 are determined by fitting the model to the data. The parameter c_3 can only be determined when high pressure data is available. If only data at atmospheric pressure were available, c_3 was set to zero.

The EF fluid-specific parameters for the crude oils measured in this study (development and test datasets) are provided in Table 5.5. The sample Blend 1 was prepared by mixing ME-CV-A1 with deasphalted WC-B-B2 (WC-B-B2-DAO) in a 30 to 70 mass ratio, respectively. The sample ME-CV-A2 was obtained from the same source reservoir as sample ME-CV-A1 but with slightly different physical properties. The EF model fit the viscosity data for these fluids to within a maximum absolute relative deviation (MARD) of 17% with an overall average absolute relative deviation (AARD) of 5%.

Table 5.5. Fluid specific EF model parameters for the crude oils used in this study (development and test datasets). Parameter c_3 was only determined when high pressure viscosity data were available.

Sample	ρ_s^o kg/m^3	c_2	c_3 x10^6 kPa^{-1}
WC-B-B1	1076.9	0.522	0.15
C-B-B2	1072.1	0.505	0.16
CO-B-A1	1064.4	0.544	-
ME-CV-A1	979.6	0.397	-
ME-CV-A2*	985.6	0.380	-
Blend1	1024.2	0.450	-
WC-B-B2-DAO	1043.8	0.422	0.32

* second sample from ME-CV-A oil.

Table 5.6 lists relevant physical properties and the calculated EF fluid-specific parameters for the bitumens in the independent dataset. When the value of the hydrogen-to-carbon ratio was not known, it was calculated using the emprirical relation found by Sanchez-Lemuz (2015):

$$(H/C)_{bitumen} = 3.43887 - 1.9327 SG_{bitumen} \tag{5.1}$$

where (H/C) and SG are the bitumen hydrogen-to-carbon atomic ratio and specific gravity, respectively. The EF model fits the viscosity data for these fluids to an AARD and MARD of 6 and 18%, respectively.

Table 5.6. Physical properties and EF parameters for the bitumens in the independent dataset. Parenthesis indicate calculated H/C ratios. The parameter c_3 was only calculated when high pressure data were available.

Crude Oil	SG	H/C Ratio	Viscosity at 25°C, mPa·s	ρ_s^o kg/m³	c_2	c_3 x10⁻⁶ kPa⁻¹
Athabasca 1	1.010	(1.49)	185000	1060.4	0.5075	0.24
Athabasca 2	1.015	1.50 (1.48)	540000	1062.5	0.5168	-
Athabasca 3	1.009	(1.49)	125000	1062.1	0.5070	0.24
Athabasca 4	1.010	(1.49)	184000	1060.2	0.5064	0.21
Cold Lake	1.000	1.59 (1.51)	54500	1055.9	0.5100	-
McKay River	1.008	(1.49)	87000	1065.0	0.5290	0.1

5.3 Determination of Binary Interaction Parameters

The first step was to model the viscosity of all the mixtures presented in the Development Dataset to confirm that binary interaction parameters are required to fit the data and to determine their values. The mixture viscosities were calculated from the measured density and known pressure using the EF model with the mass-based mixing rules (Equations 4.7 to 4.9). Two approaches to calculating the mixture viscosity were evaluated: 1) ideal mixing rules, *i.e.* the viscosity binary interaction parameter was set to zero (α_{ij}=0), and; 2) non-ideal mixing rules, *i.e.* a non-zero viscosity binary interaction parameter was fitted to the mixture data. The former approach provides a baseline against which to compare the model performance with non-zero interaction parameters. The latter approach demonstrates the improvement in model accuracy when binary interaction parameters are used and provides the α_{ij} values that will be used to develop a binary interaction parameter correlation.

<u>Ideal Mixing Rules</u>

Figure 5.1 show the measured and predicted viscosity for mixtures of pure hydrocarbons. Predictions calculated assuming ideal mixing have lower deviations for mixtures of hydrocarbons that belong to the same chemical family, such as the binaries of *n*-octane and *n*-tetradecane (Figure 5.1a), but it increases for components from different chemical families, such as binaries of cyclohexane and toluene (Figure 5.1b). In general, the absolute

average relative deviation (AARD) and maximum absolute relative deviation (MARD) for the EF model predictions for pure hydrocarbons, calculated assuming ideal mixing, were 3% and 17%, respectively. A summary of the deviations of pure hydrocarbon pairs is presented in Table 5.7.
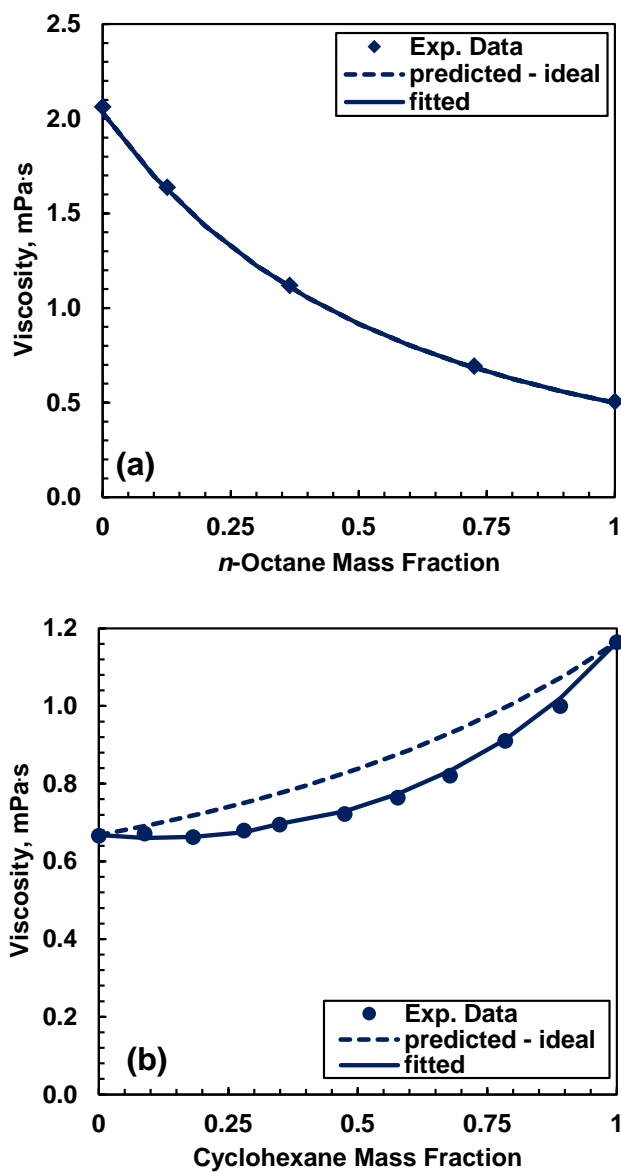
Figure 5.1. Experimental and predicted viscosities at 25°C and 0.1 MPa of pure hydrocarbon binaries: a) *n*-octane/*n*-tetradecane (Chevalier *et al*., 1990); b) cyclohexane/toluene (Silva *et al*., 2009).

Table 5.7. Summary of the deviations of the calculated viscosities of pure hydrocarbon binaries in the development data set. NB is number of binaries.

Binary	NB	Ideal Mixing Rules ($\alpha_{ij}=0$)		Mixing Rules with Fitted α_{ij}		Mixing Rules with Correlated α_{ij}	
		AARD %	MARD %	AARD %	MARD %	AARD %	MARD %
Alkane/Alkane	16	0.7	6	0.4	4	1	7
Alkane/Branched	11	2	7	0.6	2	3	8
Aromatic/Aromatic	6	1	3	0.3	1	3	9
Aromatic/Alkane	10	6	17	0.9	2	4	15
Aromatic/Cyclic	5	5	10	0.5	1	2	6
Cyclic/Alkane	5	3	5	0.7	3	1	4

Figure 5.2a shows the experimental viscosity and ideal mixing predictions for WC-B-B1 and WC-B-B2 bitumens diluted with n-alkane solvents from C1 to C20. In general, the deviations are the highest for the lower carbon number solvents where the viscosity reduction is greatest. Figure 5.2b shows the experimental viscosity and ideal mixing predictions for WC-B-B1 and WC-B-B2 bitumens diluted with n-heptane, cyclohexane and toluene. Note that the ideal mixing predictions deviates more from the experimental data as the solvent becomes more aromatic.The deviations from ideal mixing also increase as the solvent content increases and this trend is observed at all temperatures and pressures, as shown for toluene diluted bitumen in Figure 5.3. The EF model fitted to pure toluene and to the bitumen modeled as a single component are also shown in Figure 5.3 for comparison purposes. The higher deviations at higher solvent contents suggest that the ideal mixing rules do not accurately describe the mixtures. Similar results were obtained for the other mixtures and a summary of the deviations is presented in Table 5.8. The predictions are within an order of the magnitude of the measured values with overall AARD and MARD of 36% and 225%, respectively.
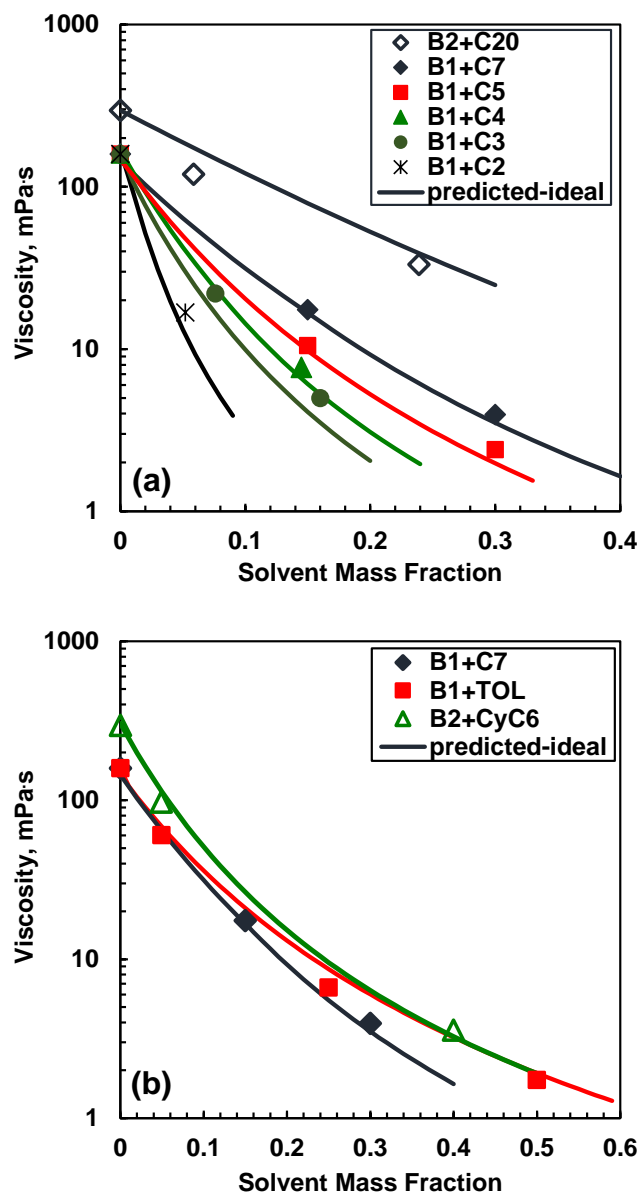
Figure 5.2. Measured and ideal mixing predicted viscosities ($\alpha_{ij} = 0$) of bitumens WC-B-B1 (B1) (closed symbols) and WC-B-B2 (B2) (open symbols) at 100°C and 5MPa diluted with: a) *n*-alkanes; b) *n*-heptane, cyclohexane (CyC6), and toluene (Tol).
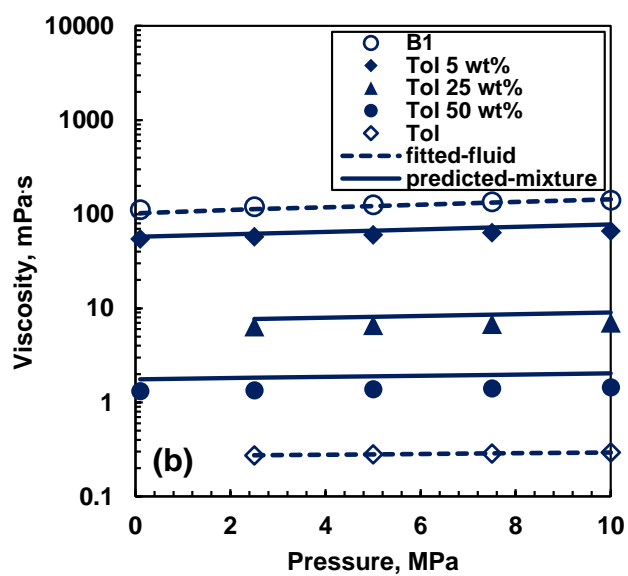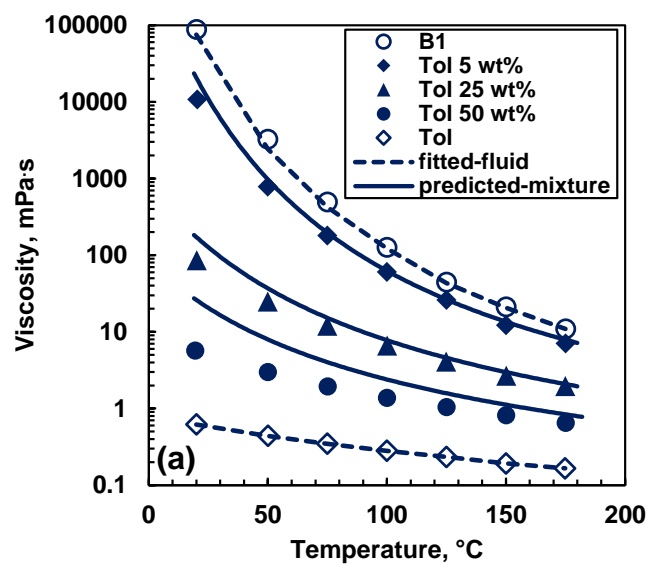
Figure 5.3. Measured and ideal mixing predicted viscosities ($\alpha_{ij} = 0$) of bitumen WC-B-B1 (B1) diluted with toluene (Tol): a) at 5MPa; b) at 50°C.

Table 5.8. Summary of the deviations of the calculated viscosities of diluted crude oils in the development dataset.

Mixture	Ideal Mixing Rules ($\alpha_{ij}=0$)		Mixing Rules with Fitted α_{ij}			Mixing Rules with Correlated α_{ij}		
	AARD %	MARD %	α_{ij}	AARD %	MARD %	α_{ij}	AARD %	MARD %
B1/ethane	20	48	-0.0520	12	32	-0.0625	18	45
B1/ propane	43	76	-0.0460	19	52	-0.0316	28	62
B1/n-butane	21	63	-0.0160	12	54	-0.0177	11	53
B1/n-pentane	21	44	-0.0154	9	24	-0.0101	13	30
B1/n-heptane	14	52	-0.0037	10	47	-0.0013	12	50
B1/toluene	33	125	+0.0211	8	30	+0.0210	7	30
B2/n-eicosane	38	126	+0.0193	11	34	+0.0127	14	51
B2/cyclohexane	17	41	+0.0077	12	27	+0.0114	13	30
B2/MN	103	225	+0.0213	0.5	1	+0.0210	1	2

Non-Ideal Mixing Rules

Since the ideal mixing rules did not accurately describe the mixture viscosities in all cases, the EF model was fit to the data using non-zero values for α_{ij}. To preserve the simplicity and generality of the correlation, the α_{ij} values were assumed to be independent of temperature, pressure, and composition for each pseudo-binary. The optimum values of α_{ij} for each component pair in the Development Dataset were calculated by minimizing the deviations of the EF predictions from the measured viscosity data of the binary or pseudo-binary mixtures.

Figure 5.1 ('fitted' lines) shows that incorporating binary interaction parameters fit to the data greatly improves the viscosity predictions for pure hydrocarbon mixtures, particularly for mixtures of species of different chemical family. Table 5.7 presents a summary of deviations for the pure hydrocarbon binaries in the development dataset comparing predictions with ideal mixing rules and with fitted α_{ij} values. Similarly, Table 5.8 shows a summary of deviations and fitted α_{ij} values for the bitumen/solvent pseudo-binaries in this study. . The use of binary interaction parameters reduced the overall AARD and MARD

for pure hydrocarbons to 0.6% and 9%, respectively (compared with 3% and 17%, respectively, with α_{ij}=0).

Similarly, the use of binary interaction parameters improved the viscosity predictions for solvent diluted bitumen, Figure 5.4. The improvement was observed at all temperatures (and pressures) as shown for toluene diluted bitumen in Figure 5.5. A single value of α_{ij} *(+0.0221)* for the pair bitumen WC-B-B1/toluene, independent of temperature, pressure and composition, was sufficient to fit all the experimental data with an AARD and MARD of 4% and 12%, respectively. A similar result was obtained for the other mixtures. The calculated α_{ij} values for the bitumen/solvent pseudo-pairs in the Development Dataset as well as the average and maximum deviations for each pseudo-binary are summarized in Table 5.8. The use of binary interaction parameters reduced the overall AARD and MARD for the diluted bitumens to 11% and 54%, respectively (compared with overall AARD and MARD of 34% and 225% with $\alpha_{ij} = 0$).

The maximum deviations were generally found at low temperature. Figures 5.3a and 5.5a show that, at low temperature, the viscosity changes significantly with small changes in temperature. The density of the fluid approaches the ρ_s^o value at lower temperatures; hence, small deviations in the input density can cause high deviations in the viscosity prediction at low temperature.
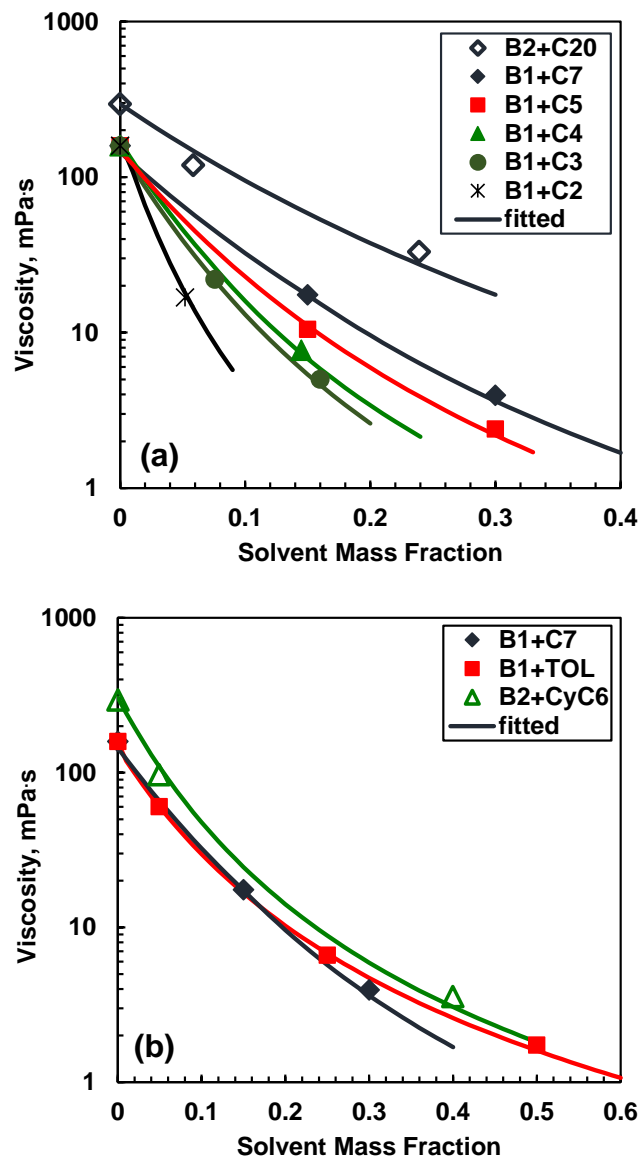
Figure 5.4. Measured and fitted viscosities (fitted α_{ij}) of bitumens B1 (closed symbols) and B2 (open symbols) at 100°C and 5MPa diluted with: a) *n*-alkanes; b) *n*-heptane, cyclohexane (CyC6), and toluene (Tol).
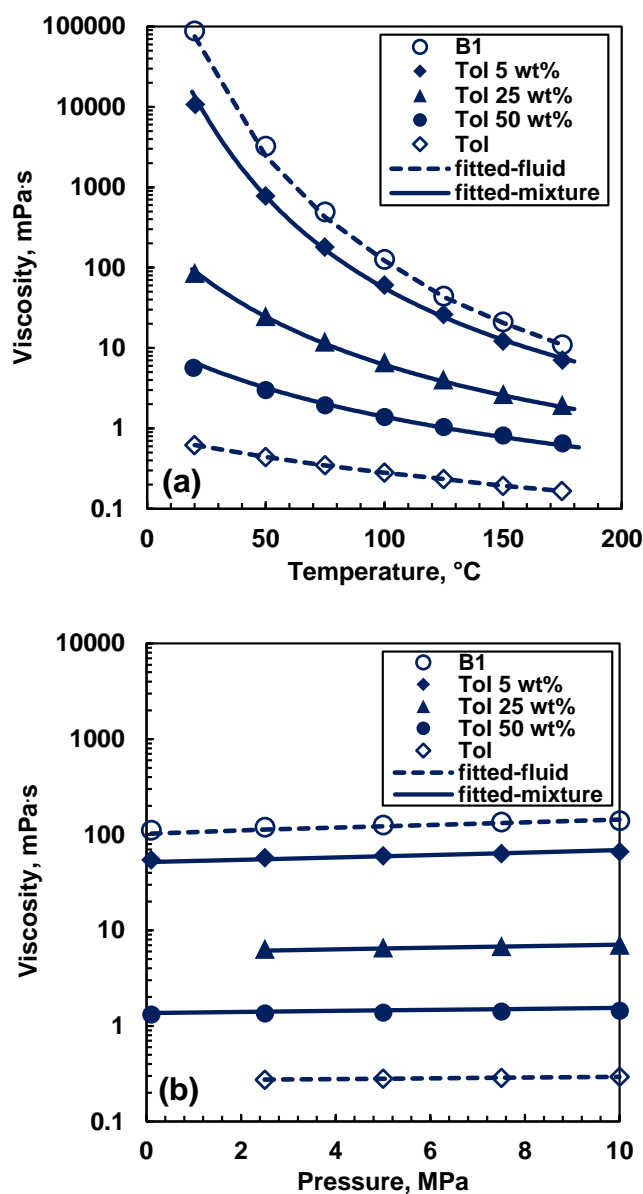
Figure 5.5. Measured and predicted viscosities ($\alpha_{ij} = +0.0221$) of bitumen B1 diluted with toluene (Tol): a) at 5MPa; b) at 100°C.

5.4 Generalization of Viscosity Binary Interaction Parameters

The second step was to develop a generalized correlation for the viscosity binary interaction parameters based on the calculated α_{ij} values for the Development Dataset mixtures. Since viscosity can be correlated to density, it is plausible that there is some relationship between viscosity binary interaction parameters and density binary interaction

parameters. Saryazdi *et al*. (2013) found that the binary interaction parameters for the density of mixtures of bitumen and solvent correlated to the normalized specific gravity defined as:

$$\Delta SG_{norm} = \frac{2\left|SG_i - SG_j\right|}{SG_i + SG_j}$$

(5.2)

where *SG* is the specific gravity of the components *i* and *j*. Therefore, the α_{ij} values were plotted against the normalize difference of specific gravity of the paired components, Figure 5.6a.
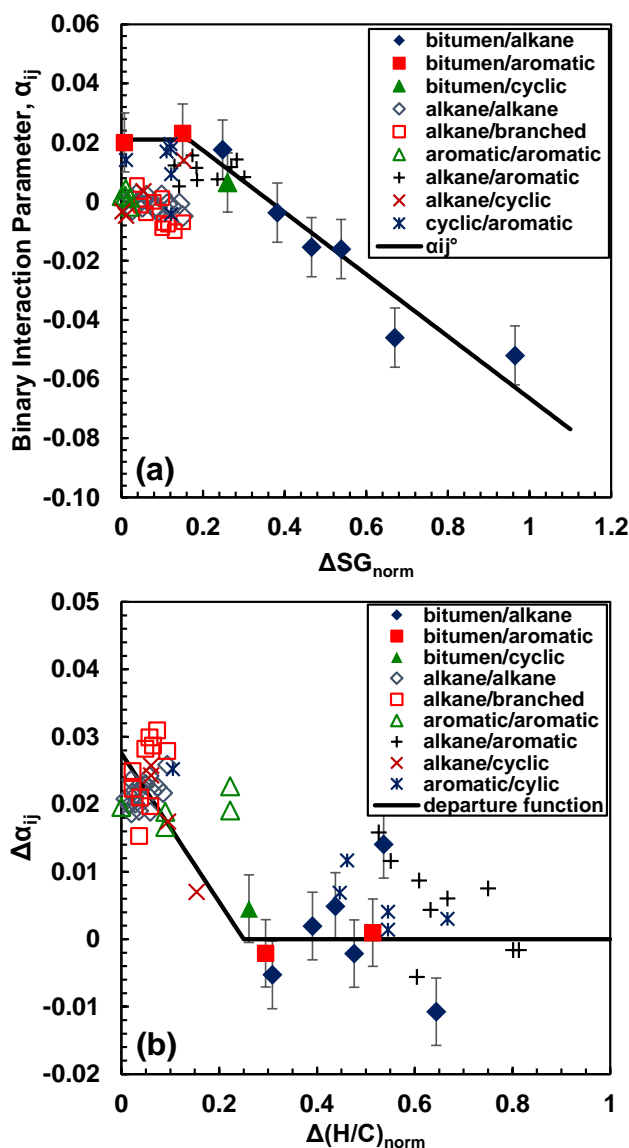
Figure 5.6. a) Viscosity binary interaction parameter, α_{ij}, versus ΔSG_{norm}. Solid and open symbols correspond to pseudo-binaries bitumen/solvent or pure hydrocarbon pairs respectively. (b) Departure term, $\Delta\alpha_{ij}$, versus $\Delta(H/C)_{norm}$ for the pseudo-binaries and binaries in the developing data set.

Figure 5.6a provides two notable observations: 1) the bitumen/solvent α_{ij} are constant below $\Delta SG_{norm}= 0.165$ and decrease linearly above this value, and; 2) the pure hydrocarbon α_{ij} appear to cluster according to differences in chemical family. These observations suggest that the viscosity binary interaction parameters can be determined from a reference

function to ΔSG_{norm} and a departure function that accounts for the differences in chemical family:

$$\alpha_{ij} = \alpha_{ij}^o - \Delta\alpha_{ij} \tag{5.3}$$

where α_{ij}^o is the reference value and $\Delta\alpha_{ij}$ is the departure function. The bitumen/solvent trend was selected as a reference function and the bitumen/solvent data of Figure 5.6a were fitted to obtain the following expression:

$$\Delta SG_{norm} \leq 0.165: \qquad\qquad \alpha_{ij}^o = 0.021 \tag{5.4}$$

$$\Delta SG_{norm} > 0.165: \quad \alpha_{ij}^o = 0.038304 - 0.10478\Delta SG_{norm} \tag{5.5}$$

Figure 5.6b shows that the departure from the reference function (the difference between the reference binary interaction parameter and the fitted value, $\Delta\alpha_{ij}$) correlates to the normalized difference in hydrogen-to-carbon ratio of the paired components defined as:

$$\Delta(H/C)_{norm} = \frac{2\left|(H/C)_i - (H/C)_j\right|}{(H/C)_i + (H/C)_j} \tag{5.6}$$

where (H/C) is the atomic hydrogen to carbon ratio of components i and j. The data in Figure. 5.6b were fitted to obtain the following expression for the departure function:

$$\Delta(H/C)_{norm} \leq 0.25: \Delta\alpha_{ij} = 0.02756 - 0.1103\Delta(H/C)_{norm} \tag{5.7}$$

$$\Delta(H/C)_{norm} > 0.25: \qquad\qquad \Delta\alpha_{ij} = 0 \tag{5.8}$$

where $\alpha_{ii} = \alpha_{jj} = 0$.

The viscosity binary interaction parameter for each pair in the Development Dataset was calculated using Equations 5.3 to 5.8 and then used to calculate the mixture viscosities. The correlated α_{ij} values for the bitumen/solvent pseudo-binaries in the Development Dataset as well as the average and maximum deviations for each pseudo-binary are summarized in Table 5.8. The overall AARD and MARD for the pure hydrocarbon binaries were only reduced slightly to 2.4% and 15%, respectively (compared with 3% and 17%, respectively, with $\alpha_{ij}=0$). However, the overall AARD and MARD for the bitumen/solvent pseudo-binaries were reduced significantly to 13% and 62%, respectively (compared with overall AARD and MARD of 34% and 225% with $\alpha_{ij} = 0$).

The improvement in accuracy with the generalized correlation was only slightly less than that obtained using fitted values (overall AARD and MARD of 12% and 54% with fitted α_{ij}).

5.5 Assessment of the Binary Interaction Parameter Correlation - Test Dataset

The validity of the proposed correlation for α_{ij} was assessed against the Test Dataset which included data for hydrocarbon mixtures, diluted crude oils, and diluted deasphalted oils. The viscosity predictions with the correlated and zero α_{ij} are compared for each type of mixture below.

Hydrocarbon Mixtures

The deviations of the viscosity predictions for the hydrocarbon mixtures in the Test Dataset are listed in Table 5.9. For binaries, the overall AARD and MARD were of 4% and 16%, respectively, when correlated α_{ij} were used compared with 6% and 21% respectively when α_{ij} was set to zero. The results demonstrate that a single correlated value of α_{ij} is sufficient to reasonably predict the viscosity of the mixtures regardless temperature, pressure, and composition, Figure 5.7. The improvement was more significant for the more asymmetric mixtures, Figure 5.7a.

For multi-component hydrocarbon mixtures, the overall AARD and MARD were 3.7% and 12%, respectively, for viscosity predictions calculated using correlated α_{ij} values compared with 4.3% and 22%, respectively, with ideal mixing rules. Binary pair interactions alone were sufficient to predict the viscosity of multi-component mixtures at any temperature, pressure, or composition shown in Figure 5.7b.
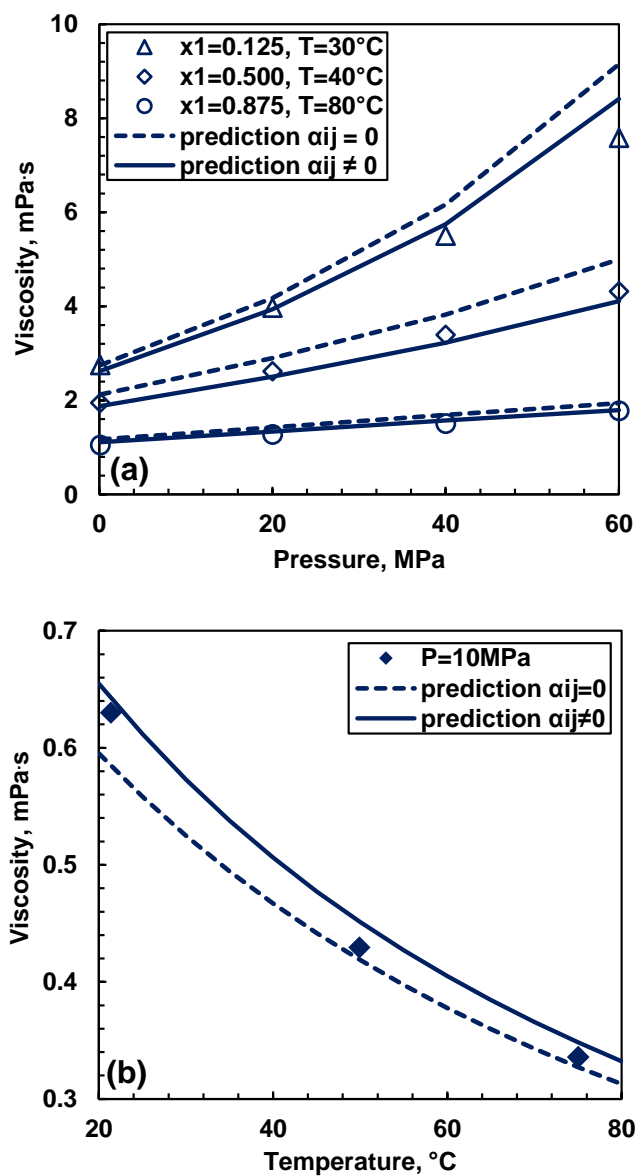
Figure 5.7. Viscosity of hydrocarbon mixtures: a) versus pressure for 1-methylnaphthalene(1)/2,2,4,4,6,8,8-heptamethylnonane(2), Canet et al. (2001); b) versus temperature for 10.5 wt% pentane, 20 wt% heptane, 5 wt% octane, 3.5 wt% pentadecane, 29 wt% cyclohexane, 29 wt% toluene, data from this study.

Table 5.9. Summary of the deviations of the calculated viscosities for the pure hydrocarbon mixtures in the test dataset. EtBz, HMN, MCyC6, HBz and CyC6 stand for ethylbenzene, 2,2,4,4,6,8,8-heptamethylnonane, methylcyclohexane, heptylbenzene and cyclohexane, respectively.

Mixture	Ideal Mixing Rules ($\alpha_{ij}=0$)		Mixing Rules with Correlated α_{ij}	
	AARD %	MARD %	AARD %	MARD %
Binary				
C7/C24	8	11	8	10
Tol/C5	10	18	9	16
EtBz/C8	2	4	2	4
EtBz/CyC6	4	8	3	6
C7/MN	0.5	1	0.8	3
CyC6/Decalin	1	3	4	6
MN/C13	7	13	1	3
MN/HMN	11	21	4	10
Multicomponent				
C8/C9/HBz	4	6	6	8
C7/MCyC6/MN	2	7	1	7
Tol/C8/EtBz/C14	5	16	3	7
Tol/C8/EtBz/C16	1	6	4	8
Tol/EtBz/C14/C16	4	8	4	8
C8/EtBz/C14/C16	3	10	4	12
Tol/C8/C14/C16	1	6	2	5
C13/HMN/MCyC6/HBz/MN	13	23	5	10
C5/C7/C8/C15/CyC6/Tol	5	12	3	7

Diluted Crude Oils

First consider the pseudo-binary test data from this study, which are summarized in Table 5.3. The two crude oils in this dataset (CO-B-A1 from Colombia, B3 in legends; and ME-CV-A1 from the Middle East, CV1 in legends) are from different geographical locations than the two Western Canadian bitumens (WC-B-B1 and WC-B-B2) used to develop the α_{ij} correlation and have significantly different density and viscosity, Table 5.1.

Figure 5.8a shows that using the α_{ij} correlation improves the accuracy of the predicted viscosity for both oils despite the difference in their properties and asphaltene content. The improvement was observed for all three solvents considered (*n*-heptane results are not

shown on the figure because the data are very similar to the toluene data). Figure 5.8b shows that the predictions are improved over the full range of temperatures and pressures considered. A summary of the deviations is presented in Table 5.10. The overall AARD and MARD were 10% and 32%, respectively, with correlated α_{ij} compared with 57% and 282%, respectively, with ideal mixing rules.

Note, the properties of the sample ME-CV-A2 (CV2) used to prepare the pseudo-binary with n-pentane were slightly different from the ME-CV-A1 sample used previously, see Table 5.5. Its viscosity was only measured at atmospheric pressure and therefore the parameter c_3 could not be determined from the data and was instead calculated from a correlation developed by Motahhari (2013) and presented in Equation 4.13. The molecular weight of the ME-CV-A2 crude oil was 475 g/mol (Powers, 2014) and the calculated c_3 was $2.8 \ 10^{-7}$ kPa^{-1}.
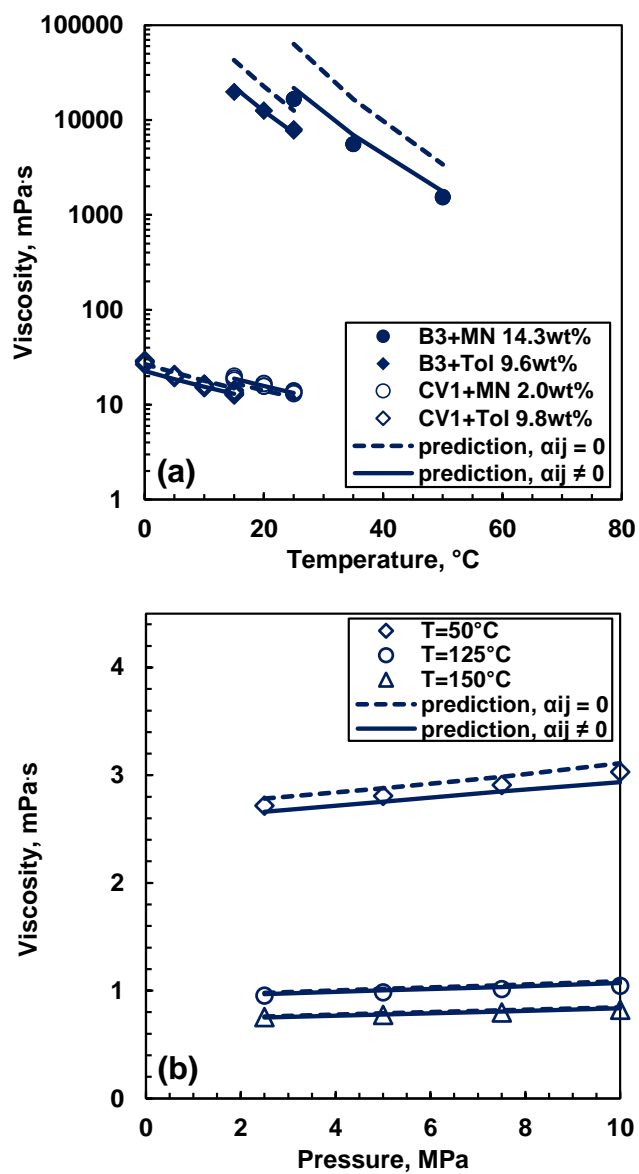
Figure 5.8. Viscosity of diluted crude oil: a) versus temperature at 0.1 MPa for CO-B-A1 (B3 in legend) and ME-CV-A1 (CV1 in legend) diluted with toluene (Tol) and 1-methylnaphthalene (NM); b) versus pressure for 90 wt% ME-CV-A2 and 10 wt% *n*-pentane.

Table 5.10. Summary of deviations of calculated viscosities of diluted crude oils in the Test Dataset.

Mixture	Ideal Mixing Rules ($\alpha_{ij}=0$)		Mixing Rules with Correlated α_{ij}	
	AARD,%	MARD,%	AARD,%	MARD,%
Binaries				
B3/toluene	76	117	10	26
B3/MN	200	282	24	32
CV2/*n*-pentane	4	9	3	6
CV1/toluene	22	18	5	13
CV1/MN	31	47	13	30
Blend1	10	36	7	16
Ternaries				
B2/heptol	18	146	10	68
Blend1/*n*-tetradecane	30	66	11	25
Blend1/MN	56	103	9	20

Viscosity and density data for three pseudo-ternary mixtures were collected at the conditions shown in Table 5.3. Recall that heptol is an equimass mixture of *n*-heptane and toluene and that Blend 1 is a mixture of 30 wt% ME-CV-A1 with 70 wt% deasphalted WC-B-B2. Figure 5.9a shows the measured and modeled viscosity for ternaries made from heptol. Figure 5.9b shows the measured and modeled viscosity for Blend1 and a pseudo-ternary made from Blend1. A summary of the deviations is provided in Table 5.10. The overall AARD and MARD for Blend1 were 7 and 16%, respectively, with correlated α_{ij} values compared with 10 and 36%, respectively, for α_{ij} set to zero. The overall AARD and MARD for the ternaries were 10 and 68%, respectively, with correlated α_{ij} values and 35 and 146%, respectively, for α_{ij} set to zero. While the use of correlated α_{ij} improve the viscosity predictions, the MARD is still quite high. The high MARD occurs at 20°C where the data are least reliable and the assumption of Newtonian behavior in the bitumen may begin to break down.
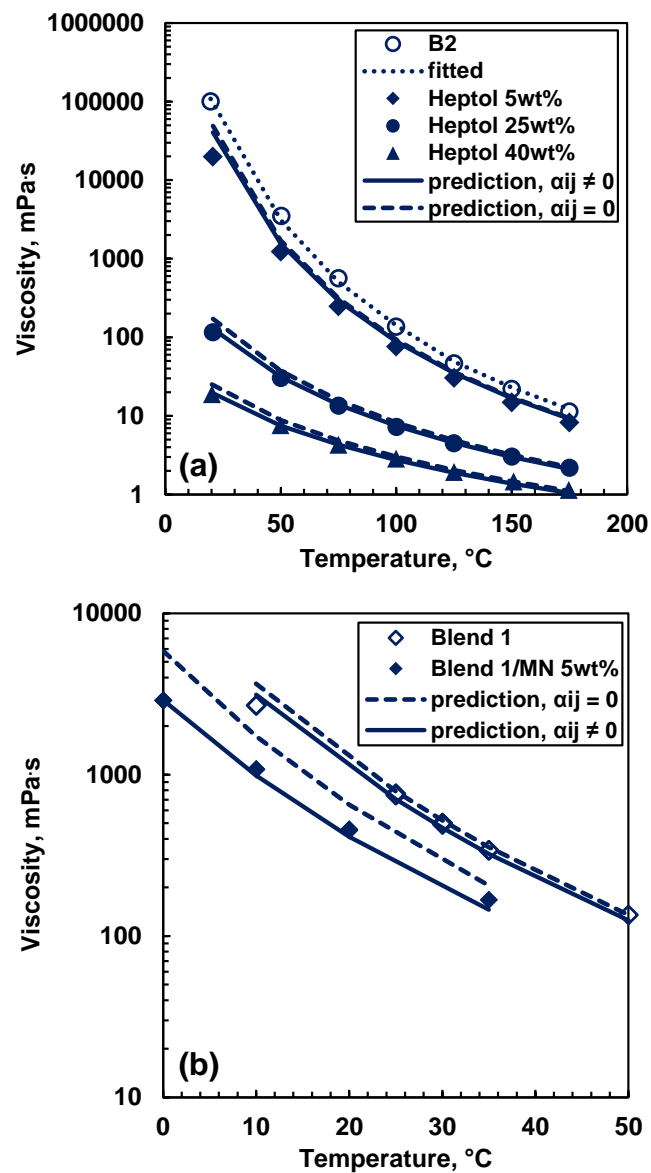
Figure 5.9. Viscosity versus temperature of: a) WC-B-B2 (B2) diluted with heptol (50 wt% heptane and 50 wt% toluene) at 10 MPa; b) Blend 1 and Blend 1/1-methylnaphthalene (MN) 5 wt% at 0.1 MPa.

<u>Deasphalted Oil/Solvent Mixtures</u>

Deasphalted bitumen has significantly lower density and viscosity than the source bitumen (see Table 5.1) and therefore provides a test of the robustness of the correlation. Also, a comparison of deasphalted versus whole bitumen viscosity demonstrates if the EF and α_{ij} correlations correctly account for the contribution of asphaltenes. Asphaltenes self-associate and may not follow the correlated trends. For example, at low temperatures, asphaltenes are known to contribute to non-Newtonian behavior (Bazyleva *et al*., 2010; Abivin *et al*, 2012) and the EF model would no longer apply. It is possible that the previous fitting to diluted bitumen data was skewed. If so, the correlation would deviate for oils with little or no asphaltenes. On the other hand, if the EF correlation with the proposed interaction parameter correlation can be used to predict the viscosity of mixtures with deasphalted bitumen, then it suggests that the contributions from asphaltene association/structure formation can be neglected over the temperatures considered in this study (that is, at temperatures above the expected range of non-Newtonian behavior).

The viscosity of mixtures of deasphalted WC-B-B2 bitumen with *n*-octane, *n*-dodecane and toluene are shown in Figure 5.10. The EF fluid specific parameters of deasphalted bitumen were determined by fitting the correlation to the undiluted deasphalted bitumen data. Then, the viscosity of the mixtures was predicted with the binary interaction parameters set to zero and with the correlated binary interaction parameters, Figure 5.10. The average and maximum deviations are summarized in Table 5.11. In general, using the correlated interaction parameters improves the viscosity prediction (overall AARD and MARD of 7% and 30%, respectively) compared with no interaction parameters (overall AARD and MARD of 12% and 40% respectively). The EF correlation provides similar quality predictions for the deasphalted oil mixtures as for the whole bitumen mixtures. Hence, it appears that any structural contributions of the asphaltenes to the viscosity can be neglected at temperatures above 21°C for bitumens and lighter oils, where non-Newtonian behavior is negligible.
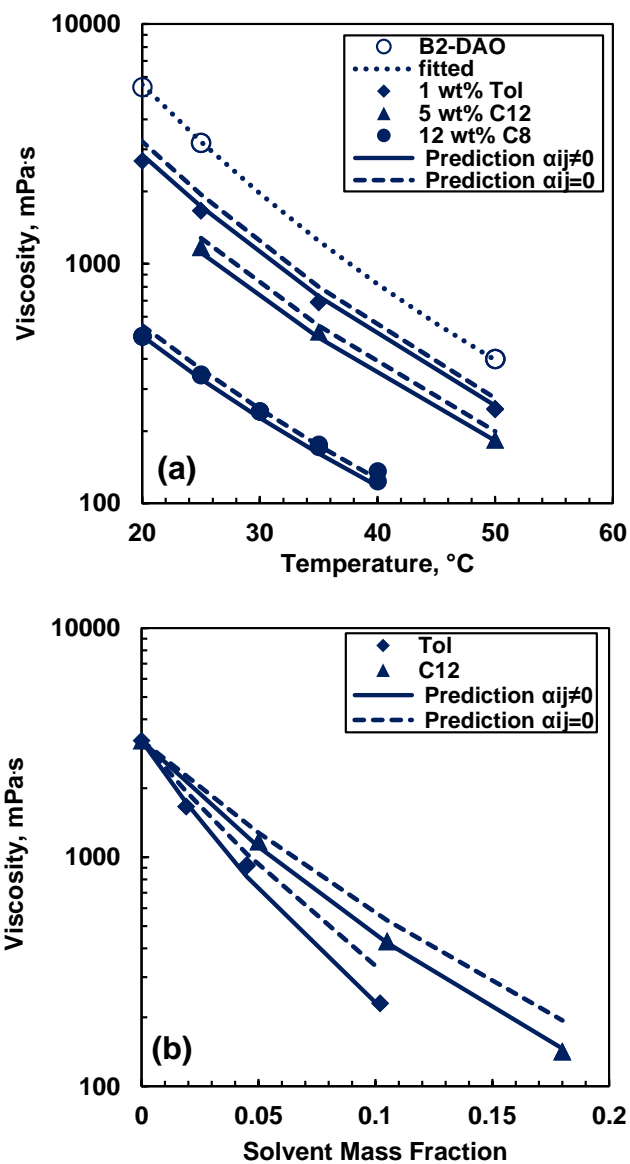
Figure 5.10. Effect of temperature (a) and dilution at 25°C (b) on the viscosity of deasphalted bitumen WC-B-B2 (B2-DAO in legends) diluted with *n*-octane (C8), *n*-dodecane (C12) and toluene (Tol) at 0.1 MPa.

Table 5.11. Summary of deviations of calculated viscosities for dilute deasphalted bitumen WC-B-B2 (B2-DAO). NP stands for number of data points.

Mixture	NP	Ideal Mixing Rules $(\alpha_{ij}=0)$		Mixing Rules with Correlated α_{ij}		
		AARD %	MARD %	α_{ij}	AARD %	MARD %
B2-DAO/octane	15	5	11	+0.0038	5	13
B2-DAO/dodecane	25	17	37	+0.0107	3	6
B2-DAO/toluene	30	13	40	+0.0210	12	30

5.6 Assessment of the Binary Interaction Parameter Correlation - Independent Dataset

The validity of the proposed correlation for the viscosity binary interaction parameters was also assessed against the Independent Dataset. A total of over 1500 data points were compiled from different diluted Western Canada bitumens and one diluted Canadian heavy oil for a variety of diluents and conditions, Table 5.4. The EF fluid-specific parameters, specific gravity and atomic Hydrogen-to-Carbon ratio for the oils in the Independent Dataset are shown in Table 5.6.

The Independent Dataset was modeling using both ideal mixing rules and mixing rules with correlated binary interaction parameters (Equations 5.3 to 5.8). A summary of the deviations is presented in Table 5.12. As expected, the use of correlated interaction parameters improved the viscosity prediction (overall AARD and MARD of 14 and 73%, respectively) compared with no interaction parameters (overall AARD and MARD of 30 and 200% respectively). As with the Test Dataset, the maximum deviations were found at room temperature where the potential error in the data is highest and the fluid may exhibit non-Newtonian behavior (Bazyleva *et al*., 2010).

Table 5.12. Summary of deviations of viscosity predictions for diluted bitumens from the Independent Dataset.

Mixture	Ideal Mixing Rules ($\alpha_{ij} = 0$)		Mixing Rules with Correlated α_{ij}	
	AARD,%	MARD,%	AARD,%	MARD,%
Athabasca 1/toluene	43	60	6	16
Athabasca 1/xylene	33	50	10	22
Athabasca 2/pentane	17	37	12	26
Athabasca 3/decane	8	35	9	38
Athabasca 4/tetradecane	24	48	9	32
Cold Lake /toluene	17	53	10	25
McKay River/hexane	19	37	16	25
McKay River/decane	22	48	24	53
McKay River/toluene	68	200	37	73
McKay River/Mixture1	17	34	16	28
McKay River/Mixture2	34	74	19	38

Finally, the viscosity model was tested on the pseudo-ternary bitumen/solvent/solvent mixtures, Figure 5.11. Both zero and correlated α_{ij} values predict the viscosity of the pseudo-ternary with similar accuracy. This result is not surprising considering that Mixture 1 is composed by 75 wt% of n-hexane and the correlated interaction parameter between this component and the McKay River bitumen has a numerical value of -0.0047, which is too small to significantly alter the viscosity predicted with ideal mixing. The other correlated interaction parameters for the pairs McKay River bitumen/toluene and n-hexane/toluene are +0.021 and +0.0098, respectively. In general, the presence of aromatic solvents in a mixture leads to a more non-ideal behavior. Hence, correlated α_{ij} values become very important in order to capture the non-ideality of the mixture to produce more accurate predictions. Therefore, it is expected that as the mass composition of toluene in the mixture increases, the deviation from ideal behaviour also increases as can be seen in Figure 5.11b with Mixture 2 (25 wt% n-hexane). Using the correlated interaction parameters again improved the viscosity prediction (overall AARD and MARD of 18 and 40%, respectively) compared with interaction parameters set to zero (overall AARD and MARD of 25 and 74% respectively). A summary of the deviations is presented in Table 5.12.
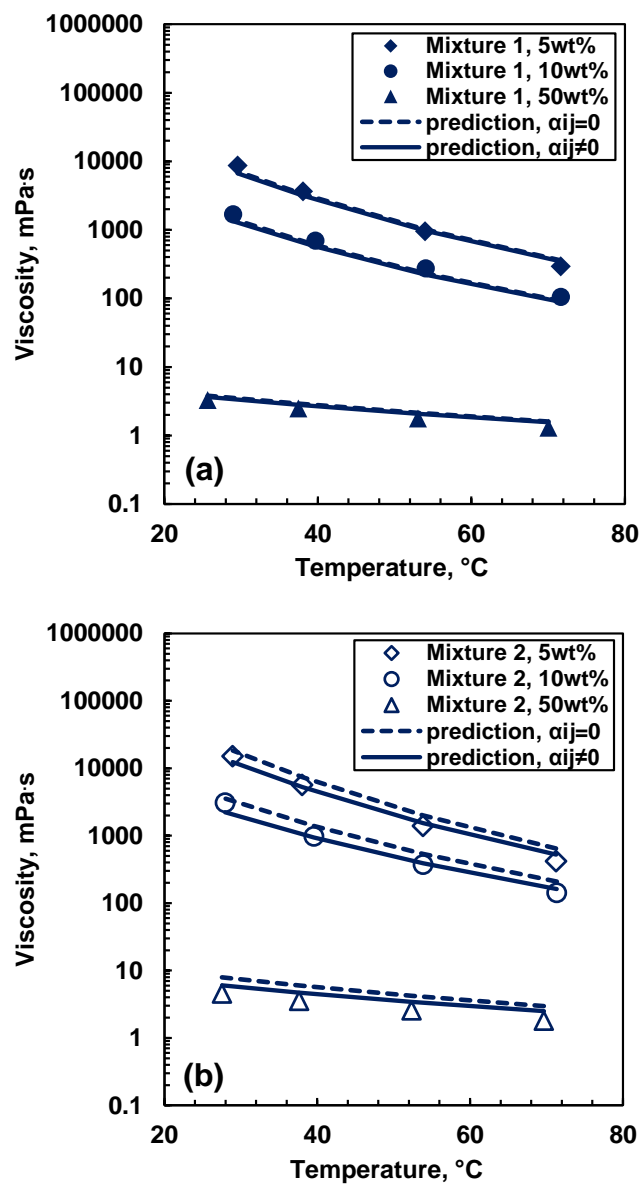
Figure 5.11. Effect of temperature and solvent content on the viscosity of dilute Mc Kay River bitumen (Khan *et al*. 2014): a) diluent: Mixture 1, *n*-hexane/toluene (75% wt *n*-hexane) at 3MPa; b) diluent: Mixture 2, *n*-hexane/toluene (25% wt *n*-hexane) at 10MPa.

5.7 Summary

The binary interaction parameter for the EF model mixing rules, α_{ij}, was found to be independent of temperature, pressure, and solvent content. In addition, binary interaction parameters were found to be sufficient to model the viscosity of multi-component mixtures.

The viscosity binary interaction parameter was correlated to the specific gravity and atomic hydrogen-to-carbon ratio of paired components. The correlation was developed from a dataset of the density and viscosity of pure hydrocarbon binaries from the literature and pseudo-binaries of bitumen and solvent from this study. The data for the bitumen/solvent pseudo-binaries were collected at temperatures from 21 to 175°C, pressures up to 10 MPa, and solvent contents up to 50 wt%. Paraffinic, cyclic, and aromatic solvents were included.

The proposed correlation was assessed on a test dataset which included pure hydrocarbon binaries and multi-component mixtures from the literature, as well as bitumen/solvent pseudo-binaries and pseudo-ternaries, and deasphalted bitumen/solvent pseudo-binaries from this study. The data for pure hydrocarbon mixtures were reported at temperatures from 20 to 80°C and pressures up 100 MPa over the entire range of composition. The data for the bitumen/solvent mixtures were collected at temperatures from 20 to 175°C, pressures up to 10 MPa, and solvent contents up to 40 wt%. The proposed correlation was also assessed on an independent dataset from the literature which included Western Canada bitumens diluted with paraffinic and aromatic solvents. These data were reported at temperatures from 20 to 200°C, pressures up to 10 MPa, and solvent contents up to 50 wt%.

Table 5.13 compares the AARD and MARD of the viscosities calculated with fitted α_{ij} and predicted with α_{ij} set to zero (ideal mixing rule) and with correlated α_{ij}. The use of correlated α_{ij} provides a modest improvement over the ideal mixing rules for the prediction of the viscosity of hydrocarbon mixtures and a significant improvement for diluted bitumens. The deviations obtained with the correlated α_{ij} are almost as low as those obtained with the fitted α_{ij}.

Table 5.13. Comparison of deviations of viscosity predictions for development, test, and independent datasets.

Dataset	Mixing Rules with Fitted α_{ij}		Ideal Mixing Rules ($\alpha_{ij}=0$)		Mixing Rules with Correlated α_{ij}	
	AARD %	MARD %	AARD %	MARD %	AARD %	MARD %
Development – Hydrocarbons	0.6	9	3	17	2.4	15
Development – Diluted Oils	11	54	36	225	13	62
Test – Hydrocarbons	1.5	12	5	23	3.7	16
Test – Diluted Oils	6	22	50	282	10	68
Independent – Diluted Oils	13	48	30	200	14	73

CHAPTER SIX: VISCOSITY OF DISTILLATION CHARACTERIZED OILS AND THEIR FRACTIONS USING THE EXPANDED FLUID MODEL[2]

This chapter presents the extension of the EF model to predict the viscosity of pseudo-component characterized crude oils based on a distillation assay. A distillation assay was chosen, rather than a GC assay, to avoid the high uncertainties related to the extrapolation required to characterize the heaviest fraction of the GC assay (see Section 4.4). The proposed methodology is expected to predict the viscosity of single and multiple phases more accurately as a function of their composition.

6.1 Introduction

For phase behavior modeling, the heavy oil composition is normally represented as a mixture of defined components and pseudo-components that represent boiling point intervals (Whitson and Brule, 2000). The mass fraction for each boiling point interval (*i.e.* pseudo-component) is assigned based on a distillation assay obtained from true boiling point distillation (ASTM, 2009), spinning band distillation (Powers, 2014), simulated distillation (ASTM, 2015), or deep-vacuum fractionation (Castellanos-Diaz 2012). Since less than 50 wt% of a heavy oil is distillable, the distillable fraction data must be extrapolated to define the heavy fractions and complete the oil characterization (Castellanos-Diaz *et al.* 2011). Once the pseudo-components are defined, the normal boiling point, specific gravity, and molecular weight of each pseudo-component must be measured or determined from correlations. Critical properties and acentric factor, can be calculated using another set of correlations. Finally, the physical properties of the crude oil are calculated by combining the properties of the pseudo-components. This approach can also be extended to viscosity modeling.

---

[2] The contents of this chapter were published in *Energy & Fuels*, 30(9), **2016**, 7134-7157.

Several viscosity models have incorporated the compositional approach into their calculation schemes. Those models were reviewed in Chapter 2, Sections 2.5.1 and 2.5.2. However, these models were developed based on experimental data collected from conventional oil distillation cuts. They have been tested on whole heavy oils but not their fractions. Heavy oils and bitumens have a greater proportion of high boiling point components than conventional oils because they have a higher content of polycyclic aromatic and naphthenic compounds (Riazi 2005). Hence, there is significant uncertainty in attempting to predict heavy oil fraction properties using correlations based on conventional oil cuts. Recently, a deep vacuum fractionation apparatus was developed and used to obtain physical samples of heavy oil distillation cuts representing approximately 50 wt% of the heavy oil (Castellanos Díaz *et al*. 2014; Sanchez-Lemus *et al*., 2014). This dataset provided an opportunity to develop and test viscosity characterization methodologies for heavy oils.

The objectives that are focus of this chapter are: 1) measure the viscosities of these heavy boiling cuts as well as lighter boiling cuts, and asphaltenes, and; 2) develop a pseudo-component based method for heavy oil viscosity prediction based on these measurements. The proposed oil characterization and viscosity modeling methodology is tested on measured viscosities of heavy oils and on similar data obtained from the literature. A simple tuning procedure is proposed for cases where at least one viscosity measurement is available.

6.2 Oil Characterization Methodology

A schematic of the characterization procedure is provided in Figure 6.1. The maltene and C5-asphaltene fractions of each oil were characterized separately as recommended by Catellanos-Diaz *et al*. (2011). The asphaltenes are characterized separately because they self-associate and their properties do not follow the same trends as the maltenes versus cumulative wt% distilled. The asphaltene fraction was treated as a single component for viscosity modeling purposes.
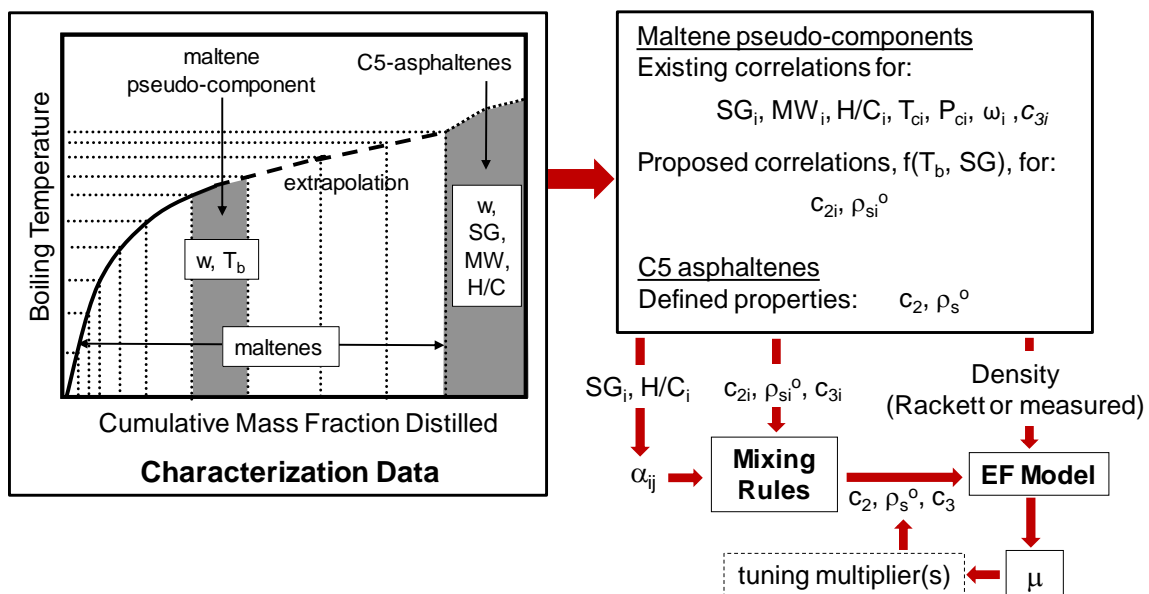
Figure 6.1. Schematic of characterization procedure for predicting crude oil viscosity.

Maltene Characterization

Unless otherwise stated, the maltene fraction was characterized from its distillation assay. Since the maltenes are not fully distillable, a Gaussian extrapolation was performed to extend the distillation curve over the entire concentration range of maltenes, as indicated in Figure 6.1. The distillation curve was divided into pseudo-components, each representing a boiling point interval of the same width (ΔT_b) as recommended by Catellanos-Diaz *et al*. (2011). The pseudo-component properties required for the viscosity parameter correlations (to be developed later) are the boiling point from the characterization as well as the specific gravity, molecular weight, and H/C ratio. The critical properties and acentric factor are also required to determine pseudo-component densities at different temperatures and pressures for input into the viscosity model.

The molecular weight and initial estimate of the specific gravity of each maltene pseudo-component were calculated using the Lee-Kesler (Kesler and Lee, 1976) and the Katz-Firoozabadi correlations (Katz and Firoozabadi, 1978), respectively. The H/C ratio for each pseudo-component in the maltene fraction was calculated using the empirical correlation

developed by Sanchez-Lemuz (2015):

$$H/C = 3.4388 - 1.932SG \qquad (6.1)$$

where *H/C* is the atomic hydrogen-to-carbon ratio and *SG* is the specific gravity. The critical temperature, critical pressure, and acentric factor of each pseudo-component in the maltene fraction were calculated from the Lee-Kesler correlations (Kesler and Lee, 1976; Lee and Kesler, 1975) as suggested by Catellanos-Diaz *et al.* (2011).

The initial specific gravities of the pseudo-components were tuned to match the density of the whole maltenes with a single constant multiplier and therefore, the predicted density of the whole maltenes was also required. The following empirical relation is proposed for cases where the experimental specific gravity of the maltenes is not available:

$$SG_{malt} = 0.8254SG_{oil} + 0.1496 \qquad (6.2)$$

where SG_{malt} and SG_{oil} are the specific gravity of the maltenes and crude oil respectively. Equation 6.2 was found to correlate to the measured SG_{mal} with an average absolute deviation of 0.5%. The maltenes were obtained from crude oils with specific gravities between 0.87 and 1.1.

C5-Asphaltene Characterization

The asphaltene fraction was represented by a single pseudo-component for viscosity modeling purposes and its EF model parameters, specific gravity, molecular weight, and H/C are the only required input properties for the viscosity model. The EF model parameters are discussed later. The H/C ratio was determined from Equation 6.1. The specific gravity and molecular weight were determined indirectly from the measured oil properties, the characterized maltene properties, and the measured mass fraction of C5-asphaltenes in the oil. First, the maltenes were characterized as described above and their bulk molecular weight and specific gravity determined. Then, the asphaltene molecular weight was calculated from a molar mixing rule and the specific gravity was determined from the following regular solution mixing rule:

$$\frac{1}{\rho_{oil}} = \sum_{i}^{n} \frac{w_i}{\rho_i} \qquad (6.3)$$

where $n=2$, i refers to maltenes or asphaltenes, ρ is the density of the component, in this case at 15.6°C, and, w is the mass fraction.

6.3 Application to Pseudo-Components

To apply the EF model to pseudo-components, the fluid specific parameters (c_2 c_3, and ρ_s^o) and the density of each pseudo-component at the specified temperature and pressure are required. Correlations for the c_2 and ρ_s^o parameters as a function of normal boiling point and specific gravity are developed later. The c_2 and ρ_s^o parameters for the single component asphaltenes are also discussed later. The pressure dependency parameter c_3 was calculated using Equation. 4.13. When predicting crude oil viscosities, the binary interaction parameters between the pseudo-components were determined with Equations 5.2 to 5.8 and the required H/C ratio of each pseudo-component was determined with Equation 6.1.

The density of the whole crude oil at a given temperature and pressure was predicted from those of the maltenes and asphaltenes at the same conditions using Equation 6.3. The density of the maltenes was determined from the pseudo-component densities using Equation 6.3 as described previously. The methods used to determine the density of the maltene pseudo-components and the asphaltenes at any given temperature and pressure are described below.

Maltene Pseudo-Components

For the maltenes produced from the precipitation of C5-asphaltenes, the density of a pseudo-component at a given temperature and pressure was determined using the Tait-COSTALD correlation (Thomson *et al.* 1982):

$$\rho_{T,P} = \rho_{T,P_o}\left[1-C\ln\left(\frac{B+P}{B+P_o}\right)\right]^{-1}$$

(6.4)

where $\rho_{T,P}$ is the density of the fluid at a temperature, T, and pressure, P, and $\rho_{T,Po}$ is the density at T and atmospheric pressure, P_o. The parameters C and B are given by:

$$C = 0.0861488 + 0.0344483\omega$$

(6.5)

$$\frac{B}{P_c} = -1 - 9.0702(1-T_r)^{1/3} + 62.45326(1-T_r)^{2/3} - 135.1102(1-T_r) + e(1-T_r)^{4/3} \quad (6.6)$$

$$e = \exp\left(4.79594 + 0.250047\omega + 1.14188\omega^2\right) \quad (6.7)$$

where ω, P_c and T_r are the acentric factor, critical pressure, and reduced temperature, respectively.

The density of the pseudo-components at atmospheric pressure, $\rho_{T,Po}$, was assumed equal to that of the saturated liquid and was calculated from the modified Rackett correlation given by (Spencer and Danner 1972):

$$v_s = \frac{RT_c}{P_c} Z_{RA}^{\left[1 + \left(1 - T/T_c\right)^{2/7}\right]} \quad (6.8)$$

where v_s is the molar volume of the saturated liquid at temperature T, T_c is the critical temperature, P_c is the critical pressure, and Z_{RA} is the Rackett compressibility factor. The density is simply the component molecular weight divided by the calculated saturated molar volume. The density of the pseudo-component at atmospheric pressure was assumed equal to that of the saturated liquid at the same temperature because the compression correction between saturation pressure and atmospheric pressure is very small (Motahhari *et al.*, 2013). The Rackett compressibility factor was determined by tuning Equation 6.8 applied at 15.6°C to fit the previously determined specific gravity. Equation 6.4 predicted the density of the maltenes of bitumen WC-B-B1 with an average and maximum deviation of 0.2% and 0.5%, respectively, at temperatures and pressures up to 175°C and 10 MPa.

C5-Asphaltenes

Due to the lack of data, it was assumed that the C5-asphaltenes were incompressible and only the temperature dependence of their density was considered. The following empirical relation was found to fit the density data calculated from the asphaltene/toluene solutions assuming that they form a regular solution (Equation. 6.3):

$$\rho_{asph} = 1000SG_{asph} - \left(6.7424 - 5.098SG_{asph}\right)\left(T - 15.6\right) \quad (6.9)$$

where ρ_{asph} and SG_{asph} are the density at temperature, T, in °C and the specific gravity of

the asphaltenes at 15.6°C, respectively. Equation 6.9 fitted the estimated C5-asphaltene density from the WC-B-B1, WC-B-A1, CO-B-A1, and EU-HO-A1 oils with average and maximum absolute deviations of 2 and 5 kg/m^3, respectively, at temperatures up to 90°C at atmospheric pressure.

6.4 Data Collected and Organization of Datasets

In order to develop correlations for the maltene pseudo-components, the density and viscosity of the distillation cuts from six heavy oils were measured. Similarly, the density and viscosity of molten asphaltenes were measured to determine the EF model parameters for the asphaltenes. Density and viscosity data for maltenes, partially deasphalted oils, and whole oils were also measured to validate the proposed approach for EF model parameters and model mixing rules. The data collected in this study are summarized below. Note, the capillary viscometer apparatus covered a broader range of temperatures and pressures than the cone and plate apparatus but required more sample and time. Therefore, most samples were run with the cone and plate apparatus with a small subset run with the capillary viscometer when sample size permitted. The data collected in this study were supplemented from the literature where applicable and organized into development and test datasets as described below.

6.4.1 *Data Collected in This Study*
<u>Whole Oils</u>

The density and viscosity of the WC-B-B1, WC-B-A2 and WC-B-A3 whole oils were measured at temperatures and pressures up to 175°C and 10 MPa using the capillary viscometer. The viscosities of the WC-B-B1, WC-B-A1, US-HO-A1, MX-HO-A1, CO-B-B1, and EU-HO-A1 whole oils were measured in the cone and plate rheometer at atmospheric pressure and temperatures up to 125°C. The whole oil viscosities of the CO-B-A1 at temperatures up to 75°C and ME-CV-A1 at 25°C were also measured in the cone and plare rheometer at atmospheric pressure. For the cone and plate measurements, fresh sample (around 2 mL) was used every time the temperature was changed to minimize the potential for light end losses. Testing at higher temperatures was avoided in the cone and

plate apparatus in order to minimize the evaporation of light components. The density of the samples from the cone and plate measurement set was measured in the Anton Paar density meter at atmospheric pressure at temperatures up to 90°C. The molecular weight and H/C ratio of the crude oils were measured by Sanchez-Lemuz (2015). The whole oil density and viscosity values are summarized in Appendix C.

Distillation Cuts

The viscosities of the WC-B-B1, WC-B-A1, US-HO-A1, MX-HO-A1, CO-B-B1, and CO-B-A1 distillation cuts (40 in total) were measured in the cone and plate rheometer at atmospheric pressure and temperatures up to 150°C. For these measurements, the sample was not replaced when the temperature was ramped because there was a limited amount of sample. The viscosity of the distillation cuts was found to be stable as long as the temperature was kept well below their boiling point.

The density of the distillation cuts of sample CO-B-A1 were measured in the Anton Paar density meter at temperatures up to 70°C at atmospheric pressure. The same apparatus was employed to measure a single density data point at 15.6°C for the other distillation cuts in order to determine their specific gravity. Densities at different temperatures were not measured due to the limited amount of sample available. The molecular weight and H/C ratio of the distillation cuts and maltenes were measured by Sanchez-Lemuz (2015). The cut properties are summarized in the Appendix C.

Maltenes

The viscosity and density of maltenes obtained from sample WC-B-B1 were measured at temperatures and pressures up to 175°C and 10 MPa using the capillary viscometer apparatus. The viscosities of the C5-maltenes obtained from samples WC-B-A1, WC-B-A2, US-HO-A1, MX-HO-A1, CO-B-B1, and CO-B-A1 were measured in the cone and plate rheometer at atmospheric pressure at temperatures up to 120°C. The densities of these maltenes were measured in the Anton Paar density meter at atmospheric pressure at temperatures up to 90°C. The maltene properties are summarized in the Appendix C.

Partially De-Asphalted Oils

WC-B-B3 bitumen was diluted with *n*-pentane at three conditions (50, 60, and 67 wt% *n*-pentane) to obtain three partially deasphalted oils with residual asphaltene contents of 16, 4, and 3 wt%, respectively. The viscosity and density of these samples were measured at atmospheric pressure and temperatures up to 75°C using the cone and plate rheometer and Anton Paar density meter, respectively. The density and viscosity data of the deasphalted oils are provided in the Appendix C.

C5-Asphaltenes

The viscosities of WC-B-B1 and CO-B-A1 C5-asphaltenes were measured in the cone and plate rheometer at temperatures between 175°C to 200°C at atmospheric pressure and at shear rates between 0.01 s^{-1} and 10 s^{-1}. The data was collected at these temperatures to ensure that the asphaltenes were completely molten (Laštovka *et al*.,2008). The shear rate range was chosen to obtain Newtonian behavior; shear thinning was observed at shear rates higher than 10 s^{-1}.

The density of the WC-B-B1 C5-asphaltenes was determined indirectly from the density of asphaltene/toluene solutions measured in the Anton Paar density meter at atmospheric pressure and temperatures between 25°C and 90°C as described previously. The densities could not be measured at higher temperatures because 90°C is the upper temperature of the apparatus. Instead, the asphaltene densities were linearly extrapolated to the temperatures at which the viscosities were measured. The measured asphaltene densities and viscosities are provided in the Appendix C.

In order to validate the density extrapolation, data were collected in the capillary viscometer for one asphaltene/toluene mixture (5 wt% WC-B-B1 C5-asphaltenes) at temperatures from 21 to 175°C (for density) and from 21 to 100°C (for viscosity) all at pressures up to 9 MPa. Note, viscosity data were not collected at higher temperatures because the viscosity was too low for an accurate measurement. The mixture densities were then predicted using the previously extrapolated WC-B-B1 C5-asphaltene densities.

Regular solution behavior was assumed and the asphaltenes were assumed to be incompressible. The density of toluene was obtained from the NIST database (2008). Figure 6.2 shows experimental and predicted density of the mixture asphaltenes/toluene. The average and maximum absolute relative deviations are 0.3% and 0.5%, respectively. Hence, the extrapolated asphaltene densities are sufficiently accurate for predicting mixture densities. These data were also used to evaluate the viscosity correlations and are provided in the Appendix C.
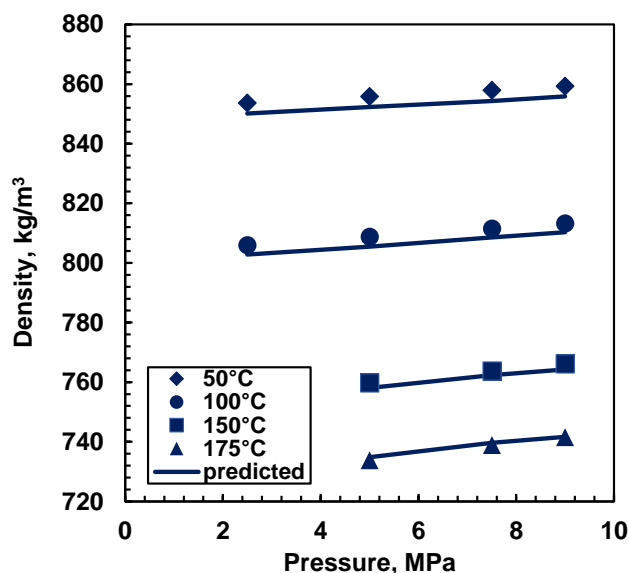
Figure 6.2. Measured and predicted density of a mixture of 5 wt% C5-asphaltenes in toluene.

6.4.2 *Datasets*

Development Dataset 1: Distillation Cuts and Pure Hydrocarbons.

This dataset was used to develop correlations for the maltene pseudo-component EF model parameters. It includes the EF model parameters, normal boiling point, specific gravity and molecular weight of the distillation cuts from this study and pure hydrocarbons. The normal boiling point and specific gravity are required for the EF model parameter correlations. The molecular weight is required to calculate the density of the distillation cuts from Equation 6.8 and is also used to determine the c_3 parameter for the EF model for high

pressure applications (Equation 4.13). The atomic hydrogen-to-carbon ratio was not included in this dataset because it is only used to calculate the viscosity binary interaction parameter in the mass-based mixing rules (Equations 5.3 to 5.8) and is not required for modeling single pseudo-components.

The EF parameters, c_2 and ρ_s^o, for the distillation cuts were calculated by fitting the correlation to the experimental viscosity data measured in this study and using the calculated density as input. The cut density was determined at any temperature using Equation 6.8 with a Rackett compressibility factor fitted to the measured density at 15.6°C. The EF model parameters for each cut are provided in the Appendix C.

The EF model parameters for each pure hydrocarbon were determined by fitting the model to measured viscosity data and using the measured density as input. The density and viscosity of pure hydrocarbons: normal alkanes (C5 to C36) and assorted pure hydrocarbons were gathered from the literature (NIST 2008; API ,1966). The assorted pure hydrocarbon group includes aromatics and alkylbenzenes (17components), fused aromatics (10 components), non-fused aromatics (11 components) alkyl cycloalkanes (33 components), branched alkanes (16 components), fused naphthenics (18 components), and non-fused naphthenics (13 components). The EF model parameters for the pure hydrocarbons are provided in the Appendix D.

Development Dataset 2: C5-Asphaltenes)
This dataset was used to determine the EF model parameters of C5-asphaltenes. It includes density and viscosity data for C5-asphaltenes from the WC-B-B1 and CO-B-A1 oils. The fitting of the EF model parameters is discussed later.

Test Dataset 1: Distillation Cuts
This dataset was used to test the proposed correlations for the EF model parameters for maltene pseudo-components. It includes literature data for over 120 distillation cuts collected from the 19 crude oils listed in Table 6.1. In most cases, the data reported for

each distillation cut were the kinematic viscosity versus temperature at atmospheric pressure, and physical properties such as normal boiling point and specific gravity. Critical temperature, critical pressure, and molecular weight were calculated from the Lee-Kesler correlations (Kesler and Lee 1976). The density of the cuts was calculated from Euation 6.8 using calculated critical properties and molecular weight, as described for Development Dataset 1. The calculated density was also used to convert the reported kinematic viscosities to dynamic viscosities. Each distillation cut was modeled as a single pseudo-component with EF model parameters determined from proposed correlations (presented later).

Table 6.1. Summary of range of selected physical properties of the distillation cuts in Test Dataset 1.

Crude Oil	Number of Cuts	SG Range	Tb Range, °C	Viscosity Range, mPa·s	Reference
Alaska North Slope	11	0.80-0.98	196-593	57-0.4	API, 2000
Altamont	11	0.76-0.88	196-649	13-0.5	API, 2000
Arab Berry	3	0.75-0.84	149-301	0.4-14	Beg *et al.*, 1988
Arabian Light	8	0.77-0.99	156-411	0.4-3.0	Kanti *et al.*, 1989
Boscan	3	0.81-0.88	182-290	0.7-4	Beg *et al.*, 1988
California	3	0.78-0.81	137-187	0.3-0.9	Beg *et al.*, 1988
Iranian Export	4	0.71-0.80	90-223	0.3-1.2	Beg *et al.*, 1988
Kern River	3	0.95-1.01	393-621	$44\text{-}1\times10^6$	Altgelt et al., 1994
Light Valley	3	0.79-0.86	159-252	0.6-2.1	Beg *et al.*, 1988
Maya	3	0.82-0.95	232-387	1-14	Altgelt et al., 1994
Midway Special	3	0.74-0.87	100-245	0.4-1.9	Beg *et al.*, 1988
Minas Sumatra	4	0.69-0.81	83-266	0.3-1.1	Beg *et al.*, 1988
Oklahoma	3	0.75-0.82	137-237	0.3-4	Beg *et al.*, 1988
Pennsylvania	3	0.74-0.70	137-237	0.3-1.5	Beg *et al.*, 1988
Safania	2	0.74-0.78	144-201	0.5-1	Beg *et al.*, 1988
Sahara	1	0.83	289	1.7-5	Queimada *et al.*, 2006
San Joaquin Valley	9	0.85-1.00	196-537	0.9-1700	API, 2000
Stabilized Arabian	3	0.73-0.78	118-196	0.4-0.9	Beg *et al.*, 1988
Waxy Crude Oil	3	0.76-0.82	124-217	0.4-1.2	Beg *et al.*, 1988
Wyoming	3	0.76-0.82	137-237	0.3-1.6	Beg *et al.*, 1988
Cracked Residue	3	0.99-1.02	404-411	205-1920	Watson *et al.*, 1935

Test Dataset 2: Maltenes

This dataset was used to assess the proposed viscosity modeling methodology for maltenes, and includes viscosity and density data of C5-maltenes obtained from the WC-B-B1, WC-B-A1, US-HO-A1, MX-HO-A1, CO-B-B1, CO-B-A1 oils (the oils from which the distillation cuts were obtained) and from the WC-B-A2 oil. The maltenes were characterized as a set of pseudo-components as described previously. The EF model parameters of each pseudo-component were determined from the proposed correlations.

Test Dataset 3: Whole and Partially De-Asphalted Oil, and Asphaltenes in Toluene

This dataset was used to assess if crude oil viscosity could be predicted from the known maltene and asphaltene contents and the EF model parameters determined for the maltenes and the asphaltenes. It includes density and viscosity data collected in this study for: 1) a whole heavy oil WC-B-B1; 2) a partially deasphalted heavy oil WC-B-B3, and; 3) an asphaltene/toluene mixture. In this case, the oils were characterized as a pseudo-binary mixture of maltenes and C5-asphaltenes. The EF parameters of the maltenes were determined by fitting their measured density and viscosity. The EF parameters for the asphaltenes are discussed later. The dataset also included the measured H/C ratios of the maltenes and the asphaltenes which were required to determine the binary interaction parameter.

Test Dataset 4: Heavy Oils and Bitumens

This dataset was used to assess the proposed viscosity modeling methodology for whole oils. It includes the density and viscosity of the oil samples used to provide the distillation cuts for the Development Dataset 1 (WC-B-B1, WC-B-A1, US-HO-A1, MX-HO-A1, CO-B-B1 and CO-B-B1). The same type of data is also included for the EU-HO-A1, WC-B-A2, WC-B-A3 and ME-CV-A1 oils. The maltenes were characterized as a set of pseudo-components and the asphaltenes as single component. The EF model parameters of the pseudo-components were determined from the proposed correlations. The parameters for the asphaltenes are presented later. The H/C ratios required to determine the binary

140

interaction parameter between the asphaltenes and maltenes were determined from a correlation (Equation 6.1) and therefore H/C data were not required for this dataset.

Test Dataset 5: Crude Oils

This dataset provided an independent test of the viscosity modeling methodology. Viscosity and density of four crude oils at atmospheric pressure was collected from the literature. The selected crude oils were chosen because a distillation essay was also reported. For these fluids, the distillation assays were performed on the entire oil, not just the maltenes, and the asphaltene content was not always reported with the data. When the asphaltene content was not reported, it was obtained from other publications on the same oil. The distillation assay was extrapolated to characterize the maltenes and the asphaltenes were treated as a single pseudo-component, as described for Test Dataset 4.

Table 6.2 presents a summary of some physical properties of the crude oils grouped in the independent dataset. The asphaltene contents of crude oils Alaska North Slope and San Joaquin Valley were not reported in the work from which distillation assay, viscosity and density were taken but rather by Mclean and Kilpatrick (1997) who used samples from the same regions. These samples have similar specific gravity and viscosity at 37.7°C as those reported in the original source. Similarly, Catellanos-Diaz *et al*. (2011) reported distillation data for the Athabasca bitumen sample while Badamchi-Zadeh *et al*. (2009) reported density and viscosity for the same bitumen sample.

Table 6.2. Selected physical properties of the crude oils in the Test Dataset 5.

Crude Oil	SG	Asph. wt%	Viscosity mPa·s	Source
Alaska North Slope	0.891	3.35	28.1 (15.6°C)	API, 2000; Mclean *et al*., 1997
Athabasca	1.007	22.7	30,090 (35.5°C)	Catellanos-Diaz *et al*. 2011; Badamchi-Zadeh *et al*. 2009
Boscan	0.993	18	485,500 (15.6°C)	EST, 2001
San Joaquin Valley	0.977	4.57	1,376 (40°C)	API, 2000; Mclean *et al*., 1997

6.5   Results and Discussion

6.5.1 *Development of Correlations for Maltene Pseudo-Component EF Parameters*

As discussed previously, the heavy oils are each characterized as a set of maltene fractions plus a single asphaltene fraction. The objective is to find correlations for the EF model parameters of the maltene cuts and to determine the model parameters for the asphaltene fraction. This section focuses on the maltenes; the asphaltenes are discussed later.

There are three EF model parameters (c_2, c_3, ρ_s^o) to be determined. The parameter c_3 was calculated from Equation 4.13 and was found to provide satisfactory predictions for the higher pressure viscosity data and therefore was not modified. The following steps were taken to develop correlations for the c_2 and ρ_s^o parameters:

1. Validate the accuracy of input density. Since the accuracy of the EF model depends on the accuracy of the input density, the accuracy of the Rackett correlation for the maltene cut densities was evaluated before proceeding to the correlations.

2. Develop a correlation for the c_2 parameter. Since the maltene characterization is based on a distillation assay, the boiling point was selected as the main input parameter. However, boiling point alone was insufficient to obtain a good correlation and specific gravity was added as a second input parameter. Note, these two physical properties roughly characterize molecular energy and size respectively, and have been widely used as inputs to crude oil property correlations (Riazi 2005).

3. Develop a correlation for the ρ_s^o parameter. The EF model is very sensitive to the ρ_s^o parameter and a sufficiently accurate correlation of ρ_s^o to the known physical properties was not found. Instead, a separate correlation was developed for a synthetic viscosity data point at a single temperature and atmospheric pressure. The EF model equation (Equation 4.1) was then rearranged to obtain an expression for ρ_s^o which incorporated the synthetic data point.

Each step is discussed in detail below. The combined correlations are then evaluated on the Development Dataset 1 and Test Dataset 1 viscosities.

Validation of Rackett Correlation Densities for Maltene Cuts

Ideally, the density of each cut would be measured at the conditions of each viscosity measurement. However, the sample volumes were limited and the experimental density data for most of the cuts in this study were only collected at 15.6°C. As discussed previously, the cut densities at any temperature were determined from the Rackett correlation tuned to match the one measured density. In order to validate this approach, the density of the six distillation cuts from the bitumen CO-B-A1 were measured from 20 to 70°C at atmospheric pressure. The correlated densities are compared to the measured values in Figure. 6.3. The average absolute relative deviation (AARD) and maximum absolute relative deviation (MARD) are 0.1% and 0.3% respectively. The EF model using the calculated densities fits the distillation cut viscosity data with an AARD and MARD of 2% and 22%, respectively, compared with an AARD and MARD of 1.8 and 20% using the measured densities. Therefore, we conclude that the densities from the tuned Rackett correlation are sufficiently accurate for the viscosity modeling at atmospheric pressure.
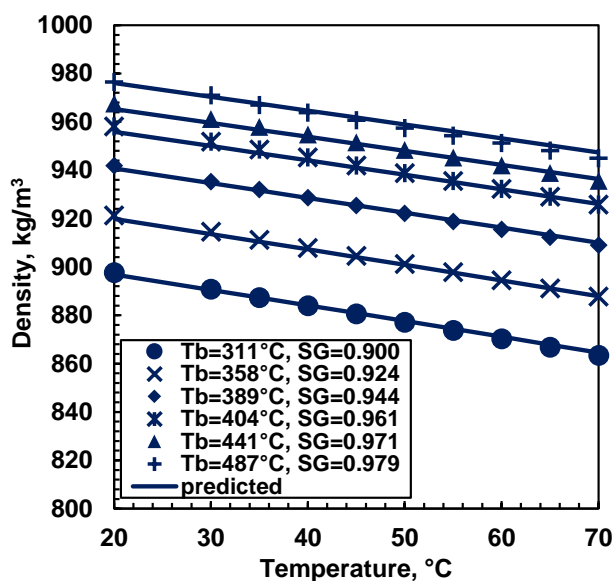
Figure 6.3. Measured and predicted densities of the distillation cuts from CO-B-A1 bitumen at atmospheric pressure.

Correlation of EF Model Parameter c_2

The symbols in Figure 6.4 shows the c_2 parameters of Development Dataset 1 versus normal boiling point (T_b). Both distillation cut and pure hydrocarbon compound parameters are shown and the parameters for the distillation cuts are similar to the majority of the aromatic compounds, in agreement with the high aromatic content that have been reported for heavy oil distillation cuts (Altgelt and Boduszynski, 1994). In general, the c_2 parameter increases monotonically for each well-defined chemical family but decreases with aromaticity when moving along a constant boiling point line. Hence boiling point alone is insufficient for correlating this parameter. One approach to improve the correlation is to choose a reference family for a correlation of c_2 to T_b for this one family, and then determine a departure function based on a second property such as specific gravity. The c_2 parameter is then given by:

$$c_2 = c_2^o - \Delta c_2 \tag{6.10}$$

where $c_2{}^o$ is the reference value and Δc_2 is a departure value which captures the difference of c_2 values between a component and the reference substance with the same normal boiling point.

Normal alkanes have been used as a reference system to predict viscosity, critical properties of distillation cuts (Twu 1984,1985), and EF fluid-specific parameters for pseudo-components (Motahhari *et al*., 2013). However, as the normal boiling point and molecular weight increase, the properties of the normal alkanes highly deviate from those of the pseudo-components and the prediction of their properties becomes challenging. We found that better results were obtained when the distillation cuts were used as the reference system rather than pure hydrocarbons. This system is not a true chemical family but represents the monotonic polycyclic aromatic progression typical of heavy petroleum fluids.

The reference function was obtained by fitting the distillation cut data from Development Dataset 1. Note that the viscosity and specific gravity of light distillation cuts (and hence their EF model parameters) are similar to those of *n*-alkanes and; therefore, the reference

function was constrained to approach *n*-alkane values at low boiling points ($c_2 \to 0.199$ as the boiling point goes to 0°C). The proposed reference function is given by:

$$c_2^o = 1.882 \times 10^{-3} \exp\left(0.0058855 T_b\right) + 0.3674 T_b^{-0.1177} \qquad (6.11)$$

where T_b is the normal boiling point temperature in K. The solid line in Figure 6.4 shows the reference function. While this correlation alone may be sufficient for these heavy, highly aromatic distillation cuts, it will likely deviate for lighter, more paraffinic cuts. Light paraffinic cuts have properties similar to mixtures of alkanes with relatively small amounts of cyclic and aromatic compounds. Figure 6.4a shows that the correlation does not accurately represent the alkanes and cyclics. Therefore, a departure function was developed based on specific gravity in order to account for differences in cut chemistries.
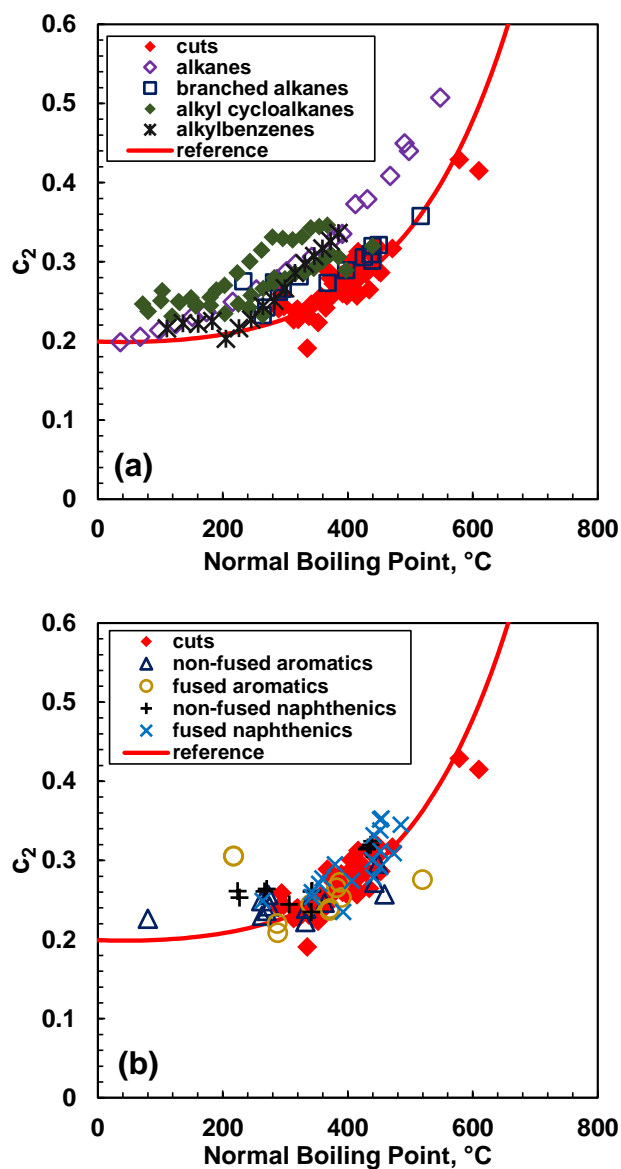
Figure 6.4. Parameter c_2 versus normal boiling point for Development Dataset 1: (a) alkanes, branched alkanes, alkyl cycloalkanes and alkylbenzenes; (b) non-fused aromatics, fused aromatics, non-fused naphthenics and fused naphthenics. Distillation cuts are included in both (a) and (b).

The first step in developing the departure function is to find an expression for the specific gravity of the reference distillation cuts. The measured specific gravities of the distillation cuts were correlated to their normal boiling point with the following two constraints. First, the reference specific gravity must tend to that of normal alkanes at low boiling point

because the reference function for c_2 tends to the n-alkanes at low boiling points. Hence, the specific gravity of the reference family must also tend to that of n-alkanes to ensure that the value of the departure function is zero. Second, at high boiling points, the specific gravity approaches an asymptote. This maximum value was set equal to the average measured specific gravity of the C5-asphaltenes from the WC-B-B1 bitumen ($SG_{max}=1.098$). This specific gravity is comparable to those reported elsewhere (Rogel and Carbognani, 2003; Barrera et $al.$ 2013). The constrained fitted equation for the reference specific gravity is given by:

$$SG^o = 1.098\left[1 - \exp\left(-0.00148T_b^{1.1128}\right)\right] \tag{6.12}$$

where SG^o is the specific gravity of the reference distillation cut. As indicated by the line in Figure 6.5a, the proposed correlation fits the specific gravity data of the reference distillation cuts with an AARD and MARD of 0.8% and 2%, respectively.
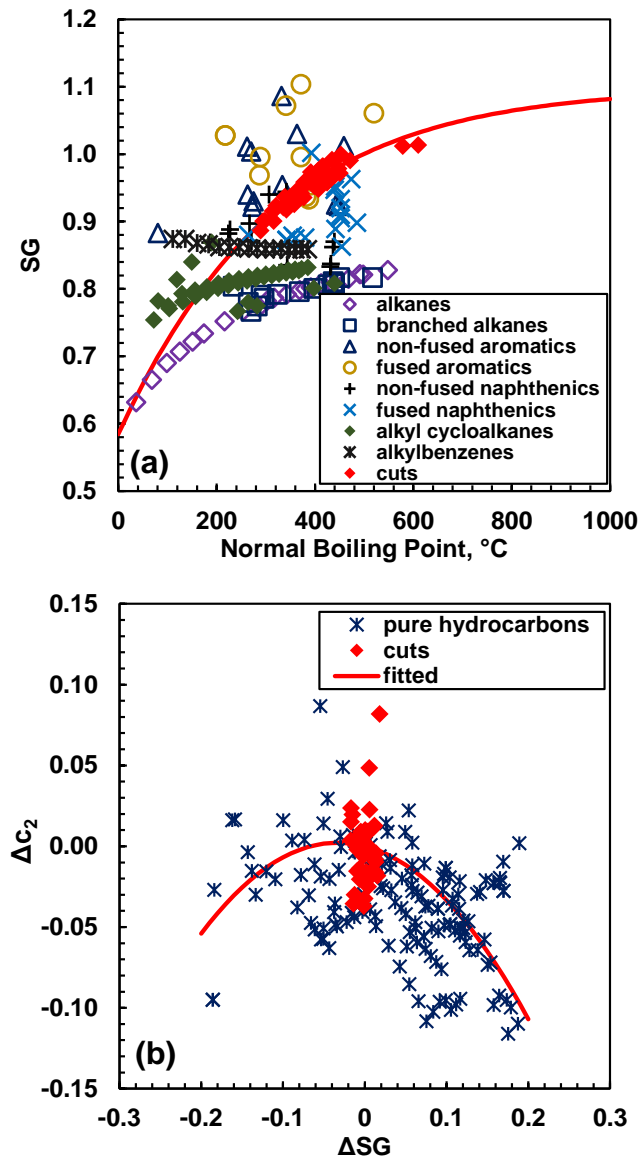
Figure 6.5. The two parts of the correlation for the c_2 parameter: a) the reference function shown with the specific gravity of the cuts and pure hydrocarbons in Development Dataset 1; b) Δc_2 versus ΔSG.

The final step is to determine the departure values, ($\Delta c_2 = c_2^o - c_2$ and $\Delta SG = SG^o - SG$) and find a correlation between them. The following equation was found to fit the data to within $\pm 30\%$, Figure 6.5b:

$$\Delta c_2 = -2.01417 \Delta SG^2 - 0.1324 \Delta SG \qquad (6.13)$$

The complete correlation for c_2 is then given by Equations 6.10 to 6.13. The deviation between fitted and correlated c_2 parameters for Development Dataset 1 is shown in Figure 6.6. Although the deviations in the calculation of Δc_2 seem to be high, the actual difference between fitted and calculated c_2 is not enough to cause large deviations in the viscosity. The AARD and MARD in the predicted c_2 values were 10 and 30%, respectively for pure hydrocarbons, including n-alkanes, and 5 and 20% respectively for the heavy oil distillation cuts. Note the correlation was developed using the data presented in Figure 6.4 and its validity for boiling points lower than 0°C was not investigated.
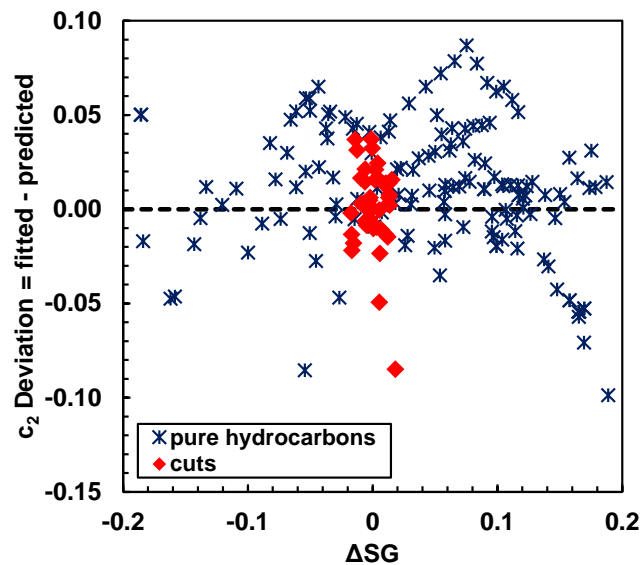
Figure 6.6. Relative deviation of predicted c_2 parameter versus ΔSG for Development Dataset 1.

Correlation of EF Model Parameter: ρ_s^o

As mentioned, the EF correlation is highly sensitive to the ρ_s^o value; therefore, the uncertainty in ρ_s^o must be kept to a minimum to produce accurate modeling results. Various forms of direct correlations were attempted for this parameter but all gave unacceptably high errors. Instead, an indirect approach was developed where ρ_s^o is calculated with the EF model (using the correlated c_2 parameter) from a single viscosity data point at a reference temperature and atmospheric pressure, as follows:

$$\rho_s^o = \rho_T \left\langle 1 + \ln\left[1 + \frac{c_2}{\ln\left(1 + \frac{\mu_T - \mu_G}{0.165}\right)} \right] \right\rangle^{\frac{1}{0.65}} \tag{6.14}$$

where ρ_T and μ_T are the density and viscosity in kg/m^3 and mPa·s, respectively, at a reference temperature T and μ_G is the dilute gas viscosity. The atmospheric pressure viscosity data point, μ_T, can be measured or predicted using a correlation. Note that Equation 6.14 is the EF model written explicitly in terms of ρ_s^o.

The Abbott (1971), Twu (1985), and API (1997) correlations were assessed for the prediction of μ_T. The output of the correlations is the kinematic viscosity and the density is required to determine the dynamic viscosity. The inputs in all cases are the normal boiling point and specific gravity, and the correlations only predict the viscosity at two temperatures, 37.7°C and 98.8°C, at atmospheric pressure. The temperature of 37.7°C was selected as the reference temperature. To test the accuracy of these correlations, the predicted viscosity data point at 37.7°C was compared to the measured value for the heavy oil distillation cuts of the Development Dataset 1. In general, the viscosity of the heavy oil distillation cuts at 37.7°C was predicted with average deviations of 100%, 60%, and 70% with the Abbott, Twu, and API correlations, respectively. The high deviations are not surprising considering that the correlations were developed based on conventional oil distillation cuts.

The Twu correlation was modified in order to improve the accuracy of the viscosity prediction at 37.7°C for heavy cuts. In the original correlation, the viscosity of a cut is calculated as a departure from the viscosity of *n*-alkanes. Here, the viscosity at 37.7°C of a cut or pure hydrocarbon is calculated as a departure from the viscosity of the cuts in the Development Dataset 1 at the same temperature at atmospheric pressure. Hence the experimental viscosity of the heavy oil cuts at 37.7°C was used to develop the reference function defined as:

$$\log\left[\log\left(v_{37.7}^o + 1\right)\right] = (0.0036T_b - 2.0942)0.95^{T_b/200} \tag{6.15}$$

where $v_{37.7}{}^o$ and T_b are the reference kinematic viscosity in cSt at 37.7°C and the normal boiling point in K respectively. Note that the form of Equation 6.15 is different from the original reference function proposed by Twu at 37.7°C. Figure 6.7 shows that the new reference function is consistent with the original correlation for light cuts but follows the trend of the heavy cut viscosities.

The departure function was retuned against the data collected in this study for pure components to obtain the following equations:

$$\ln\left(v_{37.7} + \frac{250}{T_b}\right) = \ln\left(v_{37.7}^o + \frac{250}{T_b}\right)\left(\frac{1+2f}{1-2f}\right)^2 \tag{6.16}$$

$$f = -|x|\Delta SG + 53.2315\frac{\Delta SG^2}{T_b^{0.5}} \tag{6.17}$$

$$x = 3.7012 - \frac{73.02779}{T_b^{0.5}} \tag{6.18}$$

where $v_{37.7}$ is the kinematic viscosity in cSt of the distillation cut at 37.7°C and atmospheric pressure. *ΔSG* (*ΔSG = SGᵒ-SG)* is determined as described in the previous section with reference specific gravity, *SGᵒ*, calculated from Equation 6.12. The AARD and MARD of modified correlation for the viscosity at 37.7°C are 29% and 90%, respectively, for the pure hydrocarbons and 35% and 95%, respectively, for the distillation cuts in Development Dataset 1. Note that the correlation presented here is applicable to cuts and pure

151

hydrocarbons. The original correlation by Twu has an extra set of equations for pure hydrocarbons.
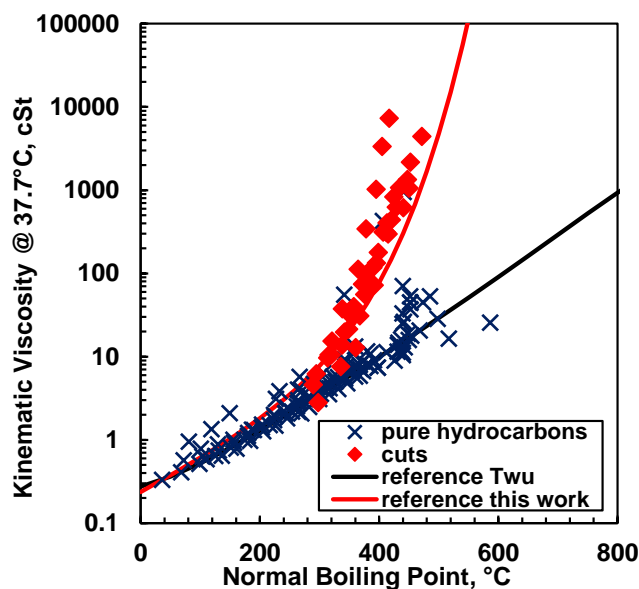
Figure 6.7. Kinematic viscosity at 37.7°C of heavy oil distillation cuts and pure hydrocarbons from Development Dataset 1 versus normal boiling point. The new reference kinematic viscosity function (this study) as well as original reference kinematic viscosity developed by Twu (1985) are also shown.

Testing on Distillation Cuts

The proposed correlations were used to calculate the EF model parameters and predict the viscosity of the distillation cuts in Development Dataset 1 and in Test Dataset 1. Note that the densities of the distillation cuts were calculated from the modified Rackett correlation after tuning to match the specific gravity of the cut, as described previously. The viscosities of the distillation cuts from Development Dataset 1 were "predicted" with an overall AARD, MARD and bias of 49, 106 and -28%, respectively. The viscosities for the distillation cuts from Test Dataset 1 were predicted with an overall AARD, MARD and bias of 24, 130, and -10%, respectively, Table 6.3. A typical example of the predicted cut data is provided in Figure 6.8.

The deviations are comparable to the errors in estimating the viscosity at 37.7°C indicating that the single point viscosity prediction (Equations 6.15 to 6.18) is the main source of error

in the overall correlation. In general, the EF model with correlated parameters tends to under-predict the viscosity of heavy cuts with higher deviations for high boiling point cuts, as indicated in Figure 6.9a. Although the correlation was developed from heavy oil distillation cut data, it provided better AARD for the lighter cuts that made up the test dataset. It appears that the departure function based on pure hydrocarbon data is able to compensate for the different chemistry of the lighter cuts compared with the heavier cuts, as indicated in Figure 6.9b.

Table 6.3. Summary of the deviations and bias in the predicted viscosity of the distillation cuts from Test Dataset 1.

Crude Oil	AARD %	MARD %	Bias %
Alaska North Slope	33	130	+21
Altamont	31	100	+27
Arab Berry	8	31	+3
Arabian Light	10	47	+4
Boscan	22	38	+22
California	14	29	+13
Iranian Export	28	44	+23
Kern River	62	83	-62
Light Valley	32	46	+32
Maya	16	29	+7
Midway Special	20	51	-16
Minas Sumatra	25	36	+25
Oklahoma	28	58	+28
Pennsylvania	24	50	+24
Safania	20	35	+20
Sahara	8	12	-8
San Joaquin Valley	16	63	-5
Stabilized Arabian	28	40	+28
Waxy Crude Oil	33	41	+33
Wyoming	16	28	+16
Cracked Residue	22	35	-20
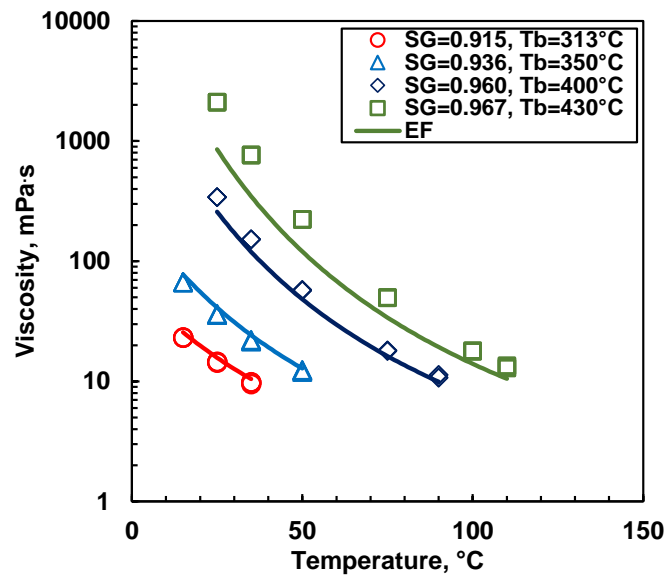
Figure 6.8. Measured and predicted viscosities for the cuts obtained from WC-B-A1 bitumen at atmospheric pressure.
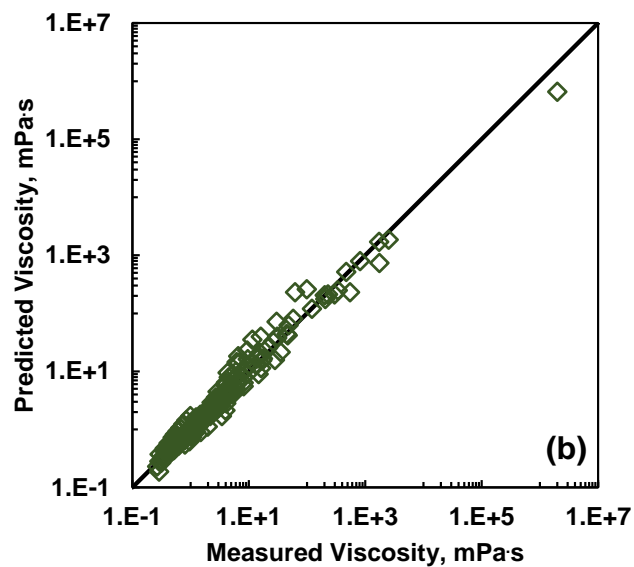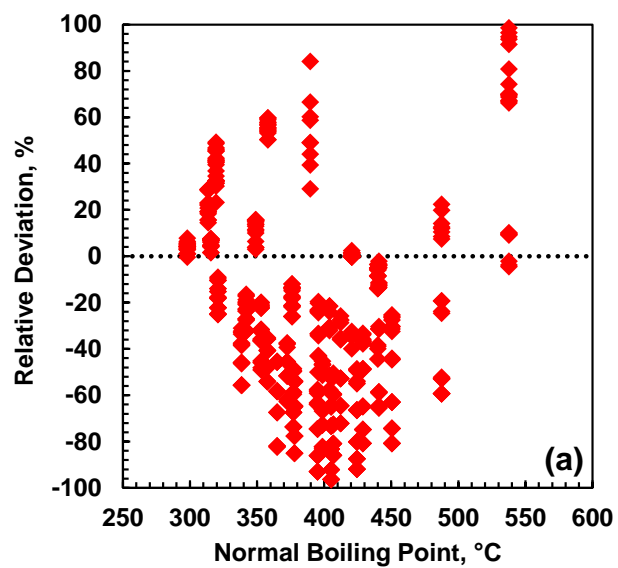
Figure 6.9. Illustration of errors in the predicted viscosities of distillation cuts: a) relative deviation (100x(Predicted- Measured)/Measured) versus normal boiling point for the cuts in Development Dataset 1; b) predicted versus measured viscosities for Test Dataset 1.

Testing on C5-Maltenes

Another test for the proposed methodology is the ability to predict the viscosity of the maltenes from a pseudo-component characterization. This prediction depends on both the correlations for the pseudo-component EF model parameters and the EF model mixing rules. The proposed methodology was tested on the maltenes in Test Dataset 2. The measured and predicted viscosities for maltenes are shown in Figure 6.10 as an example. Overall, when experimental density was the input to the viscosity model, the viscosity of the maltenes was predicted with an overall AARD, MARD, and bias of 62, 90, and -62%, respectively. When predicted density was the input, the overall AARD, MARD, and bias were 59, 91, and -55%, respectively, Table 6.4. In contrast, when the EF correlation was fitted directly to the measured viscosity, the overall AARD, MARD and bias were 2, 11, and -1%, Table 6.5.

The predictions are significantly less accurate than directly fitting the data and, in general, the viscosity of the maltenes is under-predicted. The density prediction is not the main source of error because the results with measured and predicted densities are similar. The magnitude of the error is similar to the errors observed when predicting the cut viscosities. Hence, much of the error can be attributed to the EF parameter correlations. It is also possible that binary interaction parameters used to predict the maltene viscosity were incorrect; however, the values required to fit the maltene viscosity were unrealistically large compared to the binary interaction parameters for all other similar materials (Ramos-Pallares *et al*. 2016a). The maltene tests indicate that the errors in predicting the viscosity of a whole oil without any tuning could be in the order of 60%. While this potential error is significant, the untuned model captures the correct trends with pressure and temperature, suggesting that tuning to a single data point should be sufficient to produce an accurate viscosity model.
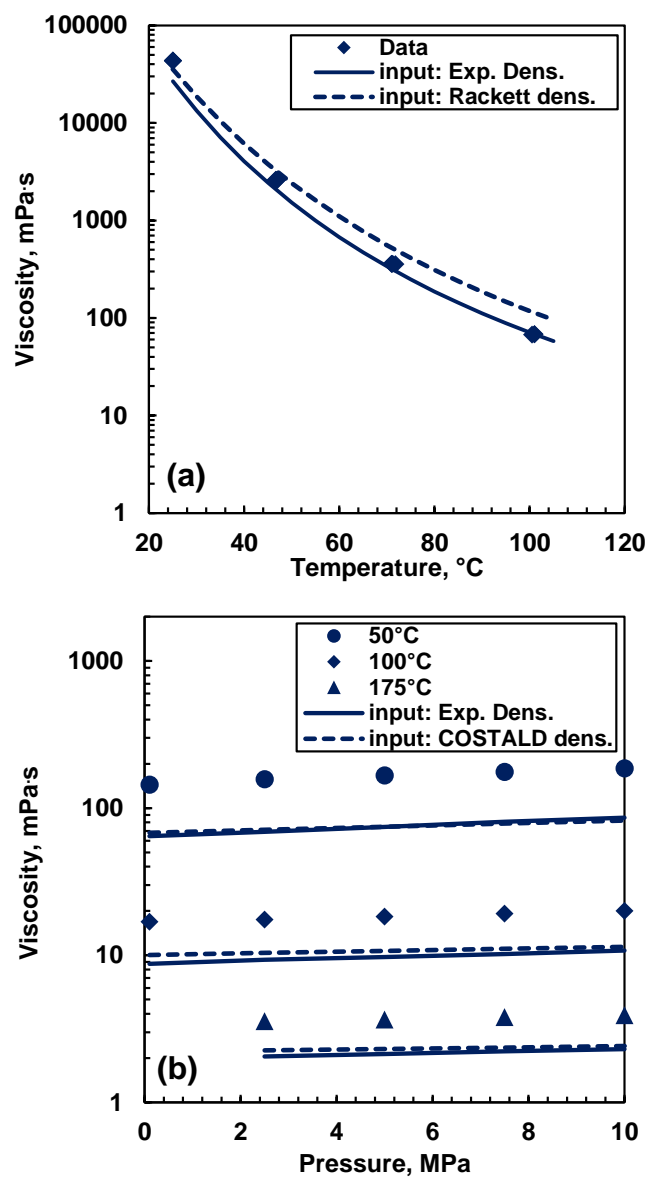
Figure 6.10. Measured and predicted viscosity of C5-maltenes: a) WC-B-A2-DAO at atmospheric pressure; b) WC-B-B1-DAO. The solid line is the EF with the measured density (Exp. Dens.) as input and the dashed line is the EF with predicted density as input. DAO stands for deasphalted oil. Recall that COSTALD becomes Rackett correlation at atmospheric pressure.

Table 6.4. Calculated EF correlation parameters for C5-maltenes, and the average and maximum relative deviation and bias of the predicted viscosity with experimental and predicted density as input. DAO stands for deasphalted sample according to procedure described previously.

C5-Maltenes	c_2	ρ_s^o kg/m³	EF with Experimental Density			EF with Predicted Density		
			AARD %	MARD %	Bias %	AARD %	MARD %	Bias %
Used for correlations								
WC-B-B1-DAO	0.3115	1037.7	50	55	-50	47	56	-22
WC-B-A1-DAO	0.3809	1032.1	51	63	-51	42	61	-42
US-HO-A1-DAO	0.2835	1010.9	83	90	-83	83	90	-83
MX-HO-A1-DAO	0.3065	1019.6	73	79	-74	72	79	-72
CO-B-B1-DAO	0.2697	1013.9	63	65	-63	83	91	-83
CO-B-A1-DAO	0.3809	1032.1	51	63	-51	42	61	-42
Not used for correlations								
WC-B-A2-DAO	0.3653	1045.1	44	48	-44	14	30	-12

Table 6.5. Fitted EF correlation parameters for C5-maltenes, and the average and maximum relative deviation and bias of the fitted viscosity. The measured density was used to fit the EF to viscosity data. DAO stands for deasphalted sample according to procedure described previously.

C5-Maltenes	c_2	ρ_s^o kg/m³	AARD %	MARD %	Bias %
Used for correlations					
WC-B-B1-DAO	0.3964	1047.3	2	4	0
WC-B-A1-DAO	0.4042	1030.7	3	11	-3
US-HO-A1-DAO	0.4017	1013.3	1	4	-1
MX-HO-A1-DAO	0.4214	1027.5	3	5	0
CO-B-B1-DAO	0.4338	1033.1	2	3	-2
CO-B-A1-DAO	0.4042	1030.7	3	11	-3
Not used for correlations					
WC-B-A2-DAO	0.4114	1048.3	2	7	0

6.6 EF Model Parameters for Asphaltenes

The EF fluid-specific parameters for C5-asphaltenes were estimated by fitting the correlation to the viscosity data (and density data as the input) for the C5-asphaltenes in Development Dataset 2, Figure 6.11. Although the two asphaltene samples were obtained from heavy oils from different geographical locations, they both have similar viscosity values. Therefore, it was assumed that all C5-asphaltenes have the same EF fluid-specific parameters when they are modeled as a single component. The EF correlation fitted the experimental viscosity data with an AARD and MARD of 5% and 24%, respectively. The fitted parameters c_2 and ρ_s^o were 0.9057 and 1113.7 kg/m³, respectively.
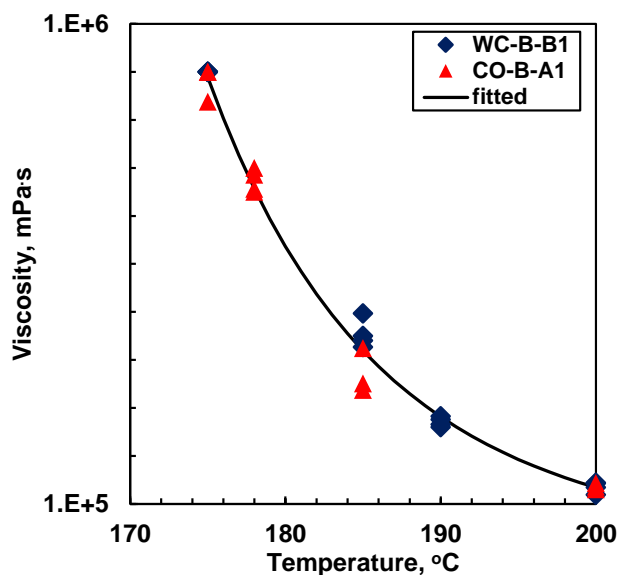
Figure 6.11. Viscosity versus temperature of molten C5-asphaltenes from the WC-B-B1 and CO-B-A1 bitumens. The viscosity was measured in a shear rate range of 0.01 s^{-1} to 10 s^{-1}. Note this is a Cartesian plot.

Testing the Asphaltene EF Model Parameters

To test the asphaltene EF model parameters, the accuracy of the EF model was evaluated when asphaltenes were part of the mixture to be modeled. Any errors in the asphaltene parameters would be expected to propagate to the viscosity prediction for the mixture. The parameters were first tested on the simplest possible mixture: a 5 wt% solution of asphaltenes in toluene from Test Dataset 3. The measured density was used as the input. The EF model parameters for toluene were taken from Ramos-Pallares *et al*. (2016a).The

EF model parameters for the mixture were calculated using the mass-based mixing rules with an interaction parameter calculated from Equations 5.3 to 5.8 using the the the H/C ratio of 1.192 measured for the WC-B-B1 C5-asphaltenes. The molecular weight of the asphaltenes for the calculation of c_3 from Equation 4.13 was estimated from the known mass fractions of maltenes and asphaltenes and the known molecular weight of the whole oil and the maltenes (M_{oil} = 558 g/mol, M_{malt}= 483 g/mol). To date, Equation 4.13 has only been used to estimate c_3 parameters for pure hydrocarbons and distillation cuts. However, the results shown here suggest that the calculated value is suitable for the modeling of asphaltenes represented as a single component.

The EF model predictions are compared with the experimental data at 9 MPa in Figure 6.12. The viscosity of toluene is also shown for comparison purposes. The viscosity of the mixture was predicted with an AARD, MARD and bias of 4, 9 and -0.6%, respectively. The accuracy of the prediction demonstrates that the asphaltene EF model parameters determined from molten asphaltenes can be applied to simple mixtures.
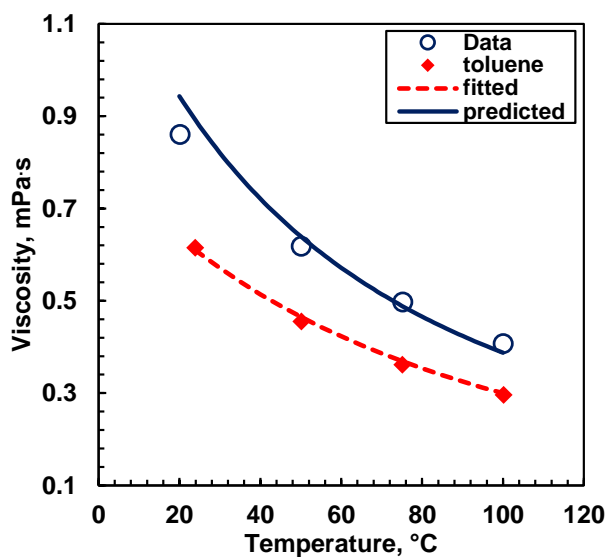
Figure 6.12. Viscosity versus temperature for a mixture of 5 wt% C5-asphaltenes in toluene at 9 MPa. The toluene data are from NIST database (2008).

The EF model parameters for the asphaltenes were next tested on viscosity data for whole WC-B-B1 bitumen from Test Dataset 3. In this case, the bitumen was modeled as a two component mixture of maltenes and asphaltenes and the measured density was used as the input to the EF model. The maltenes were treated as a single component to avoid introducing error from the characterization procedure. The EF fluid-specific parameters for the maltenes were determined from experimental viscosity and density data at atmospheric pressure (c_2=0.3959, ρ_s^o=1047.2 kg/m^3). The EF fluid-specific parameters for the heavy oil were calculated using the mass-based mixing rules. The binary interaction parameter was calculated from Equations 5.3 to 5.8 using the measured specific gravities (SG_{malt}=0.986, SG_{asph}=1.098) and H/C ratios for maltenes and asphaltenes (H/C_{mal} =1.533, H/C_{asph}=1.192). Note, the asphaltenes from this oil were part of the dataset used to determine the asphaltene EF model parameters.

Figure 6.13a shows that the model predicts the viscosity of the whole bitumen with an AARD, MARD and bias of 20, 80 and +20%, respectively. In comparison, the EF correlation directly fitted to bitumen viscosity data at atmospheric pressure has an AARD, MARD and bias of 8, 16 and -1%, respectively. Note that the maximum deviation was found at room temperature for which large uncertainties in the density measurement have been noted. The small loss in accuracy with the model predictions may be caused by inaccuracy in the predicted binary interaction parameters. The satisfactory accuracy of the prediction indicates that the EF model parameters determined for the asphaltenes can be applied as part of a petroleum mixture without modification. The results also demonstrate that, for viscosity modeling purposes, asphaltenes in a crude oil and asphaltenes dissolved in a hydrocarbon solvent can be treated in the same way, even though they may self-associate differently.
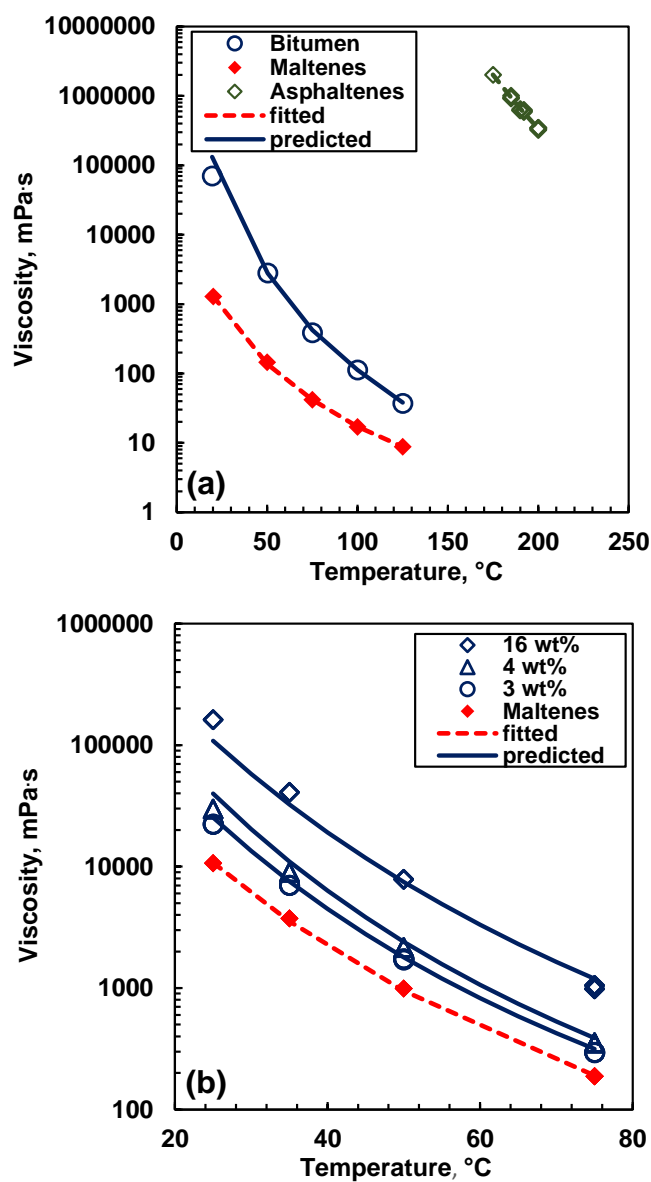
Figure 6.13. Measured and predicted viscosity of: a) WC-B-B1 bitumen and its C5-maltenes and C5-asphaltenes at 0.1 MPa; b) partially deasphalted WC-B-B3 bitumen. Mass percentage in the label corresponds to asphaltene content.

Recall that the asphaltenes were treated as a single component even though they are a complex multi-component mixture. Therefore, partially deasphalted oils from the WC-B-B3 bitumen (Test Dataset 3) were examined to determine the sensitivity of the model predictions when the asphaltenes are fractionated. The partially deasphalted samples were

modeled as a two pseudo-component mixture of maltenes and asphaltenes, as described for the whole bitumen test. The EF model parameters for the asphaltenes were not altered. Figure 6.13b shows that the model predicts the viscosity of the partially deasphalted bitumens with an AARD, MARD, and bias of 12, 33%, and -4%, respectively. In comparison, the data were fitted directly with the EF model and the AARD, MARD, and bias were 3, 5% and 0.5%, respectively. Hence, using a single set of EF model parameters for the asphaltenes provides satisfactory viscosity predictions even when the asphaltenes are fractionated. It appears that the effect of asphaltenes on the viscosity does not significantly depend on small differences in their molecular weight, self-association, or structural configuration in the crude oil.

6.7 Predicting and Tuning the Viscosity of Crude Oils

Viscosity Prediction

The proposed correlations and modeling approach were tested on the whole oils from Test Dataset 4. Note, four of the 10 oils in this dataset (WC-B-A2, WC-B-A3, EU-HO-A1, and ME-CV-A1) were not used to develop the EF model parameter correlations. To predict the viscosity of any crude oil using the EF model, only the distillation curve, the asphaltene content, and the specific gravity and molecular weight of the whole oil are required. Either experimental or predicted whole oil density can be used as input and here both are evaluated. The density of the whole oil was predicted as described previously.

The oils were characterized as described previously and as shown in the Appendix E. The boiling point curve was extended over the entire maltene fraction following a Gaussian extrapolation. The maltene fraction was split into pseudo-components and their properties calculated from existing correlations. The EF parameters, c_2 and ρ_s^o, for each pseudo-component were calculated using the proposed correlations (Equations 6.10 to 6.18). The EF parameters of the single component asphaltene fraction were set to $c_2 = 0.9057$ and $\rho_s^o = 1113.7$ kg/m³. The c_3 parameter was calculated for each pseudo-component and the asphaltene fraction using Equation 4.13. The H/C ratio was calculated for each pseudo-component and asphaltene fraction using Equation 6.1. Finally, the EF parameters for the

whole crude oil were calculated by combining those of the pseudo-components and the asphaltene fraction using the mass-based mixing rules (Equations 4.7 to 4.9) with binary interaction parameters determined from Equations 5.3 to 5.8.

Figure 6.14 shows the viscosity predictions for the WC-B-A2 bitumen using predicted densities as the input (solid line). Note, bitumen WC-B-A2 was not used to develop the EF parameter correlations or to tune the asphaltene density correlation (Equation 6.9). The maltene fraction was modeled using 12 pseudo-components. The AARD and MARD were 31 and 38%, respectively, when experimental densities were used as input and 37 and 49%, respectively, when predicted densities were used as input. In comparison, the AARD and MARD for the model directly fitted to the whole oil data are 2 and 7%, respectively. The untuned predictions are not as accurate as the directly fitted model but follow the correct trends with pressure and temperature. The same behavior was observed for all the oils. For example, Figure 6.15 shows the measured and predicted viscosity versus temperature for EU-HO-A1 heavy oil, a sample from a different geographical region. Note, that high pressure viscosities were not measured for this oil.

To determine the sensitivity of the viscosity model to the number of pseudo-components in the maltene fraction, the viscosity of the heavy oil EU-HO-A1 at atmospheric pressure was predicted for 1, 3, 4, 6, and 12 pseudo-components using experimental density as input, Figure 6.15. The EU-HO-A1 heavy oil was not used for any of the model development. The AARD for 1, 3, 4, 6 and 12 pseudo-components were 60, 53, 52, 52, 52 and 52% respectively. 4 pseudo-components are sufficient to minimize the error and significant deviations are only observed for 3 or fewer pseudo-components.
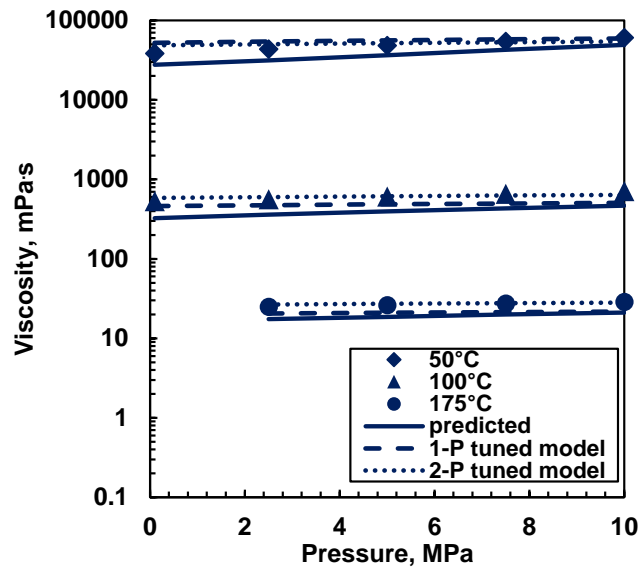
Figure 6.14. Measured and predicted viscosities of WC-B-A2 bitumen. Dashed and dotted lines corresponds to EF predictions after tuning one parameter, c_2, and both model parameters, c_2 and ρ_s^o, respectively. 1-P and 2-P stand for 1 or 2 parameters tuned model.
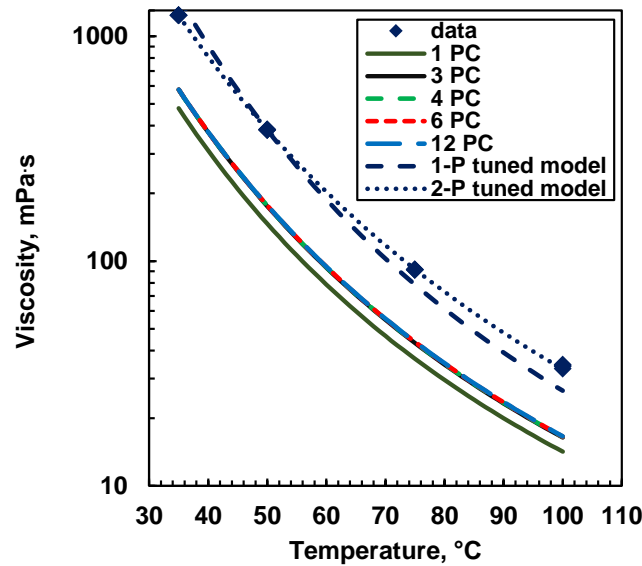
Figure 6.15. The effect of the number of pseudo-components (PC) on the predicted viscosities of EU-HO-A1 bitumen at atmospheric pressure. 1-P and 2-P stand for 1 or 2 parameters tuned model.

The calculated EF model parameters, the deviations, and the bias are provided for all of the oils in Test Dataset 4 in Table 6.6. The maltene fractions were modeled with 12 pseudo-components. When measured density was used as the input, the overall AARD, MARD, and bias of the crude oil samples in the Test Dataset 4 were 40, 98, and -27%, respectively. When predicted density was used as the input, the overall AARD, MARD, and bias were 43, 99, and -29%, respectively. Note that the deviations presented in Table 6.6 (and all following error tables in this section) were calculated over the entire dataset including data at high pressure. There was no significant difference in the errors between the oils whose cuts were used in the development datasets and those which were not. The deviations with the measured or predicted density as the input are similar, indicating that the proposed method for the prediction of crude oil density is not contributing significantly to the error in the viscosity predictions.

For the model prediction where the viscosities were fitted directly with the EF model (using measured density as the input), the fitted parameters and errors are provided in Table 6.7. The overall AARD, MARD, and bias of the fitted viscosities were 3.2%, 35%, and +0.5%, respectively. As found for the maltenes, the predictions are significantly less accurate than the fitted model. In addition, the predicted EF parameters, c_2 and ρ_s^o, are, in general, lower than the fitted values. The deviation in the predicted viscosities are similar to those obtained for the distillation cuts (with no asphaltene content) and it appears that the main source of error is the prediction of the single data point at 37.7°C for the pseudo-components in the maltene fraction. Nevertheless, the results demonstrate that the characterization approach using maltene pseudo-components and a single asphaltene component can provide crude oil viscosity predictions with an accuracy within ±40%.

Table 6.6. Calculated EF model parameters for whole crude oils, and the average and maximum relative deviation and bias of the predicted viscosity.

Oil	c_2	ρ_s^o kg/m³	EF with Measured Density			EF with Predicted Density		
			AARD %	MARD %	Bias %	AARD %	MARD %	Bias %
Used for correlations								
WC-B-B1	0.4077	1056.3	20	30	-12	29	85	-24
WC-B-A1	0.4002	1041.3	32	47	-27	37	54	-32
US-HO-A1	0.3618	1011.3	22	35	-7	36	61	-29
MX-HO-A1	0.4241	1043.9	98	98	-98	99	99	-99
CO-B-B1	0.4027	1038.3	32	45	-32	35	51	-35
CO-B-A1	0.4657	1050.9	42	50	-77	44	67	-44
Not used for correlations								
WC-B-A2	0.4721	1064.4	31	38	-2	37	49	-37
WC-B-A3	0.3959	1046.3	26	33	-21	19	35	-8
EU-HO-A1	0.3376	1014.1	52	54	-42	53	55	-33
ME-CV-A1	0.3335	956.1	46	62	+-46	47	57	+46

Table 6.7. Fitted EF model parameters for whole crude oils, and the average and maximum relative deviation and bias of the fitted viscosity. The measured density was used to fit the EF to viscosity data.

Oil	c_2	ρ_s^o kg/m³	AARD %	MARD %	Bias %
Used for correlations					
WC-B-B1	0.5050	1072.1	7	20	4
WC-B-A1	0.5091	1055.1	2	7	-0.1
US-HO-A1	0.4472	1026.2	3	10	0.1
MX-HO-A1	0.6923	1041.8	0.7	1	0
CO-B-B1	0.5143	1054.1	1	2	0
CO-B-A1	0.5895	1064.3	3	6	-0.1
Not used for correlations					
WC-B-A2	0.5281	1069.5	3	6	-0.2
WC-B-A3	0.4845	1057.2	8	32	1
EU-HO-A1	0.4214	1024.8	1	3	0
ME-CV-A1	0.3959	979.3	3	7	-0.1

Model Tuning

If data are available, the EF correlation parameters can be tuned with single multipliers applied to c_2 alone or to both c_2 and ρ_s^o. The parameter c_2 was chosen for the single multiplier adjustment because the tuning process converges faster, although the outcome is similar for either parameter. In this study, the model was tuned to dead oil atmospheric pressure data. A single viscosity data point was chosen when c_2 was adjusted and two data points when c_2 and ρ_s^o were adjusted. As an example, the single and two parameter tuned viscosities for the bitumen WC-B-A2 (with predicted density used as input) and the heavy oil EU-HO-A1 (with measured density used as input) are compared with the predicted viscosities in Figures 6.14 and 6.15, respectively. The tuning reduced the overall AARD of both samples to 14% (single parameter) and 6% (two parameter) compared with 42% without tuning.

The model, tuned with a single multiplier for c_2 and using measured density as the input, matched the viscosity of the crude oils in Test Dataset 4 with an AARD, MARD, and bias of 17, 56, and -7%, respectively, Table 6.8. The deviations after tuning are approximately half those obtained for with no tuning. The model, tuned with single multipliers to both c_2 and ρ_s^o and using measured density as the input, reduced the AARD, MARD, and bias to 4, 21, and +1%, respectively, Table 6.9. These errors are comparable to errors obtained when directly fitting the data, Table 6.7.

Table 6.8. The average and maximum relative deviation and bias of the tuned (single multiplier to c_2 parameter only; measured density input) viscosities for Test Dataset 4. NP stands for number of experimental data points in the dataset.

Oil	NP	c_2 multiplier	AARD %	MARD %	Bias %
Used for correlations					
WC-B-B1	25	0.9605	21	35	-19
WC-B-A1	22	1.0157	31	47	-15
US-HO-A1	22	0.9560	25	56	+4
MX-HO-A1	12	1.6738	2	5	+2
CO-B-B1	16	1.0080	28	43	-28
CO-B-A1	13	1.0542	21	39	-0.2
Not used for correlations					
WC-B-A2	27	1.0410	14	22	-12
WC-B-A3	27	1.0025	17	32	-11
EU-HO-A1	16	1.0753	14	23	-4
ME-CV-A1	16	0.9462	11	20	+10

Table 6.9. The average and maximum relative deviation and bias of the tuned (single multipliers to both c_2 and ρ_s^o; measured density input) viscosities for Test Dataset 4. NP stands for number of experimental data points in the dataset.

Oil	NP	c_2 multiplier	ρ_s^o multiplier	AARD %	MARD %	Bias %
Used for correlations						
WC-B-B1	25	1.1893	1.0166	3	9	0
WC-B-A1	22	1.3036	1.0148	4	9	+3
US-HO-A1	22	1.3094	1.0156	2	13	-2
MX-HO-A1	12	1.6493	0.9988	1	3	+0.6
CO-B-B1	16	1.3026	1.0167	2	6	+2
CO-B-A1	13	1.5771	1.0240	8	21	+0.8
Not used for correlations						
WC-B-A2	27	1.1643	1.0067	6	18	+9
WC-B-A3	27	1.2489	1.0144	7	17	+6
EU-HO-A1	16	1.2398	1.0100	1	4	-0.5
ME-CV-A1	16	1.8028	1.0829	7	17	-5

Testing the Model on an Independent Dataset

Finally, the proposed characterization and modeling approach was also evaluated on the four crude oils from the literature in Test Dataset 5. The oils were characterized as described above for the bitumens. Note, the crude oil density at the temperature of the viscosity measurements was not always reported (only the specific gravity of the whole

crude oil); therefore, the densities of all the crude oils in this dataset were predicted as described previously.

Figure 6.16 compares the predicted and tuned viscosities with measured data for the best prediction (Athabasca bitumen) and the worst prediction (Alaska North Slope crude oil). The EF correlation predicted the viscosity of the Athabasca bitumen with an AARD 8%, almost within the accuracy of the tuned model. The non-tuned predictions for the Alaska North Slope oil have an AARD of 64%. However, tuning substantially improves the model (AARD 5% with single parameter tuning and 0.1% with two parameter tuning). The deviations for all four oils are provided in Table 6.10. The overall AARD, MARD, and bias were 43, 100, and +19% without tuning, 16, 66, and -5% when c_2 was adjusted, and 7, 26, and +0.6% when both c_2 and ρ_s^o were adjusted.
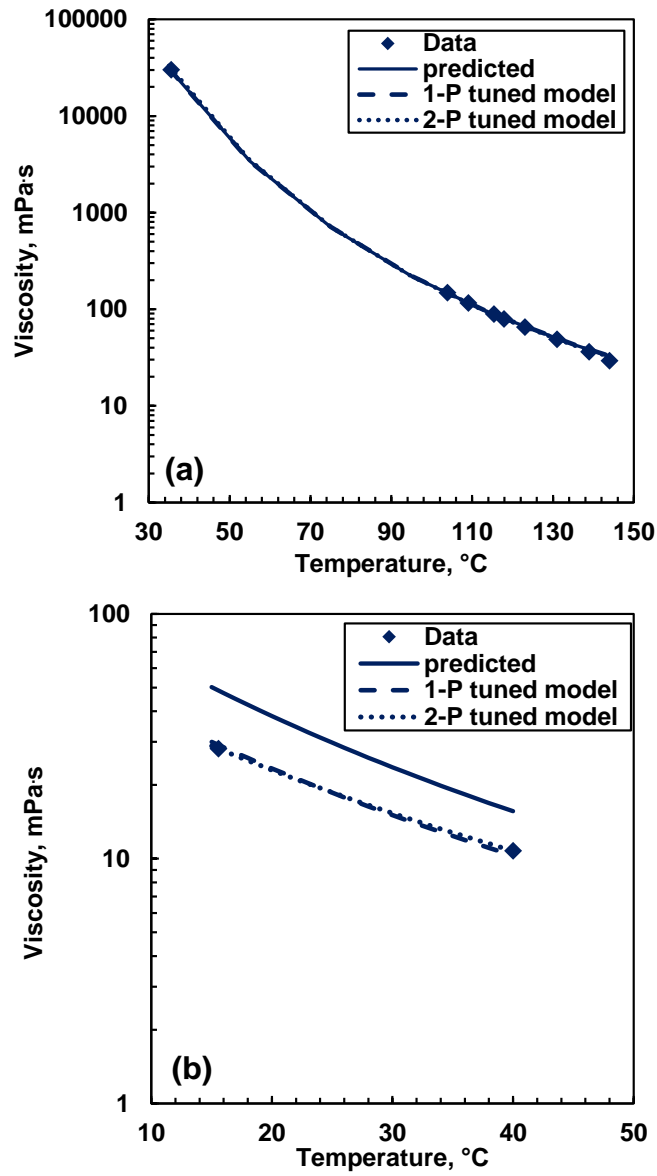
Figure 6.16. Measured and modeled viscosity versus temperature at atmospheric pressure for Athabasca bitumen (a) and Alaska North Slope crude oil (b). Dashed and dotted lines corresponds to EF predictions after tuning one parameter, c_2, and both model parameters, c_2 and ρ_s^o, respectively.

Table 6.10. Average and maximum relative deviations and bias of predicted and tuned viscosities for Test Dataset 5. Predicted densities were used as input.

Crude Oil	Predicted			Tuned c_2			Tuned c_2, $\rho_s{}^o$		
	AARD	MARD	Bias	AARD	MARD	Bias	AARD	MARD	Bias
	%	%	%	%	%	%	%	%	%
Alaska North Slope	64	75	+64	5	9	+5	0	0	0
Athabasca	8	43	+8	3	11	+1	3	9	1
Boscan	55	100	+47	19	44	-9	22	26	2
San Joaquin Valley	44	61	-44	30	60	+18	4	10	-4

6.8 Summary

Density and viscosity data were collected for distillation cuts from heavy oils, maltenes, C5-asphaltenes, partially deasphalted heavy oils, and whole oils. The data were used to develop and test correlations for the EF viscosity model parameters (c_2 and $\rho_s{}^o$) of distillation cuts (equivalent to distillation based pseudo-components).

A methodology was proposed to predict viscosity from a distillation assay with maltenes characterized as a set of pseudo-components and C5-asphaltenes treated as a single component. Densities were predicted using the modified Rackett correlation. The EF model predictions with predicted density as an input were of similar accuracy as those with measured densities as the input. The proposed methodology predicted the viscosity of the oils in the development and test datasets with overall AARDs of 40 and 42%, respectively. Single multiplier tuning of the c_2 parameter to a single atmospheric pressure data point reduced the AARDs to 21 and 14%, respectively. Single multiplier tuning of each of the c_2 and $\rho_s{}^o$ parameters (using two atmospheric pressure data points) reduced the AARDs to 4 and 7%, respectively. The latter deviations were almost the same as the deviations from directly fitting the EF model to the data.

The proposed methodology only requires a distillation assay, the asphaltene mass content, specific gravity and molecular weight of the oil to provide a reasonable viscosity

prediction. Two atmospheric viscosity data point are sufficient for predictions within experimental error. As few as four maltene pseudo-components are sufficient for a consistent viscosity prediction.

CHAPTER SEVEN: PREDICTION OF THE LIQUID VISCOSITY OF CHARACTERIZED OILS USING THE GENERALIZED WALTHER MODEL[3]

This chapter presents a methodology to predict the liquid viscosity of characterized oils using the Generalized Walther model (GW). The proposed approach is based on a distillation assay rather than a GC assay in order to avoid uncertainties related to the extrapolation of the GC heaviest fraction. The GW model has potential application in a reservoir simulator because of its simplicity and fast convergence; however, a more accurate extension to characterized oils is required for its application in compositional analysis.

7.1 Background

Typically, a compositional model is employed for situations where multiple phases can form. In this case, the fluid is characterized into a set of pseudo-components that represent the property distribution in the fluid and allows for components to partition between phases. A full phase model requires viscosity prediction in the gas and liquid regions including near the critical point. However, most heavy oil processes do not operate near the critical region and there are well established methods to determine gas phase viscosities. Hence, the focus here is on a viscosity model for the liquid phase of crude oils characterized into pseudo-components. The model must be applicable over a wide range of temperatures, pressures, and compositions and must also be rapid and easy to implement for use in reservoir simulators.

The objective of focus for this chapter is to extend the generalized Walther model (GW) to predict the liquid viscosity of crude oils characterized from a distillation assay. This model was selected because it is simple and fast and only requires temperature and pressure as

---

inputs. As presented in Chapter 6, the maltenes are characterized as a set of pseudo-components while the asphaltenes are treated as a single component. Model parameters and correlations are developed and tested on datasets collected from the literature that include the viscosities of bitumens, heavy oils, conventional oils, and molten asphaltenes.

7.2 Range of Application

The generalized Walther model is only applicable to liquids far from their critical point. To determine the applicable range more precisely, the generalized Walther model (Equations 4.14 to 4.16) was fit to viscosity data of *n*-alkanes from methane to dodecane, benzene, toluene and cyclohexane from the saturation pressure up to 100 MPa. Those compounds were chosen because there were data available in the vicinity of the critical point and over the full phase diagram (NIST, 2008). As an example, Figure 7.1 shows the measured and modeled viscosities for methane, *n*-hexane, benzene, and cyclohexane along the saturated liquid line. In all cases, the model deviates from the data in the vicinity of the critical point when viscosity decreases rapidly. The selected criterion for model applicability was an error of less than 5% because other viscosity models implemented in simulators such as the Corresponding States, the *f*-theory and the Expanded Fluid (EF) are capable of fitting oil viscosity within 5% (Pedersen *et al*., 1984; Quiñones-Cisneros *et al*., 2003; Yarranton and Satyro, 2009). The reduced temperature at which the model deviates by more than 5% depends on the fluid but was at least 0.75 in all cases. Hence, the generalized Walther model is applicable at reduced temperatures below 0.75 and pressures above the saturation pressure.
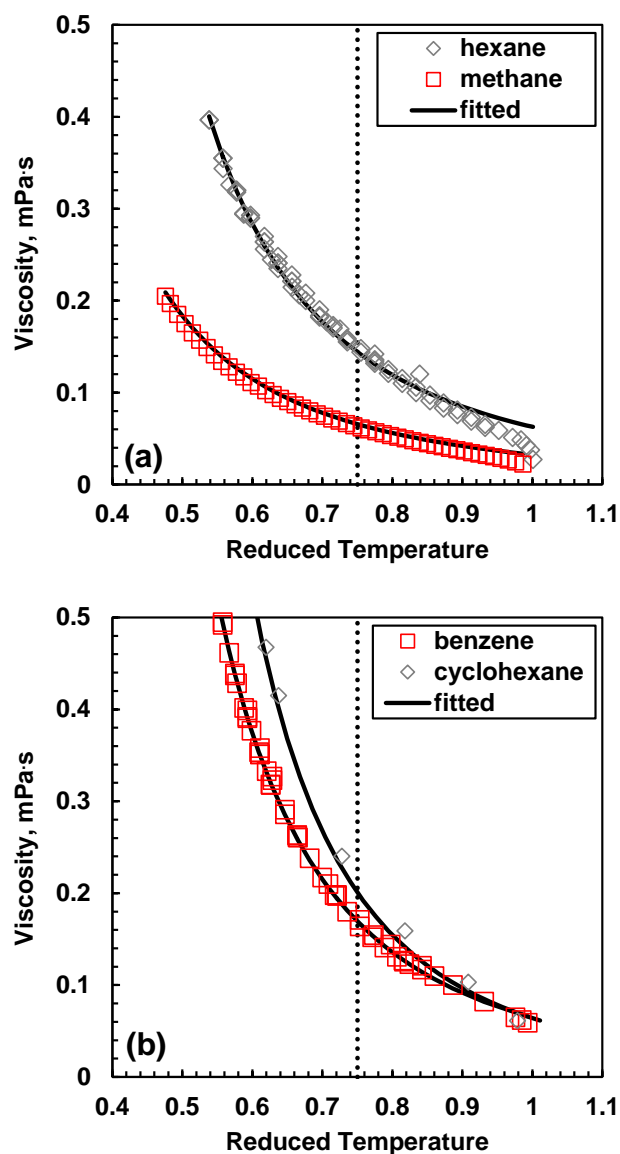
Figure 7.1. Viscosity versus reduced temperature for: a) methane and *n*-hexane, and; b) benzene and cyclohexene. The dotted lines correspond to a reduced temperature of 0.75.

7.3 Oil Characterization

The crude oils were characterized based on distillation assays and divided into pseudo-components as shown in Figure 7.2. The approach is the same as used for the EF model and presented in Chapter 6. Maltenes and asphaltenes were characterized separately as recommended by Catellanos-Diaz *et al*. (2011)**.** A Gaussian extrapolation was performed

to extend the distillation curve to the end of the maltenes. The distillation curve was divided into pseudo-components each representing a boiling point interval of the same width. Asphaltenes were characterized as a single component for viscosity modeling purposes, as recommended by Ramos-Pallares *et al.* (2016b).
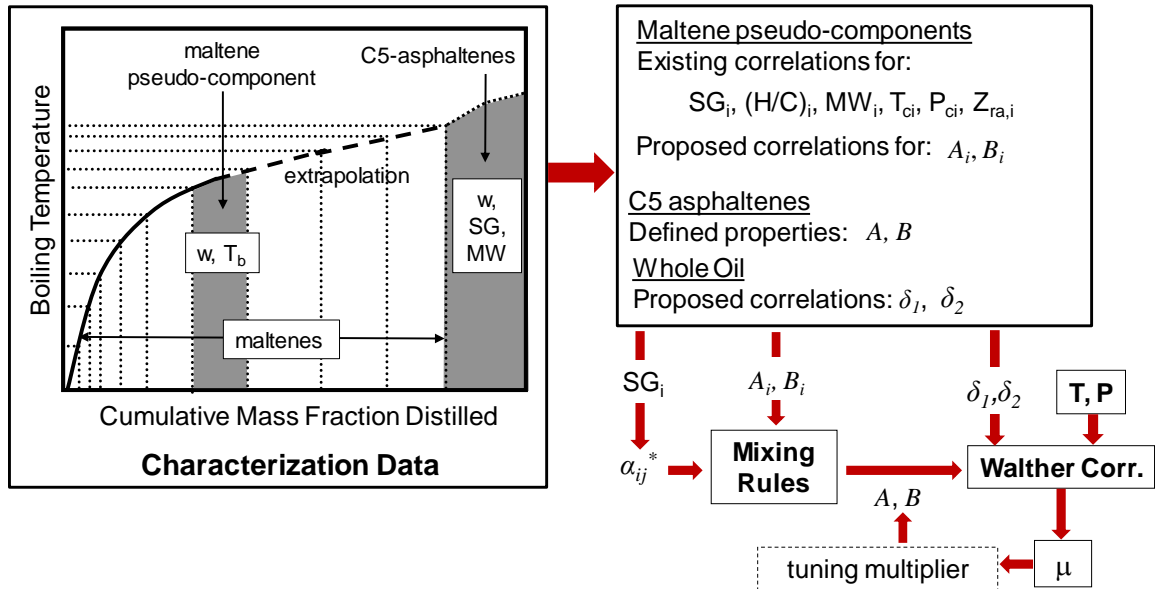
Figure 7.2. Schematic of characterization procedure for predicting crude oil viscosity from the generalized Walther model.

Maltene Pseudo-Components

The pseudo-component properties required for the model parameter correlations (development provided in Section 7.5) are the normal boiling point, the specific gravity, the molecular weight, Rackett compressibility, and critical properties. The initial specific gravity and molecular weight of each maltene pseudo-component were calculated using the Katz-Firoozabadi (Katz and Firoozabadi, 1978) and the Lee-Kesler (Kesler and Lee, 1976) correlations, respectively. The critical temperature and pressure of each pseudo-component in the maltene fraction were calculated using the Lee-Kesler correlations (Kesler and Lee, 1976).

The modified Rackett correlation (Spencer and Danner, 1972), given in Equation 6.8, was used to calculate the density of each pseudo-component at 37.7°C for input into the correlations developed later. The Rackett compressibility factor for each pseudo-component was calculated by fitting the modified Rackett correlation at 15.6°C to match the tuned specific gravity of the pseudo-component. The difference between the saturated density and the density at atmospheric pressure was assumed to be negligible at 15.6°C.

The specific gravities of the pseudo-components were tuned to match the specific gravity of the maltenes. The specific gravity of the whole maltene fraction was calculated from the initial specific gravities of the pseudo-components using a regular solution mixing rule (Equation 6.3). A single constant multiplier was then applied to all of the pseudo-components to match the measured maltene specific gravity. Equation 6.2 was used to determine the maltene specific gravity when the measured value was not available.

C5-Asphaltene Component

The experimentally determined Walther model parameters for the single component asphaltenes are presented in Section 7.5.1.2. The only required input property is the asphaltene specific gravity. The specific gravity was determined indirectly from the measured oil properties, the characterized maltene properties, and the measured mass fraction of C5-asphaltenes in the oil. First, the maltenes were characterized as described above and their bulk specific gravity determined. Then, the asphaltene specific gravity was determined from that of the whole crude oil and maltenes using a regular solution mixing rule (Equation 6.3).

7.4 Datasets

The datasets used to develop the correlations for the maltene pseudo-component Walther parameters and to determine the Walther parameters for the asphaltenes are presented below. The datasets used to test the proposed approach are also presented.

Development Dataset 1: Distillation Cuts and Pure Hydrocarbons

This dataset was used to develop a correlation for the Walther parameters A and B for the pseudo-components in the maltenes. It includes the Walther parameters, normal boiling point and specific gravity of 40 distillation cuts obtained from 6 different heavy oils and bitumens from disparate geographical locations (WC-B-B1 and WC-B-A1: Western Canada, US-HO-A1: United States, MX-HO-A1: Mexico and CO-B-B1 and CO-B-A1: Colombia) collected in this study. The dataset also contains assorted pure hydrocarbons including *n*-alkanes (carbon numbers from C1 to C24), branched alkanes (17 compounds), aromatics and alkylbenzenes (19 compounds), fused aromatics (10 compounds), non-fused aromatics (11 compounds), cycloalkanes and alkyl cycloalkanes (36 compounds), fused naphthenics (19 compounds), and non-fused naphthenics (13 compounds) (NIST, 2008; API, 1966). The normal boiling point and specific gravities were reported for each fluid. The Walther parameters were calculated by fitting the correlation to the reported viscosity data at atmospheric pressure. All the viscosity data in this dataset are at atmospheric pressure. The Walther parameters A and B of the pure components in the Development Dataset 1 are summarized in Appendix F.

The density at 37.7°C of the cuts, which is used as input for the correlations presented later, was calculated using the modified Rackett correlation (Equation 6.8) tuned to match the reported specific gravity of the cut. The critical temperature, critical pressure, and the molecular weight used in the Rackett correlation were calculated using the Lee-Kesler correlations (Kesler and Lee, 1976).

Development Dataset 2: C5-Asphaltenes

This dataset was used to calculate the Walther correlation parameters A and B for C5-asphaltenes by fitting the model to measured low shear (Newtonian) viscosity of molten C5-asphaltenes at temperatures between 175°C and 200°C at atmospheric pressure. The viscosities of C5-asphaltenes from Western Canada bitumen WC-B-B1 and Colombian bitumen CO-B-A1 were measured in this study.

Development Dataset 3: Viscosity at High Pressure of Pure Hydrocarbons and Crude Oils.

This dataset was used to develop a correlation for the viscosibility parameters δ_1 and δ_2 for the whole crude oil. The viscosibility parameters were defined in Equation 4.15 and capture how viscosity changes with pressure. This dataset includes the Walther parameters A and B, calculated viscosibility parameters δ_1 and δ_2 as well as the molecular weight of pure hydrocarbons and crude oils collected from the literature. The parameters δ_1 and δ_2 were calculated from high pressure viscosity data of 12 n-alkanes (from methane to dodecane), 2 branched alkanes (isopentane and 2, 3-dimethylpentane), 4 aromatics (benzene, ethylbenzene, toluene and 1-methylnapthalene), 3 cyclics (cyclohexane, methylcyclohexane and decaline), 2 Western Canada bitumens (WC-B-B1 and WC-B-B2), 1 Western Canada heavy oil (WC-HO-1) and a condensate. The viscosity data of pure components was collected from the NIST database (2008), that of WC-B-B1 and WC-B-B2 was collected in this study and that of WC-HO-1 was reported by Yarranton *et al.* (2013), respectively.

Development Dataset 4: Pure Hydrocarbon Binaries and Bitumen/Solvent Pseudo-Binaries

This dataset was used to develop a correlation for the viscosity binary interaction parameters. It includes the Walther binary interaction parameters, α_{ij}^*, of 58 pure hydrocarbon binaries (Chevalier *et al.*, 1990), and 9 bitumen/solvent pseudo-binaries (this study). The dataset also includes the Walther parameters A and B, the specific gravity and molecular weight of the different pure components and bitumens from which the binaries and pseudo-binaries were prepared.

The pure hydrocarbon binaries include alkane/alkane, alkane/branched alkane, aromatic/aromatic, aromatic/alkane, aromatic/cyclic and cyclic/alkane. Their viscosities were reported at 25°C and atmospheric pressure over the entire range of compositions. The binary interaction parameters were determined by fitting the Walther model (Equation 4.16), with mixture parameters calculated from the model mixing rules (Equations 4.17 and 4.18), to the data. The bitumen/solvent pseudo-binaries include mixtures of two Western Canada bitumens, WC-B-B1 and WC-B-B2, with solvents such as ethane,

propane, *n*-butane, *n*-pentane, *n*-heptane, *n*-eicosane, cyclohexane, toluene and 1-methylnaphthalene. Their viscosity was measured at temperatures from 21 to 175°C, pressures up to 10 MPa, and solvent contents up to 50 wt%. The binary interaction parameters were determined as described for pure hydrocarbon binaries. The crude oils were modelled as single components.

Test Dataset 1: Distillation Cuts

The predictive approach developed for the maltene pseudo-components was tested on a dataset containing distillation cuts from the 20 different oils listed in Table 6.1. This dataset is the same one used to test the EF maltene pseudo-component model parameters. The normal boiling point, specific gravity and viscosity (usually kinematic viscosity) were reported. The Rackett correlation, tuned to match the reported specific gravity, was used to model the density of the cuts to convert kinematic into dynamic viscosity. The molecular weight, when not reported, and critical properties to be used in the Racket correlation were calculated as described for the cuts in Development Dataset 1.

Test Dataset 2: Partially Deasphalted Bitumen

This dataset was used to test the C5-asphaltene Walther parameters. It includes the viscosity of 3 partially deasphalted bitumen samples collected in this study and a completely deasphalted sample from the same crude oil. The specific gravities of the samples were also included in the dataset.

Test Dataset 3: Diluted Crude Oils

This dataset was used to test the proposed correlations for the viscosibility parameters and the Walther viscosity binary interaction parameter. It includes viscosity data, the fitted Walther parameters A and B, the molecular weight, and the specific gravity of several crude oil/solvent pseudo-binaries. The dataset also contains the viscosity of the crude oils used to prepare the pseudo-binaries measured at the conditions showed in Table 7.1, except for Cold Lake 2 and Athabasca 3 whose viscosities were reported at atmospheric pressure. Note, the molecular weight of crude oils Athabasca 1 and 2, McKay River and Cold Lake

2 were not reported in the work from which viscosity data was taken, but rather by Nourozieh *et al*. (2013), Coates *et al*. (2005) and Mehrotra (1990), respectively, who used samples from the same regions. The specific gravity of bitumen Cold Lake 2 was reported by Mehrotra (1990) at 25°C. Badamchi-Zadeh *et al.* (2009) reports viscosities of the pseudo-binary Athabasca 2/pentane at solvent content up to 26 wt%; however, the data for solvent content higher than 10 wt% was not considered here because of the possibility of asphaltene precipitation at high solvent content. The Walther parameters for the solvent in the pseudo-binary Athabasca 1/xylene were calculated by fitting the model to data in the source paper because the solvent is a mixture of xylenes.

Table 7.1. Crude oil/solvent pseudo-binaries in the Test Dataset 3. MN stands for 1-methyl naphthalene and C14 for tetradecane. Oil samples CO-B-A1 and ME-CV-A1 corresponds to a Colombian bitumen and a Middle East conventional oil. * indicates that the property was taken from the second reference.

Mixture	SG_{oil}	M_{oil} g/mol	Range of Conditions			Source
			Temp. °C	Pressure MPa	Solvent wt%	
Athabasca 1/toluene	1.010	512*	25 - 71	0.1 - 10	5 - 50	Guan, 2013 Nourozieh, 2013
Athabasca 1/xylene	1.010	512*	25 - 71	0.1 - 10	5 - 50	Guan 2013 Nourozieh, 2013
Athabasca 1/decane	1.010	512	25 - 71	0.1 - 10	5 - 50	Nourozieh, 2013
Athabasca 1/C14	1.010	512	25 - 71	0.1 - 10	5 - 50	Kariznovi, 2013
Athabasca 2/pentane	1.015	512*	50 - 200	1	5 - 10	Argüelles-Vivas, 2012 Nourozieh, 2013
Athabasca 3/propane	1.007	552	11 - 75	0.8 - 5	5 - 10	Badamchi-Zadeh, 2009
Cold Lake 1 /toluene	1.000	582	25 - 100	0.1	1 - 10	Mehrotra, 1990
McKay River/decane	1.008	611*	25 - 71	1 - 10	35 - 50	Khan, 2014; Coates, 2005
McKay River/toluene	1.008	611*	25 - 71	1 - 10	5 - 50	Khan, 2014; Coates, 2005
Cold Lake 2/methane	0.995*	582*	26 - 103	2.5 - 10	saturated	Mehrotra,1988, 1990
Cold Lake 2/ethane	0.995*	582*	22 - 102	1 - 10	saturated	Mehrotra, 1988, 1990
CO-B-A1/toluene	1.106	603	20 - 35	0.1	5 - 10	This Study
CO-B-A1/MN	1.106	603	25 - 50	0.1	14.3	This Study
ME-CV-A1/toluene	0.872	475	0 - 15	0.1	6 - 10	This Study
ME-CV-A1/MN	0.872	475	10 - 25	0.1	2 - 8	This Study

Test Dataset 4: C5-Maltenes

This dataset was used to test the Walther parameter correlations and the correlated viscosity binary interaction parameters applied to maltene pseudo-components. It contains viscosity and distillation assay data collected in this study of seven C5-maltene samples, molecular weight and specific gravity. Six of the C5-maltene samples were used to obtain the distillation cuts in Development Dataset 1 and their viscosities were measured at atmospheric pressure. The viscosity of the C5-maltene sample obtained from WC-B-B1 bitumen was measured at temperatures from 21 to 175°C and pressures up to 10 MPa. The other C5-maltene sample corresponds to that obtained from bitumen WC-B-A2. This bitumen was not used in the development of correlations.

Test Dataset 5: Whole Crude Oils

This dataset was used to test the proposed approach to predict the viscosity of crude oils. It includes the viscosity, distillation assay, molecular weight, specific gravity, and asphaltene mass content of each of the crude oils presented in Table 7.2. The range of conditions at which the viscosity of those oils was measured is also included in Table 7.2. Approximately half of the crude oils in this dataset were used to obtain the distillation cuts grouped into the Development Dataset 1. Note, the asphaltene content of the Alaska North Slope and San Joaquin Valley oils were not reported in the original source and were instead obtained from other publications (McLean *et al.*, 1997) on crude oils from the same geographical regions with similar API gravity and viscosity at 37.7°C. Similarly, distillation data for the Athabasca bitumen sample were obtained from Castellanos-Diaz *et al.* (2011) while the density and viscosity for the same oil were obtained from Badamchi-Zadeh *et al.*(2009). Note that the fluids included in this dataset were also used to test the EF extension to characterized oils presented in the previous Chapter.

Table 7.2. Ranges of the physical properties for the crude oils in Test Dataset 5. WC, US, MX, CO, EU and ME stand for Western Canada, United States, Mexico, Colombia, Europe and Middle East; B, HO and CV stands for bitumen, heavy oil and conventional oil, and the third term indicates sample number. ANS and SJV stand for Alaska North Slope and San Joaquin Valley oils, respectively.

Crude Oil	SG	Asph. Content wt%	Viscosity at 20°C mPa·s	T Range °C	P Range MPa	Source
Used in Correlations						
WC-B-B1	1.012	17	89,200	20 - 175	0.1 - 10	This Study
WC-B-A1	0.996	16	33,737	25 - 125	0.1	"
US-HO-A1	0.961	14	5,627	25 - 125	0.1	"
MX-HO-A1	0.976	21	831,600	25 - 125	0.1	"
CO-B-B1	0.992	22	106,500	25 - 100	0.1	"
CO-B-A1	1.106	27	2,800,000	40 - 75	0.1	"
Not Used in Correlations						
WC-B-A2	1.026	22	7,500,000	50 - 175	0.1 - 10	"
WC-B-A3	1.101	18	33,737	50 - 175	0.1 - 10	"
EU-HO-A1	0.968	7	5,036	35 - 100	0.1	"
ME-CV-A1	0.872	3.8	18.1		0.1	"
ANS	0.891	3.3	28.1 (15.6°C)	15 - 40	0.1	API, 2000 Mclean, 1997
Athabasca	1.007	22.7	30,090 (35.5°C)	35 - 144	0.1	Catellanos,2011 Badamchi, 2009
Boscan	0.993	18	485,500 (15.6°C)	15 - 37	0.1	EST, 2001
SJV	0.977	4.6	1,376 (40°C)	40 - 125	0.1	API, 2000 Mclean, 1997

7.5 Results and Discussion

The development of the correlations for all of the Walther model parameters are presented and then the testing of each correlation is discussed. The predictive method is then tested on data for maltenes and whole crude oils. Finally, a tuning procedure is provided for cases where at least one viscosity data point is available.

7.5.1 *Development of Walther Model Parameter Correlations*

The proposed approach to predict crude oil viscosity was shown in Figure 7.2 and involved the following steps: 1) determine the Walther parameters (A and B) for the maltene pseudo-components; 2) determine the Walther parameters for the C5-asphaltenes; 3) determine the binary interaction parameters, α_{ij}^*, and predict the viscosity of the whole oil at atmospheric

184

pressure from Equation 4.16; 4) determine the parameters δ_1 and δ_2 for the whole crude oil and calculate the viscosity at a given pressure as a departure from the atmospheric value using Equations 4.14 and 4.15. Correlations are required for A, B, δ_1, δ_2, and α_{ij}^{*}.

7.5.1.1 Walther Model Parameter Correlations for Maltene Pseudo-Components

It proved to be challenging to develop a direct correlation for both of the Walther parameters (A and B) based on physical properties such as molecular weight, boiling point or specific gravity. Due to the double logarithm in the Walther model, small deviations in the parameters cause large deviations in the predicted viscosity. Instead, a correlation was developed only for the A parameter and the B parameter was determined by fitting the model to a single viscosity calculated from another correlation.

Correlation for Parameter A

The parameter A in the Walther model represents the hypothetical viscosity of a liquid as the logarithm of the absolute temperature tends to zero at atmospheric pressure. In reality, the viscosity will tend to infinity as the liquid becomes a solid (or a glass for petroleum fluids) and therefore the glass transition temperature is used as the reference temperature instead of absolute zero. In general, when the Walther correlation is fitted to a fluid with a lower glass transition temperature, a lower value of the A parameter is found to fit the data. While the A parameter correlated approximately to the glass transition temperature, a better correlation was found to the fragility ratio. The fragility ratio is defined as the quotient between the normal boiling point, T_b, and the glass transition temperature both in Kelvin (Alba *et al.*, 1990). It is related to the change in viscosity of a liquid in the vicinity of the glass transition temperature: low values indicate a dramatic increase of viscosity near the glass transition and *vice versa*.

Data for the glass transition temperature of hydrocarbons and petroleum fluids is scarce; therefore, the glass transition temperature was assumed to be the temperature at which the viscosity of fluid reached 10^{15} mPa·s (Abivin *et al.*, 2011). This proxy glass transition temperature can be calculated from the Walther model (Equation 4.16) as follows:

185

$$\log\left(T_g^W\right) = \frac{A - \log\left[\log\left(10^{15} + 1\right)\right]}{B} \tag{7.1}$$

where T_g^W in K is the proxy glass transition temperature calculated from the Walther model and A and B are the Walther parameters calculated by fitting the model to data at atmospheric pressure. Note that Equation 7.1 is not intended to predict the exact glass transition temperature but rather an approximate value suitable for correlation purposes. The proxy glass transition temperatures calculated from Equation 7.1 were compared to measured values for some hydrocarbons reported by Miller (1968) and Alba *et al.* (1990). In general, the calculated values were 1.05 times lower than the experimental values.

The proxy glass transition temperature and the fragility ratio were then calculated for all the pure components and cuts in Development Dataset 1 using Equation 7.1 and the quotient between T_b and T_g^W, respectively. Since the fragility ratio will later be required to predict viscosity, a method is required to predict it independently of the Walther model parameters. The T_g^W calculated from Equation 7.1 were found to correlate to molecular weight, M, as follows:

$$\frac{1}{T_g^W} = 0.9482\left(\frac{1}{M}\right) + 0.027 \tag{7.2}$$

Figure 7.3 shows the relationship between parameter A and fragility ratio (with T_g determined from Equation 7.1) for Development Dataset 1. The A parameter increases as the fragility ratio decreases indicating a more dramatic change of viscosity near the glass transition temperature for fluids with high values of parameter A. Note that heavy oils and bitumens were found to have A parameters between 8 and 11; that is, they are fragile materials with a dramatic increase of viscosity at low temperatures, as observed by Abivin *et al.* (2011).
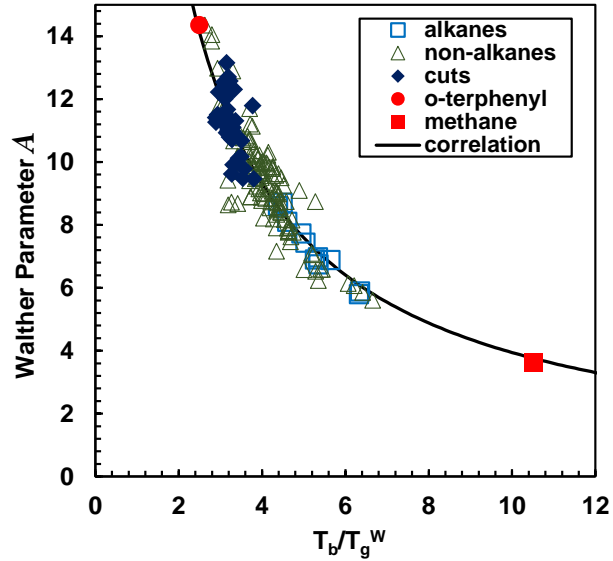
Figure 7.3. The relationship between Walther parameter *A* and the fragility ratio for the fluids in Development Dataset 1.

A correlation to fit the data shown in Figure 7.3 was developed subject to two constraints: 1) fit the fluid with the lowest fragility ratio (and highest value of the *A* parameter); that is, o-terphenyl (Angell, 1988), and; 2) fit the fluid with the highest fragility ratio; that is methane. The proposed correlation is given by:

$$A = \frac{1000}{9.8071 + 24.3836\left(\dfrac{T_b}{T_g^W}\right)} \tag{7.3}$$

where T_b is the normal boiling point in K. The values of the parameter *A* for the components and cuts in the Development Dataset 1 were recalculated using Equations 7.2 and 7.3 and compared to the fitted values. The average absolute relative deviation (AARD), maximum absolute relative deviation (MARD) and bias were of 6, 32 and -0.2%, respectively.

<u>Calculation of Parameter B</u>

The Walther parameter B was indirectly calculated using the correlated parameter A and a synthetic viscosity data point at 37.7°C as follows:

$$B = \frac{A - \log\left[\log\left(\mu_{37.7°C} + 1\right)\right]}{\log(310.7)}$$

(7.4)

where $\mu_{37.7°C}$ is the viscosity at 37.7°C (310.7 K) and atmospheric pressure predicted from Equations 6.15 to 6.18.

7.5.1.2 Walther Model Parameter Correlations for C5-Asphaltenes

The Walther parameters A and B for the C5-aspahltene pseudo component were calculated by fitting the model to the Newtonian viscosity data of asphaltenes in Development Dataset 2. Figure 7.4 shows that both asphaltene samples had similar viscosities even though they were extracted from bitumen samples from two different geographical locations (Western Canada and Colombia). Hence, it was assumed that asphaltenes regardless the origin and chemistry have the same Walther parameters when modeled as a single component. The fitted values of parameters A and B were of 8.3706 and 2.8638 respectively. The model fits the data with an AARD, MARD and bias of 5, 24 and -0.3%, respectively.
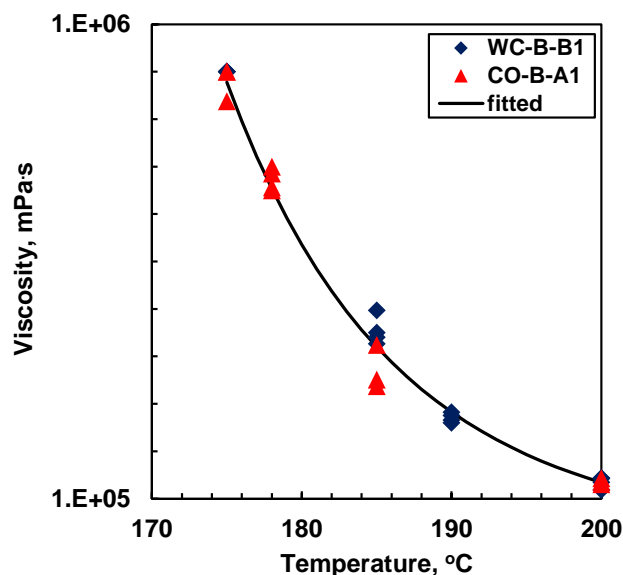
Figure 7.4. Newtonian viscosity of molten C5-asphaltenes from bitumens WC-B-B1 and CO-B-A1 at atmospheric pressure. Solid line corresponds to the Walther model (Equation 4.16) fitted to the data.

7.5.1.3 Correlation for the Viscosibility Parameters δ_1 and δ_2

Correlations for the viscosibility parameters δ_1 and δ_2 were developed using the data in Development Dataset 3. First the viscosibility parameters for each fluid were determined as follows: 1) the viscosity at atmospheric pressure was calculated using the fitted Walther parameters A and B; 2) the viscosities at higher pressure were modeled with Equations 4.14 and 4.15 and the least squares best fit values of δ_1 and δ_2 were determined. The δ_1 parameter was found to correlate with molecular weight, Figure 7.5, as follows:

$$\delta_1 = \frac{0.2715 + 1.4088 \ln(M)}{1 \times 10^5} \tag{7.5}$$

where δ_1 is in kPa^{-1}. The δ_2 parameter was almost constant and was set to a fixed average value:

$$\delta_2 = 1.48 \times 10^{-7} \tag{7.6}$$

where δ_2 is in kPa^{-1}K^{-1}.

189
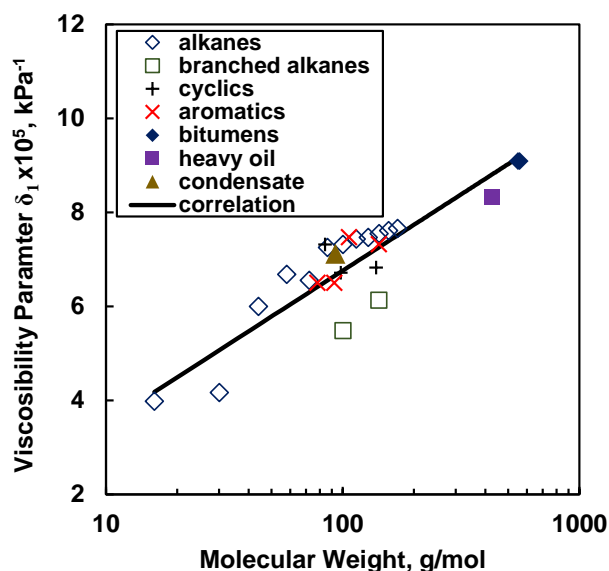
Figure 7.5. Calculated fluid-specific viscosibility parameter δ_1 versus molecular weight of the fluids in the Development Dataset 3.

7.5.1.4 Correlation for Viscosity Binary Interaction Parameter α_{ij}^*

A correlation for the prediction of the viscosity binary interaction parameters for the Walther mass-based mixing rules (Equations 4.17 and 4.18) was developed using viscosity data of pure hydrocarbon binaries and bitumen/solvent pseudo-binaries in the Development Dataset 4. For the purpose of developing the α_{ij}^* correlation, the crude oils were modeled as a single component and their model parameters calculated as in the case of pure components. First, the α_{ij}^* for each binary or pseudo-binary was determined as follows: 1) the Walther parameters A and B of both components were calculated by fitting the model to viscosity data at atmospheric pressure (except for ethane, n-propane and n-butane, which were fitted at higher pressure in order to be in the liquid region); 2) the Walther parameters A and B of the binary or pseudo-binary were calculated using the mass-based mixing rules (Equations 4.17 and 4.18) and the best fit value of α_{ij}^* was determined from the objective function defined in Equation 4.12.

The experimentally derived α_{ij}^* were used to find a correlation. The normalized specific gravity difference, ΔSG_{norm} defined in Equation 5.2, was selected as the correlating

190

parameter because it has been successfully used in correlations for density binary interaction parameters (Saryazdi *et al.*, 2013) and viscosity binary interaction parameters for the Expanded Fluid (EF) model (Section 5.4). Therefore, the α_{ij}^* values were plotted against the normalize difference of specific gravity of the paired components, Figure 7.6.
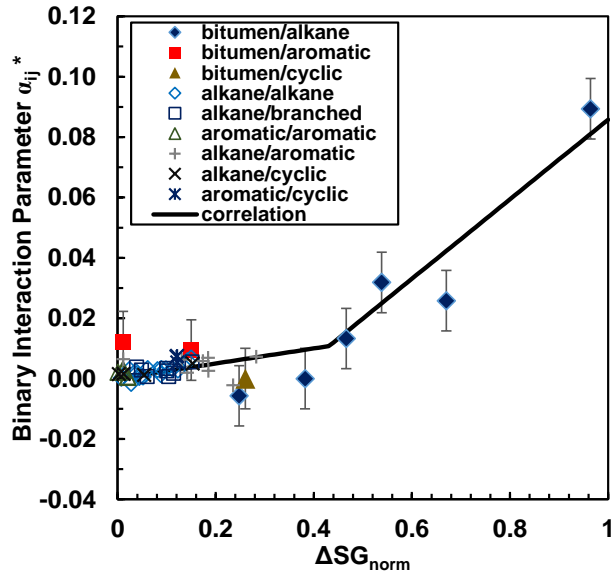
Figure 7.6. Viscosity binary interaction parameter, α_{ij}^*, versus ΔSG_{norm} for the pure hydrocarbon binaries and bitumen/solvent pseudo-binaries for the binaries and pseudo-binaries in the Development Dataset 4.

Figure 7.6 provides two notable observations: 1) the bitumen/solvent α_{ij}^* increases rapidly above $\Delta SG_{norm} = 0.431$, and; 2) below $\Delta SG_{norm} = 0.431$, the α_{ij}^* values slightly increase with ΔSG_{norm}. The trends were fit with the following correlation:

$$\Delta SG_{norm} \leq 0.431: \qquad \alpha_{ij}^* = 0.025 \Delta SG_{norm} \tag{7.7}$$

$$\Delta SG_{norm} > 0.431: \quad \alpha_{ij}^* = 0.1318 \Delta SG_{norm} - 0.04603 \tag{7.8}$$

The interaction parameters were found to be independent of temperature and composition. Since the interaction parameters apply to both pure hydrocarbon mixtures and dilute crude oils, it is also expected to apply to mixtures of pseudo-components.

7.6 Testing the Correlations for the Viscosity Model Parameters

7.6.1 *Testing the Walther Parameters for Maltene Pseudo-Components*

The correlation for parameter *A* and the calculation of parameter *B* were tested on the atmospheric pressure viscosity data of the heavy oil distillation cuts in the Development Dataset 1 and the distillation cuts in the Test Dataset 1. Each cut was modeled as a single component. As an example, Figure 7.7a shows the measured and calculated viscosity of three distillation cuts of Western Canada bitumen WC-B-A1 (solid symbols) and two distillation cuts of South East Asian conventional oil Minas Sumatra (open symbols). These crude oils are not only from different regions but also illustrate the range of viscosities in the dataset.
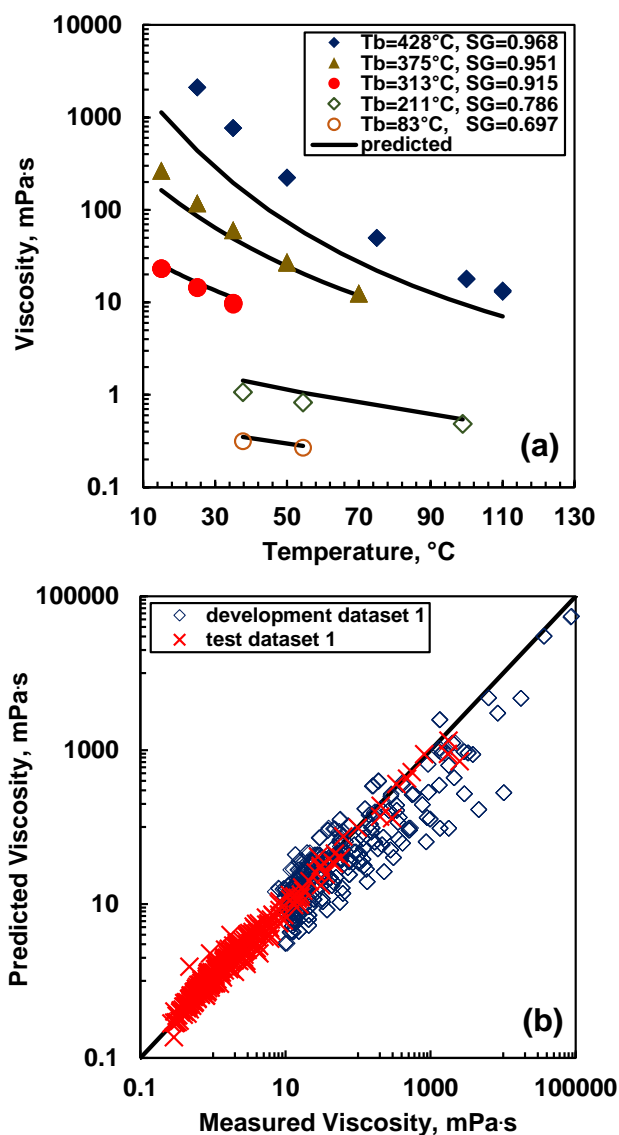
Figure 7.7. a) Viscosity versus temperatures of distillation cuts of WC-B-A1 bitumen (This Study; solid symbols) and Minas Sumatra conventional oil (Beg *et al*., 1988; open symbols); b) dispersion plot of the cuts in the Development Dataset 1 (solid symbols) and Test Dataset 1 (crosses).

In general, the Walther model with correlated parameters slightly over-predicts the viscosity of low boiling point cuts and under-predicts the viscosity of high boiling point distillation cuts. The main source of the deviations is the prediction of the single viscosity data point at 37.7°C which performs well for low and medium boiling point distillation

cuts but considerably under-predicts the data point for high boiling point cuts. The predicted viscosity of the heavy distillation cuts likely deviates because they have a relatively high content of polyaromantic compounds. A dispersion plot for all of the cuts in Development Dataset 1 and Test Dataset 1 is provided in Figure 7.7b. The overall AARD, MARD, and bias were 49, 148 and -18%, respectively, for the cuts in Development Dataset 1, and 23, 100 and +11%, respectively, for Test Dataset 1. The lower deviations in Test Dataset 1 are not surprising because this dataset consists of low viscosity conventional oils cuts.

7.6.2 *Testing the Asphaltene Walther Parameters*

The validity of Walther parameters for C5-asphaltenes was tested by predicting the viscosity of a partially deasphalted bitumen from Test Dataset 2. The maltenes and asphaltenes were each treated as single component fluids for this test. The model parameters for the maltenes were calculated by fitting the Walther model (Equation 4.16) to their viscosity data. The asphaltene parameters were determined previously (Section 7.5.1.2). The Walther parameters A and B for the whole sample were calculated using the mass-based mixing rules (Equations 4.17 and 4.18) with correlated binary interaction parameters (Equations 7.7 and 7.8).

Figure 7.8 shows that the model predicts the viscosity at 16 wt% asphaltenes (moderate deasphalting) with an AARD of just 6%. However, the model under-predicts the viscosity when most of the asphaltenes have been removed (AARDs of 23 and 32%, respectively, for 3 and 4 wt% asphaltenes). It is possible that the residual asphaltenes have different Walther parameters than the whole asphaltenes but the residual asphaltenes are expected to be more like resins and therefore have lower viscosity than the whole asphaltenes. Hence, the model would be expected to over-predict rather than under-predict the highly deasphalted oil viscosity. A more likely explanation is that some of the lighter maltene components were removed during the evaporation of the solvent (see a description of the deasphalting procedure in Section 3.2.3) leading to a mismatch between the actual composition and the composition used in the model; in other words, the composition of the

resulting material contains less lighther components, and consequently higher viscosity, than the original composition used in the model. Overall, the constant asphaltene parameters capture the trend of viscosity with asphaltene content with overall AARD, MARD, and bias of 16, 32, and -16%, respectively.
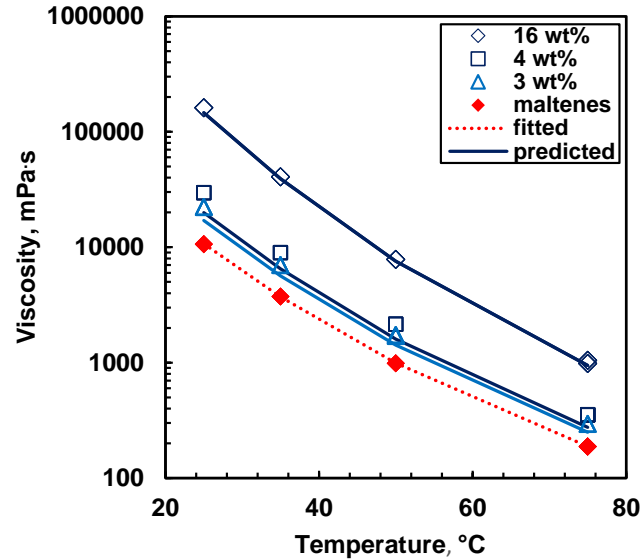
Figure 7.8. Viscosity predicted using the Walther model for three partially deasphalted samples of the same bitumen with original asphaltene content of 22 wt% (This Study). Data and predictions at atmospheric pressure.

7.6.3 *Testing the Correlations for the Viscosibility Parameters*

The viscosibility parameter (δ_1 and δ_2) correlations (Equations 7.5 and 7.6) were tested on the high pressure viscosity data for the Athabasca 1 and McKay River crude oils in Test Dataset 3. The other oils in the test dataset were not used because high pressure viscosity data was not available. For all calculations, the δ_2 parameter was set to the constant value from Equation 7.6. The crude oils were modeled as single components. The Walther parameters *A* and *B* for Athabasca 1 were determined by fitting its atmospheric viscosity data and the experimentally derived value for δ_1 was determined by fitting the model to the higher pressure data. There were no atmospheric pressure data for the McKay River crude oil; therefore, *A*, *B*, and the experimentally derived value for δ_1 were determined simultaneously by fitting the model to the higher pressure data. Finally, the higher pressure

viscosities were predicted from the GW model (Equations 4.14 to 4.16) using δ_1 and δ_2 from Equations 7.5 and 7.6, respectively. The viscosity of the oils was also calculated using fitted δ_1 for comparison purposes. Table 7.3 shows that the deviations with the correlated parameters are only slightly higher than the deviations with the fitted parameters. Overall, the model with the constant δ_2 and correlated δ_1 had average deviations below 10%.

Table 7.3. Summary of deviations of fitted and correlated δ_1 for the prediction of viscosities at high pressure of crude oils Athabasca 1 and McKay River.

Oil	Model with fitted δ_1				Model with Correlated δ_1			
	$\delta_1 \times 10^5$ kPa^{-1}	AARD %	MARD %	Bias %	$\delta_1 \times 10^5$ kPa^{-1}	AARD %	MARD %	Bias %
Athabasca 1	10	6	12	-5	9.06	9	17	-8
McKay River	9.61	7	16	+2	9.31	8	16	+2

7.6.4 *Testing the Correlation for the Binary Interaction Parameter*

The viscosities of the pure hydrocarbon binaries in Development Dataset 4 (all at atmospheric pressure) were modeled using previously fitted *A* and *B* parameters and the mixing rules (Equations 4.17 and 4.18) with both fitted and correlated α_{ij}^{*}'s. The AARD, MARD and bias were 1, 10 and -0.10%, respectively, with fitted α_{ij}^{*}'s. and 3, 24 and +2%, respectively, with correlated α_{ij}^{*}'s.

The viscosities of the bitumen/solvent pseudo-binaries in Development Dataset 4 and Test Dataset 3, including high pressure data, were also modeled using fitted *A* and *B* parameters, predicted δ_1 and δ_2 parameters, and the mixing rules (Equations 4.17 to 4.19) with both fitted and correlated α_{ij}^{*}'s. Figure 7.9 shows examples of a good prediction and a poor prediction. A summary of the deviations is presented in Table 7.4 for the pseudo-binaries in the Development Dataset 4 and Table 7.5 for Test Dataset 3. For Development Dataset 4, the overall AARD, MARD and bias were 10%, 66%, and -2%, respectively, with fitted α_{ij}^{*}'s and 27, 78, and -11%, respectively, with correlated α_{ij}^{*}'s. For Test Dataset 3, the overall AARD, MARD and bias were 8, 41, and -2%, respectively, with fitted α_{ij}^{*}'s and 22, 112, and +9%, respectively, with correlated α_{ij}^{*}'s. The largest deviations in Table 7.5 correspond to the pseudo-binaries of crude oil and toluene. Overall, in all but three cases,

the error was less than or equal to simply setting the interaction parameters to zero (not shown here). The three exceptions were the pseudo-binaries bitumen/*n*-eicosane and bitumen/cyclohexane in Development Dataset 4 and Cold Lake 2/ethane in Test Dataset 3. Significant error reductions were obtained for mixtures of heavy oils with low carbon number *n*-alkanes.
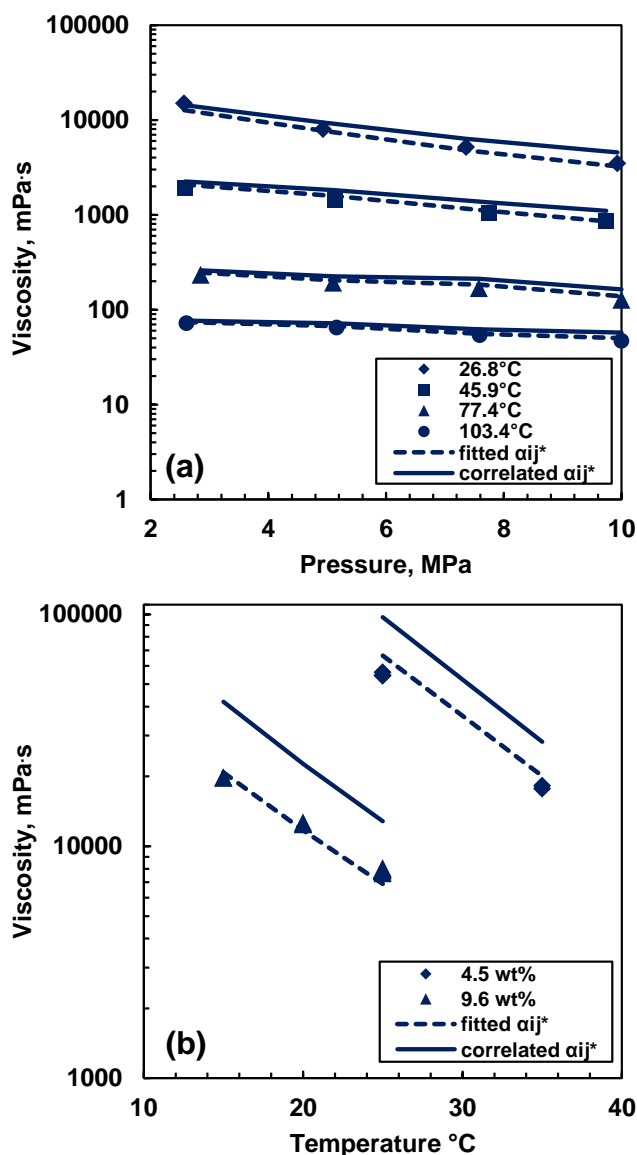
Figure 7.9. Examples of good and poor predictions using correlated viscosity binary interaction parameters: a) Cold Lake Bitumen 2 saturated with methane (Mehrotra and Svrcek, 1988), and; b) CO-B-A1 bitumen diluted with toluene, solvent contents of 4.5 and 9.6 wt% (this study). Fitted and correlated interaction parameters of both mixtures are reported in Tables 7.4 and 7.5.

Table 7.4. Summary of the deviations of the calculated viscosities of the diluted crude oils in Development Dataset 4. B1 and B2 correspond to bitumen WC-B-B1 and WC-B-B2. MN stands for 1-methylnaphthalene.

Mixture	Mixing Rules with Fitted α_{ij}^*				Mixing Rules with Correlated α_{ij}^*			
	α_{ij}	AARD %	MARD %	Bias %	α_{ij}	AARD %	MARD %	Bias %
B1/ethane	+0.0894	3	6	0	+0.0811	13	26	+13
B1/ propane	+0.0258	6	22	+2	+0.0418	27	56	-27
B1/*n*-butane	+0.0318	8	27	+1	+0.0244	18	62	+18
B1/*n*-pentane	+0.0133	7	28	+1	+0.0154	7	35	-5
B1/*n*-heptane	-0.0096	13	31	+5	+0.0096	38	69	-38
B1/toluene	+0.0094	8	29	-2	+0.0376	19	78	+18
B2/*n*-eicosane	-0.0057	19	36	-6	+0.0061	38	56	-38
B2/cyclohexane	+0.0094	21	66	-15	+0.0065	32	74	-32
B2/MN	+0.013	7	29	-3	0	54	70	-5

Table 7.5. Summary of deviations of the pseudo-binaries crude oil/solvent in Test Dataset 3. MN stands for 1-methyl naphthalene. Oil samples CO-B-A1 and ME-CV-A1 corresponds to a Colombian bitumen and a Middle East conventional oil.

Mixture	Mixing Rules with Fitted α_{ij}^*				Mixing Rules with Correlated α_{ij}^*			
	α_{ij}	AARD %	MARD %	Bias %	α_{ij}	AARD %	MARD %	Bias %
Athabasca 1/toluene	+0.0128	6	34	+5	+0.0036	49	71	+49
Athabasca 1/xylene	+0.0111	6	20	+0.4	+0.0038	35	61	+35
Athabasca 1/decane	+0.0075	7	27	+1	+0.0079	7	28	+2
Athabasca 1/tetradecane	+0.0065	7	24	+2	+0.0068	7	25	+2
Athabasca 2/pentane	+0.0154	14	41	+4	+0.0147	14	42	+5
Athabasca 3/propane	+0.0387	6	14	-12	+0.0413	6	20	-16
Cold Lake 1 /toluene	+0.0086	8	28	-4	+0.0033	17	51	+10
McKay River/decane	+0.0076	10	28	+2	+0.0079	10	29	+1
McKay River/toluene	+0.0103	7	11	+1	+0.0036	23	31	+24
Cold Lake 2/methane	+0.1349	6	15	-18	+0.0954	19	30	-5
Cold Lake 2/ethane	-0.0112	14	28	-8	+0.0789	47	75	-53
CO-B-A1/toluene	+0.0157	11	22	+1	+0.0058	76	112	+76
CO-B-A1/MN	+0.0012	2	3	-0.2	+0.0003	8	11	+8
ME-CV-A1/toluene	-0.0061	7	25	-0.5	0	11	32	-11
ME-CV-A1/MN	+0.0018	7	22	+2	+0.0041	7	24	-1

7.7 Testing the Viscosity Model Predictions

7.7.1 *C5-Maltenes*

The model predictions were first tested on the C5-maltenes in Test Dataset 4. The maltene fraction was characterized into 12 pseudo-components as described previously. The pseudo-component Walther parameters (*A* and *B*) were calculated from the correlations previously presented and then the parameters for the whole maltene fraction at atmospheric pressure were calculated from the mixing rules (Equations 4.17 and 4.18) with the correlated binary interaction parameters (Equations 7.7 and 7.8). The viscosibility parameters (δ_1 and δ_2) for the whole maltenes were calculated from the respective correlations (Equations 7.5 and 7.6). Finally, the viscosity was determined from the generalized Walther model (Equation 4.14).

Figure 7.10 shows the predicted viscosities of C5-maltenes from bitumens WC-B-A2 and WC-B-B1 (this study). Note that the pseudo-component correlations were based on cuts from the WC-B-B1 bitumen and therefore the results for this oil are not truly independent. The generalized Walther model with correlated parameters captures the change of viscosity of WC-B-A2 and WC-B-B1 C5-maltenes with temperature and pressure as shown in Figures 7.10a and 7.10b, respectively. Note that the model slightly over-predicted the viscosity of the WC-B-B1 C5-maltenes and under-predicted the viscosity of the rest of C5-maltene samples in the Test Dataset 4.

The deviations of the fitted and predicted maltene viscosities are provided in Table 7.6 and Table 7.7, respectively. The generalized Walther model predicted the viscosity of the maltenes in Test Dataset 4 with an overall AARD, MARD and bias of 56, 94 and -53% respectively. In comparison, the model could fit the data with an overall AARD, MARD and bias of 4, 15 and +0.2% respectively. The deviations for the maltene viscosities are comparable to those found for the distillation cuts, which suggest that the main source of deviation was the prediction of the synthetic viscosity data point at 37.7°C (Equations 6.15 to 6.18).
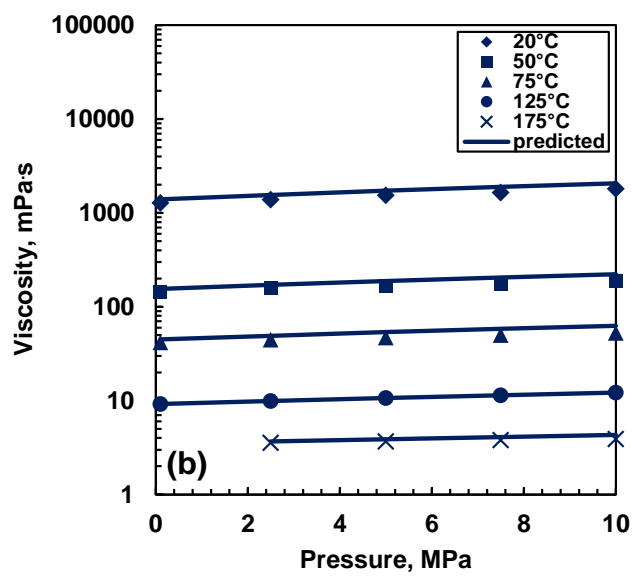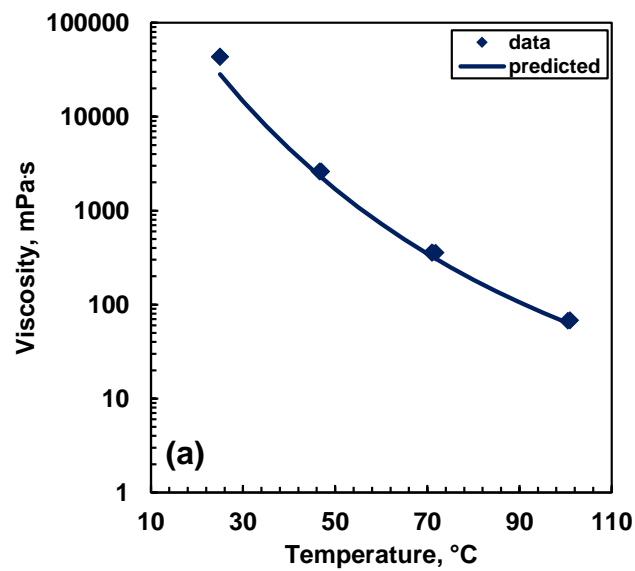
Figure 7.10. Measured and predicted viscosity of C5 maltenes: a) WC-B-A2 at atmospheric pressure and b) WC-B-B1. The viscosity of both samples was measured in this study.

200

Table 7.6. Fitted parameters and deviations of the fitted viscosities for the C5-maltenes in Test Dataset 4.

C5-Maltenes	A	B	AARD %	MARD %	Bias %
Used for Correlations					
WC-B-B1	9.765	3.758	3	9	+2
WC-B-A1	9.599	3.656	1	2	-0.1
US-HO-A1	9.646	3.711	2	5	-0.1
MX-HO-A1	9.442	3.628	4	7	0
CO-B-A1	10.879	4.133	6	15	0
CO-B-B1	9.950	3.821	5	12	0
Not Used for Correlations					
WC-B-A2	10.866	4.123	5	11	0

Table 7.7. Predicted parameters and deviations of the predicted viscosities for the C5-maltenes in Test Dataset 4.

C5-Maltenes	A	B	AARD %	MARD %	Bias %
Used for Correlations					
WC-B-B1	9.682	3.722	12	23	+12
WC-B-A1	9.673	3.731	73	84	-73
US-HO-A1	9.731	3.838	86	94	-86
MX-HO-A1	9.488	3.689	65	78	-65
CO-B-A1	9.328	3.541	55	85	-55
CO-B-B1	9.628	3.776	84	94	-84
Not Used for Correlations					
WC-B-A2	10.514	3.987	17	35	-17

7.7.2 *Whole Crude Oils*

Finally, the model predictions were tested on the whole crude oils in the Test Dataset 5. Each oil was split into maltenes and asphaltenes and each fraction characterized separately as already described. The Walther parameters for the 12 maltene pseudo-components were determined as described in the previous section. The previously determined fixed parameters were used for the single component C5-asphaltenes. The Walther parameters of the whole crude oil were calculated from the maltene pseudo-component and asphaltene parameters using the mass-based mixing rules with correlated interaction parameters. The viscosibility parameters were determined for the whole oil and its viscosity predicted as described in the previous section.

Figure 7.11 shows the predicted viscosity for the Western Canada bitumen WC-B-A2 at pressures up to 10 MPa (a good prediction) and the European heavy oil EU-HO-A1 at atmospheric pressure (a poor prediction). Note that none of those two oils was used to develop the correlations for the Walther parameters. The model under-predicts the viscosity of both crude oils; however, in the case of the Western Canada bitumen the under-predicted viscosity is remarkably close to the actual data. The model predicted the correct trends with temperature and pressure but systematically under-predicted the magnitude of the viscosity. The error is again attributed mainly to the inaccuracy of the synthetic viscosity data point at 37.7°C. In general, the model under-predicted the viscosity of heavy oils and bitumens and slightly over-predicted the viscosity of a conventional oil in the Test Dataset 5.

The deviations of the fitted and predicted whole oil viscosities are provided in Tables 7.8 and 7.9, respectively. Note that parameter δ_1 was only estimated when high pressure data was available to fit the model. The modified Walther model predicted the viscosity of the crude oils in the Test Dataset 5 with an overall AARD, MARD and bias of 57, 98 and -52% respectively. In comparison, the model could fit the data with an overall AARD, MARD and bias of 4, 37 and +0.1%, respectively. There was no significant difference in the errors between the oils whose cuts were used in the development datasets and those which were not.
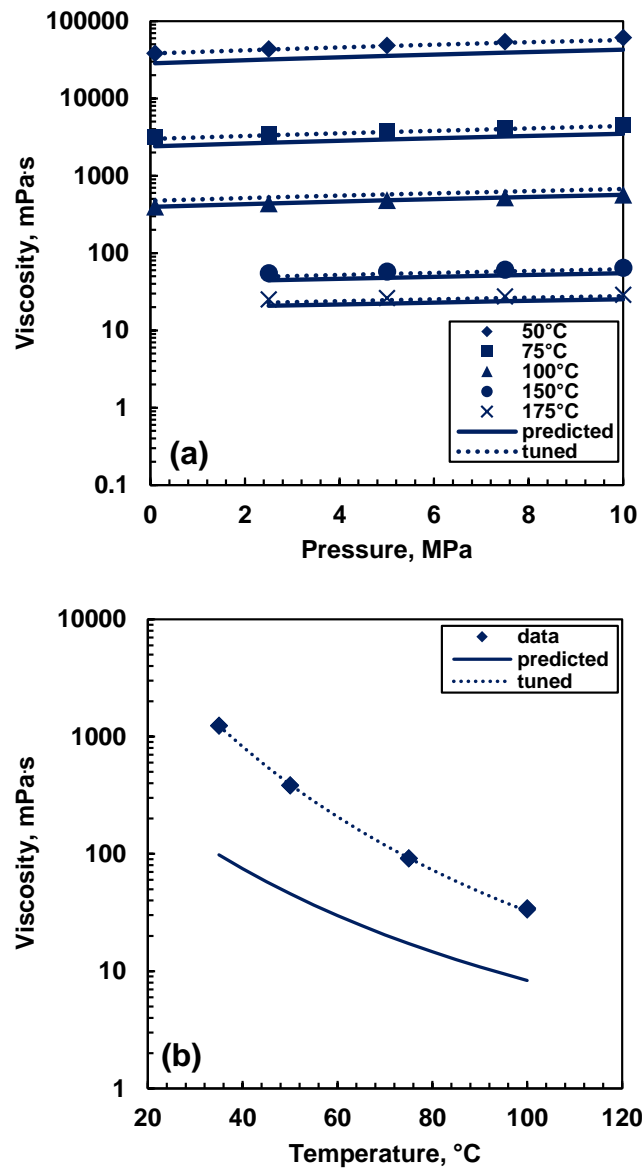
Figure 7.11. Predicted and tuned viscosities calculated from the generalized Walther model for: a) a Western Canada Bitumen (WC-B-A2) and b) a European heavy oil (EU-HO-A1).

Table 7.8. Summary of deviations and bias of fitted viscosities by the generalized Walther model for the oils in Test Dataset 5. ANS and SJV stand for Alaska North Slope and San Joaquin Valley oils respectively.

Oil	A	B	$\delta_1 \times 10^5$ kPa^{-1}	AARD %	MARD %	Bias %
Used for Correlations						
WC-B-B1	9.402	3.531	9.23	5	18	0
WC-B-A1	9.238	3.468	-	3	5	0
US-HO-A1	9.271	3.536	-	4	12	0
MX-HO-A1	9.009	3.339	-	0	1	0
CO-B-A1	9.305	3.448	-	3	8	0
CO-B-B1	9.153	3.426	-	1	4	0
Not Used for Correlations						
WC-B-A2	9.768	3.629	9.09	2	11	0
WC-B-A3	10.705	4.038	9.90	11	25	-2
EU-HO-A1	9.5832	3.654	-	2	4	0
ME-CV-A1	8.302	3.321	-	3	7	0
ANS	9.641	3.851	-	0	0	0
Athabasca	9.664	3.620	-	2	6	0
Boscan	10.127	3.813	-	25	37	+3
SJV	10.846	4.147	-	1	2	0

Table 7.9. Summary of deviations and bias of predicted viscosities from the generalized Walther model for the oils in Test Dataset 5. ANS and SJV stand for Alaska North Slope and San Joaquin Valley oils respectively.

Oil	A	B	$\delta_1 \times 10^5$ kPa^{-1}	AARD %	MARD %	Bias %
Used for Correlations						
WC-B-B1	9.448	3.575	9.15	56	83	-56
WC-B-A1	9.461	3.591	9.42	72	84	-72
US-HO-A1	9.545	3.706	8.82	79	89	-79
MX-HO-A1	9.250	3.515	9.06	96	98	-96
CO-B-A1	9.159	3.425	9.15	83	89	-83
CO-B-B1	9.334	3.573	9.01	87	95	-87
Not Used for Correlations						
WC-B-A2	10.062	3.751	9.76	21	30	-21
WC-B-A3	10.691	4.072	9.30	64	83	-64
EU-HO-A1	9.689	3.772	8.58	84	92	-84
ME-CV-A1	9.718	3.902	6.18	10	20	-10
ANS	9.477	3.770	8.38	30	33	+30
Athabasca	10.072	3.780	9.67	9	27	-3
Boscan	9.397	3.529	9.35	40	66	-40
SJV	9.646	3.719	8.65	62	85	-62

The sensitivity of the model to the number of pseudo-components in the maltene fraction was also tested. The predicted viscosities for a Middle East conventional oil (ME-CV-A1) using 1, 3, 6 and 12 pseudo-components are shown in Fig. 7.12. A minimum of three pseudo-components was required to obtain consistent predictions for this oil and for the other oils in Test Dataset 5. This observation indicates that the proposed viscosity model does not impose restrictions on the number of pseudo-components beyond what is typically required to model phase behavior data using an equation of state (Catellanos-Diaz *et al.*, 2011).
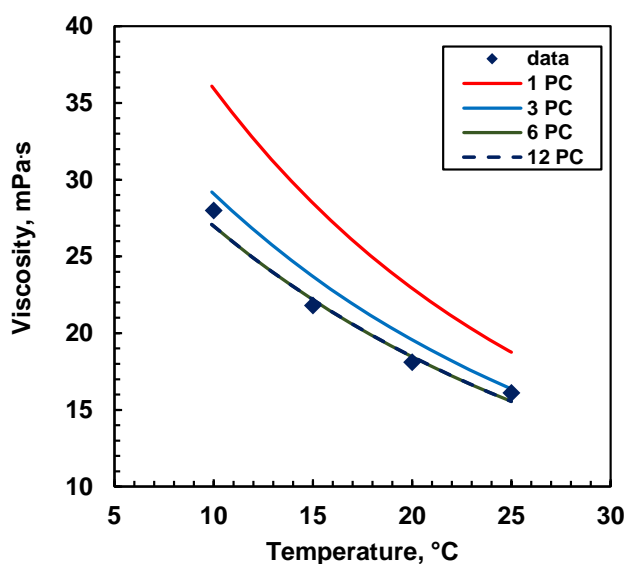
Figure 7.12. Effect of number of pseudo-components used to model the maltene fraction on the viscosity predicted from the Generalized Walther model. The data corresponds to a Middle East conventional oil (ME-CV-A1) at atmospheric (this study).

7.8 Tuning the Model

The correlated generalized Walther model can be easily tuned if a single viscosity data point is available. In this study, the model was tuned using a single data point at atmospheric pressure because such information is usually available in industrial applications. A single constant multiplier was applied to the calculated parameter B to match the viscosity data point. The results of the tuned model for a bitumen and a heavy oil are shown in Figure 7.11. In those two cases, the tuned model predicted the data within

5%. Note that once the model has been tuned to the data point at atmospheric pressure, it predicts the viscosity of the fluid at high pressures and temperatures, Figure 7.11a.

A summary of the estimated multipliers for the parameter *B* and the deviations and bias for the oils in the Test Dataset 5 are presented in Table 7.10. The overall AARD, MARD and bias were of 8, 67 and -2% respectively. In all cases, the tuned model deviations were notably reduced compared to those produced by the non-tuned model. The AARD's of the tuned model are slightly higher than those estimated when the model was fit to the data except for the San Joaquin Valley oil.

Table 7.10. Summary of deviations and bias of the tuned Walther model for the oils in the Test Dataset 5. ANS and SJV stand for Alaska North Slope and San Joaquin Valley oils respectively.

Oil	Multiplier *B*	AARD %	MARD %	Bias %
Used in Correlations				
WC-B-B1	0.993	5	21	-3
WC-B-A1	0.991	6	14	-6
US-HO-A1	0.984	4	18	-2
MX-HO-A1	0.977	3	8	-3
CO-B-A1	0.990	4	11	+3
CO-B-B1	0.979	3	9	-3
Not Used in Correlations				
WC-B-A2	0.999	5	11	-5
WC-B-A3	0.990	11	24	-4
EU-HO-A1	0.980	2	6	-0.36
ME-CV-A1	0.997	5	16	-5
ANS	1.004	1	1	+1
Athabasca	1.000	9	27	-3
Boscan	0.997	27	67	+18
SJV	0.987	21	34	-15

7.9 Validated Range of the Model

As noted previously, the model only applies to single phase Newtonian liquids at reduced temperature below 0.75. The model was tested on pure hydrocarbon at temperatures from -100 to 400 °C, pressures up to 100 MPa, and viscosities from 0.1 to 6 mPa·s. A list of

fitted Walther parameters for more than 120 pure hydrocarbons is included in Appendix F. The model has been tested on crude oils from North America, South America, Europe, and the Middle East with C5-asphaltene content up to 27 wt%, API gravities ranging from 8 to 30, and viscosities ranging from 10 to 7×10^6 mPa·s at temperatures and pressures up to 200°C and 10 MPa, respectively. It is strongly recommended to measure at least one viscosity data point for an oil so that the model can be tuned.

7.10 Summary

A predictive but tunable model for the liquid viscosity of characterized crude oils at any condition was developed based on the generalized Walther correlation. The crude oils are characterized into maltene pseudo-components and a single C5-asphaltene component. The viscosity model inputs are the absolute temperature, pressure, two component parameters (A and B), two oil parameters (δ_1 and δ_2), and binary interaction parameters. The asphaltene parameters were determined experimentally and fixed for all cases. Correlations were developed for the fluid specific parameters of the maltenes and the binary interaction parameters. The required data are the C5-asphaltene content, the specific gravity and molecular weight of the oil, and the boiling point distribution of the maltenes. The specific gravity and molecular weight distributions of the maltenes are also required but are generated from existing correlations.

The proposed model predicted the viscosity of 5 Western Canadian and 2 Colombian bitumens, 3 Americans, 1 Mexican, 1 Venezuelan and 1 European heavy oils and also a conventional oil from Middle East with an overall AARD, MARD and bias of 57, 98 and -52% respectively. The main source of inaccuracy in the model is the prediction of a synthetic data point at 37.7°C at atmospheric pressure. A simple tuning scheme was developed for use with a single measured viscosity data point using a single common multiplier for the B parameter. The overall AARD, MARD and bias were reduced to 8, 67, and -2%, respectively. For comparison, the overall AARD, MARD, and bias for the fitted model were 4, 37, and +0.1%, respectively.

CHAPTER EIGHT: MODELLING THE THERMAL CONDUCTIVITY OF PURE HYDROCARBONS, CRUDE OILS AND THEIR MIXTURES USING AN EXPANDED FLUID MODEL

This chapter presents the development and testing of a thermal conductivity model for pure hydrocarbons, crude oils and their mixtures based on the Expanded Fluid (EF) concept. The proposed model is intended for use in process simulators and therefore must be simple and rapid to implement and apply over the entire fluid phase diagram.

8.1 Background and Objectives

Thermal conductivity is a measure of a material's ability to conduct heat and it depends on the state of the material, temperature, and pressure. In this thesis, the fluid region is of interest. To illustrate the effects of temperature and pressure on non-polar hydrocarbons, consider the thermal conductivity of *n*-propane.

Figure 8.1a shows the thermal conductivity of liquid *n*-propane along the saturated liquid line and at two different pressures. In general, the thermal conductivity of the decreases linearly with temperature from the melting to the boiling point (Riazi and Faghrl, 1985). The thermal conductivity increases slightly with pressure. Note that the thermal conductivity of the saturated liquid decreases rapidly in the vicinity of the critical point.

Figure 8.1b shows the thermal conductivity of gaseous *n*-propane along the saturated vapor line and also at different pressures. At pressures below 1 MPa, the thermal conductivity increases with temperature and slightly increases with pressure. In this low pressure region, the effect of pressure on thermal conductvity is so small that it is usually neglected for engineering applications (Poling *et al*., 2001). At higher pressures, the thermal conductivity increases with temperature and pressure. Note that the effect of pressure is significant in the vicinity of the critical point. In addition, in the vicinity of the critical point, the thermal conductivity of hydrocarbon gases decrease with temperature.
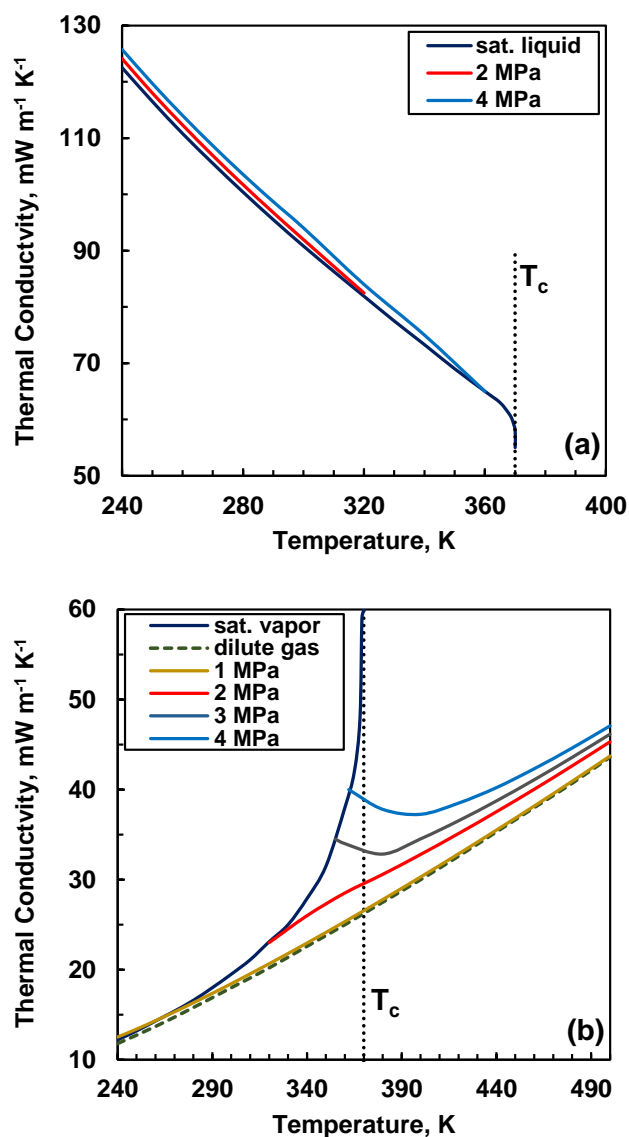
Figure 8.1. Thermal conductivity of liquid (a) and gaseous (b) *n*-propane. Data from Holland *et al*. (1979). T_c is the critical temperature (369.85 K). The critical pressure of *n*-propane is 4.25 MPa.

To date, the physical mechanisms that explain thermal conductivity behavior in fluids is not well captured in theoretical or semi-empirical models (Poling *et al*., 2001). Several empirical and semi-empirical approaches have been proposed for the modelling and prediction of thermal conductivity and most of these models only apply to the liquid phase.

Only the Corresponding States (CS) model describes the thermal conductivity of liquid and gas phases across the phase diagram; however, the application of this model is challenging because it requires complex iterative calculations for the estimation of the reference component properties and the calculation of the model parameters. In addition, the application of CS model to heavy petroleum fluids is problematic because these fluids often correspond to the reference fluid (methane or propane) at temperatures below the reference fluid's freezing point (Pedersen and Fredenslund 1987; Baltatu *et al*. 1999). The CS model as well as other empirical models for gases and liquids were presented in Section 2.5.4.

An alternative is to develop a model for thermal conductivity based on the Expanded Fluid (EF) concept. The EF concept proposes that properties that depend on the spacing between molecules, such as viscosity and thermal conductivity, decrease monotonically as the fluid expands from a compressed state near the liquid-solid phase transition to the dilute gas state. The compressed state is defined where the viscosity tends to infinity and the thermal conductivity to its liquid-solid phase transition value. This approach was successfully applied to viscosity as discussed in Chapters 5 and 6.

This chapter focuses on the following thesis objectives:
1. To develop a simple and fast convergence thermal conductivity model based on the Expanded Fluid (EF) concept applicable across the entire phase diagram.The following steps were required to complete this objective: i) assemble experimental thermal conductivity and density data of pure hydrocarbons from assorted chemical families including alkanes, cyclics and aromatics (this dataset was collected from the NIST Database, 2008); ii) find a mathematical relationship between density and thermal conductivity applicable to pure hydrocarbons regardless of chemical family; iii) collect experimental thermal conductivity and density data of crude oils; iv) test the proposed model on these data.
2. To extend the model to mixtures through simple mass-based mixing rules with adjustable binary interaction parameters. The model was extended to mixtures by developing mass-based mixing rules for the model parameters. Binary interaction

parameters were used to capture the non-ideality of the mixing process. A correlation was proposed for the estimation of binary interaction parameters. This correlation was based on literature data of pure hydrocarbon binaries and bitumen/solvent pseudo-binaries data generated in this thesis.

3. To propose a methodology to predict crude oil model parameters based on distillation assay data consistent with the methodology used for the Expanded Fluid and Generalized Walther viscosity models.The thermal conductivity model was extended to pseudo-component characterized oils by developing correlations for the pseudo-component model parameters. The predictive capability of the EF based thermal conductivity model was tested on a dataset containing 7 crude oils from disparate geographical locations.

8.2 Datasets

To develop a thermal conductivity model based on the Expanded Fluid concept, both thermal conductivity and density data were required. Other physical properties such as molecular weight, specific gravity, and boiling point were collected for the development of fluid-parameter correlations. Data for pure hydrocarbon compounds and distillation cuts of crude oils were available from the literature. Data for crude oils, diluted crude oils, and asphaltenes were collected in this thesis and are outlined below.

8.2.1 Data Collectected in This Study

The thermal conductivities of crude oils, diluted crude oils, and asphaltenes were measured using the hot wire apparatus described in Section 3.2.9. All the data were collected at Grashof numbers below 10,000 to avoid the effect of natural convection (See Section 3.2.9.5).

Crude Oils

The thermal conductivities of the crude oils samples WC-B-B3, WC-B-A3(1), WC-B-A3(2) and EU-HO-A1 and a deasphalted sample of WC-B-B3 (WC-B-B3-DAO) were measured at temperatures and pressures up to 125°C and 10 MPa, respectively. Note, 8 days were required to collect these thermal conductivity data for each crude oil. The

thermal conductivities of crude oil samples WC-B-A1, CO-B-B1 and ME-CV-A1 were measured at only two conditions: room temperature and 50°C, both at atmospheric pressure. The thermal conductivities of the crude oils are reported in Appendix G.

A distillation assay was performed and the C5-asphaltene and toluene insoluble contents were measured for each of the oils. The densities of the crude oils samples WC-B-B3, WC-B-B3-DAO, WC-B-A3(1), WC-B-A3(2) and EU-HO-A1 were measured in the capillary viscometer apparatus at temperatures and pressures up to 175°C and 10 MPa, respectively. The densities of the samples WC-B-A1, CO-B-B1 and ME-CV-A1 were measured at temperatures up to 90°C at atmospheric pressure using the Anton Paar density meter. The densities of samples WC-B-A3(1), EU-HO-A1, WC-B-A1, CO-B-B1 and ME-CV-A1 were reported by Ramos-Pallares *et al.* (2016a) and are included in Appendix G. Other physical properties of the oils are summarized in Table 8.1.

Note, the WC-B-A3(2) sample was recovered from the same reservoir as WC-B-A3(1) but had different density, viscosity, and thermal conductivity values. These values were measured as noted above. Other properties such as molecular weight and hydrogen to carbon ratio, as well as the distillation assay data, were assumed to be the same as WC-B-A3(1) sample.

Table 8.1. Properties of crude oils used in this chapter including specific gravity (SG), atomic hydrogen-to-carbon (H/C) ratio, molecular weight (M), viscosity, μ, and thermal conductivity, λ, both at 20°C and atmospheric pressure, asphaltene content, and toluene insoluble (TI) content.

Sample	SG	H/C	M	μ at 20°C mPa·s	λ at 20°C mW/m.K	C5-Asph. wt%	TI wt%
WC-B-B3	1.020	1.473	558	150000	137.0	22	0.68
WC-B-A3(1)	1.010	1.453	550	356,000	138.3	18	0.55
WC-B-A3(2)	1.009	1.453	550	300,000	139.6	18	0.55
CO-B-B1	1.000	1.473	577	158,000	136.1	22	0.74
WC-B-A1	0.996	1.577	585	72,800	137.8	16	0.51
EU-HO-A1	0.968	1.596	475	5,036	129.0	7	0.31
ME-CV-A1	0.872	1.756	475	18.1	125.0	3.8	0.03
WC-B-B3-DAO	0.984	1.533	483	1,600	133.1	0	0

Diluted Crude Oils

The thermal conductivities of the pseudo-binaries WC-B-A3(2)/*n*-pentane, WC-B-A3(2)/cyclohexane and WC-B-A3(2)/toluene were measured at temperatures from 20 to 100°C, pressures up to 10 MPa, and solvent contents up to 40 wt%. The thermal conductivities of the pseudo-binaries WC-B-A3(2)/*n*-heptane and WC-B-A3(2)/*n*-tetradecane were measured only at room temperature, atmospheric pressure, and solvent contents up to 20 wt%. The collected data is presented in Appendix G.

The densities of the pseudo-binaries WC-B-A3(2)/*n*-pentane, WC-B-A3(2)/cyclohexane and WC-B-A3(2)/toluene were measured at temperatures up to 90°C at 0.1 MPa using the Anton Paar density meter. Note, the maximum temperature of the apparatus is 90°C. The same density meter was used to determine the density of the pseudo-binaries WC-B-A3(2)/*n*-heptane and WC-B-A3(2)/*n*-tetradecane at room temperature.

The density of the pseudo-binaries WC-B-A3(2)/*n*-pentane, WC-B-A3(2)/cyclohexane and WC-B-A3(2)/toluene at high pressure was determined using the following mixing rule (Saryazdi *et al*., 2013):

$$\frac{1}{\rho_{MIX}} = \sum_i^{nc} \sum_j^{nc} \frac{w_i w_j}{2} \left(\frac{1}{\rho_i} + \frac{1}{\rho_j} \right)(1 - \beta_{ij}) \qquad (8.1)$$

where ρ is the density at a given pressure, the subscript *MIX* refers to the mixture, subscripts *i* and *j* refer to the two components (in this case the bitumen and the solvent), and β_{ij} is the density binary interaction parameter given by (Saryazdi *et al.*, 2013):

$$\beta_{ij} = \beta_{ij}^{20°C} + K(T - 293) \qquad (8.2)$$

where $\beta_{ij}^{20°C}$ is the interaction parameter at 20°C, *K* is a fitting constant and *T* is the absolute temperature in K. Note, the interaction parameter is a function of temperature only.

To use Equation. 8.1, the component densities and binary interaction parameter are required. The density of the bitumen at pressures up to 10 MPa was measured and that of the solvents was collected from the NIST database (2008). The values of $\beta_{ij}^{20°C}$ and *K* were determined for each pseudo-binary by fitting Equations 8.1 and 8.2 to the pseudo-binary density data collected at temperatures up to 90°C at 0.1 MPa. The deviations in the fitted densities were less than 0.2 kg/m³. To confirm the reliability of extrapolating to higher pressures, this calculation approach was tested on the pseudo-binary oil/solvent density data reported by Ramos-Pallares *et al*. (2016a) at temperatures and pressures up to 175°C and 10 MPa. The densities of the pseudo-binaries WC-B-B1/*n*-pentane, WC-B-B2/cyclohexane and WC-B-B1/toluene were calculated with a deviation of less than 0.3 kg/m³ over the entire range of temperatures and pressures.

C5-Asphaltene/Toluene Mixtures

Measurements were performed on C5-asphaltenes precipitated from sample WC-B-A3(1). The thermal conductivities of two C5-asphaltene/toluene mixtures (1.2 and 8.7 wt% C5-asphaltenes) were measured at temperatures from 20 to 40°C and pressures up to 10 MPa. Higher temperatures were not tested due to the onset of natural convection. The density of the mixtures was calculated using a mixing rule similar to Equation 8.1 with the interaction parameter set to zero based on the assumption that C5-asphaltenes and toluene form a regular solution (Barrera *et al.*, 2013). The density of toluene was taken from the NIST

database (2008) and the density of the C5-asphaltenes was calculated from Equation 6.9. This approach was validated in Section 6.3. The collected data is compiled in Appendix G.

8.2.2 Organization into Datasets

The fluids for which thermal conductivity and density data were collected in this thesis and from the literature included pure hydrocarbons, crude oils, pure hydrocarbon binaries, oil/solvent pseudo-binaries and distillation cuts. The data were divided into development and test datasets as described below.

Development Dataset 1

This dataset was used to develop an Expanded Fluid based model for thermal conductivity and contains over 2500 thermal conductivity and density data points across the entire phase diagram of 15 *n*-alkanes (C1 to C24) and 13 assorted pure hydrocarbons from different chemical families including branched paraffins, cyclics and aromatics. The data were taken from the NIST database (2008) and are reported at temperatures from -150 to 330°C and pressures up to 200 MPa. This dataset also includes the liquid thermal conductivity at atmospheric pressure of 6 branched paraffins, 9 cyclics, and 20 fused and non-fused aromatics reported by Yaws (1995). Yaws (1995) does not report thermal conductivity data for each compound but rather reports the fluid-specififc coefficients of the following empirical correlation:

$$\log(\lambda_{liq}) = A + B\left(1 - \frac{T}{C}\right)^{2/7}$$
(8.3)

where λ_{liq} is the liquid thermal conductivity at atmospheric pressure, in W m^{-1}K^{-1}, T is the absolute temperature in K and A, B and C are fluid-specific fitting parameters. The density of these liquids at atmospheric pressure was not reported in the original source but taken from the NIST database (2008).

The density of the fluid, when available, was used as reported. When the density was not available at a given condition, it was estimated by fitting the following empirical correlation to the reported data:

$$\rho = \left(a_1 + a_2 T\right) \exp\left\{a_3\left[1 - \exp\left[-\left(a_4 T + a_5\right)P\right]\right]\right\}$$ (8.4)

where ρ is the density of the fluid in kg/m^3, T is the temperature in °C, P is the pressure in kPa, and a_1, a_2, a_3, a_4 and a_5 are fitting parameters. Equation 8.4 is a modification of the correlation proposed by Badamchi-Zadeh *et al*. (2009) to improve its performace at higher pressure. Equation 8.4 fitted the data within ± 0.9 kg/m^3. A summary of the estimated parameters a_1, a_2, a_3 and a_4 is presented in Appendix H.

Other physical properties included in this dataset are the specific gravity, molecular weight, normal boiling point, and the EF fluid-specific parameter compressed state density, ρ_s^o. The first three properties were used for correlation purposes and were taken from the NIST database (2008). The EF parameter ρ_s^o was used as model input and was taken from Yarranton and Satyro (2009), Motahhari (2013), and Ramos-Pallares *et al*. (2016b).

Development Dataset 2

This dataset was used to develop a set of mixing rules for the thermal conductivity model parameters and to develop a correlation for the prediction of binary interaction parameters. Binary interaction parameters were included into the mixing rules to account for the non-idealities of the thermal conductivity mixing. This dataset includes thermal conductivity data of 19 pure hydrocarbon binaries at 0.1 MPa including alkane/alkane, alkane/branched paraffin, branched paraffin/branched paraffin, alkane/cyclic, alkane/aromatic, aromatic/aromatic and aromatic/cyclic (Parkinson, 1974; Saksena-and-Harminder, 1974; Ogiwara *et al*. 1980; Wada *et al*. 1985;). The density of the binaries was not reported in the original reference but rather taken from the NIST database (2008). This dataset also includes the thermal conductivities and densities of the bitumen/solvent pseudo-binaries measured in this thesis. The specific gravity and atomic hydrogen-to-carbon atomic ratio of the components were included in the dataset for correlating purposes.

Development Dataset 3

This dataset was used to develop a correlation to predict a synthetic thermal conductivity data point at a reference temperature at atmospheric pressure for maltene pseudo-

components. This dataset includes the thermal conductivity at the normal boiling point of 42 pure hydrocarbons including *n*-alkanes, branched paraffins, cyclics, and aromatics reported in the API Technical Data Book (1997). Other properties included in this dataset were the specific gravity and molecular weight which were used for correlating purposes. These properties were taken from the NIST database (2008).

This dataset also includes the thermal conductivity and distillation assay of deasphalted bitumen WC-B-B3 (WC-B-B3-DAO). The data for this deasphalted sample was used to extend the range of application of the proposed correlation toward higher molecular weights.

Development Dataset 4

This dataset was used to estimate the asphaltene thermal conductivity model parameters. Note that the asphaltenes were modelled as a single component. This dataset includes the thermal conductivity, density, molecular weight, C5-asphaltene content, and distillation assay of the bitumen WC-B-B3.

Test Dataset 1

This dataset was used to test the proposed thermal conductivity model parameter correlations for petroleum fluids with no asphaltene content. It includes the thermal conductivity at 0.1 MPa, specific gravity and normal boiling point of 46 distillation cuts collected from the literature (Baltatu, 1984; Baltatu *et al*. 1985; API, 2000), Table 8.2. The densities of the cuts were not reported by the authors but instead were calculated from the modified Rackett correlation based on their molecular weight and correlated critical properties. The Rackett compressibility factor was estimated by fitting the correlation to the reported specific gravity of the cut. The procedure is the same as described later,in Section 8.5.1, for maltene pseudo-components.

Table 8.2. Range of selected physical properties of the distillation cuts in Test Dataset 1. N. Cuts and N.P. stand for the number of cuts and the number of data points, respectively.

Crude Oil	N. Cuts	N.P.	Tb Range, °C	SG Range	Reference
Not Specified	25	64	82 - 362	0.69 - 0.95	Baltatu, 1984
Not Specified	13	8	74 - 411	0.73 - 1.00	Baltatu, 1985
Alaska North Slope	8	38	196 - 482	0.85 – 0.98	API,2000

Test Dataset 2

This dataset was used to assess if the model parameters estimated for asphaltenes can be used to predict the thermal conductivity of a mixture containing asphaltenes. The dataset includes the two C5-asphaltene/toluene mixtures from this thesis.

Test Dataset 3

This dataset was used to test the predictive capability of the thermal conductivity model and the proposed correlations for its parameters. This dataset includes the measured thermal conductivity, density, distillation assay, asphaltene content, specific gravity and molecular weight of the crude oils WC-B-B3, WC-B-A3(1), WC-B-A3(2), EU-HO-A1, WC-B-A1, CO-B-B1 and ME-CV-A1. The crude oils were characterized as a set of maltene pseudo-components and a single asphaltene pseudo-component as will be described in Section 8.5.1. The thermal conductivity model parameters for the maltene pseudo-components and the asphaltene pseudo-component are calculated as introduced in Sections 8.5.3 and 8.5.4, respectively. The thermal conductivity model parameters for the whole crude oil were determined using the proposed mixing rules with correlated binary interaction parameters. The compressed-state density, ρ_s^o, for each fluid is also required as input. This parameter was calculated as described in Section 6.5 using the same oil characterization methodology presented above.

8.3 Development of Thermal Conductivity Model – Single Component Fluids

8.3.1 Pure Components

The proposed thermal conductivity model is based on the idea that the transport properties of a fluid, specifically the viscosity and the thermal conductivity, are related to the expansion of the fluid from a compressed state. This idea was first proposed by Hildebrand (1971) and Hildebrand and Lamoreaux (1972). The concept of fluid expansion, or Expanded Fluid (EF), has been previously used to develop a full phase viscosity model for hydrocarbons, crude oils, their mixtures, distillation cuts and pseudo-components (Yarranton and Satyro 2009; Motahhari *et al*., 2011a,b; Ramos-Pallares *et al*., 2016a,b).

To illustrate the EF concept, Figure 8.2 shows how the double log of viscosity and log of thermal conductivity of ethane change with density. Density, rather than specific volume, was chosen as the correlating variable because it is bounded between zero and a maximum value referred to as the compressed state density, $\rho_s{}^o$. The specific volume (inverse of density) tends to very large values as the fluid approaches the dilute gas state. In general, the viscosity and thermal conductivity increase as the fluid is compressed from the dilute gas state. The viscosity increases rapidly with density and approaches infinity as the density of the fluid reaches a value beyond which the fluid cannot be compressed without incurring a liquid-solid phase transition. This fluid-specific parameter is defined as the compressed state density, $\rho_s{}^o$, (Yarranton and Satyro, 2009). The thermal conductivity of the fluid increases, almost linearly, and reaches a maximum value as the density reaches the compressed state value. It has been reported that, unlike viscosity, the thermal conductivity of hydrocarbons at the liquid-solid phase transition has a finite value (Forsman and Andersson, 1984; Velez *et al*., 2015). The trends shown in Figure 8.2 were observed for all of the pure hydrocarbons in the Development Dataset 1.
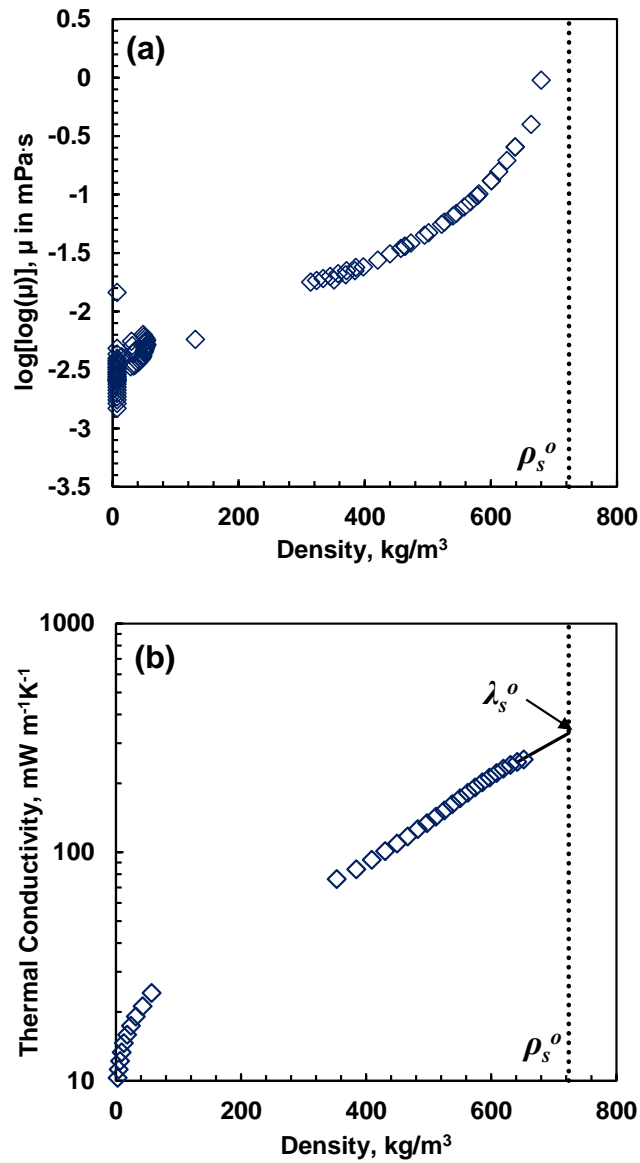
Figure 8.2. Relationship of saturated ethane viscosity (a) and thermal conductivity (b) to density. Data from the NIST database (2008). ρ_s^o is the compressed state density of ethane with a value of 724 kg/m³ determined by modeling the viscosity (Yarranton and Satyro, 2009). Solid line in (b) is a linear extrapolation of the data.

The following expression was used to capture the relation between thermal conductivity and fluid expansion (inverse of density) shown in Figure 8.2b:

$$\ln\left(\frac{\lambda - \lambda_G}{\lambda_s^o - \lambda_G}\right) = -c_{2\lambda}\left[\left(\frac{\rho_s^o}{\rho}\right)^n - 1\right] \tag{8.5}$$

where λ in mW m^{-1}K^{-1} is the thermal conductivity of the fluid, λ_G in mW m^{-1}K^{-1} is the thermal conductivity of the dilute gas, λ_s^o in mW m^{-1}K^{-1} is the thermal conductivity at the compressed state, $c_{2\lambda}$ (dimensionsless) scales the thermal conductivity change to the fluid expansion, and n is an empirical exponent that improves the model fit in the transition from saturated liquid to saturated vapor. Note that in Equation 8.5 the thermal conductivity of the fluid approaches the dilute gas value as the density of the fluid tends to zero and to the compressed state value, λ_s^o, as the density approaches the compressed state value, ρ_s^o. The exponent is to be fixed to a constant value for all fluids. The parameters λ_G, λ_s^o and $c_{2\lambda}$, and ρ_s^o must be determined for each fluid.

Equation 8.5 was found adequate at atmospheric pressure but was modified as follows to better match the data at higher pressures:

$$\ln\left(\frac{\lambda - \lambda_G}{\lambda_s^* - \lambda_G}\right) = -c_{2\lambda}\left[\left(\frac{\rho_s^o}{\rho}\right)^n - 1\right] \tag{8.6}$$

where

$$\lambda_s^* = \frac{\lambda_s^o}{\exp\left(-c_{3\lambda}P\right)} \tag{8.7}$$

and P is the pressure and $c_{3\lambda}$ is an empirical high pressure parameter.

The dilute gas thermal conductivity for a pure component was calculated from the following empirical correlation (Yaws, 2008):

$$\lambda_G = A_{o,\lambda} + B_{o,\lambda}T + C_{o,\lambda}T^2 + D_{o,\lambda}T^3 \tag{8.8}$$

where T is the absolute temperature, in K, and $A_{o,\lambda}$, $B_{o,\lambda}$, $C_{o,\lambda}$ and $D_{o,\lambda}$ are fluid-specific parameters usually reported at atmospheric pressure. The numerical values of these parameters were taken from Yaws (2008). For pseudo-components, the dilute gas thermal

221

conductivity was calculated from Equation 8.8 using the parameters of the *n*-alkane with the same molecular weight. This assumption was validated by calculating the dilute gas thermal conductivity of 20 isomers of *n*-heptane (including branched alkanes, cyclics and toluene) in a temperature range between 0 to 800 °C. In general, the dilute gas thermal conductivity of the components was within 10% of that of the *n*-heptane.

The value of ρ_s^o was determined by fitting the EF viscosity model, Equation 4.1, to viscosity data for each fluid (see details in Section 4.1). The compressed state density values of over 150 pure hydrocarbons were reported by Motahhari (2013) and Ramos-Pallares *et al.* (2016b). Note if the EF viscosity model is not used to fit viscosity data, the value of the compressed state density can be determined using the procedure introduced in Chapter 6 for characterized oils.

The fluid-specific parameters λ_s^o and $c_{2\lambda}$ were determined for each hydrocarbon in the Development Dataset 1 by fitting Equation 8.6 to its thermal conductivity data at atmospheric pressure. Note that $c_{3\lambda}$ is equal to zero at atmospheric pressure. The parameter $c_{3\lambda}$ was only estimated for the components in the Development Dataset 1 for which high pressure data were available. The optimum set of parameters were those that minimized the following objective function:

$$OF = \sum \left(\lambda_{meas} - \lambda_{corr} \right)^2 \tag{8.9}$$

where the subscripts "*meas*" and "*corr*" indicate measured and correlated values. A global optimization was performed to determine *n* where the parameters for each fluid were optimized at each choice of *n*. The optimum value for *n* was 0.2. Hence, the Expanded Fluid (EF) thermal conductivity model is given by:

$$\lambda - \lambda_G = \left(\lambda_s^* - \lambda_G \right) \exp \left\{ -c_{2\lambda} \left[\left(\frac{\rho_s^o}{\rho} \right)^{0.2} - 1 \right] \right\} \tag{8.10}$$

Equation 8.10 describes the thermal conductivity of a pure hydrocarbon across the entire fluid phase diagram using density, pressure, dilute gas viscosity (calculated from

Equation 8.8) and four fluid-specific parameters $\lambda_s{}^o$, $c_{2\lambda}$ $c_{3\lambda}$ and $\rho_s{}^o$ as inputs. Equation 8.10 will henceforth be referred to as the Expanded Fluid (EF) thermal conductivity model.

The EF thermal conductivity model, Equation 8.10, fit the data in the two-phase region for n-alkanes, from C1 to C20, and hydrocarbons from different chemical families including branched paraffins, cyclics and aromatics in the Development Dataset 1. Figure 8.3 shows the model fit to thermal conductivity data for saturated ethane and benzene. Note that Equation 8.10 is continuous along the two-phase envelope including the critical point. However, the model is not capable of predicting the thermal conductivity enhancement observed at the critical point and described in Section 2.4.4. The model also fits thermal conductivity data at pressures up to 500 MPa, as shown in Figure 8.4 for compressed n-octane and cyclohexane.

Table 8.3 provides the fitted fluid-specific parameters and deviations for the hydrocarbons from Development Dataset 1 that are later used in the development of correlations. The parameters for the rest of fluids in Development Dataset 1 are presented in Appendix I. The thermal conductivity model fits the data of pure hydrocarbons in the Development Dataset 1 with an average absolute relative deviation (AARD) of 4%, a maximum absolute relative deviation (MARD) of 58%, and a bias of 2 %. The maximum deviations were found at reduced temperatures between 0.97 and 1.1 where the critical enhancement occurs. If the critical enhancement region is excluded, the AARD, MARD and bias decrease to 2, 25 and 1.2%, respectively.
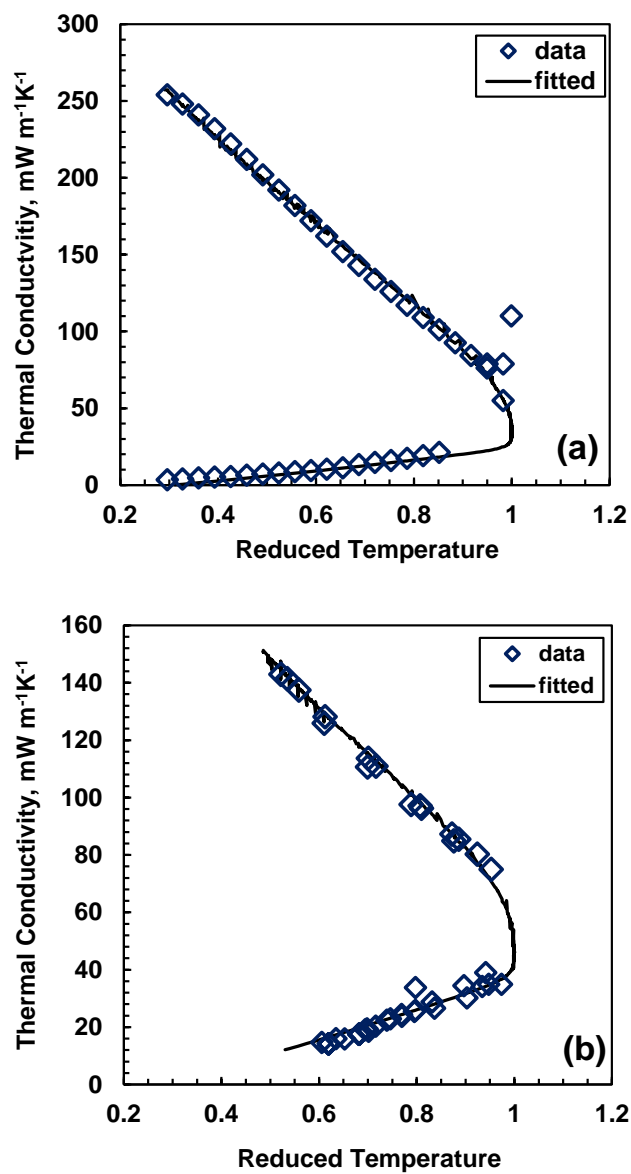
Figure 8.3. Measured and modeled thermal conductivity of saturated: a) ethane; b) benzene. Data from NIST (2008). Note the high deviations near the critical point due to critical enhancement. Note, irregularities (spikes) in the modeled thermal conductivities in this and other figures are the result of scatter in the density data used as an input; these data were not smoothed prior to applying the model.
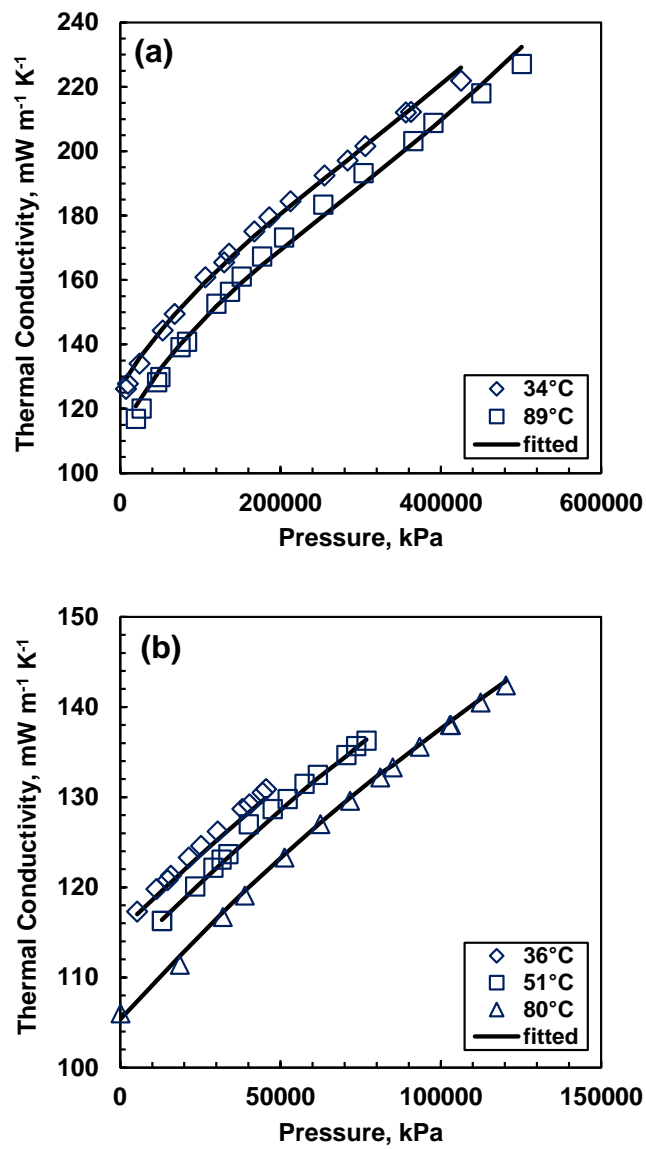
Figure 8.4. Measured and modeled thermal conductivity of compressed: a) *n*-octane (Li *et al*., 1984); b) cyclohexane (NIST, 2008).

Table 8.3. Thermal conductivity model parameters and deviations for selected hydrocarbons from Development Dataset 1. NP stands for number of data points. $c_{3\lambda}$ was only calculated for the components for which high pressure data were available.

Component	NP	ρ_s^o kg/m³	$c_{2\lambda}$	λ_s^o mW/m.K	$c_{3\lambda}$ x10⁷ kPa⁻¹	AARD %	MARD %	Bias %
methane	337	540.0	12.285	341.2	0	14	58	-4
ethane	138	724.0	11.927	331.4	0	14	55	-13
propane	128	778.0	10.411	241.8	5.7	11	52	-8
n-butane	156	813.0	12.569	249.5	5.5	10	35	-8
n-pentane	71	837.0	11.996	221.4	8.0	2	6	0
n-hexane	195	849.1	11.152	209.7	7.9	2	11	1
n-heptane	241	857.8	11.517	202.8	5.0	1	6	0
n-octane	51	862.7	11.846	201.6	3.6	1	4	0
n-decane	47	868.1	10.483	189.7	-	1	2	0
n-dodecane	6	871.4	10.250	182.7	-	0.2	0.4	0
n-tetradecane	7	875.5	8.648	178.7	-	0.1	0.1	0
n-octadecane	151	885.1	8.038	185.4	9.0	2	11	1
n-eicosane	8	885.5	10.422	195.0	-	0.1	0.2	0
n-docosane	8	885.2	10.512	198.3	-	0.2	0.5	0
n-tricosane	7	891.4	9.947	197.5	-	0.1	0.1	0
n-tetracosane	28	893.2	10.344	203.5	10.0	1	2	0.7
benzene	200	1066.4	10.384	212.0	9.0	2	4.7	0
ethylbenzene	50	1052.0	9.343	182.5	5.0	1	3.3	0
o-xylene	60	1052.9	10.139	182.1	10.0	1	4.0	0
p-xylene	70	1045.5	11.637	196.8	10.0	0	1.6	0
toluene	400	1049.6	11.542	203.6	3.0	1	6.5	0
cyclohexane	80	922.1	10.136	163.6	8.9	4	8.4	-3

8.3.2 Crude Oils Represented as a Single Component Fluid

The EF thermal conductivity model was tested on the crude oils in Test Dataset 3. The crude oils were modeled as single components and Equation 8.10 was fit to the experimental thermal conductivity data. The measured density was used as the model input. The dilute gas thermal conductivity for each fluid was calculated from Equation 8.8 using the coefficients of the *n*-alkane with the same molecular weight as the crude oil. The compressed state density, ρ_s^o, was determined by fitting the EF viscosity model, Equation 4.1, to viscosity data for the same oils.

The EF thermal conductivity model not only fits the data of the crude oils but also captured the correct trend between thermal conductivity and temperature, as illustrated in Figure 8.5 for Western Canada bitumen WC-B-A3(1). The model predicts a linear decrease in the thermal conductivity with temperature as has been observed for pure hydrocarbons, distillation cuts, and crude oils (Baltatu *et al*. 1985; Guzman *et al*. 1989; Riazi 2005). The conductivity model fitted the thermal conductivity of the oils in the Test Dataset 3 with an AARD, MARD, and Bias of 0.14, 0.57 and -0.01 %, respectively. A summary of the deviations and fitted model parameters are provided in Table 8.4. Note that the AARD, MARD and bias of samples WC-B-A1, CO-B-B1 and ME-CV-A1 are zero as the model matches the only two data points collected for each one of those samples.
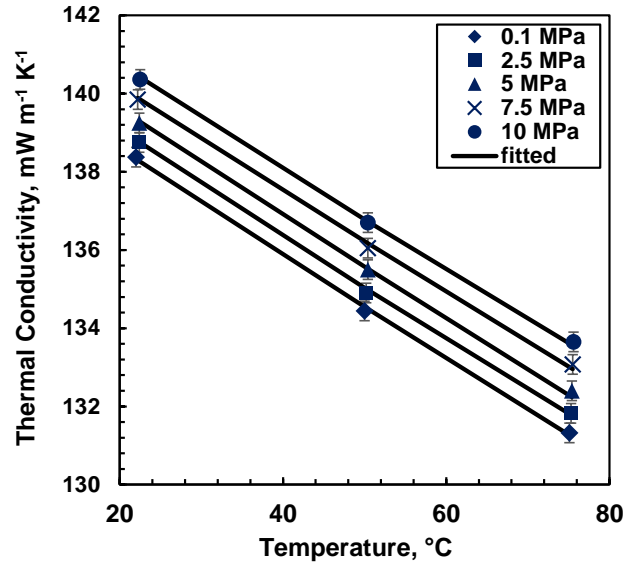
Figure 8.5. Measured and modeled thermal conductivity of the Western Canada bitumen WC-B-A3(1).

Table 8.4. Summary of fitted model parameters and deviations for the crude oils in Test Dataset 3. NP stands for number of points. $c_{3\lambda}$ was only determined when high pressure data were available.

Sample	NP	ρ_s^o kg/m³	$c_{2\lambda}$	λ_s^o mW/m.K	$c_{3\lambda}$ x10⁷ kPa⁻¹	AARD %	MARD %	Bias %
WC-B-B3	14	1070.0	8.254	147.1	9.4	0.3	0.6	-0.03
WC-B-A3(1)	15	1057.2	8.372	149.3	8.5	0.1	0.1	0.00
WC-B-A3(2)	20	1060.0	7.552	149.2	7.3	0.1	0.3	-0.05
EU-HO-A1	15	1024.8	8.048	142.5	8.3	0.1	0.2	0.00
WC-B-A1	2	1057.2	8.174	151.7	-	0	0	0
CO-B-B1	2	1054.1	4.937	143.2	-	0	0	0
ME-CV-A1	2	979.3	10.424	164.7	-	0	0	0

8.4 Extension of Thermal Conductivity Model to Mixtures

The EF thermal conductivity model treats a mixture as a single pseudo-component with model parameters calculated from those of the pure components using mixing rules. Hence mixing rules are required for the parameters λ_G, ρ_s^o, $c_{3\lambda}$, λ_s^o and $c_{2\lambda}$.

The dilute gas thermal conductivity of the mixture was calculated using the Wassiljewa method (1904) with parameters calculated from the Mason and Saxena equation (1958). This calculation method was introduced in Section 2.5.6.1. The mixing rule for the compressed state density, ρ_s^o, was defined in Equation 4.8 and its binary interaction parameter is calculated from Equations. 5.3 to 5.8.

The model is relatively insensitive to the parameter $c_{3\lambda}$ and therefore the following simple mixing rule was applied without further testing:

$$c_{3\lambda,mix} = \left(\sum_i^{nc} \frac{w_i}{c_{3\lambda,i}} \right)^{-1}$$

(8.11)

where w is the mass fraction and nc refers to the number of components in the mixture. The form of the mixing rule for $c_{3\lambda}$ is identical to that for the EF viscosity model high pressure parameter c_3 defined in Equation 4.9.

The following mixing rules were evaluated for the parameter λ_s^o:

Mixing Rule A1:
$$\lambda_{s,mix}^o = \left(\sum_i^{nc} \frac{w_i}{\lambda_{s,i}^o} \right)^{-1}$$
(8.12)

Mixing Rule A2:
$$\lambda_{s,mix}^o = \sum_i^{nc} w_i \lambda_{s,i}^o$$
(8.13)

where the subscript *mix* indicates a mixture parameter. Mixing rules A1 and A2 are similar to those recommended by Wada *et al*. (1985) and Poling *et al*. (2001) for the estimation of thermal conduccivity of liquid mixtures. A similar set of mixing rules was evaluated for the parameter $c_{2\lambda}$:

Mixing Rule B1:
$$c_{2\lambda,mix} = \left(\sum_i^{nc} \frac{w_i}{c_{2\lambda,i}} \right)^{-1}$$
(8.14)

Mixing Rule B2:
$$c_{2\lambda,mix} = \sum_i^{nc} w_i c_{2\lambda,i}$$
(8.15)

The mixing rules for the parameters λ_s^o and $c_{2\lambda}$ were divided into four sets for purposes of evaluation, as presented in Table 8.5. Each set of mixing rules was used to predict the thermal conductivity of the binaries and pseudo-binary mixtures in Development Dataset 2. The thermal conductivity of the mixtures was calculated using the mass composition, the EF thermal conductivity model parameters of the pure components, and the mixing rules. Recall that the interaction parameter for the ρ_s^o mixing rule (Equation 4.7) is different from zero and calculated from Equations 5.3 to 5.8.

When necessary, the model parameters of the pure components were tuned to fit the pure component thermal conductivity reported in the source data so that the only deviation results from the mixing rules. The model parameters for the bitumen WC-B-A3(2), used to prepare the pseudo-binaries in Development Dataset 2, are reported in Table 8.4.

Table 8.5. Sets of mixing rules tested for thermal conductivity model parameters λ_s^o and $c_{2\lambda}$. MR stands for mixing rule.

Set	MR λ_s^o	MR $c_{2\lambda}$
1	MR A1 (Eq. 8.12)	MR B1 (Eq. 8.14)
2	MR A1 (Eq. 8.12)	MR B2 (Eq. 8.15)
3	MR A2 (Eq. 8.13)	MR B1 (Eq. 8.14)
4	MR A2 (Eq. 8.13)	MR B2 (Eq. 8.15)

Tables 8.6 and 8.7 are a summary of the deviations for mixing rule Sets 1 and 2 and Sets 3 and 4, respectively. In general, the four sets of mixing rules predict the thermal conductivity of the pure hydrocarbon binaries and the bitumen/solvent pseudo-binaries to within 3 and 5%, respectively. The maximum deviations occurred with the aromatic/aromatic binaries and the bitumen/toluene and bitumen/cyclohexane pseudo-binaries. All four sets of mixing rules produce similar deviations for the pure hydrocarbon binaries. However, Set 2 produces the lowest deviations for the bitumen/solvent pseudo-binaries. Therefore, Set 2 (Equations 8.12 and 8.15) is the recommended set of mixing rules.

Table 8.6. Summary of deviations for mixing rule Sets 1 and 2. NB stands for number of binaries or pseudo-binaries.

Binary	NB	Set 1			Set 2		
		AARD %	MARD %	Bias %	AARD %	MARD %	Bias %
Pure Hydrocarbon Binaries							
alkane/alkane	7	0.2	0.5	0.2	0.2	0.5	0.1
alkane/branched	2	0.5	1.1	0.5	0.5	1.1	0.5
alkane/cyclic	2	0.3	0.6	0.3	0.3	0.6	-0.2
alkane/aromatic	4	0.3	1.1	0.3	0.3	1.1	-0.1
cyclic/cyclic	1	0.6	1.1	0.6	0.2	0.4	0.2
aromatic/aromatic	3	1.1	3.6	1.1	1.1	3.5	0.8
Overall Deviation		0.5	3.6	0.5	0.4	3.5	0.2
Oil/Solvent Pseudo-Binaries							
oil/pentane	1	2.4	3.0	2.4	2.0	2.5	-2.0
oil/heptane	1	3.5	4.0	3.5	3.3	3.8	3.3
oil/tetradecane	2	2.1	4.0	2.1	2.0	4.0	2.0
oil/toluene	2	2.0	5.0	-2.0	1.5	3.5	-1.4
oil/cyclohexane	2	2.0	5.0	-2.0	2.0	4.5	2.0
Overall Deviation		2.4	5.0	-0.2	2.0	4.5	0.8

Table 8.7. Summary of deviations for sets of mixing rule Sets 3 and 4. NB stands for number of binaries or pseudo-binaries.

Binary	NB	Set 3			Set 4		
		AARD %	MARD %	Bias %	AARD %	MARD %	Bias %
Pure Hydrocarbon Binaries							
alkane/alkane	7	0.2	0.6	0.2	0.2	0.5	0.2
alkane/branched	2	0.8	2.1	0.8	0.8	1.9	0.8
alkane/cyclic	2	0.2	0.5	0.2	0.2	0.5	0.2
alkane/aromatic	4	0.3	1.4	0.8	0.2	0.6	0.2
cyclic/cyclic	1	1.2	2.2	1.2	1.2	2.2	1.2
aromatic/aromatic	3	1.1	3.6	1.1	1.0	3.5	1.0
Overall Deviation		0.6	3.6	0.7	0.6	3.5	0.6
Oil/Solvent Pseudo-Binaries							
oil/pentane	1	3.1	3.7	-3.1	3.0	3.5	-3.0
oil/heptane	1	4.3	4.9	4.3	4.2	4.7	4.2
oil/tetradecane	2	2.5	4.5	2.5	2.4	4.5	2.4
oil/toluene	2	3.5	7.0	-3.5	2.9	5.8	-2.9
oil/cyclohexane	2	2.0	5.0	-2.0	2.0	5.0	-2.0
Overall Deviation		3.0	7.0	-0.4	3	5.8	-0.3

The performance of the model using mixing rule Set 2 (henceforth referred to as ideal) was evaluated using Development Dataset 2. Figure 8.6a shows that the ideal predictions for the cyclopentane/heptane binary are within 0.5% across the entire range of composition. Similar results were obtained for the other binaries in Development Dataset 2, Table 8.8. Figure 8.6b shows that the deviation between data and ideal predictions for the WC-B-A3(2)/toluene pseudo-binary can be significant at intermediate solvent contents. Similar deviations were observed for all the pseudo-binaries in Development Dataset 2, Table 8.8.
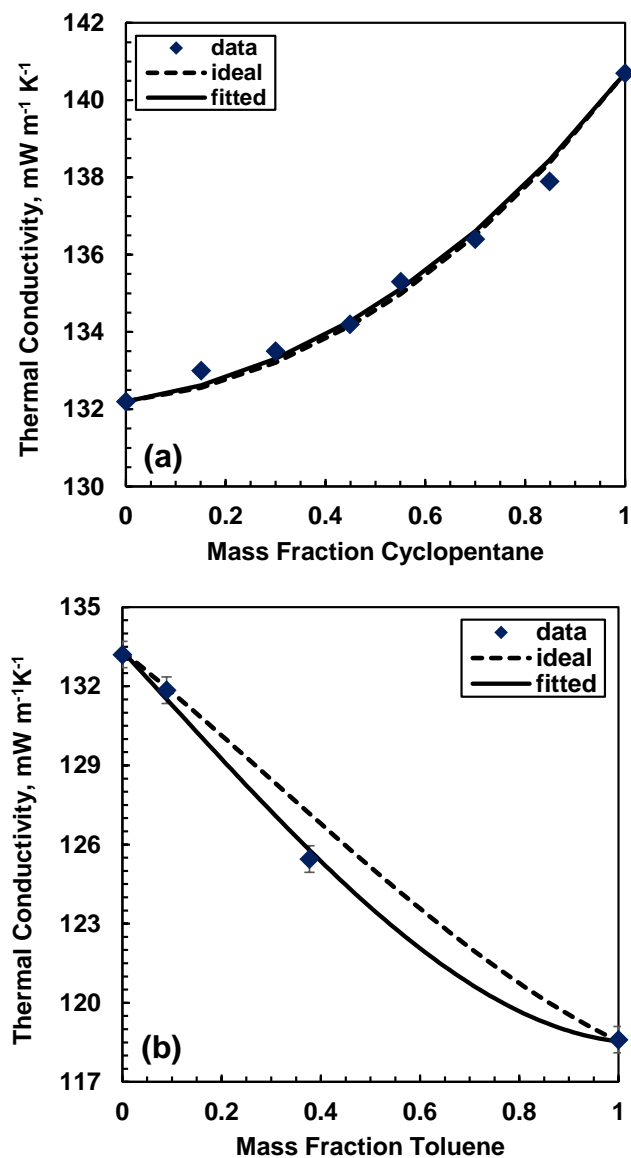
Figure 8.6. Measured and modeled thermal conductivity of: a) cyclopentane/heptane binary at 0°C and 0.1 MPa (Parkinson, 1974) fitted with $\theta_{ij} = 0.0013$; b) WC-B-A3(2)/toluene pseudo-binary at 75°C and 2.5 MPa fitted with $\theta_{ij} = -0.0192$.

233

Table 8.8. Deviations and bias of EF thermal conductivity model for mixtures from Development Dataset 2. The deviations were calculated over the entire dataset including high pressure data.

System	AARD %	MARD %	Bias %
Ideal			
binaries	0.5	3.5	0.2
pseudo-binaries	2.0	4.5	1.5
Fitted			
binaries	0.2	1.0	0.1
pseudo-binaries	0.4	2.0	0
Correlated			
binaries	0.5	3.5	0.1
pseudo-binaries	0.5	3.0	0

Therefore, the Set 2 mixing rules (Equations 8.12 and 8.15) were modified to include a binary interaction parameter as follows:

$$\lambda_{s,MIX}^{o} = \left[\sum_{i}^{nc}\sum_{j}^{nc} \frac{w_i w_j}{2}\left(\frac{1}{\lambda_{s,i}^{o}} + \frac{1}{\lambda_{s,j}^{o}} \right)\left(1-\theta_{ij}\right) \right]^{-1} \tag{8.16}$$

$$c_{2\lambda,MIX} = \sum_{i}^{nc}\sum_{j}^{nc} \frac{w_i w_j}{2}\left(c_{2\lambda,i} + c_{2\lambda,j} \right)\left(1-\theta_{ij}\right) \tag{8.17}$$

where θ_{ij} is the thermal conductivity binary interaction parameter between components i and j. When the interaction parameter is zero, Equations 8.16 and 8.17 reduce to the Set 2 mixing rules (Equations 8.12 and 8.15). The binary interaction parameter is set to zero when $i = j$. For simplicity, it was assumed that the interaction parameters are independent of temperature, pressure, and solvent content.

The binary interaction parameters for each of the binaries and pseudo-binaries in the Development Dataset 2 were determined by fitting the model to the mixture data. The fitted interaction parameters are provided in the Appendix J. Figure 8.6 shows the model fitted to data using non-zero interaction parameters. Table 8.8 shows that the deviations with the fitted model are significantly lower than the ideal case.

In order to make the EF thermal conductivity model predictive for mixtures, it is necessary to develop a correlation for the calculation of binary interaction parameters, θ_{ij}. Recall that a correlation has been already developed for interaction parameter in the ρ_s^o mixing rule (Equations 5.3 to 5.8). Figure 8.7 shows the calculated binary interaction parameters plotted against the normalized difference of specific gravity, ΔSG_{norm}, defined in Equation 5.2. ΔSG_{norm} was chosen as correlation parameter as it has been successfully used to correlate density (Saryazdi *et al.*, 2013) and viscosity interaction parameters (Ramos-Pallares *et al.*, 2016a).
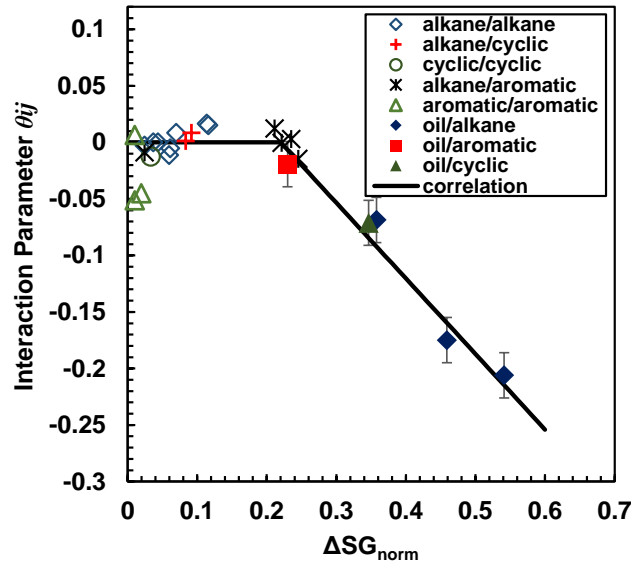
Figure 8.7. Thermal conductivity binary interaction parameter, θ_{ij}, versus the normalized difference of specific gravity, ΔSG_{norm}. Solid and open symbols correspond to the WC-B-A3(2)/solvent pseudo-binaries and the pure hydrocarbon binaries, respectively.

The following correlation was used to fit to the data in Figure 8.7:

$$\Delta SG_{norm} < 0.22: \qquad\qquad \theta_{ij} = 0 \qquad\qquad\qquad (8.18)$$

$$\Delta SG_{norm} \geq 0.22: \qquad \theta_{ij} = 0.1471 - 0.6686\Delta SG_{norm} \qquad (8.19)$$

where $\theta_{ii} = \theta_{jj} = 0$. The thermal conductivity of the binaries and pseudo-binaries in the Development Dataset 2 was recalculated using correlated interaction parameters. Table 8.8 shows that the correlation has almost no impact on the predictions for the binary mixtures

as it predicts zero interaction parameters for mixtures of pure hydrocarbons. Note that high deviations are expected for aromatic/aromatic binaries as their actual interaction parameters are far from the correlated values, as seen in Figure 8.7. It is possible that the non-idealities of the thermal conductivity mixing of aromatic binaries arise not only from the differences in molecular size but are also affected by the strong intermolecular interactions resulting from the stacking of aromatic rings (Headen *et al*., 2010)

Table 8.8 also shows that using correlated interaction parameters significantly improves the predictions for the pseudo-binaries bitumen/solvent. Figure 8.8 shows examples of a poor and good prediction for the aromatic binary toluene/benzene and for the pseudo-binary bitumen/cyclohexane, respectively. The poor prediction for the aromatic/aromatic binary in Figure 8.8a occurs because, as noted above, the predicted binary interaction parameters is zero but the actual value is non-zero. The good prediction shown in Figure 8.8b is representative of the results obtained for all other types of pure hydrocarbon mixtures and for bitumen/solvent mixtures.
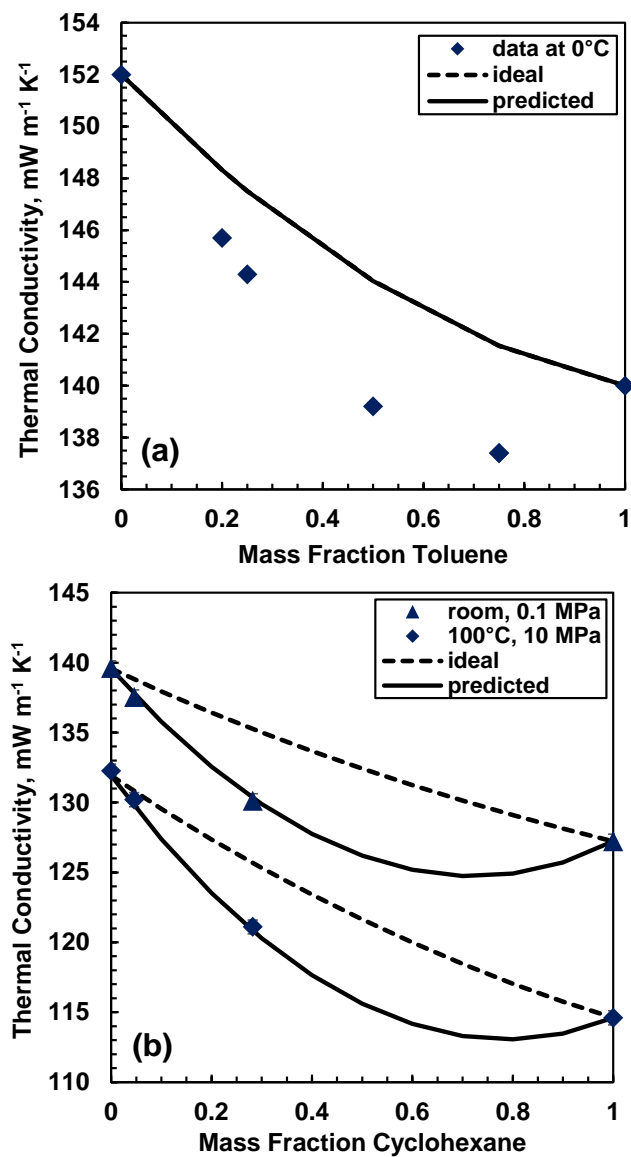
Figure 8.8. Measured and predicted thermal conductivity of a) toluene/benzene binary at 0°C and 0.1 MPa (predicted θ_{ij}=0) (Saksena-and-Harminder, 1974), and, of b) WC-B-A3(2)/cyclohexane pseudo-binary (predicted θ_{ij}= -0.0844). Dotted and solid lines are the model with ideal mixing rules and with correlated interaction parameters, respectively. The thermal conductivity of the pseudo-binary was calculated across the entire range of composition; however, for this mixture the onset of asphaltene precipitation occurs around 0.8 wt% cyclohexane.

8.5 Thermal Conductivity Model for Characterized Crude Oils

The next step is to extend the model to predict the thermal conductivity of pseudo-component characterized oils. As previously described, crude oils are each characterized as a set of maltene pseudo-components and asphaltene single pseudo-component. Therefore, it is necessary to develop correlations for the prediction of the model parameters $c_{3\lambda}$, , λ_s^o, $c_{2\lambda}$ and ρ_s^o for the maltene pseudo-components and the single asphaltene pseudo-component. The model parameters $c_{3\lambda}$, λ_s^o and $c_{2\lambda}$ for the whole oil are then calculated by combining those of the maltene pseudo-components and asphaltene pseudo-component using the mass-based mixing rules (Equations 8.11, 8.16 and 8.17) with correlated interaction parameters estimated from Equations 8.18 and 8.19, Figure 8.9. The parameter ρ_s^o for the whole oil is calculated from those of the maltene pseudo-components and asphaltene pseudo-component using the corresponding mixing rule (Equation 4.7) with correlated interaction parameters from Equations 5.3 to 5.8, Figure 8.9. This section begins with a description of the oil characterization methodology and an approach to predict the density of characterized crude oils. Predicted density rather than measured will be used as model input. Then, the development and testing of correlations for maltene pseudo-components and the estimation and testing of asphaltene pseudo-component model parameters are presented.

8.5.1 Oil Characterization Methodology

The proposed oil characterization methodology is the same as that used for the prediction of the EF viscosity model parameters as presented in Section 6.2. A schematic of the characterization procedure is provided in Figure 8.9. The maltene and C5-asphaltene fractions of each oil were characterized separately as recommended by Catellanos-Diaz *et al*. (2011). The maltenes are characterized based on boiling cuts. The asphaltenes are characterized separately because they self-associate and their properties do not follow the same trends as the maltenes versus cumulative wt% distilled. The asphaltene fraction was treated as a single component for thermal conductivity modeling purposes.
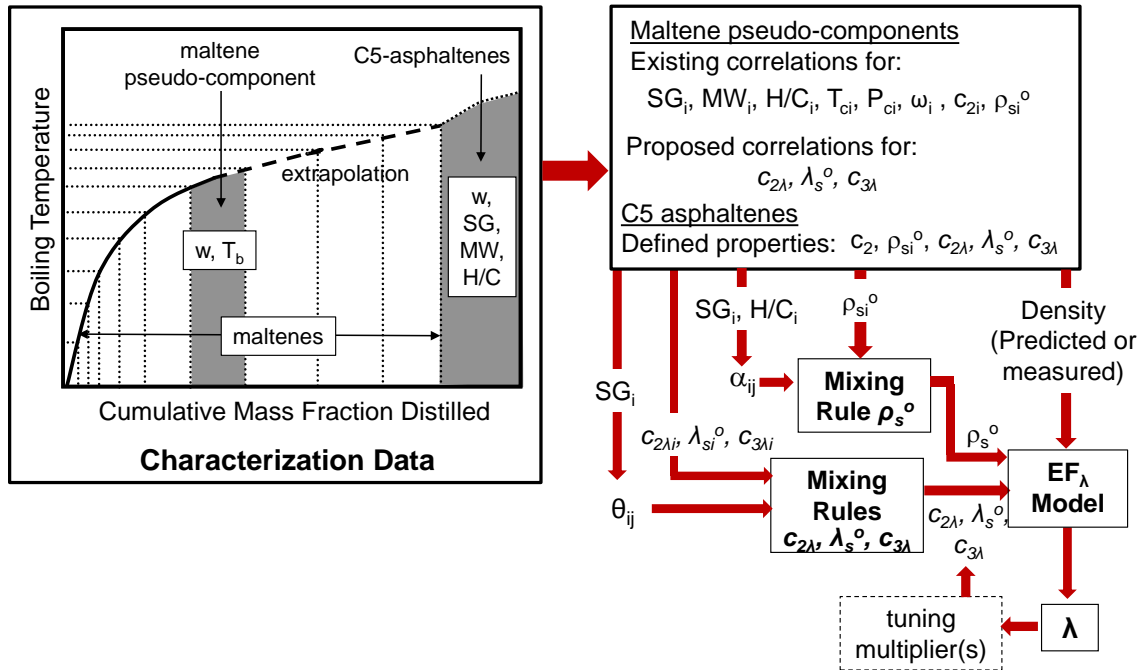
Figure 8.9. Schematic of characterization procedure for predicting crude oil thermal conductivity. MR stands for mixing rule and λ indicates thermal conductivity.

Maltene Characterization

Unless otherwise stated, the maltene fraction was characterized from its distillation assay. Since the maltenes are not fully distillable, a Gaussian extrapolation was performed to extend the distillation curve over the entire concentration range of maltenes. The distillation curve was divided into pseudo-components, each representing a boiling point interval of the same width (ΔT_b) as recommended by Catellanos-Diaz *et al.* (2011). The pseudo-component properties required for the thermal conductivity parameter correlations (to be developed later) are the boiling point from the characterization as well as the specific gravity, molecular weight, and H/C ratio. The critical properties and acentric factor are also required to determine pseudo-component densities at different temperatures and pressures for input into the conductivity model.

The molecular weight and initial estimate of the specific gravity of each maltene pseudo-

component were calculated using the Lee-Kesler (Kesler and Lee, 1976) and the Katz-Firoozabadi correlations (Katz and Firoozabadi, 1978), respectively. The H/C ratio for each pseudo-component in the maltene fraction was calculated as a function of the specific gravity using Equation 6.1. The critical temperature, critical pressure, and acentric factor of each pseudo-component in the maltene fraction were calculated from the Lee-Kesler correlations (Kesler and Lee, 1976; Lee and Kesler, 1975) as suggested by Catellanos-Diaz *et al.* (2011). The initial specific gravities of the pseudo-components were tuned to match the specific gravity of the whole maltenes with a single constant multiplier. Note, if the experimental specific gravity of the maltenes is not available, it can be calculated as a function the the specific gravity of the oil using Equation 6.2.

C5-Asphaltene Characterization

The asphaltene fraction was represented by a single pseudo-component and its model parameters, specific gravity, molecular weight, and H/C are the only required input properties for the thermal conductivity model. The model parameters are discussed in Section 8.5.4. The H/C ratio was determined from Equation 6.1. The specific gravity and molecular weight were determined indirectly from the measured oil properties, the characterized maltene properties, and the measured mass fraction of C5-asphaltenes in the oil. First, the maltenes were characterized as described above and their bulk molecular weight and specific gravity determined. Then, the asphaltene molecular weight was calculated from a molar mixing rule and the specific gravity was determined from the regular solution mixing rule, Equation 6.3.

8.5.2 Crude Oil and Cut Density Prediction

The EF thermal conductivity model (Equation 8.6) lrequires the density of the fluid as an input; therefore, in order to make the model totally predictive, the following procedure was proposed to predict crude oil density at any temperature and pressure. This predictive approach is the same as that proposed for the EF viscosity model and presented in Section 6.3. Briefly, the density of the whole crude oil at a given temperature and pressure was predicted from those of the maltenes and asphaltenes at the same conditions using a regular

solution mixing rule (Equation 6.3). The density of the maltenes was determined from the pseudo-component densities using a regular solution mixing rule (Equation 6.3) as described previously. The methods used to determine the density of the maltene pseudo-components and the asphaltenes at any given temperature and pressure are described below.

Maltene Pseudo-Components

For the maltenes produced from the precipitation of C5-asphaltenes, the density of a pseudo-component at a given temperature and pressure was determined using the Tait-COSTALD correlation, presented in Equation 6.4, which uses pressure, three fluid-specific parameters, and the density at atmospheric pressure as inputs. The fluid-specific parameters are calculated from Equations 6.5 to 6.7. The critical temperature, critical pressure, and acentric factor of the pseudo-components required as inputs in Equations 6.5 to 6.7 are calculated as described previously. The density of the pseudo-components at atmospheric pressure was calculated from the modified Rackett correlation, given in Equation 6.8, which uses temperature, critical temperature, critical pressure, molecular weight and an adjustable parameter, known as Rackett compressibility factor, as inputs. The critical temperature and pressure and the molecular weight are determined as described previously. The Rackett compressibility factor was determined by tuning the correlation applied at 15.6°C to fit the previously determined specific gravity. The Racket correlation predicts molar volume rather than density; the density is simply the pseudo-component molecular weight divided by the calculated molar volume.

C5-Asphaltenes

The density of the asphaltenes was assumed to be independent of pressure and only a function of temperature as introduced in Section 6.3. The density of the asphaltenes is calculated from Equation6.9 which requires the specific gravity of the asphaltenes as input. The specific gravity of the asphaltenes is determined from the specific gravity of the crude oil, specific gravity of the maltenes and the asphaltene mass content using the regular solution mixing rule defined in Equation 6.3.

8.5.3 Development of Correlations for Maltene Pseudo-Component Parameters

To apply the EF thermal conductivity model to the maltenes, correlations are required for the model parameters ρ_s^o, λ_s^o, $c_{2\lambda}$ and $c_{3\lambda}$.

Parameter ρ_s^o

The parameter ρ_s^o for maltene pseudo-components is calculated using the correlation developed in Chapter 6 for the EF viscosity model without further modification. It is repeated here for the reader's convenience.

$$\rho_s^o = \rho_T \left\langle 1 + \ln\left[1 + \frac{c_2}{\ln\left(1 + \frac{\mu_{37.7°C} - \mu_G}{0.165}\right)} \right] \right\rangle^{\frac{1}{0.65}} \tag{8.20}$$

$$c_2 = c_2^o - \Delta c_2 \tag{8.21}$$

$$c_2^o = 1.882 \times 10^{-3} \exp\left(0.0058855 T_b\right) + 0.3674 T_b^{-0.1177} \tag{8.22}$$

$$\Delta c_2 = -2.01417 \Delta SG^2 - 0.1324 \Delta SG \tag{8.23}$$

$$\Delta SG = SG^o - SG \tag{8.24}$$

$$SG^o = 1.098\left[1 - \exp\left(-0.00148 T_b^{1.1128}\right)\right] \tag{8.25}$$

where T_b and SG are the pseudo-component normal boiling point in K and specific gravity, respectively. μ_G is the dilute gas viscosity calculated from Equation 4.6 using the parameters of the n-alkane with the same molecular weight as the pseudo-component. $\mu_{37.7°C}$ is calculated from the kinematic viscosity of the pseudo-component at 37.7°C and atmospheric pressure predicted from the following correlation presented in Chapter 6:

$$\ln\left(v_{37.7} + \frac{250}{T_b}\right) = \ln\left(v_{37.7}^o + \frac{250}{T_b}\right)\left(\frac{1 + 2f}{1 - 2f}\right)^2 \tag{8.26}$$

$$f = -|x|\Delta SG + 53.2315 \frac{\Delta SG^2}{T_b^{0.5}} \tag{8.27}$$

$$x = 3.7012 - \frac{73.02779}{T_b^{0.5}} \tag{8.28}$$

$$\log\left[\log\left(v_{37.7}^{o} + 1\right)\right] = (0.0036T_b - 2.0942)0.95^{T_b/200} \tag{8.29}$$

The calculated pseudo-component density at 37.7°c from the rackett correlation (Equation 6.8) is used to convert kinematic into dynamic viscosity.

Parameter λ_s^{o}

The compressed state thermal conductivity was found to correlate to molecular weight. Figure 8.10 shows the previously fitted compressed state thermal conductivity for the pure hydrocarbons in Development Dataset 1 (summarized in Table 8.3 and Appendix I) and the crude oils in Test Dataset 3 (Table 8.4) versus their molecular weight. The fitted parameters of the oils were used here to demonstrate the behavior of λ_s^{o} at higher molecular weights. Note that the maximum molecular weight of the pure hydrocarbons in the Development Dataset 1 is 350 g/mol, Figure 8.10. Most of the data follow a monotonically decreasing trend versus molecular weight that appears to reach an asymptote above a molecular weight of 300 g/mol. This asymptotic behavior might be the consequence of a suppression of rotational and translational degrees of freedom as the chain length growths. A similar behavior has been observed for other properties dependent on the rotational and translational degrees of freedom such as the mass-based heat capacity (Huang *et al*., 2005). For simplicity, it was assumed that the chemical family of the component does not have a significant influence on the value of the parameter λ_s^{o}. However, the deviations observed for *n*-alkanes at molecular weight higher than 220 g/mol might indicate that λ_s^{o} is dependent on the chemical family. There were too few data available to investigate further at this time.
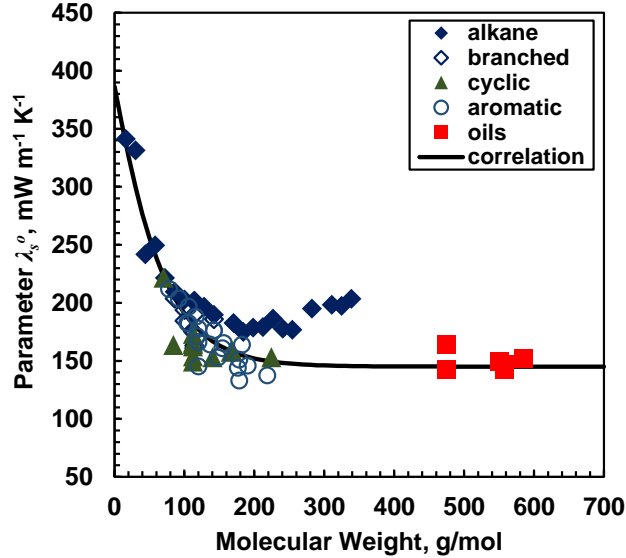
Figure 8.10. Calculated parameter λ_s^o versus molecular weight for the pure hydrocarbons in Development Dataset 1 and the crude oils in Test Dataset 3.

A correlation for λ_s^o was developed subjected to two constraints: 1) it must fit the λ_s^o for methane which is the lowest molecular weight component shown in Figure 8.10, and, 2) it must tend to a constant value at higher molecular weights. The correlation is given by:

$$\lambda_s^o = 241.34\exp\left(-0.01075M^{1.0939}\right)+145.1 \tag{8.30}$$

where λ_s^o is the compressed state thermal conductivity in mWm^{-1}K^{-1}. Equation 8.30 was defined to fit the data of cyclics, aromatics, and crude oils in order to be more representative of the high content of aromatics and cyclics found in heavy oil distillation cuts and pseudo-components (Altgelt and Boduszynsky, 1994). The AARD, MARD and bias of the correlated λ_s^o values were 9, 28, -1%, respectively. Not surprisingly, the maximum deviations were found for *n*-alkanes, Figure 8.11.
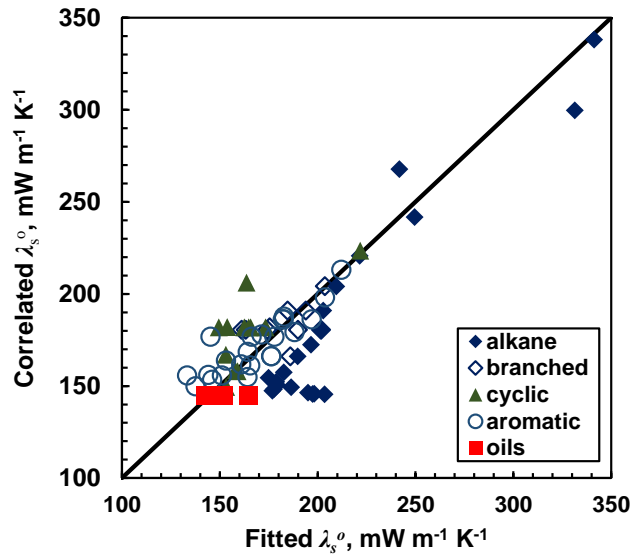
Figure 8.11. Dispersion plot of the correlated versus fitted λ_s^o parameter. The pure components and crude oils shown in the figure are those from the Development Dataset 1 and Test Dataset 3, respectively.

Parameter $c_{2\lambda}$

It was challenging to correlate the parameter $c_{2\lambda}$ directly to physical properties. The EF thermal conductivity model is sensitive to the value of this parameter and small deviations substantially affect the predicted thermal conductivities. Therefore, the $c_{2\lambda}$ parameter was instead determined indirectly from the EF thermal conductivity model using the correlated λ_s^o (Equation 8.30) and a synthetic thermal conductivity data point at a reference temperature at atmospheric pressure, λ_{REF}:

$$c_{2\lambda} = -\left[\left(\frac{\rho_s^o}{\rho_{REF}}\right)^{0.2} - 1\right]^{-1} \ln\left(\frac{\lambda_{REF} - \lambda_G}{\lambda_s^o - \lambda_G}\right)$$

(8.31)

where subscript *REF* indicates the reference condition. Equation 8.31 is simply the EF thermal conductivity model (Equation 8.10) written explicitly in terms of $c_{2\lambda}$. Recall that $\lambda_s^o = \lambda_s^*$ at atmospheric pressure.

The data in the Development Dataset 3 were used to develop a correlation for the prediction of the synthetic data point. This dataset contains experimental thermal conductivity of pure hydrocarbons at the normal boiling point and therefore the normal boiling point of each component was chosen as the reference temperature for that component, *i.e.* $\lambda_{REF} = \lambda_{Tb}$ for each component. The normal boiling point is also a convenient reference for boiling cut based pseudo-components. Figure 8.12 shows the relationship between thermal conductivity at the boiling point and molecular weight. The thermal conductivity at the boiling point shows a similar trend as that of the compressed state thermal conductivity, λ_s^o, Figure 8.10. It was assumed that the chemical family of the components does not have a significant effect on the thermal conductivity for the purpose of developing the correlation.
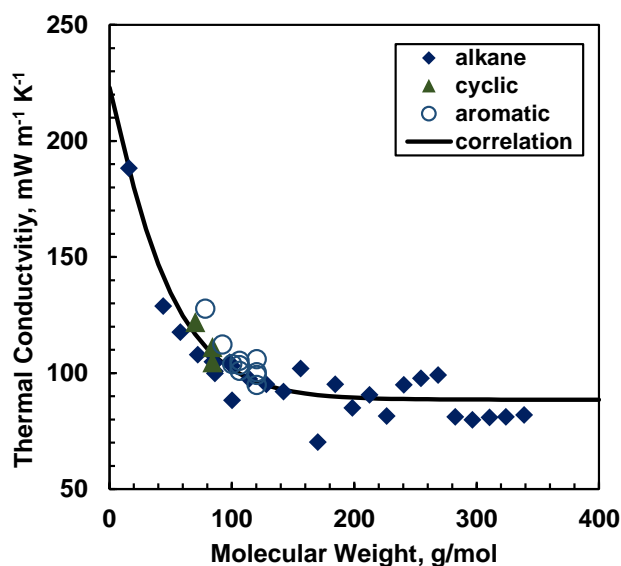
Figure 8.12. Thermal conductivity at the normal boiling point of the pure hydrocarbons in the Development Dataset 3. The data was taken from the API Technical Data Book (1997).

The data in Figure 8.12 are limited to molecular weights below 350 g/mol. The thermal conductivity at atmospheric pressure of the deasphalted bitumen sample WC-B-B3-DAO was used to guide the extrapolation to higher molecular weights. Note that the actual thermal conductivity at the boiling point of the deasphalted oil is not known, nor is its boiling point. The extrapolation was performed as follows:

246

1. The deasphalted bitumen was divided into twelve pseudo-components and their physical properties calculated as described in Section 8.5.

2. The parameter λ_s^o for each pseudo-component was calculated from Equation 8.30.

3. The parameter $c_{2\lambda}$ for the pseudo-components was calculated from Equation 8.31 using the thermal conductivity of each pseudo-component at the boiling point as input. This value of thermal conductivity was calculated from an initial correlation fitted to the data in Figure 8.12.. As to the other inputs for Equation 8.31, density was calculated from the Rackett correlation evaluated at the boiling point and ρ_s^o was calculated from Equations 8.20 to 8.29.

4. The parameters $c_{2\lambda}$ and λ_s^o for the whole deasphalted oil were calculated from those of the pseudo-component parameter values using the corresponding mixing rules (Equations 8.16 and 8.17) with correlated interaction parameters (Equations 8.18 and 8.19). Similarly, the parameter ρ_s^o for for the whole deasphalted oil was calculated from the corresponding mixing rule (Equation 4.7) using correlated interaction parameters from Equations 5.3 to 5.8.

5. The thermal conductivity of the deasphalted oil at 0.1 MPa was estimated using the calculated model parameters using experimental density as input.

Finally, the coefficients of the initial correlation for the calculation of the thermal conductivity at the boiling point were adjusted to match the experimental data of the deasphalted oil at atmospheric pressure. The correlation was constrained to converge to a fixed value at higher molecular weights as in the case of λ_s^o. The final correlation is given by:

$$\lambda_{REF} = \lambda_{Tb} = 134.48\exp\left(-0.01352M^{1.1178}\right)+88.5 \qquad (8.32)$$

where λ_{Tb} is the thermal conductivity at the normal boiling point. Equation. 8.32 predicts the thermal conductivity at the boiling point of the 42 pure components in the Development Dataset 3 with AARD, MARD and bias of 6, 28 and 1%, respectively.

<u>Parameter $c_{3\lambda}$</u>

The parameter $c_{3\lambda}$ calculated for the pure components in Development Dataset 1 and the crude oils in the Test Dataset 3 were also correlated to molecular weight as shown in Figure 8.13. The previously fitted values of these parameters can be found in Tables 8.3 and 8.4 for the respective datasets. The correlation is given by:

$$c_{3\lambda} = 9 \times 10^{-7} \left\{ 1 - \exp\left[-0.0252(M-16)^{0.974} \right] \right\}$$ (8.33)

where $c_{3\lambda}$ is in kPa^{-1}. Equation 8.33 is valid for molecular weights higher than 16 g/mol and converges to a fixed value of 9×10^{-7} kPa^{-1} at higher molecular weights. Although there is not enough data to fully justify the inclusion of an asymptote in Equation 8.33, this assumption proved to be advantageous when predicting the thermal conductivity of pseudo-component characterized oils, as will be discussed later.

Equation 8.33 fits the data for the $c_{3\lambda}$ parameter with an AARD of 28%. However, the EF thermal conductivity model is not very sensitive to the value of this parameter and therefore using the correlated values does not significantly affect the performance of the model. Note that a better correlation it is not feasible at this time because high pressure thermal conductivity data for pure hydrocarbons are scarce.
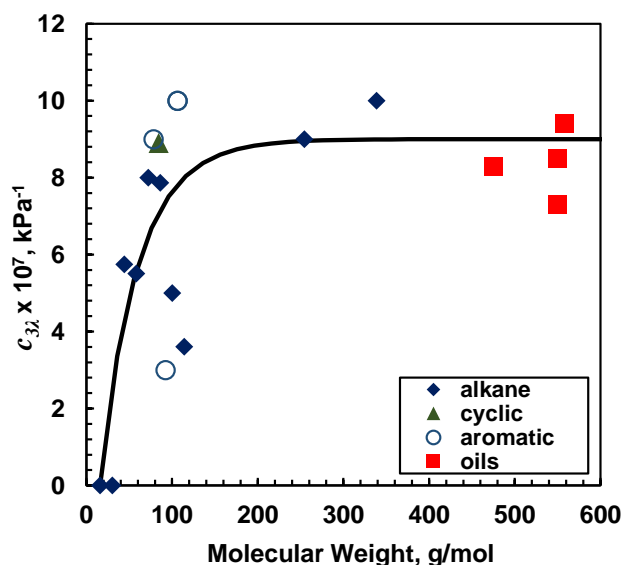
Figure 8.13. Relationship between parameter $c_{3\lambda}$ and molecular weight.

Testing the Parameter Correlations for Maltenes

The proposed correlations for parameters λ_s^o and $c_{2\lambda}$ were tested on the distillation cuts in Test Dataset 1. Note that only atmospheric pressure data were available for distillation cuts and therefore, the correlation for the parameter $c_{3\lambda}$ could not be tested. The thermal conductivities were predicted using the EF model (Equation 8.10) with correlated parameters λ_s^o and $c_{2\lambda}$ (Equations 8.30 and 8.31). The cuts were modeled as single components; therefore, no mixing rules for model parameters were required. The parameter ρ_s^o for each cut was calculated for each cut from Equations 8.20 to 8.29. The density and dilute gas thermal conductivity, required as model inputs, were calculated using the Rackett correlation (Equation 6.8) and Equation 8.8, respectively, as previously described. The EF thermal conductivity model approach is totally predictive requiring only the boiling point and specific gravity of the cut. For comparison purposes, the thermal conductivity of the cuts was also predicted using the Pedersen and Fredenslund (1987) version of the Corresponding States (CS) model presented in Section 2.5.4.1. The CS is another full-phase model widely used in petroleum applications.

Figure 8.14 shows the performance of the EF and the CS models for predicting the thermal conductivity of two representative distillation cuts. Figure 8.15 shows the deviation for each model as a function of the boiling point of the cut. In general, both models tend to underpredict the thermal conductivity of the cuts in Test Dataset 1. However, the relative deviation of the EF model is independent of the boiling point while the relative deviation for the CS model tends to increase with boiling point and has higher maximum deviations. The EF model predicted the thermal conductivity of the cuts in the Test Dataset 1 with an AARD, MARD and bias of 7, 19 and -5 %, respectively. These deviations are similar to those obtained from the prediction of the synthetic thermal conductivity data point suggesting that it is the main source of error. The AARD, MARD and bias of the CS model are 12, 40 and -6 %, respectively.
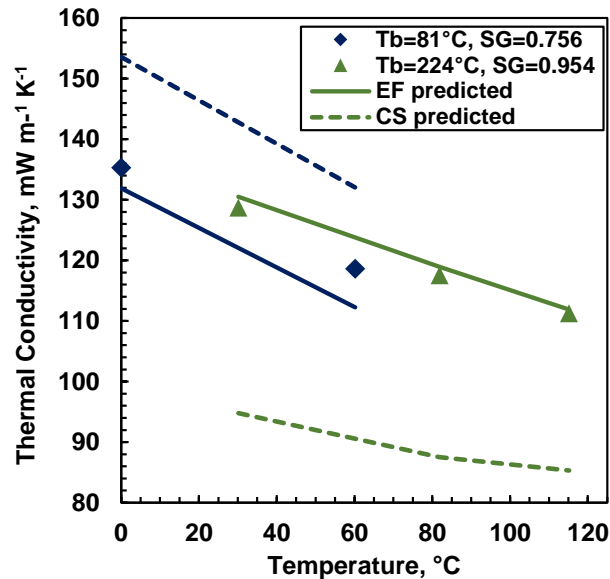
Figure 8.14. Thermal conductivity at atmospheric pressure versus temperature for two distillation cuts in the Test Dataset 1(Baltatu, 1984).
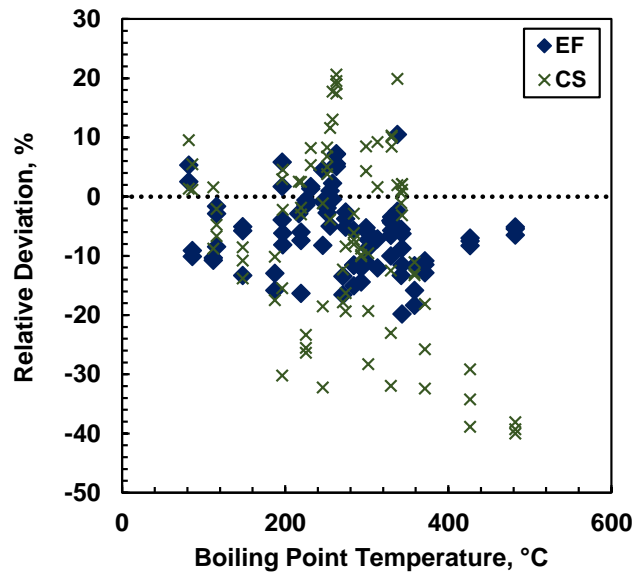
Figure 8.15. Relative deviation (100x (Predicted-Experimental)/Predicted) versus boiling point for the cuts in the Test Dataset 1. CS stands for Corresponding States Model.

The proposed correlation for the $c_{3\lambda}$ parameter was tested on the deasphalted bitumen sample WC-B-B3-DAO. The procedure for the calculation of the model parameters λ_s^o and $c_{2\lambda}$ for the deasphalted sample WC-B-B3-DAO was described in the previous section. Recall that this sample was represented as a set of pseudo-components and its thermal conductivity at atmospheric pressure was used in the development of the correlation for $c_{2\lambda}$. Figure 8.16 shows the prediction at high pressure using correlated $c_{3\lambda}$ parameters. This parameter was calculated for the whole fluid by combining those of the pseudo-components, calculated from Equation 8.33, using the mixing rule defined in Equation 8.11. The EF thermal conductivity model with correlated parameters predicted the thermal conductivity for this sample with an AARD, MARD and bias of 0.1, 0.25, and 0.01 %, respectively.
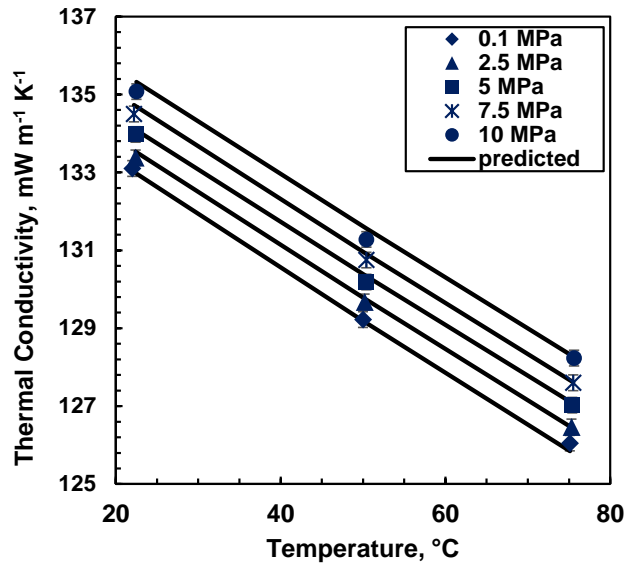
Figure 8.16. Predicted thermal conductivity for the deasphalted bitumen WC-B-B3-DAO.

8.5.4 Asphaltene Parameters

For thermal conductivity modelling purposes, the asphaltene fraction was represented as a single pseudo-component with fixed model parameters. These fixed parameters were not determined experimentally, as in the case of viscosity (refer to Section 6.6), because injection of molten asphaltenes into the hot wire apparatus cell would break the platinum wire.

Instead, the fixed asphaltene parameters for the thermal conductivity model were determined by tuning the model prediction to match the experimental thermal conductivity data of the sample WC-B-B3 using the experimental thermal conductivity of its C5-maltenes and C5-asphaltene content as inputs. The asphaltene parameters were determined as follows:

1. the bitumen was represented as a pseudo-binary mixture of maltenes and asphaltenes;
2. the maltene EF thermal conductivity model parameters $c_{2\lambda}$ and λ_s^o were determined by fitting the model to maltene thermal conductivity data at 0.1 MPa.

3. the whole oil parameters $c_{2\lambda}$ and λ_s^o were determined by fitting the model to the whole oil thermal conductivity data at 0.1 MPa. The value of ρ_s^o for the whole bitumen was calculated by fitting the EF viscosity model to measured viscosity data. The measured density was used as an input. Note that the EF viscosity model parameters c_2 and ρ_s^o for asphaltenes, estimated by fitting the model to experimental asphaltene data, were 0.9057 and 1113.7 kg/m³, respectively (Section 6.6).

4. the mass-based mixing rules (Equations 8.16 and 8.17) that relate the whole oil parameters to the maltene and asphaltene parameters were rearranged to determine the asphaltene parameters. The correlated interaction parameter (Equations 8.18 and 8.19) was used in the mixing rules.

The estimated asphaltene parameters $c_{2\lambda}$ and λ_s^o were 3.881 and 145.6 mW m^{-1} K^{-1}, respectively. The fitted λ_s^o value is close to the asymptotic value λ_s^o of 145.1 mW m^{-1} K^{-1} found for pure hydrocarbons at higher molecular weights(refer to Figure 8.10). The estimated asphaltene parameters were retuned in order to match this asymptotic value in order to ensure a smooth transition of the parameter λ_s^o from maltene pseudo-components to asphaltenes. The final set of parameters $c_{2\lambda}$ and λ_s^o for asphaltenes were 3.718 and 145.1 mWm^{-1}K^{-1}, respectively.

Figure 8.17 shows the model with fitted maltene and asphaltene parameters (solid line) and model predictions at pressures up to 10 MPa (dashed lines). High pressure predictions were calculated using the parameter $c_{3\lambda}$ for the whole bitumen estimated from those of the maltenes and asphaltenes using the mixing rule defined in Equation 8.11. The $c_{3\lambda}$ parameter for the maltenes and asphaltenes was calculated from Equation 8.33 using the molecular weight of each the fraction as input ($M_{mal} = 483$ g/mol, $M_{asph} = 1240$ g/mol). The EF thermal conductivity model fits the data at 0.1 MPa with AARD, MARD and bias of 0.03, 0.06 and -0.02%, respectively. The model predicts the data at high pressure with AARD, MARD and bias of 0.04, 0.1, and 0.02%, respectively.
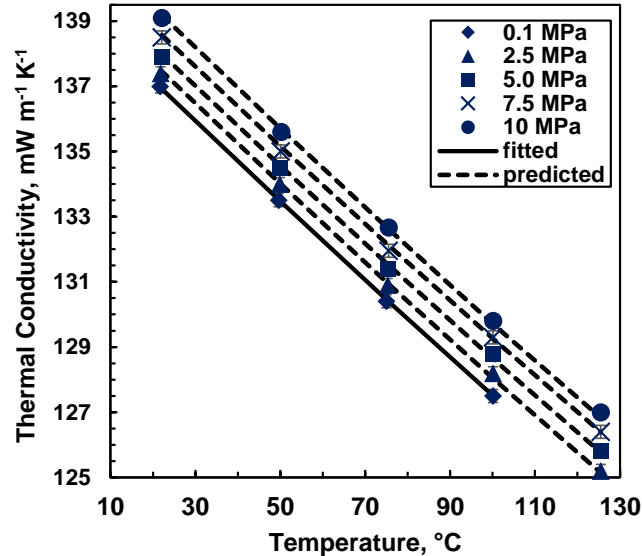
Figure 8.17. Measured and calculated thermal conductivity of Western Canada bitumen WC-B-B3. Solid line corresponds to the EF thermal conductivity model with maltene and asphaltene fitted parameters and dashed lines correspond to model predictions at high pressure.

Testing the Asphaltene Parameters

As the fixed asphaltene parameters were estimated by tuning the data of a particular sample, it is necessary to evaluate if they are applicable to different asphaltenes obtained from other crude oils. Therefore, the accuracy of the model was evaluated for mixtures containing asphaltenes. Any errors in the asphaltene parameters are expected to propagate to the thermal conductivity prediction of the mixture.

The asphaltene parameters were tested on two C5-asphaltene/toluene mixtures from the Test Dataset 2. The C5-asphaltenes used here were obtained from the Western Canada bitumen WC-B-A3(1); a sample from the same country but from a different reservoir than that used to determine the asphaltene parameters (WC-B-B3). The two mixtures were modelled as pseudo-binaries with model parameters $c_{2\lambda}$ and λ_s^o calculated from those of the asphaltenes and toluene using the mass-based mixing rules (Equations 8.16 and 8.17) with correlated interaction parameters estimated from Equations 8.18 and 8.19. The high

254

pressure parameter, $c_{3\lambda}$, for both components was calculated from Equation 8.33 and that of the mixture was calculated from the corresponding mass-based mixing rule (Equation 8.11). The ρ_s^o of the pseudo-binaries was calculated from its mixing rule (Equation 4.7) with correlated interaction parameters (Equations 5.3 to 5.8). The interaction parameters for the ρ_s^o mixing rule were calculated using the experimental atomic hydrogen-to-carbon ratio (H/C$_{asph}$= 1.185) and specific gravity (SG$_{asph}$=1.094) of the C5-asphaltenes as input. The density of the mixtures, used as input, was estimated as discussed in Section 8.2.1.

Figure 8.18 shows the model predictions at 5 MPa. The data of pure toluene has been included in the figure as a reference. The model predicted the thermal conductivity of the pseudo-binary mixtures with AARD, MARD and bias of 0.2, 0.5 and 0.01%, respectively. Note, the deviations were estimated over the entire dataset not just the data at 5 MPa. The accuracy of the prediction demonstrates that the fixed asphaltene model parameters can be applied to simple mixtures regardless of small differences in molecular weight or self-association.
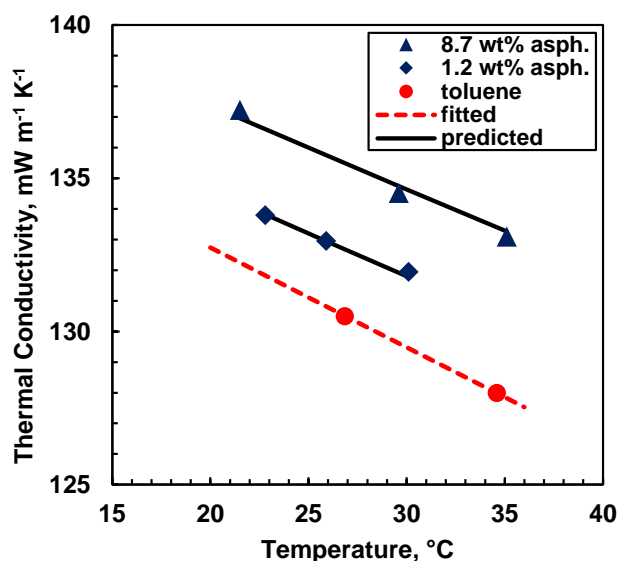
Figure 8.18. Thermal conductivity of pure toluene and pseudo-binaries with 1.2 and 8.7 wt% C5-asphaltene in toluene at 5 MPa. The EF thermal conductivity model was fit to toluene data from 26 to 200°C at 5 MPa (NIST, 2008). The C5-asphaltenes were precipitated from sample WC-B-A3(1).

8.6 Predicting and Tuning the Thermal Conductivity of Characterized Crude Oils

8.6.1 Thermal Conductivity Prediction

The proposed correlations and modelling approach were tested on the crude oils from the Test Dataset 3. Note that only the sample WC-B-B3 was used to develop correlations. Previously, the EF thermal conductivity model was fitted to the crude oils from the Test Dataset 3 but they were modelled as single component fluids. The fitted model parameters are summarized in Table 8.4. To predict the thermal conductivity of each crude oil using the EF thermal conductivity model, the only required input oil properties are its distillation curve, specific gravity, molecular weight, and C5-asphaltene content. Either experimental or predicted density is also required as input. The results presented here were obtained using the density predicted as described in Section 8.5.2; no additional input data were required.

The crude oils were characterized as shown in Figure 8.9 and in Appendix E. The boiling point curve was extended over the entire maltene fraction following a Gaussian extrapolation. The maltene fraction was divided into a set of pseudo-components and their properties calculated from a set of correlations described in Section 8.5.1. The parameter $\rho_s{}^o$ for each maltene pseudo-component was calculated from Equations 8.20 to 8.29 using boiling point and specific gravity as inputs. The EF parameters $\lambda_s{}^o$ and $c_{2\lambda}$ for each pseudo-component were calculated from Equations 8.30 and 8.31, respectively. The asphaltene fraction was characterized as a single component with EF parameters set to $\lambda_s{}^o=145.1$ mW/m.K, $c_{2\lambda} = 3.718$ and $\rho_s{}^o = 1113.7$ kg/m^3. The high pressure parameter $c_{3\lambda}$ was calculated for each pseudo-component and asphaltene fraction using Equation 8.33.

The parameter $\rho_s{}^o$ for the whole oil was estimated by combining those of the pseudo-components and asphaltenes using the corresponding mass-based mixing rule (Equation 4.7) with interaction parameters calculated from Equations 5.3 to 5.8. The specific gravity and atomic hydrogen to carbon ratio of pseudo-components and asphaltenes are required for the calculation of interaction parameters for the $\rho_s{}^o$ mixing rule. Both properties are calculated as described in Section 8.5.1. The whole oil EF parameters $c_{3\lambda}$, $\lambda_s{}^o$ and $c_{2\lambda}$ and were calculated by combining those of the pseudo-components and asphaltenes using mass-based mixing rules (Equations 8.11, 8.16 and 8.17, respectively) with correlated interaction parameters determined from Equations 8.18 and 8.19. These thermal conductivity interaction parameters are only a function of the specific gravity of the asphaltene and maltene pseudo-components and are calculated as described in Section 8.5.1.

All crude oils were modelled using 13 pseudo-components for the maltene fraction and 1 pseudo-component for asphatlenes. Figure 8.19a shows the predicted thermal conductivity of the European heavy oil EU-HO-A1 at temperatures from 22 to 75°C and pressures up to 10 MPa. Figure 8.19b shows the model predictions at 0.1 MPa for three different oils from disparate geographical locations (Colombia, Europe and Middle East) with different API gravities (10°, 15° and 30°). The deviations for the model predictions for each crude

oil are reported in Table 8.9. The EF thermal conductivity model captured the trends of thermal conductivity with temperature, pressure, and oil API gravity; however, the deviations were significantly higher than the fitted model (Table 8.4). The AARD, MARD and bias of the EF model predictions for this dataset were 2.1, 3.0 and 1.4%, respectively, compared with 0.2, 0.6 and -0.01%, respectively, for the fitted model. Note that these and the rest of the deviations reported here are estimated over the entire dataset including high pressure data.
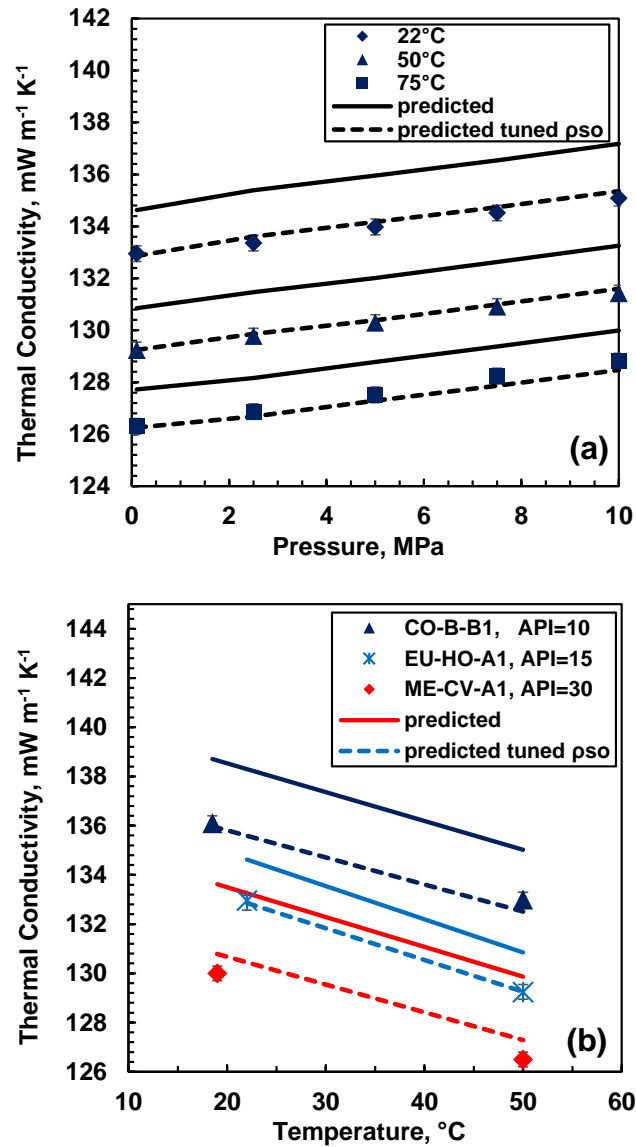
Figure 8.19. Measured and predicted thermal conductivity of: a) European heavy oil EU-HO-A1 at 22 to 75°C and 0.1 to 10 MPa; b) crude oils CO-B-B1, EU-HO-A1 and ME-CV-A1 at room temperature and 50°C at 0.1 MPa. Solid and dashed lines correspond to predicted and predicted with tuned ρ_s^o, respectively.

Table 8.9. EF thermal conductivity model parameters and deviations for the crude oils from the Test Dataset 3.

Oil	ρ_s^o kg/m^3	$c_{2\lambda}$	λ_s^o, mW m^{-1}K^{-1}	$c_{3\lambda}$, x10^7 kPa^{-1}	AARD %	MARD %	Bias %
WC-B-B3	1052.0	7.214	146.0	8.9	2.4	2.6	2.4
WC-B-A3(1)	1046.3	8.545	146.0	8.8	1.5	2.0	1.3
WC-B-A3(2)	1050.0	7.594	146.1	8.9	2.5	3.0	-2.5
EU-HO-A1	1014.1	8.170	146.5	8.9	1.3	1.5	1.3
WC-B-A1	1041.3	7.916	146.4	8.9	2.9	3.0	2.9
CO-B-B1	1038.3	7.148	146.3	9.0	1.7	1.9	1.7
ME-CV-A1	956.1	5.948	148.7	8.8	2.7	2.8	2.7

Effect of Tuning ρ_s^o

The predictive procedure for thermal conductivity depends on the calculation of the EF parameter ρ_s^o. As pointed out in Section 6.5, the value of the predicted ρ_s^o is uncertain because it depends on the accurate prediction of a single viscosity data point. The estimated ρ_s^o values for the maltene pseudo-components (calculated from Equations 8.20 to 8.29) and asphaltene fraction ($\rho_{s\ asph}^o$=1113.7 kg/m³) were tuned using a constant common multiplier to match a single experimental viscosity data point of the fluid at 0.1 MPa. Details of this tuning procedure are presented in Section 6.7. This tuning was previously shown to substantially improve the viscosity model predictions. Therefore, the thermal conductivity of the crude oils from the Test Dataset 3 was predicted using the EF thermal conductivity model with tuned ρ_s^o.

Tuning the compressed state density substantially improved the thermal conductivity predictions as shown in Figure 8.19 and Table 8.10. Note that using tuned or untuned ρ_s^o only affects the value of the parameter $c_{2\lambda}$ (see Equation 8.31). The parameters λ_s^o and $c_{3\lambda}$ are independent of the value of ρ_s^o; therefore, they are not shown in Table 8.10. The AARD, MARD and bias of the EF model with tuned ρ_s^o were 0.6, 1.8, 0.1%, respectively, similar to the AARD, MARD and bias of 0.2, 0.6 and -0.01%, respectively, for the fitted model.

Clearly, the main source of error in the EF models for viscosity and thermal conductivity is the accurate determination of ρ_s^o.

Note the highest deviations were observed for WC-B-A3(2). Recall that the molecular weight and distillation curve for this sample were assumed to be identical to those of sample WC-B-A3(1). Both samples proceed from the same reservoir source but they have different density, viscosity, and thermal conductivity. The relatively high errors may arise from a non-representative distillation curve.

Table 8.10. Summary of EF thermal conductivity model parameters (tuned ρ_s^o) and deviations for the crude oils from the Test Dataset 3. Note that after tuning ρ_s^o only the value of $c_{2\lambda}$ is affected. Values of λ_s^o and $c_{3\lambda}$ are not shown as they are the same as those presented in Table 8.9.

Oil	Tuned ρ_s^o, kg/m³	$c_{2\lambda}$,	AARD %	MARD %	Bias %
WC-B-B3	1069.5	6.960	0.5	0.8	0.5
WC-B-A3(1)	1057.2	8.062	0.2	0.4	-0.2
WC-B-A3(2)	1060.0	7.165	1.4	1.8	-1.4
EU-HO-A1	1024.3	7.967	0.1	0.3	0.0
WC-B-A1	1055.2	7.670	1.2	1.3	1.2
CO-B-B1	1055.6	6.896	0.2	0.4	-0.2
ME-CV-A1	979.6	5.666	0.6	0.6	0.6

Sensitivity to Number of Pseudo-Components

To evaluate the sensitivity of the model to the number of pseudo-components used to represent the maltene fraction, the thermal conductivity of the Western Canada bitumen WC-B-A3(2) was predicted for 1, 3, 6 and 12 pseudo-components, using tuned ρ_s^o values, Figure 8.20. The AARD of 1, 3, 6 and 12 pseudo-components were 1.4, 1.2, 1.2, 1.1%, respectively. Three pseudo-components were sufficient to minimize the error not only for sample WC-B-A3(2) but also for the other crude oils in the Test Dataset 3.
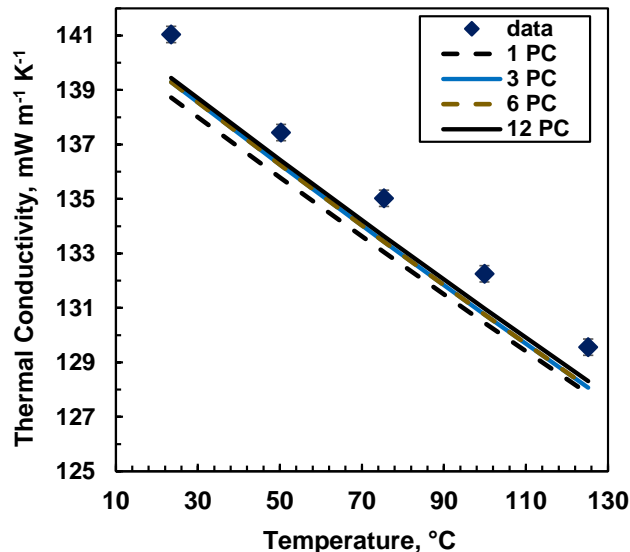
Figure 8.20. Experimental and modelled thermal conductivity of Western Canada bitumen WC-B-A3(2) at 10 MPa (the worst prediction for the oils from the Test Dataset 3). PC stands for number of pseudo-components used to represent the maltene fraction.

8.6.2 Tuning the Model

If thermal conductivity data are available, the EF thermal conductivity model can be easily tuned using single common multipliers applied to the model parameters of the maltene pseudo-components and asphaltene pseudo-component. As previously described, either calculated or tuned ρ_s^o parameters can be used. Using predicted or tuned ρ_s^o parameters produce thermal conductivity values within 3 and 1% of experimental data, respectively. However, using tuned ρ_s^o demands at least a single viscosity data point measured at 0.1 MPa. A description of the approach to tune the model when using predicted and tuned ρ_s^o is presented below.

Model with Predicted ρ_s^o

If the ρ_s^o values for maltene pseudo-components and asphaltene pseudo-component were predicted as described in Sections 8.5.3 and 8.5.4, respectively, the EF thermal conductivity model can be tuned by applying a single constant multiplier to the parameter λ_s^o to match a thermal conductivity data point at room temperature (or any other

262

temperature) and atmospheric pressure. Table 8.11 shows a summary of the multipliers to the parameter λ_s^o and deviations for the oils from the Test Dataset 3. The overall AARD, MARD and bias were of 0.2, 0.6 and 0.01%, respectively. In comparison, the overall AARD, MARD and bias of the fitted model were of 0.2, 0.6 and -0.01%, respectively. The deviations of the tuned model are almost identical to those of the fitted model. Note that once the model is tuned at atmospheric pressure, it is predictive at high pressure.

Table 8.11. Single common multipliers, deviations, and bias of the tuned EF thermal conductivity model with predicted ρ_s^o for the oils from the Test Dataset 3. Deviations were calculated over the entire dataset including high pressure.

Sample	multiplier λ_s^o	AARD %	MARD %	Bias %
WC-B-B3	0.976	0.45	0.60	0.15
WC-B-A3(1)	1.004	0.20	0.27	0.14
WC-B-A3(2)	0.999	0.18	0.22	0.18
EU-HO-A1	0.988	0.17	0.35	0.00
WC-B-A1	0.971	0.14	0.29	-0.14
CO-B-B1	0.981	0.19	0.38	-0.19
ME-CV-A1	0.973	0.06	0.12	-0.06

Model with Tuned ρ_s^o

In order to maintain the consistency between EF viscosity and thermal conductivity models, it is recommended to tune ρ_s^o against a single viscosity data point and then tune the parameter λ_s^o using a single constant multiplier to match a thermal conductivity data point at room temperature (or any other temperature) and atmospheric pressure. This approach is recommended when using the EF viscosity and thermal conductivity models simultaneously. A summary of the estimated multipliers for the parameter λ_s^o and the deviations and bias for the oils in Test Dataset 3 are presented in Table 8.12. The overall AARD, MARD and bias were 0.2, 0.6 and -0.06% respectively, compared with the AARD, MARD and bias of 0.2, 0.6 and -0.01%, respectively, for the fitted model. Note that after tuning, the overall deviations were similar for the model with predicted and tuned ρ_s^o, respectively. Once the model has been tuned to the data point at atmospheric pressure, it

263

predicts the thermal conductivity of the fluid at high pressures and temperatures to within 0.5%.

Table 8.12. Single common multipliers, deviations, and bias of the tuned EF thermal conductivity model with tuned ρ_s^o for the oils from the Test Dataset 3. Deviations were calculated over the entire dataset including high pressure.

Sample	multiplier λ_s^o	AARD %	MARD %	Bias %
WC-B-B3	0.996	0.40	0.45	0.16
WC-B-A3(1)	1.003	0.15	0.27	0.14
WC-B-A3(2)	0.998	0.18	0.22	0.18
EU-HO-A1	1.001	0.26	0.61	-0.26
WC-B-A1	0.987	0.35	0.45	-0.35
CO-B-B1	1.001	0.34	0.48	-0.34
ME-CV-A1	0.994	0.00	0.00	0.00

8.7 Comparison of the EF and Corresponding States Thermal Conductivity Models

The version of the Corresponding States (CS) model evaluated here was proposed by Pedersen and Fredenslund (1987) which has been formulated for crude oil characterized based on a GC assay. Briefly, the thermal conductivity of a fluid is divided into two contributions: one arising from transport of energy due to translational effects, λ', and the other from the transfer of energy due to internal degrees of freedom, λ'':

$$\lambda = \lambda' + \lambda'' \tag{8.34}$$

The translational part is calculated as:

$$\lambda' = \left(\frac{T_{c,x}}{T_{c,o}}\right)^{-1/6}\left(\frac{P_{c,x}}{P_{c,o}}\right)^{2/3}\left(\frac{M_x}{M_o}\right)^{-1/2}\left(\frac{\alpha_x}{\alpha_o}\right)\left(\lambda_o' - \lambda_o''\right) + \lambda_x'' \tag{8.35}$$

where T, P, M and α are the temperature, pressure, molecular weight and a correction factor, respectively; subscript c indicate a critical property of the fluid x and the reference component o (methane). The translational thermal conductivity of characterized crude oils is calculated using Equation 8.35 with critical properties, molecular weight and parameter α calculated from those of the pseudo-components using the mixing rules developed by

Christensen and Fredenslund (1980). The parameter α is calculated according to the expression proposed by Pedersen and Fredenslund (1987). The properties of methane, used as reference component, are calculated from the equations presented by Pedersen and Fredenslund (1987). Finally, the internal degrees of freedom thermal conductivity is calculated according to the correlation developed by Christensen and Fredenslund (1980).

The oil characterization approach for the CS model applications are described in detail by Pedersen *et al*. (1984b) and is briefly summarized here. The first step is to characterize the oil into carbon number (effectively molecular weight) based pseudo-components based on the GC assay. Since up to 70 wt% of a bitumen falls into the C30+ residue of a GC assay, the assay must be extrapolated to completely characterize the oil. The molar distribution in the carbon number fractions in the C30+ residue was assumed to follow an exponential distribution. The molar distribution was extrapolated up to C100. The average molecular weight of this distribution was adjusted to match the molecular weight of the whole oil calculated from all fractions including the residue. The specific gravities of the carbon number fractions were calculated from a logarithmic dependence between specific gravity and carbon number adjusted to fit the experimental value of the oil. The boiling points of the carbon number fractions were estimated from the expressions proposed by Katz and Firoozabadi (1978), for fractions up to C45, and by Pedersen *et al*. (1984b), for heavier fractions. The critical properties of the carbon number fractions were calculated from the Cavett correlations (Cavett, 1962) which require specific gravity and boiling point as inputs. Once the complete description of the oil was constructed, the oil was divided into pseudo-components. A set of consecutive carbon number fractions were lumped into a pseudo-component. A total of 13 pseudo-components were defined.

Given the high uncertainties related with the calculation of critical properties of heavier pseudo-components, the authors recommended to tune these properties in order to match phase behavior data. However, as no phase behavior data was available, no tuning of critical properties was performed here.

To evaluate the predictive capabilities of the EF and the CS thermal conductivity models for characterized oils, the thermal conductivity of the Western Canada bitumen WC-B-B3 was predicted using both approaches. This example was chosen because it was the only oil for which GC assay data were available. Note that this oil was used in the development of the EF model correlations; however, considering that there were no significant differences in the errors between this sample and the others which were not used in the development of correlations, the results for sample WC-B-B3 are considered valid for comparison purposes.

Figure 8.21 shows the EF and the CS thermal conductivity predictions at 0.1 MPa. Although both models capture the correct trend between thermal conductivity and temperature; the rate at which CS predictions decrease with temperature is much faster than that of the experimental data and EF predictions with tuned and untuned ρ_s^o. The accuracy of the CS model predictions depends mostly on two factors: 1) the thermal conductivity of methane used as reference component and, 2) the calculation of the critical properties of the fluid (see Equation 8.35).

In the great majority of cases, heavy oils correspond to methane at conditions below its freezing point (-182°C) for which thermal conductivity data is not available; therefore, the thermal conductivity must be determined by extrapolation. However, the extrapolated values might not coincide with the actual data considering that the thermal conductivity of methane shows several anomalies at -182, -223 and -248°C due to transition between crystal phases (Jezowski *et al*., 1997; Konstantinov *et al*., 1999).

Regarding the second factor, the accuracy of the calculated critical properties the Cavett correlations (Cavett, 1962) greatly depends on the specific gravity and boiling point of the carbon number fractions used as input. However, for heavier carbon number fractions, these two properties are estimated from extrapolation which introduces high uncertainties which in turn impacts the estimated critical properties. The accuracy of the EF thermal conductivity model mostly depends on the estimation of ρ_s^o. As previously mentioned, the

calculation of this parameter is subjected to high uncertainties. Nonetheless, the model predicted the thermal conductivity of the oils from the Test Dataset 3 within 3% of experimental values.

The CS model predicted the thermal conductivity of the Western Canada bitumen WC-B-B3 with an AARD, MARD and bias of 12, 17 and -12%, respectively. The EF thermal conductivity model predicted the thermal conductivity of the same fluid with AARD, MARD and bias of 2.4, 2.6 and 2.4%, respectively. When the estimated ρ_s^o for the EF thermal conductivity model was tuned against a single viscosity data point, as described in Section 6.7, the AARD, MARD and bias were reduced to 0.5, 0.8, 0.5%, respectively.
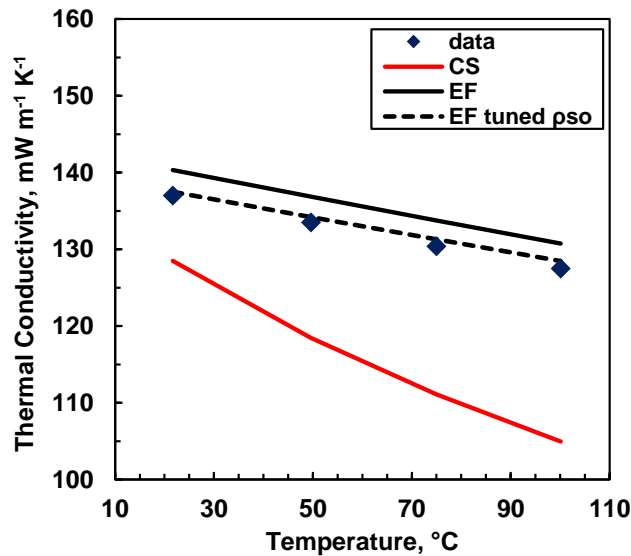
Figure 8.21. Measured and predicted thermal conductivity data at 0.1 MPa of Western Canada bitumen WC-B-B3. The solid and dashed lines are the EF model predictions with untuned and tuned ρ_s^o, and the dashed line is the Corresponding States model prediction.

8.8 Summary

A full phase thermal conductivity model for pure hydrocarbons, crude oils, and their mixtures was developed based on the concept that the fluid properties that depend on the spacing between molecules, such as viscosity and thermal conductivity, decrease monotonically as the fluid expands from the liquid-solid phase transition to the dilute gas

state. The model requires density, pressure and four fluid-specific parameters, ρ_s^o, λ_s^o, $c_{2\lambda}$, and $c_{3\lambda}$ as inputs.

The model was developed based on a dataset collected from the literature for *n*-alkanes, branched alkanes, aromatics and cyclics at temperatures and pressures up to 500°C and 100 MPa, respectively. The model was tested on the thermal conductivity data for 7 crude oils, each modeled as a single component fluid, at temperatures and pressures up to 125°C and 10 MPa, respectively. The model fit the data for over 50 different hydrocarbons to within 5% and the data for the 7 crude oils to within 0.5%.

Mass-based mixing rules including binary interaction parameters were developed for the correlation parameters to model mixtures. The model with tuned interaction parameters fit the data of 20 pure hydrocarbon binaries and 5 oil/solvent pseudo-binaries with average deviations of 0.2 and 0.5%, respectively. A correlation was developed for the interaction parameters as function of specific gravity.

A method was developed to predict the thermal conductivity of crude oils based on a distillation assay, asphaltene content, molecular weight and specific gravity of the oil. Predicted density rather than experimental values were used as inputs in this study. This method relies on a separate characterization for maltenes and asphaltenes. The maltene fraction is represented as pseudo-components with model parameters calculated as a function of molecular weight and boiling point. The asphaltene fraction is represented as a single component with fixed model parameters. The parameters of the whole fluid are calculated by combining those of the maltene pseudo-components and asphaltenes using the mixing rules with correlated interaction parameters. The required pseudo-component paramters are, ρ_s^o, λ_s^o, $c_{2\lambda}$, and $c_{3\lambda}$. A correlation for the parameter ρ_s^o was previously developed and presented in Section 6.5.1 and briefly summarized in Section 8.5.3. Correlations for the fluid-specific parameters $c_{2\lambda}$, $c_{3\lambda}$ and λ_s^o were developed in this chapter. The model with untuned ρ_s^o predicted the thermal conductivity of 7 crude oils with an AARD, MARD and bias of 2.1, 3, and 1.4%, respectively. The accuracy of the predictions improved significantly when the ρ_s^o values were tuned against viscosity data. The EF model

with tuned $\rho_s{}^o$ predicted the thermal conductivity of the same 7 crude oils with an AARD, MARD and bias of 0.6, 1.8, and 0.1%, respectively.

CHAPTER NINE: CONCLUSIONS AND RECOMMENDATIONS

The main objective of this thesis was to develop a predictive methodology for the viscosity and thermal conductivity of heavy oils and bitumens for use in process and reservoir simulation. For process simulation, the Expanded Fluid viscosity model was extended to characterized oils and a new thermal conductivity model was developed based on the Expanded Fluid concept. For reservoir simulation, the Walther viscosity model was updated for oils characterized based on a distillation assay. This chapter presents a summary of the conclusions drawn from this study and recommendations for future research projects in this field.

9.1 Dissertation Contributions and Conclusions
The major contributions from this thesis are:

- the collection of viscosity data for whole and diluted heavy oils, totally and partially deasphalted heavy oils, heavy oil distillation cuts and asphaltenes.
- the application of the Expanded Fluid and Walther viscosity models to oils characterized based on a distillation assay,
- the development of a method to predict compressed liquid phase density for input into the Expanded Fluid model,
- the design and commissioning of an apparatus to measure the thermal conductivity of heavy oil, solvents, and their mixtures,
- the collection of thermal conductivity data for whole and diluted heavy oils, deasphalted oils and C5-asphaltene/toluene mixtures,
- the development of an Expanded Fluid thermal conductivity model for pure components, characterized crude oils, and mixtures.

Each contribution and the associated conclusions are discussed below.

<u>Viscosity Data</u>

A comprehensive set of viscosity and density data was gathered as summarized below.

Diluted Bitumen:

- 9 pseudo-binary and 1 pseudo-ternary mixture of crude oil and solvent(s) at temperatures from 20 to 175°C, pressures up to 10 MPa, and solvent contents up to 40 wt%. The solvents used to prepare the mixtures were ethane, propane, butane, pentane, heptane, eicosane, toluene, cyclohexane and heptol (a mixture 50 wt% heptane and 50 wt% toluene).

- 7 pseudo-binary and 1 pseudo-ternary mixture of crude oil and solvent(s) and 3 pseudo-binary mixtures of deasphalted oil and solvent at temperatures from 10 to 50°C at atmospheric pressure and solvent contents up to 15 wt%. The solvents used to prepare the mixture these mixtures were pentane, dodecane, tetradecane and 1-methylnaphthalene.

Whole Oils, Totally and Partially Deasphalted Oils:

- 15 different crude oils from disparate geographical locations at temperatures from 20 to 175°C and pressures up to 10 MPa; oil API gravity from 8 to 30° and asphaltene contents from 3 to 25 wt%.

- 6 totally deasphalted oils at temperatures from 20 to 150°C at atmospheric pressure.

- 1 totally deasphalted samples at temperatures from 20 to 175°C and pressures up to 10 MPa.

- a bitumen partially deasphalted to residual asphaltene contents of 16, 4 and 3% at temperatures from 20 to 75°C at atmospheric pressure.

Distillation Cuts:

- 40 distillation cuts obtained from 7 different heavy oils from disparate geographical locations at temperatures from 20 to 125°C at atmospheric pressure.

Asphaltenes:

- 2 molten C5-asphaltenes samples obtained from 2 different bitumens at temperatures from 175 to 200°C at atmospheric pressure.
- a 5 wt% C5-asphaltene in toluene solution at temperatures from 21 to 175° and pressures up to 9 MPa.

The dataset is well suited for developing and testing viscosity models because it encompasses a wide range of temperatures, pressures and solvent contents. It also includes deasphalted oils and distillation cuts, for which available data are scarce, and pseudo-binaries of bitumen with solvents, such as *n*-eicosane, cyclohexane, 1-methylnaphthalene, for which data have not been yet reported in the literature. To the author's knowledge, this is the first measurement of molten asphaltene properties to be reported in the public domain.

Expanded Fluid and Walther Viscosity Model for Characterized Oils

A methodology was developed to predict the viscosity of hydrocarbon mixtures, diluted crude oils, distillation cuts, totally and partially deasphalted oils, and, whole crude oils using the Expanded Fluid (EF) and Generalized Walther (GW) viscosity model. The oils are characterized into pseudo-components based on a distillation assay. The physical and critical properties of the pseudo-components are determined from existing correlations. New correlations were developed for the viscosity model parameters and for the binary interaction parameters in the viscosity model mixing rules. A methodology was adapted to predict the input density. The models include a tuning procedure using a single common multiplier. The required inputs are a distillation assay, the asphaltene content of the oil, and the specific gravity of the oil. The models provide viscosity predictions to within 50 % of measured values. Both models can be easily tuned against one single experimental viscosity datapoint. Tuned models provide viscosity predictions within 5% of measured values. The previous EF and GW versions, based on GC characterized oils, predicted the viscosity of the oils within 130% of measured values.

Compressed Liquid Density Model for Characterized Oils

The density of compressed liquid crude oils was predicted based on the same characterization methodology used for the viscosity model. The density of maltene pseudo-components was predicted using the Rackett and Tait-COSTALD correlations whereas that of asphaltenes (represented as a single component) was estimated from an empirical correlation developed in this thesis. This empirical correlation was obtained by fitting asphaltene/toluene density data assuming asphaltenes/toluene mixtures form regular solutions. The correlation accounts for the effect of temperature on asphaltene density but neglects the effect of pressure due to the limited data available. This methodology predicted the density of the crude oils in this study with an average absolute deviation of 2 kg/m^3. The error from the assumption that asphaltenes were incompressible was negligible, at least at pressures below 10 MPa. Unlike other density prediction methods, such as cubic equations of state coupled with volume translation, the proposed approach does not require the calculation of asphaltene critical parameters and accentric factors (which introduce large errors) or an iterative algorithm to estimate the asphaltene density.

Apparatus to Measure Thermal Conductivity

An apparatus was designed and a procedure developed to measure the thermal conductivity of liquid hydrocarbons, heavy oils, and diluted oils. The apparatus was constructed around a commercially available hot wire probe and was designed to collect data at temperatures from room to 200°C and pressures up to 10 MPa. A procedure was developed to collect thermal conductities and was validated using pure hydrocarbons and water. The measured thermal conductivities were within 5% of the literature values for Grashof numbers below 10,000. At higher Grashof numbers, natural convection became too significant to obtain accurate data.

Thermal Conductivity Data

The aforementioned apparatus was used to collect thermal conductivity data as summarized below.

Whole Oils:

- 4 crude oils and 1 deasphalted oil at temperatures from 20 to 150°C and pressures up to 10 MPa.

- 3 crude oils at 21 and 50°C and atmospheric pressure; all seven crude oils were obtained from different disparate geographical locations with API gravities between 8 and 30.

Diluted Oils:

- 5 pseudo-binary mixtures of bitumen and solvent at temperatures between 20 and 100°C, pressures up to 10 MPa, and solvent contents up to 40 wt%. The solvents were *n*-pentane, *n*-heptane, *n*-tetradecane, cyclohexane and toluene.

This dataset, particularly the high pressure data, adds significantly to the few datasets for crude oils available from the literature, which are mostly at atmospheric pressure. To the author's knowledge, these are the first oil/solvent pseudo-binary thermal conductivity data to be reported in the public domain.

Expanded Fluid Thermal Conductivity Model

An Expanded Fluid (EF) based thermal conductvity model was developed based on pure hydrocarbon data. The proposed model has three thermal conductivity fluid-specific parameters and an additional parameter, the compressed or "glassy" state density, determined from viscosity data. Other inputs are the fluid density, pressure, and the dilute gas thermal conductivity. The latter is calculated from well-established correlations. The model is applicable across the phase diagram and fits pure hydrocarbon data at temperatures from -150 to 330°C and pressures up to 200 MPa with an average deviation of 4%. The model also fits crude oil data, represented as a single fluid, with an average

deviation of 1% at temperatures from 20 to 150°C and pressures up to 10 MPa. The model was extended to mixtures through mass-based mixing rules for the model parameters. Correlated binary interaction parameters are used to improve the performace of the model for mixtures.

The model was also extended to predict the thermal conductivity of oils characterized based on a distillation assay as described for the viscosity models. A set of correlations for the model parameters were developed. The whole oil model parameters are calculated using the mixing rules with correlated interaction parameters. The model is easily tunable against either a single viscosity or thermal conductivity datapoint. The required inputs are a distillation assay, the asphaltene content of the oil, and the specific gravity of the oil. The density of the oil, used as input, is predicted as described previousy.

The EF thermal conductivity model has several advantages over the Corresponding States (CS) model, another full-phase model used in petroleum applications. First, it does not require a reference fluid and therefore is applicable to heavy oils without modification. Methane or propane, which are used as CS reference fluids, correspond poorly to heavy oils at conditions below the reference fluid freezing point. Second, the model is not computationally intensive and is well suited for implementation in a process simulator. In contrast, the CS model requires the calculation of reference component properties, usually with iterative algorithms. Third, the EF thermal conductivity model can be easily tuned by adjusting one parameter to match only one datapoint. . Finally, the EF model was more accurate than the CS model for the test dataset examined in this thesis. In general, the EF model predictions were within 3% of the data versus 12% with the CS model.

9.2 Recommendations

The recommendations for future studies are as follows:

1. The main source of uncertainty in the prediction of crude oil viscosity using the EF and GW models is the prediction of the synthetic viscosity data point for maltene pseudo-components. The data point correlation proposed here (the modified Twu

275

correlation) captures the effect of intermolecular forces and chemical family on viscosity by means of the boiling point and specific gravity of the pseudo-component or distillation cut, respectively. However, it was observed that the viscosity of two different cuts (from different oil sources) can vary greatly even though their boiling points and specific gravities are similar. This situation was not only observed in the dataset collected here but also in that reported in the literature. Note that in this case the proposed data point correlation would predict a similar viscosity for both cuts. The elemental analysis of the cuts indicated that, even though they have similar boiling point and specific gravity, their elemental composition was different. Hence, it is recommended to collect data on the elemental composition of the cuts and use these data to improve the synthetic data point correlation.

2. The predictive viscosity methodology for distillation characterized oils proposed in this thesis was developed from heavy crude oil fractions obtained from native crude oils. In some refinery operations, crude oils undergo thermal or hydro cracking to reduce their viscosity. However, the chemical composition of a cracked crude oil is different from that of a native oil. In addition, the viscosity parameters for cracked and native pseudo-components might be different. Therefore, it is recommended that viscosity data be collected from distillation cuts and asphaltenes obtained from reacted crude oils in order to determine how cracking changes the EF and GW model parameters. Note that although the correlations proposed in this thesis are based on native crude oils, the general approach developed to generate those correlations can be applied to reacted oils if data are available.

3. Collecting thermal conductivity data over a broad range of temperatures and pressures proved to be a challenging task because natural convection occurred and altered the measurement. In general, crude oil thermal conductivity data were not collected at temperatures higher than 125°C for this reason. In order to obtain data at higher temperature, it is recommended to modify the current hot wire apparatus

set up to use a longer wire. It has been documented in the literature that the increasing the length of the wire can significantly retard the onset of natural convection (Mani, 1971; De Groot *et al*., 1974).

4. The experimental determination of thermal conductivity of molten asphaltenes could not be performed in this study due to experimental limitations. It is recommended to measure it using a different experimental set up, such as a paralell plate apparatus, specifically designed to deal with sticky molten solids like asphaltenes. It would then be possible to determine the actual EF thermal conductivity model asphaltene parameters.

5. It is recommended to extend to Expanded Fluid (EF) concept to correlate the self-diffusivity of pure hydrocarbons and crude oils. The mechanistic analogy between the transfer of momentum, heat, and mass has been described in the literature (Hirschfelder *et al*., 1954; Bird *et al*., 2002). In particular, transport properties are controlled by intermolecular forces that determine molecular velocities and intermolecular interactions. Those intermolecular forces change as a function of distance between molecules, *i.e.*, they change as a function of fluid expansion. For instance in the low density gas state, for which intermolecular forces are negligible, the transport of momentum, heat and mass is controlled by the rate at which molecules collide which is proportional to density (Hirschfelder *et al*., 1954; Bird *et al*., 2002). In the liquid state, transport properties are no longer determined by collision rate but rather by strong intermolecular forces that are a function of molecular density which changes with fluid expansion (Irving and Kirkwood, 1950).

References

Abivin, P., Indo, K., Cheng, Y., Freed, D., and Taylor, S. D. (2011). Glass Transition and Heavy Oil Dynamics at Low Temperature. In *World Heavy oil Congress*. Edmonton, Alberta, Canada.

Abivin, P., Taylor, S. D., and Freed, D. (2012). Thermal Behavior and Viscoelasticity of Heavy Oils. *Energy and Fuels*, **26**, 3448–3461.

Aboul-Seoud, A., and Moharam, H. M. (1999). A Simple Thermal Conductivity-Temperature Correlation for Undefined Petroleum and Coal Liquid Fractions. *Chem. Eng. Res. Des.*, **77**(3), 248–252.

AEUB. (2006). Alberta Energy Reserves 2005 and Supply/Demand Outlook for 2006-2015. Calgary, Alberta, Canada: Alberta Energy and Utilities Board.

Alba, C., Busse, L. E., List, D. J., and Angell, C. A. (1990). Thermodynamic Aspects of The Vitrification of Toluene, and Xylene Isomers, and the Fragility of Liquid Hydrocarbons. *J. Chem. Phys.*, **92**(1), 617–624.

Al-Besharah, J. M., and Akashah, S. A. (1987). Viscosity of Crude Oil Blends. *Ind. Eng. Chem. Res.*, **12**, 2445–2449.

Alder, B. J. (1966). *Prediction of Transport Properties of Dense Gases and Liquids*. Berkeley, California: University of California.

Al-Gherwi, W. A., Nhaesi, A. H., and Asfour, A. F. A. (2006). Densities and Kinematic Viscosities of Ten Binary Liquid Regular Solutions at 308.15 and 313.15 K. *J. Solution Chem.*, **35**, 455–470.

Altgelt, K. H., and Boduszynski, M. M. (1994). *Composition and Analysis of Heavy Petroleum Fractions*. New York: Marcel Deckker, Inc.

Angell, C. A. (1988). Perspectives on the Glass Transition. *J. Phys. Chem. Solids*, **49**(8), 863–871.

AOSTRA. (1984). *The Thermodynamics and Transport Properties of Bitumens and Heavy Oils*. Calgary, Alberta, Canada: Alberta Oil Sands Technology and Research Authority (AOSTRA).

API. (1966). *Properties of Hydrocarbons of High Molecular Weight, Research Project 42*. Washington, D. C.

API. (1978). *Technical Data Book-Petroleum Refining*. New York: American Petroleum Institute (API).

API. (1997). *API Technical Data Book-Petroleum Refining*. (T. E. Daubert & R. P. Danner, Eds.). Washington D.C.: American Petroleum Institute (API).

API. (2000). *Comprehensive Report of API Crude Oil Characterization Measurements*. Washington, D. C.

Argillier, J.-F., Hénaut, I., Gateau, P., Héraud, J.-P., and Glénat, P. (2005). Heavy-Oil Dilution. In *SPE International Thermal Operations and Heavy Oil Symposium*. Calgary, Alberta, Canada.

Argüelles-Vivas, F. J., Babadagli, T., Little, L., Romaniuk, N., and Ozum, B. (2012). High Temperature Density, Viscosity, and Interfacial Tension Measurements of Bitumen–Pentane–Biodiesel and Process Water Mixtures. *J. Chem. Eng. Data*, **57**, 2878–2889.

Arrhenius, S. (1887). Uber die Dissociation der in Wasser Gelosten Stoffe. *Phys. Chem.*, **1**, 631–648.

Assael, M. J., Antoniadis, K. D., and Wakeham, W. A. (2010). Historical evolution of the transient hot-wire technique. *Int. J. Thermophys.*, **31**(6), 1051–1072.

ASTM. (2009). *Test Method for Distillation of Crude Oils (15-Theoretical Plate Column)*. ASTM D2892, 2009. Standard Test Method for Distillation of Crude Petroleum (15-Theoretical Plate Column).

ASTM. (2015). *ASTM D2887-Standard Test Method for Boiling Range Distribution of Petroleum Fractions by Gas Chromatography*.

Badamchi-Zadeh, A., Yarranton, H. W., Svrcek, W. Y., and Maini, B. B. (2009). Phase Behaviour and Physical Property Measurements for VAPEX Solvents: Part I. Propane and Athabasca Bitumen. *J. Can. Pet. Technol.*, **48**, 54–61.

Baird, C. T. (1989). *Guide to Petroleum Product Blending*. Flagstaff, Arizona: HPI Consultants, Inc.

Baltatu, M. E. (1982). Prediction of the Liquid Viscosity for Petroleum Fractions. *Ind. Eng. Chem. Process Des. Dev.*, **21**, 192–195.

Baltatu, M. E. (1984). Prediction of The Transport Properties of Petroleum Fraction. In *Proc. AICHE winter meeting*. Atlanta, GA.

Baltatu, M. E., Chong, R. A., and Huber, M. L. (1999). Transport Properties of Petroleum Fractions. *Int. J. Thermophys.*, **20**, 85–95.

Baltatu, M. E., Ely, J. F., and Hanley, H. J. M. (1985). Thermal Conductivity of Coal-Derived Liquids and Petroleum Fractions. *Ind. Eng. Chem. Process Des. Dev.*, **24**, 325–332.

Barker, D. A., and Wilson, D. I. (2006). Temperature Profiles in a Controlled-Stress Parallel Plate Rheometer. *Rheo. Acta*, **46**, 23–31.

Barrera, D. M., Ortiz, D. P., and Yarranton, H. W. (2013). Molecular Weight Distribution of Asphaltenes from Crude Oils. *Energy and Fuels*, **27**, 2474–2487.

Barrufet, M. A., and Setiadarma, A. (2003). Reliable Heavy Oil-Solvent Viscosity Mixing Rules for Viscosities up to 450 K, Oil-Solvent Viscosity Ratios up to 4x 10E5, and Any Solvent Proportion. *Fluid Phase Equilib.*, **213**(1-2), 65–79.

Batschinski, A. J. (1913). Untersuchungen Uber Die Innere Reibung von Fliissigkeiten. *Zeitschrift Fur Physikalische Chemie*, **84**, 643–705.

Baylaucq, A., Boned, C., Dauge, P., and Lagourette, B. (1997). Measurement of the Viscosity and Density of Three Hydrocarbons and the Three Associated Binary Mixtures versus Temperature and Pressure. *Int. J. Thermophys.*, **18**, 3–23.

Baylaucq, A., Daugue, P., and Boned, C. (1997). Viscosity and Density of the Ternary Mixture Heptane+Methylcyclohexane+1-methylnaphthalene. *Int. J. Thermophys.*, **18**, 1089–1107.

Bazyleva, A. B., Hasan, A., Fulem, M., Becerra, M., and Shaw, J. (2010). Bitumen and Heavy Oil Rheological Properties: Reconciliation with Viscosity Measurements. *J. Chem. Eng. Data*, **55**, 1389–1397.

Beg, S. A., Amin, M. B., and Hussain, I. (1988). Generalized Kinematic Viscosity-Temperature Correlation for Undefined Petroleum Fractions S. *Chem. Eng. J.*, **38**, 123–136.

Bingham, E. C. (1914). The Viscosity of Binary Mixtures. *J. Phys. Chem.*, **18**, 157–165.

Bird, R. B., Stewart, W. E., and Lightfoot, E. N. (2002). *Transport Phenomena* (2 ed.). New York: John Wiley and Sons, Inc.

Bland, W. F., and Davidson, R. L. (1967). *Petroleum Processing handbook*. New York: McGraw Hill.

Boduszynski, M. M. (1987). Composition of Heavy Petroleums. 1. Molecular Weight, Hydrogen Deficiency, and Heteroatom Concetration as a Function of Atmospheric Equivalent Boiling Point up to 1400F (760C). *Energy and Fuels*, **1**(1), 2–11.

Boduszynski, M. M., Rechsteiner, C. E., Shafizadeh, A. S. G., and Carlson, R. M. K. (1998). Composition and Properties of Heavy Crudes. *UNITAR Centre for Hevy Crude and Tar Sands*, 1–12.

Boned, C., Zéberg-Mikkelsen, C. K., Baylaucq, A., and Daugé, P. (2003). High-Pressure Dynamic Viscosity and Density of Two Synthetic Hydrocarbon Mixtures Representative of Some Heavy Petroleum Distillation Cuts. *Fluid Phase Equilb.*, **212**, 143–164.

Butler, R. M. (1997). *The Thermal Recovery of Oil and Bitumen* (1st. Ed.). Calgary, Alberta, Canada: GravDrain Inc.

Canet, X., Daugé, P., Baylaucq, A., Boned, C., and Stenby, E. H. (2001). Density and Viscosity of the 1-Methylnaphthalene +2,2,4,4,6,8,8-Heptamethylnonane System at Pressures Up to 100 MPa. *Int. J. Thermophys.*, **22**, 1669–1689.

Castellanos Díaz, O., Sánchez-Lemus, M. C., Schoeggl, F. F., Satyro, M. A., Taylor, S. D., and Yarranton, H. W. (2014). Deep-Vacuum Fractionation of Heavy Oil and Bitumen, Part I: Apparatus and Standardized Procedure. *Energy and Fuels*, **28**(5), 2857–2865.

Castellanos-Diaz, O. (2012). *Measurement and Modeling Methodology for Heavy Oil and Bitumen Vapor Pressure*. Ph.D. Thesis, University of Calgary, Calgary, Canada.

Catellanos-Diaz, O., Modaresghazani, J., Satyro, M. A., and Yarranton, H. W. (2011). Modeling the Phase Behavior of Heavy Oil and Solvent Mixtures. *Fluid Phase Equilib.*, **304**, 74–85.

Cavett, R. H. (1962). Physical Data for Distillation Calculations, Vapor-Liquid Equilibria. In *Proc. 27th API Meeting* (pp. 351–366). San Francisco, CA, USA.

Centeno, G., Sanchez-Reyna, G., Ancheyta, J., Munoz, J. A. D., and Cardona, N. (2011). Testing various mixing rules for calculation of viscosity of petroleum blends. *Fuel*, **90**(12), 3561–3570.

Chapman, S., and Cowling, T. G. (1939). *The Mathematical Theory of Nonuniform Gases* (3rd Ed.). Cambridge, UK.: Cambridge University Press.

Chevalier, J. L. E., Petrino, P. J., and Gaston-Bonhomme, Y. H. (1990). Viscosity and Density of some Aliphatic, Cyclic, and Aromatic Hydrocarbons Binary liquid Mixtures. *J. Chem. Eng. Data*, **35**(2), 206–212.

Chhabra, R. P., Sridhar, T., Uhlherr, P. H. T., and Potter, O. E. (1980). Predicting Transport Coefficients of Liquids - A Unified Approach. *AICHE J.*, **26**(3), 522–525.

Christensen, P. L., and Fredenslund, A. A. (1980). A Corresponding States Model for The Thermal Conductivity of Gases and Liquids. *Chem. Eng. Sci.*, **35**(4), 871–875.

Chung, T. H., Ajlan, M., Lee, L. L., and Starling, K. E. (1988). Generalized Multiparameter Correlation for Nonpolar and Polar Fluid Transport Properties. *Ind. Eng. Chem. Res.*, **27**, 671–679.

Chung, T., Lee, L. L., and E., S. K. (1984). Applications of Kinetic Gas Theories and Multiparameter Correlations for Prediction of Dilute Gas Viscosity and Thermal Conductivity. *Ind. Eng. Chem. Fundam.*, **23**(1), 8–13.

Churchill, S. W., and Chu, H. H. S. (1975). Correlating Equations for Laminar and Turbulent Free Convection from Horizontal Cylinder. *Int. J. Heat Mass Tranf*, **18**, 1049–1053.

CMG. (2011). CMG: Winprop User Manual Version 2011. Calgary, Alberta, Canada.

Coates, R., Pierce, G., and Fung, H. (2005). *Impact of Methane Loss on Bitumen Viscosity - Joint Industry Project*. Edmonton, Alberta, Canada.

Cornelius, C. D. (1987). Classification of natural bitumen: a physical and chemical approach. In R. F. Meyer (Ed.), *Exploration for heavy crude oil and natural bitumen* (Vol. 25, pp. 165–174). Tulsa, OK. USA: American Association of Petroleum Geologists.

Cragoe, C. S. (1933). Changes in the Viscosity of Liquids with Temperature, Pressure and Composition. *Proc. World. Pet. Cong. London*, **2**, 529–541.

Cullinan, H. T., & Kosanovich, G. (1975). The Concept of Ultimate Volume of Liquid Mixtures. *AICHE J.*, **21**(1), 195–197.

Dauge, P., Canet, X., Baylaucq, A., and Boned, C. (1999). Measurement of the Density and Viscosity of the Tridecane + 2,2,4,4,6,8,8-heptamethylnonane Mixtures in the Temperature Range 293.15- 353.15K at Pressures up to 1000MPa. *High Temp. High Press.*, **31**, 665–680.

De Groot, J. J., Kestin, J., and Sookiazian, H. (1974). Instrument to Measure the Thermal Conductivity of Gases. *Physica*, **75**(3), 454–482.

Diller, D. E., and Van Poolen, L. J. (1985). Measurements of Viscosities of Saturated and Compressed Liquid Normal Butane and Isobutane. *Int. J. Thermophys.*, **6**, 43–62.

Dutt, N. V. K. (1990). A Simple Method of Estimating the Viscosity of Petroleum Crude Oil and Fractions. *Chem. Eng. J.*, **45**(2), 83–86.

Efendiev, M. F. (1973). New Method for The Calculating Thermal Conductivity of Petroleum Oils. *Chem. Technol. Fuels Oils*, **9**(4), 321–323.

Eicher, L. D., and Zwolinsky, B. J. (1972). Limitations of the Hildebrand-Batschinski Shear Viscosity Equation. *Science*, **177**, 369.

Elam, S. K., Tokura, I., Saito, K., and Altenkirch, R. A. (1989). Thermal Conductivity of Crude Oils. *Exp.Therm. Fluid Sci.*, **2**, 1–6.

Ely, J. F., and Hanley, H. J. M. (1981). Prediction of Transport Properties. 1. Viscosity of Fluids and Mixtures. *Ind. Eng. Chem. Fundam.*, **20**, 323–332.

Ely, J. F., and Hanley, H. J. M. (1983). Prediction of Transport Properties. 2. Thermal Conductivity of Pure Fluids and Mixtures. *Ind. Eng. Chem. Fundam.*, **22**(1), 90–97.

EST. (2001). *Oil Properties Database*. Ottawa, Ontario, Canada: Emergency Service and Technology Division.

Forsman, H., and Andersson, P. (1984). Thermal Conductivity at High Pressure of Solid Odd-Numbered n-Alkanes Ranging From C9H20 to C19H40. *J. Chem. Phys.*, **80**, 2804–2807.

Grigor'ev, B. A., and Svidchenko, A. I. (1979). Methods for Calculating Thermal Conductivity of Liquid Petroleum Crudes and Products. *Chem. Technol. Fuels Oils*, **15**(8), 613–617.

Grigor'ev, B. A., and Svidchenko, A. I. (1980). Effect of Pressure on Thermal Conductivity of Crude Oils and Products. *Chem. Technol. Fuels Oils*, **16**(2), 131–134.

Grunberg, L., and Nissan, A. H. (1949). Mixture Law for Viscosity. *Nature*, **164**, 799-800.

Guan, J. G., Kariznovi, M., Nourozieh, H., and Abedi, J. (2013). Density and Viscosity for Mixtures of Athabasca Bitumen and Aromatic Solvents. *J. Chem. Eng. Data*, **58**, 611–624.

Guildner, L. A. (1958). The Thermal Conductivity of Carbon Dioxide in The Region of The Critical Point. *Proceedings of the National Academy of Sciences of the United States of America*, **44**(11), 1149–1153.

Guzman, C., Montero, C., Briceno, M. I., Chirinos, M. L., and Layrisse, I. . (1989). Physical Properties and Characterization of Venezuelan Heavy and Extra Heavy Crude Oils. *Fuel Sci. Techn. Int.*, **7**, 571–598.

Hanley, H. J. M. (1976). Prediction of the viscosity and thermal conductivity coefficients of mixtures. *Cryogenics*, **16**(11), 643–651.

Hanley, H. J. M., and McCarty, R. D. (1972). Analysis of the Application of the Transport Coefficients for Simple Dense Fluids: Application of the o Modified Enskog Theory. *Physica*, **60**, 322–356.

Harman, J. W. (1969). *Accurate Method for the Determination of the Thermal Conductivity of Gases*. Ph. D. Thesis, Technishe Hogeschool, DELFT, the Netherlands.

Healy, J. J., de Groot, J. J., and Kestin, J. (1976). The Theory of the Transient Hot-Wire Method for Measuring Thermal Conductivity. *Physica*, **82**, 392–408.

Hildebrand, J. H. (1971). Motions of Molecules in Liquids: Viscosity and Diffusivity. *Science*, **174**, 490–493.

Hildebrand, J. H., and Lamoreaux, R. H. (1972). Fluidity: A General Theory. *Proc. Natl. Acad. Sci. U.S.A.*, **69**(11), 3428–31.

Hildebrand, J. H., and Lamoreaux, R. H. (1974). Viscosity Along Continuous Paths Between Liquid and Gas. *Physica*, **74**, 416–422.

Hirshfelder, J. H., Curtiss, C. F., and Bird, R. B. (1954)."*Molecular Theory of Gases and Liquids*". John Wiley and Sons, New York.

Holland, P. M., Hanley, H. J. M., Gubbins, K. E., and Haile, J. M. (1979) A Correlation of the Viscosity and Thermal Conductvity of Gaseous and Liquid Propane. *J. Phys. Chem. Ref. Data*. **8**, 559-575.

Horrocks, J. K., and McLaughlin, E. (1963). Non-Steady-State Measurements of the Thermal Conductivity of Liquids Polyphenyls. *Proc. R. Soc. Lond.*, **273**, 259–274.

Huang, D., Simon, S. L., and McKenna, G. B. (2005). Chain Length Dependence of the Thermodynamic Properties of Linear and Cyclic Alkanes and Polymers. *J. Chem. Phys.*, **122**, 084907.1–084907.6.

Iloukhani, H., and Rezaei-Sameti, M. (2005). Viscosities and Excess Molar Volumes of the Ternary System Toluene (1) + Cyclohexane (2) + Pentane (3) at 298.15 K. *J. Chem. Eng. Data*, **50**, 1928–1931.

Irving, J. H., and Kirkwood, J. G. The Statistical Mechanical Theory of Transport Processes. IV. The Equations of Hydrodynamics. *J. Chem. Phys*. **18**, 817-829.

Jamieson, D. T., Irving, J. . B., and Tudhope, J. . S. (1975). Prediction of The Thermal Conductivity of Petroleum Products. *Wear*, **33**, 75–83.

Jezowski, A., Misiorek, H., Sumarokov, V. V., and Gorodilov, B. Y. (1997). Thermal Conductivity of Solid Methane. *Phys. Rev. B*, **55**, 5578–5580.

Johnson, S. E., Svrcek, W. Y., and Mehrotra, A. K. (1987). Viscosity Prediction of Athabasca Bitumen Using the Extended Principle of Corresponding States. *Ind. Eng. Chem. Res.*, **26**(11), 2290–2298.

Kanti, M., Zhou, H., Ye, S., Boned, C., Lagourette, B., Xans, P., and Montelt, F. (1989). Viscosity of Liquid Hydrocarbons, Mixtures and Petroleum Cuts, as a Function of Pressure and Temperature. *J. Phys. Chem.*, **93**, 3860–3864.

Kariznovi, M., Nourozieh, H., Guan, J. G., and Abedi, J. (2013). Measurement and Modeling of Density and Viscosity for Mixtures of Athabasca Bitumen and Heavy n-Alkane. *Fuel*, **112**, 83–95.

Katz, D. L., and Firoozabadi, A. (1978). Predicting Phase Behavior of Condensate/Crude-Oil Systems Using Methane Interaction Coefficients. *J. Petrol. Technol.*, **30**, 1649–1655.

Kendall, J., and Monroe, K. (1917). The Viscosity of Liquids II. The Viscosity Composition-Curve for Ideal Liquid Mixtures. *J. Am. Chem. Soc.*, **39**(9), 1787–1802.

Kesler, M. G., and Lee, B. I. (1976). Improved Predictions of Enthalpy of Fractions. *Hydro. Proc.*, **55**, 153–158.

Khan, A. (2014). *Measurement of the Physical Properties of MacKay River Bitumen and Solvent Mixtures*. M. Sc. Thesis, University of Calgary, Calgary, Alberta, Canada.

Kidnay, A. J., Parrish, W. R., and McCartney, D. G. (2011). *Fundamentals of Gas Natural Processing*. Boca Raton, FL, USA: CRC Press.

Konstantinov, V. A., Manzhelii, V. G., Revyakin, V. P., and Smirnov, S. A. (1999). Heat Transfer in the Orientationally Disordered Phase of Solid Methane. *Physica B*, **262**, 421–425.

Laštovka, V., Fulem, M., Becerra, M., and Shaw, J. M. (2008). A Similarity Variable For Estimating the Heat Capacity of Solid Organic Compounds Part II. Application: Heat Capacity Calculation for ill-Defined Organic Solids. *Fluid Phase Equilib.*, **268**, 134–141.

Latini, G., Cocci-Griffoni, R., and Passerini, G. (2006). *Transport Properties of Organic Liquids*. Southhampton, UK.: WIT Press.

Lee, B. I., and Kesler, M. G. (1975). A generalized Thermodynamic Correlation Based on Three-Parameter Corresponding States. *AIChE J.*, **21**, 510–527.

Lee, H. (1987). Thermal Conductivity Enhancement of Pure Fluids Along the Critical Isochore. *AICHE J.*, **33**(8), 1401–1404.

Li, C. C. (1976). Thermal Conductivity of Liquid Mixtures. *AIChE J.*, **22**(5), 927–930.

Li, S. F. ., Maitland, G. C., and Wakeham, W. A. (1984). The Thermal Conductivity of *n*-Hexane and *n*-Octane at Pressures Up to 0.64 GPa in the Temperature Range 34-90°C. *Ber. Bunsenges. Phys. Chem.*, **88**, 32–36.

Lindeloff, N., Pedersen, K. S., Calsep, A. S., Rønningsen, H. P., and Milter, J. (2004). The Corresponding States Viscosity Model Applied to Heavy Oil Systems. *J. Can. Pet. Technol.*, **43**(9), 47–53.

Lindsay, A. L., and Bromley, L. A. (1950). Thermal Conductivity of Gas Mixtures. *Ind. Eng. Chem.*, 42, 1508–1511.

M. M. Abbott, Kaufmann, T. D., and Domash, L. (1971). A Correlation for Predicting Liquid Viscosities of Petroleum Fractions. *Can. J. Chem. Eng.*, **49**, 379–384.

Mago, A. L., Barrufet, M. A., and Nogueira, M. C. (2005). Assessing the Impact of Oil Viscosity Mixing Rules in Cyclic Steam Stimulation of Extra-Heavy Oils. In *SPE Annual Technical Conference and Exhibition, ATCE 2005*. Dallas, Tx., USA.

Mani, N. (1971). *Precise Determination of the Thermal Conductivity of Fluids Using the Absolute Transient Hot Wire Technique*. M. Sc. Thesis, University of Calgary, Calgary, Alberta, Canada.

Masliyah, J.; Czarnecki, J.; Xu, Z. (2011). *Handbook on Theory and Practice of Bitumen Recovery from Athabasca Oil Sands, Vol 1: Theoretical Basis*. Calgary, Alberta, Canada: Kingsley.

Mason, E. A., and Saxena, S. C. (1958). Approximate Formula for The Thermal Conductivity of Gas Mixtures. *Phys. Fluids*, **1**, 361–370.

McCain, W. D. (1990). *The Properties of Petroleum Fluids*. Tulsa, OK. USA: PennWell Publising Company.

McKenna, A. M., Donald, L. J., Fitzsimmons, J. E., Juyal, P., Spicer, V., Standing, K. G., Marshall, A. G., and Rodgers, R. P. (2013). Heavy Petroleum Composition. 3. Asphaltene Aggregation. *Energy and Fuels*, **27**(3), 1246–1256.

McLaughlin, E. (1964). The Thermal Conductivity of Liquids and Dense gases. *Chem. Rev.*, **64**, 389–428.

Mclean, J. D., & Kilpatrick, P. K. (1997). Effects of Asphaltene Solvency on Stability of Water-in-Crude-Oil Emulsions. *J. Colloid Interface Sci.*, **189**, 242–253.

Mehrotra, A. K. (1990). Development of Mixing Rules for Predicting the Viscosity of Bitumen and its Fractions Blended with Toluene. *Can. J. Chem. Eng.*, **68**, 839–848.

Mehrotra, A. K., Eastick, R. R., and Svrcek, W. Y. (1989). Viscosity of cold lake bitumen and its fractions. *Can. J. Chem. Eng.*, **67**(6), 1004–1009.

Mehrotra, A. K., Monnery, W. D., and Svrcek, W. Y. (1996). A Review of Practical Calculation Methods for the Viscosity of Liquid Hydrocarbons and Their Mixtures. *Fluid Phase Equilb.*, **117**, 344–355.

Mehrotra, A. K., and Svrcek, W. Y. (1987). Corresponding States Method for Calculating Bitumen Viscosity. *J. Can. Pet. Technol.*, **26**, 60–66.

Mehrotra, A. K., & Svrcek, W. Y. (1988). Properties of cold lake bitumen saturated with pure gases and gas mixtures. *Can. J. Chem. Eng.*, **66**(4), 656–665.

Miadonye, A., Puttagunta, V. R., and Singh, B. (1993). Viscosity Modelling of American Crude Oil Fractions. *Fuel Sci. Techn. Int.*, **11**(10), 1483–1507.

Miller, A. A. (1968). Kinetic Interpretation of the Glass Transition: *J. Polym. Sci. A.*, **6**, 249–257.

Mitchell, D. L., and Speight, J. G. (1973). The Solubility of Asphaltenes in Hydrocarbon Solvents. *Fuels*, **52**, 149–152.

Motahhari, H. (2013). *Development of Viscosity Model for Petroleum Industry Applications*. Ph. D. Thesis, University of Calgary, Calgary, Alberta, Canada.

Motahhari, H., Satyro, M. a., Taylor, S. D., and Yarranton, H. W. (2013). Extension of the expanded fluid viscosity model to characterized oils. *Energy and Fuels*, **27**, 1881–1898.

Motahhari, H., Satyro, M. A., and Yarranton, H. W. (2011a). Predicting the viscosity of asymmetric hydrocarbon mixtures with the expanded fluid viscosity correlation. *Ind. Eng. Chem. Res.*, **50**(22), 12831–12843.

Motahhari, H., Schoeggl, F. F., and Satyro, M. A. (2011b). Prediction of the Viscosity of Solvent Diluted Live Bitumen at Temperatures Up to 175 ° C. In *Canadian Unconventional Resources Conference* (pp. 1–19). Calgary, Alberta, Canada.

Mullins, O. C. (2007). Petroleomics and Structure-Function Relations of Crude Oil and Asphaltenes. In *Asphaltenes, Heavy Oils and Petroleomics* (pp. 1–16). New York: Springer.

Naldrett, S. N., and Maass, O. (1940). The Viscosity of Carbon Dioxide in The Critical Region. *Can. J. Res.*, **18**b(10), 322–332.

Neindre, B. L., Garrabos, Y., and Tufeu, R. (1991). The Critical Thermal-Conductivity Enhancement Along the Critical Isochore. *Int. J. Thermophys.*, **12**(2), 307–321.

Nhaesi, A., and Asfour, A. B. (2005). Densities and Viscosities of the Regular Quinary System: Toluene (1) + Octane (2) + Ethylbenzene (3) + Tetradecane (4) + Hexadecane (5) and Its Quaternary Subsystems at (308.15 and 313.15) K. *J. Chem. Eng. Data*, **50**, 149–153.

Nieto, C. A., Li, S. F., Maitland, G. C., and Wakeham, W. A. (1983). Thermal Conductivity of Toluene in the Temperature Range 35-90°C at Pressures up to 600 MPa. *International Journal of Thermophysics*, **4**(4), 311–327.

NIST. (2008). *Standard Reference Database*. Gaithersburg, MD.

Nourozieh, H., Kariznovi, M., Guan, J. G., and Abedi, J. (2013). Measurement of Thermophysical Properties and Modeling for Pseudo-Binary mixtures of n-Decane and Athabasca Bitumen. *Fluid Phase Equilb.*, **347**, 62–75.

Ogiwara, K., Arai, Y., and Saito, S. (1980). Thermal Conductivities of Liquid Hydrocarbons and Their Binary Mixtures. *Ind. Eng. Chem. Fundam.*, **19**, 295–300.

Parkinson, W. J. (1974). *Thermal Conductvity of Binary Liquid Mixtures*. Ph. D. Thesis, University of Southern California, Los Angeles.

Pedersen, K. S., and Fredenslund, A. (1987). An Improved Corresponding States Model for the Prediction of Oil and Gas viscosities and Thermal Conductivities. *Chem. Eng. Sci.*, **42**(1), 182–186.

Pedersen, K. S., Fredenslund, A., and Christensen, P. L. (1984). Viscosity of Crude Oils. *Chem. Eng. Sci.*, **39**(6), 1011–1016.

Pedersen, K. S., Thomassen, P., and Fredenslund, A. A. (1984). Thermodynamics of Petroleum Mixtures Containing Heavy Hydrocarbons. 1. Phase Envelope Calculations by Use of the Soave-Redlich-Kwong Equation of State. *Ind. Eng. Chem. Process Des. Dev.*, **23**, 123–170.

Perkins, R. A., and Sengers, J. V. (2013). A Note on the Critical Enhancement of Transport Properties and Correlation Length of Fluids. *Int. J. Thermophys.*, **34**(11), 2046–2052.

Poling, B. E., Prausnitz, J. M., and O'Connell, J. P. (2001). *The Properties of Gases and Liquids* (5 ed., Vol. 1). New York: McGraw-Hill.

Powers, D. P. (2014). *Characterization and Asphaltene Precipitation Modeling of Native and Reacted Crude Oils*. Ph. D. Thesis University of Calgary, Calgary, Alberta, Canada.

Przezdziecki, J. W., and Sridhar, T. (1985). Prediction of Liquid Viscosities. *AIChE J.*, **31**(2), 333–335.

Queimada, A. J., Quinonez-Cisneros, S. E., Marrucho, I. M., Coutinho, J. A. P., and Stenby, E. H. (2003). Viscosity and Liquid Density of Asymmetric Hydrocarbon Mixtures. *Int. J. Thermophys.*, **24**, 1221–1239.

Queimada, A. J., Rolo, L. I., Caco, I., A., Marrucho, I. M., Stenby, E. H., and Coutinho, J. A. P. (2006). Prediction of viscosities and surface tensions of fuels using a new corresponding states model. *Fuel*, **85**, 874–877.

Quiñones-Cisneros, S. E., Zéberg-Mikkelsen, C. K., Baylaucq, A., and Boned, C. (2004). Viscosity Modeling and Prediction of Reservoir Fluids: From Natural gas to Heavy oils. *Int. J. Thermophys.*, **25**(5), 1353–1366.

Quiñones-Cisneros, S. E., Zeberg-Mikkelsen, C. K., and Stemby, E. H. (2000). The Friction Theory (f-theory) for Viscosity Modeling. *Fluid Phase Equilb.*, **169**, 249–276.

Quiñones-Cisneros, S. E., Zéberg-Mikkelsen, C. K., and Stenby, E. H. (2001a). One parameter friction theory models for viscosity. *Fluid Phase Equilb.*, **178**, 1–16.

Quiñones-Cisneros, S. E., Zéberg-Mikkelsen, C. K., and Stenby, E. H. (2001b). The Friction Theory for Viscosity Modeling: Extension to Crude Oil Systems. *Chem. Eng. Sci.*, **56**, 7007–7015.

Quiñones-Cisneros, S. E., Zéberg-Mikkelsen, C. K., and Stenby, E. H. (2003). Friction theory prediction of crude oil viscosity at reservoir conditions based on dead oil properties. *Fluid Phase Equilib.*, **212**, 233–243.

Quinonez-Cisneros, S. E., Andersen, S. I., and Creek, J. (2005). Density and Viscosity Modeling and Characterization of Heavy Oils. *Energy and Fuels*, 19(8), 1314–1318.

Ramos-Pallares, F., Schoeggl, F. F., Taylor, S. D., Satyro, M. A., and Yarranton, H. W. (2016a). Predicting the Viscosity of Hydrocarbon Mixtures and Diluted Heavy Oils Using the Expanded Fluid Model. *Energy and Fuels*, **30**, 3575–3595.

Ramos-Pallares, F., Taylor, S. D., Satyro, M. A., Marriott, R. A., & Yarranton, H. W. (2016b). Prediction of Characterized Oils and Their Fractions Using the Expanded Fluid Model. *Energy and Fuels*, **30**, 7134–7157.

Rastorguev, Y. L., & Grigor'ev, B. A. (1968). Thermal Conductivity of Petroleums. *Chem. Technol. Fuels Oils*, **4**(11), 788–793.

Riazi, M. R., and Faghrl, A. (1985). Thermal Conductivity of Liquid and Vapor Hydrocarbon Systems: Pentanes and Heavier at Low Pressure. *Ind. Eng. Chem. Process Des. Dev*. **24**, 398-401.

Riazi, M. R. (2005). *Characterization and Properties of Petroleum Fractions*. West Conshohocken, PA: ASTM International.

Richardson, W. (2016). *Diffusivity of Light Hydrocarbon Gases in Bitumen*. Ph.D. Thesis, University of Calgary, Calgary, Alberta, Canada.

Rogel, E., and Carbognani, L. (2003). Density Estimation of Asphaltenes Using Molecular Dynamics Simulations. *Energy and Fuels*, **17**, 378–386.

Rowley, R. L., White, G. L., and Chiu, M. (1988). Ternary Liquid Mixture Thermal Conductivity. *Chem. Eng. Sci.*, **43**, 361–371.

Saksena-and-Harminder, M. P. (1974). Thermal Conductivity of Binary Liquid Mixtures. *Ind. Eng. Chem. Fundam.*, **13**, 245–247.

Sanchez-Lemus, M.C. Schoeggl, F. Taylor, S.D.; Ruzicka, K., Fulem, M., and Yarranton, H. W. (2014). Deep-Vacuum Fractionation of Heravy Oil and Bitumen, Part II: Interconversion Method. *Energy and Fuels*, **28**, 2866–2873.

Sanchez-Lemuz, M. C. (2015). *Extended Distillation and Property Correlation for Heavy Oil*. Ph. D. Thesis, University of Calgary, Calgary, Canada.

Saryazdi, F., Motahhari, H., Schoeggl, F. F., Taylor, S. D., and Yarranton, H. W. (2013). Density of Hydrocarbon Mixtures and Bitumen Diluted with Solvents and Dissolved Gases. *Energy and Fuels*, **27**, 3666–3678.

Satyro, M. A., and Yarranton, H. W. (2010). Expanded Fluid -Based Viscosity Correlation for Hydrocarbons Using an Equation of State. *Fluid Phase Equilb.*, **298**, 1–11.

Schramm, G. (2000). *A Practical Approach to Rheology and Rheometry* (2nd Ed.). Karlsruhe, Germany: HAAKE Rheology.

Schumberger. (2010). ECLIPSE Reservoir Simulator, Manual and Technical Description. Houston, TX.

Sengers, J. V. (1965). Thermal Conductivity and Viscosity of Simple Fluids. *Int. J. Heat Mass Tranf.*, **8**(8), 1103–1116.

Sengers, J. V. (1985). Transport Properties of Fluids Near Critical Points. *Int. J. Thermophys.*, **6**, 203–232.

Sengers, J. V., and Watson, J, T. R. (1986). Improved International Formulations for the Viscosity and Thermal Conductivity of Water Substance. *J. Phys. Chem. Ref. Data*, **15**, 1291–1314.

SER. (2010). *2010 Survey of Energy Resources*. London.

Shu, W. R. (1984). A Viscosity Correlation for Mixtures of Heavy Oil, Bitumen, and Petroleum Fractions. *SPE J.*, **24**(3), 277–282.

Silva, A. A., Reis, R. A., and Paredes, L. L. (2009). Density and Viscosity of Decalin , Cyclohexane , and Toluene Binary Mixtures at (283 . 15 , 293 . 15 , 303 . 15 , 313 . 15 , and 323 . 15) K. *J. Chem. Eng. Data*, **54**, 2067–2072.

Speight, J. G. (2007). *The Chemistry and Technology of Petroleum* (4 Ed.). Boca Raton, FL, USA: CRC Press.

Spencer, C. F., and Danner, R. P. (1972). Improved Equation For Prediction of Saturated Liquid Density. *J. Chem. Eng. Data*, **17**, 236–241.

Stâlhane, B., and Pyk, S. (1931). Ny Method for Bestamning av Varmelednings-Koefficienter. *Teknisk Tidskrift*, **61**, 389–393.

Sutton, R., and Bergman, D. (2012). Application of the Bergman-Sutton Method for Determining Blend Viscosity. *SPE Prod. Oper.*, **27**, 106–124.

TEMA. (1968). *Standards for Tubular Exchanger Manufacturers Association* (5th Ed.).

Thomson, G. H., Brobst, K. R., and Hankinson, R. W. (1982). An Improved Correlation for Densities of Compressed Liquids and Liquid Mixtures. *AIChE J.*, **28**, 671–676.

Total. (2007). *Extra-Heavy Oils and Bitumen Reserves for The Future*. Courbevoie, France: Total.

Twu, C. H. (1984). An Internally Consistent Correlation for Predicting the Critical Properties and Molecular Weights of Petroleum and Coal-Tar Liquids. *Fluid Phase Equilib.*, **16**, 137–150.

Twu, C. H. (1985). Internally Consistent Correlation for Predicting Liquid Viscosities of Petroleum Fractions. *Ind. Eng. Chem. Process Des. Dev.*, **24**, 1287–1293.

Twu, C. H. (1986). Generalized Method for Predicting Viscosities of Petroleum Fractions. *AICHE J.*, **32**(12), 2091–2094.

van Der Held, E. F. M., Hardebol, J., and Kalshoven, J. (1953). On the Measurement of the Thermal Conductivity of Liquids by a Non-Stationary Method. *Physica*, **19**, 208–216.

van Der Held, E. F. M., and van Drunen, F. G. (1949). A Method of Measuring the Thermal Conductivity of Liquids. *Physica*, **15**, 865–881.

Vargaftik, N. B. (1949). Izv. VTI, Number 8.

Velez, C., Khayet, M., and Ortiz-De-Zarate, J. M. (2015). Temperature-Dependent Thermal Properties of Solid/Liquid Phase Change Even-Numbered n-Alkanes: n-Hexadecane, n-octadecane and n-eicosane. *Appl. Energy*, **143**, 383–394.

Viswanath, D. S., Ghosh, T. K., Prasad, D. H. L., Dutt, N. V., and Rani, K. Y. (2007). *Viscosity of Liquids*. Dordrecht, The Netherlands: Springer.

Wada, Y., Nagasaka, Y., and Nagashima, A. (1985). Measurements and Correlation of the Thermal Conductivity of Liquid n-Paraffin Hydrocarbons and Their Binary and Ternary Mixtures. *Int. J. Thermophys.*, **6**, 251–265.

Walther, C. (1931). The Evaluation of Viscosity Data. *Erdol Und Teer*, **7**, 382–384.

Wang, Z., Wang, L., and Fan, T. (2007). Densities and Viscosities of Ternary Mixtures of Heptane, Octane, Nonane and Hexyl benzene from 293.15K to 313.15K. *J. Chem. Eng. Data*, **52**, 1866–1871.

Wassiljewa, A. (1904). Warmeleitung in Gasgemische. *Physik. Z.*, **5**, 737–742.

Watson, K. M., Nelson, E. F., and Murphy, G. B. (1935). Characterization of Petroleum Fractions. *Ind. Eng. Chem.*, **27**, 1460–1464.

Wen, Y., and Kantzas, A. (2004). Evaluation of Heavy Oil / Bitumen-Solvent Mixture Viscosity Models. *J. Can. Pet. Technol.*, **45**(4), 56–61.

Whitson, C., and Brule, M. (2000). *Phase Behavior*. Richardson, TX, USA.: Society of Petroleum Engineers (SPE).

Wilke, C. R. (1950). A Viscosity Equation for Gas Mixtures. *J. Chem. Phys.*, **18**, 517–519.

Wright, W. A. (1969). An Improved Viscosity-Temperature Chart. *J. Mater.*, **4**, 19–27.

Yarranton, H. W., Alboudwarej, H., and Jakher, R. (2000). Investigation of Asphaltene Association with Vapor Pressure Osmometry and Interfacial Tension Measurements. *Ind. Eng. Chem. Res.*, **39**, 2916–2924.

Yarranton, H. W., Fox, W. B., and Svrcek, W. Y. (2007). Effect of Resins on Asphaltene Self-Association and Solubility. *Can. J. Chem. Eng*, **85**, 635–642.

Yarranton, H. W., and Masliyah, J. (1996). Molar Mass Distribution and Solubility Modeling of Asphaltenes. *AICHE J.*, **42**, 3533–3543.

Yarranton, H. W., and Satyro, M. A. (2009). Expanded Fluid-Based Viscosity Correlation for Hydrocarbons. *Ind. Eng. Chem. Res.*, **48**, 3640–3648.

Yarranton, H. W., van Dorp, J. J., Verlaan, M. L., and Lastovka, V. (2013). Wanted Dead or Live : Crude Cocktail Viscosity : A Pseudo-Component Method To Predict The Viscosity of Dead Oils, Live Oils and Mixtures. *J. Can. Pet. Technol.*, **52**(3), 176–191.

Yaws, C. L. (1995). *Handbook of Thermal Conductivity. Volume 3. Organic Compounds C8 to C28*. Houston, TX: Gulf Publishing Company.

Yaws, C. L. (2008). *Transport Properties of Hydrocarbons*. Norwich, NY: William Andrew Inc.

Zéberg-Mikkelsen, C. K., Quiñones-Cisneros, S. E., & Stenby, E. H. (2002). Viscosity Prediction of Natural Gas Using the Friction Theory. *Int. J. Thermophys.*, **23**(2), 437–454.

APPENDIX A: COLLECTED THERMAL CONDUCTIVITY DATA OF PURE COMPONENTS USED IN THE VALIDATION OF THE "HOT WIRE" METHOD

Table A.1. Measured thermal conductivity *n*-pentane.

Temp. °C	Pressure MPa	Thermal Cond. mW m^{-1} K^{-1}
20	0.1	115.5
25	0.1	113.4
30	0.1	111.9
20	5	118.2
25	5	116.5
30	5	114.8
20	10	120.6
25	10	118.9
30	10	117.2

Table A.2. Measured thermal conductivity *n*-heptane.

Temp. °C	Pressure MPa	Thermal Cond. mW m^{-1} K^{-1}
20	0.1	123.4
25	0.1	121.9
30	0.1	120.4
20	5	124.8
25	5	123.3
30	5	121.6
20	10	127.0
25	10	125.4
30	10	123.8

Table A.3. Measured thermal conductivity *n*-tetradecane.

Temp. °C	Pressure MPa	Thermal Cond. mW m^{-1} K^{-1}
23	0.1	145.8
36	0.1	141.6
45	0.1	139.3
55	0.1	136.5
65	0.1	133.6
75	0.1	130.2
23	2.5	147.2
36	2.5	143.0
45	2.5	140.4
55	2.5	137.9
65	2.5	134.9
23	5	148.1
36	5	144.1
45	5	141.5
55	5	139.0
65	5	135.8
23	7.5	149.1
36	7.5	144.9
45	7.5	142.5
55	7.5	140.2
65	7.5	136.9
23	10	150.1
36	10	146.0
45	10	143.6
55	10	141.3
65	10	138.1

Table A.4. Measured thermal conductivity toluene.

Temp. °C	Pressure MPa	Thermal Cond. mW m^{-1} K^{-1}
21	0.1	133.8
25	0.1	132.3
31	0.1	130.5
21	2.5	134.4
25	2.5	133.0
31	2.5	131.2
21	5	135.5
25	5	134.1
31	5	132.2
21	7.5	136.3
25	7.5	135.0
31	7.5	133.0
21	10	137.0
25	10	135.7
31	10	133.8

Table A.5. Measured and Reference thermal conductivity data at 0.1 MPa of ultra-deionized water provided by TermTest Inc.

Temp. °C	Measured Thermal Cond. mW m^{-1} K^{-1}	Reference Thermal Cond. mW m^{-1} K^{-1}
20	-	598.66
21	602.1	-
25	-	605.77
30	613.6	615.26
35	624.5	624.52
40	632.1	633.54
45	-	641.88
50	-	648.22
51	647.5	-
55	-	655.52
60	-	664.07
62	665.6	-

APPENDIX B: DENSITY AND VISCOSITY DATA OF CRUDE OIL/SOLVENT MIXTURES COLLECTED IN THIS STUDY

Table B.1. Density and viscosity of WC-B-B1 bitumen measured in the capillary viscometer.

Temp. °C	Pressure MPa	Density kg/m³	Viscosity mPa·s
19.6	0.1	1013.3	70400
19.6	2.5	1014.6	77800
19.6	5.0	1015.7	88500
19.6	7.5	1017.2	101000
19.6	10	1018.7	114000
50.3	0.1	992.8	2800
50.3	2.5	994.0	2950
50.3	5.0	995.5	3260
50.3	7.5	996.9	3490
50.3	10	998.2	3770
75.0	0.1	976.1	385
75.0	2.5	977.6	443
75.0	5.0	979.1	496
75.0	7.5	980.6	562
75.0	10	981.9	624
100.0	0.1	959.4	112
100.0	2.5	961.3	120
100.0	5.0	962.8	127
100.0	7.5	964.4	136
100.0	10	966.0	141
125.0	0.1	940.5	37.1
125.0	2.5	942.7	40.0
125.0	5.0	944.5	44.5
125.0	7.5	946.2	46.6
125.0	10	948.1	51.0
150.0	2.5	925.1	20.2
150.0	5.0	927.4	21.2
150.0	7.5	929.2	21.9
150.0	10	931.0	22.9
175.0	2.5	907.0	10.6
175.0	5.0	909.1	11.0
175.0	7.5	911.4	11.4
175.0	10	913.4	12.1

Table B.2. Density and viscosity of WC-B-B2 bitumen measured in the capillary viscometer.

Temp. °C	Pressure MPa	Density kg/m³	Viscosity mPa·s
19.4	0.1	1013.9	212600
19.5	2.5	1014.9	249000
19.4	5.0	1016.0	285000
19.4	7.5	1017.4	330000
19.4	10	1018.9	381000
35.0	0.1	1003.8	31400
35.0	2.5	1004.7	35500
35.0	5.0	1005.9	39400
35.0	7.5	1007.4	43700
35.0	10	1008.9	48200
50.0	0.1	994.2	6980
50.0	2.5	995.3	7570
50.0	5.0	996.7	8310
50.0	7.5	998.2	9100
50.0	10	999.5	10000
75.0	0.1	978.3	1100
75.0	2.5	979.7	1190
75.0	5.0	981.3	1280
75.0	7.5	982.7	1380
75.0	10	984.3	1450
100.0	0.1	962.9	289
100.0	2.5	964.5	308
100.0	5.0	966.2	327
100.0	7.5	967.9	348
100.0	10	969.5	370
125.0	0.1	945.7	109
125.0	2.5	947.6	116
125.0	5.0	949.5	121
125.0	7.5	951.1	128
125.0	10	953.1	135
150.0	0.1	929.2	52.3
150.0	2.5	931.3	54.4
150.0	5.0	933.4	57.1
150.0	7.5	935.4	59.9
150.0	10	937.3	62.6
175.0	2.5	915.5	30.9
175.0	5.0	917.8	32.3
175.0	7.5	920.2	33.6
175.0	10	922.2	34.9

Table B.3. Density and viscosity of WC-B-B1 bitumen diluted with 5.2 wt% ethane and measured in the capillary viscometer.

Temp. °C	Pressure MPa	Density kg/m³	Viscosity mPa·s
20	2.5	956.2	681
20	5.0	957.6	723
20	7.5	959.3	762
20	10	961.0	810
50	3.0	935.6	108
50	5.0	937.0	113
50	7.5	938.8	119
50	10	940.5	125
75	4.0	918.4	37.2
75	5.0	919.2	37.8
75	7.5	921.0	39.6
75	10	922.9	41.3
100	5.0	901.0	16.8
100	7.5	903.2	17.5
100	10	905.4	18.1
125	7.5	884.7	9.4
125	10	887.2	9.7
150	10	869.6	6.0

Table B.4. Density and viscosity of WC-B-B1 bitumen diluted with propane and measured in the capillary viscometer.

Temp. °C	Pressure MPa	8.0 wt% Propane		16 wt% Propane	
		Density kg/m³	Viscosity mPa·s	Density kg/m³	Viscosity mPa·s
19/20	2.5	956.9	1030	897.3	76.3
19/20	5.0	958.2	1100	898.9	79.5
19/20	7.5	959.9	1180	900.8	83.2
19/20	10	961.8	1260	903.0	86.9
50	2.5	934.8	133	873.3	19.3
50	5.0	936.6	140	875.4	20.2
50	7.5	938.3	149	877.5	21.0
50	10	940.0	158	879.7	22.1
75	2.5	916.8	41.5	853.6	9.0
75	5.0	918.8	43.6	856.0	9.3
75	7.5	920.6	46.2	858.4	9.6
75	10	922.5	48.7	860.6	10.0
100	5.0	901.8	19.1	836.4	5.0
100	7.5	903.9	19.8	839.2	5.2
100	10	906.1	20.7	842.0	5.4
125	5.0	883.5	10.1	-	-
125	7.5	885.7	10.5	819.3	3.3
125	10	888.2	10.8	822.7	3.4
150	7.5	868.4	6.3	799.0	2.2
150	10	870.9	6.5	802.8	2.3
175	10	853.7	4.3	-	-

Table B.5. Density and viscosity of WC-B-B1 bitumen diluted with 15 wt% *n*-butane and measured in the capillary viscometer.

Temp. °C	Pressure MPa	Density kg/m³	Viscosity mPa·s
20	2.5	925.8	145
20	5.0	927.3	151
20	7.5	928.6	157
20	10	931.0	167
50	2.5	904.0	33.6
50	5.0	905.7	35.1
50	7.5	907.6	36.3
50	10	909.6	37.9
75	2.5	885.4	14.3
75	5.0	887.6	14.8
75	7.5	889.8	15.5
75	10	891.8	16.0
100	2.5	867.2	7.5
100	5.0	869.4	7.7
100	7.5	871.7	8.0
100	10	874.1	8.3
125	2.5	848.4	4.5
125	5.0	851.0	4.7
125	7.5	853.6	4.9
125	10	856.2	5.0
150	2.5	829.3	3.0
150	5.0	832.6	3.1
150	7.5	835.6	3.2
150	10	838.3	3.3
175	2.5	810.5	2.1
175	5.0	814.1	2.2
175	7.5	817.6	2.3
175	10	820.7	2.4

Table B.6. Density and viscosity of WC-B-B1 bitumen diluted with *n*-pentane and measured in the capillary viscometer.

Temp. °C	Pressure MPa	15 wt% *n*-Pentane		30 wt% *n*-Pentane	
		Density kg/m³	Viscosity mPa·s	Density kg/m³	Viscosity mPa·s
20	0.1	936.1	216	868.2	20.6
20	2.5	937.5	224	870.1	21.9
20	5.0	938.9	238	871.8	22.5
20	7.5	940.4	247	873.4	23.4
20	10	942.4	263	875.8	24.2
50	2.5	917.2	48.6	847.5	7.9
50	5.0	918.8	51.8	849.6	8.2
50	7.5	920.5	54.9	851.6	8.5
50	10	922.3	59.1	853.8	8.8
75	2.5	899.4	20.0	827.8	4.3
75	5.0	901.3	20.8	830.2	4.4
75	7.5	903.1	21.8	832.4	4.6
75	10	905.0	22.6	834.7	4.7
100	2.5	881.3	9.6	808.0	2.7
100	5.0	883.3	9.9	810.6	2.7
100	7.5	885.4	10.4	813.1	2.8
100	10	887.6	10.8	816.1	2.9
125	2.5	863.3	5.7	788.0	1.8
125	5.0	865.7	5.9	791.3	1.9
125	7.5	868.2	6.1	794.2	1.9
125	10	870.5	6.3	797.5	2.0
150	2.5	844.9	3.7	767.2	1.3
150	5.0	847.6	3.8	771.2	1.4
150	7.5	850.3	4.0	774.7	1.4
150	10	852.9	4.1	778.3	1.5
175	2.5	826.2	2.6	-	-
175	5.0	829.5	2.7	-	-
175	7.5	832.6	2.8	-	-
175	10	835.6	2.9	-	-

Table B.7. Density and viscosity of WC-B-B1 bitumen diluted with *n*-heptane and measured in the capillary viscometer.

Temp. °C	Pressure MPa	15 wt% *n*-Heptane		30 wt% *n*-Heptane	
		Density kg/m³	Viscosity mPa·s	Density kg/m³	Viscosity mPa·s
20/19	0.1	952.2	587	893.9	41.1
20/19	2.5	953.4	634	895.4	42.7
20/19	5.0	954.7	683	896.7	44.5
20/19	7.5	956.2	737	898.4	46.8
20	10	957.9	794	900.6	48.6
50	0.1	930.4	90.7	-	-
50	2.5	931.8	96.2	872.8	12.7
50	5.0	933.5	102	874.7	13.1
50	7.5	935.2	107	876.6	13.7
50	10	936.9	113	878.6	14.3
75	0.1	913.8	31.6	-	-
75	2.5	915.5	32.9	854.8	6.4
75	5.0	917.4	34.5	857.0	6.7
75	7.5	919.1	36.3	858.9	6.9
75	10	920.9	37.9	861.0	7.2
100	0.1	896.5	14.5	-	-
100	2.5	898.4	15.2	837.3	3.8
100	5.0	900.4	15.8	839.5	4.0
100	7.5	902.4	16.5	841.8	4.1
100	10	904.3	17.2	844.3	4.2
125	0.1	878.3	8.0	-	-
125	2.5	880.6	8.3	818.9	2.5
125	5.0	882.9	8.6	821.5	2.6
125	7.5	885.0	9.0	824.2	2.7
125	10	887.3	9.3	826.8	2.8
150	2.5	863.5	5.2	-	-
150	5.0	866.1	5.3	-	-
150	7.5	868.6	5.6	-	-
150	10	871.0	5.7	-	-
175	5.0	848.9	3.6	-	-
175	7.5	851.9	3.7	-	-
175	10	854.4	3.8	-	-

Table B.8. Density and viscosity of WC-B-B2 bitumen diluted with *n*-eicosane and measured in the capillary viscometer.

Temp. °C	Pressure MPa	6.0 wt% *n*-Eicosane		24 wt% *n*-Eicosane	
		Density kg/m³	Viscosity mPa·s	Density kg/m³	Viscosity mPa·s
50	0.1	984.8	2320	939.9	257
50	2.5	986.0	2500	941.1	273
50	5.0	987.5	2740	942.6	292
50	7.5	988.9	2990	944.1	315
50	10	990.2	3190	945.6	336
75	0.1	969.0	400	922.1	77.6
75	2.5	970.6	415	923.6	81.2
75	5.0	972.2	437	925.3	86.0
75	7.5	973.6	466	927.0	91.2
75	10	974.9	503	928.6	96.0
100	2.5	953.9	114	906.6	31.7
100	5.0	955.6	120	908.5	33.2
100	7.5	957.1	127	910.3	34.8
100	10	958.8	133	912.1	36.5
125	2.5	937.5	43.3	888.2	13.1
125	5.0	939.3	45.4	890.0	13.5
125	7.5	940.9	47.7	891.9	14.3
125	10	942.8	50.1	891.9	14.9
150	2.5	921.4	20.7	873.4	7.7
150	5.0	923.6	21.5	875.6	8.0
150	7.5	925.4	22.5	877.8	8.4
150	10	927.2	23.5	879.8	8.8
175	2.5	905.0	11.5	855.8	4.9
175	5.0	907.2	11.9	858.3	5.1
175	7.5	909.6	12.4	860.8	5.3
175	10	911.4	12.8	863.0	5.5

Table B.9. Density and viscosity of WC-B-B2 bitumen diluted with cyclohexane and measured in the capillary viscometer.

Temp. °C	Pressure MPa	5.0 wt% Cyclohexane		40 wt% Cyclohexane	
		Density kg/m³	Viscosity mPa·s	Density kg/m³	Viscosity mPa·s
21	0.1	1005.3	38000	902.7	35.2
21	2.5	1006.6	42200	904.2	36.6
21	5.0	1007.8	48000	905.8	38.7
21	7.5	1009.3	54200	907.4	41.1
21	10	1010.8	60600	909.5	43.1
50	0.1	985.4	1792	881.5	12.1
50	2.5	986.8	1986	883.3	12.6
50	5.0	988.2	2140	885.2	13.1
50	7.5	989.7	2320	887.0	13.7
50	10	991.1	2510	888.9	14.4
75	0.1	968.8	324	861.9	5.9
75	2.5	970.6	333	864.0	6.0
75	5.0	972.2	352	866.3	6.3
75	7.5	973.6	369	868.3	6.5
75	10	975.1	389	870.3	6.7
100	2.5	954.2	92.2	843.6	3.5
100	5.0	955.8	97.2	845.9	3.6
100	7.5	957.6	103	848.2	3.7
100	10	959.2	109	850.8	3.8
125	2.5	937.0	35.4	822.8	2.2
125	5.0	938.9	37.1	825.6	2.3
125	7.5	940.7	38.9	828.2	2.4
125	10	942.6	40.8	830.8	2.4
150	2.5	920.2	17.1	801.0	1.5
150	5.0	922.3	17.7	804.6	1.6
150	7.5	924.3	18.5	807.7	1.6
150	10	926.3	19.3	810.8	1.7
175	2.5	903.5	9.9	779.8	1.1
175	5.0	905.9	10.1	783.8	1.2
175	7.5	908.2	10.5	787.4	1.2
175	10	910.3	10.9	790.9	1.2

Table B.10. Density and viscosity of WC-B-B1 bitumen diluted with toluene and measured in the capillary viscometer.

Temp. °C	Pressure MPa	5.0 wt% Toluene		25 wt% Toluene		50 wt% Toluene	
		Density kg/m³	Viscosity mPa·s	Density kg/m³	Viscosity mPa·s	Density kg/m³	Viscosity mPa·s
20	0.1	1004.2	8780	972.4	78.6	933.9	5.5
20	2.5	1005.5	9820	973.7	82.3	935.2	5.6
20	5.0	1006.5	10700	975.2	85.8	937.1	5.7
20	7.5	1007.9	11900	976.8	90.3	939.1	5.8
20	10	1009.0	13000	978.2	95.3	941.0	6.0
50	0.1	984.2	681	949.7	23.3	908.0	2.9
50	2.5	985.5	741	951.2	24.2	909.7	2.9
50	5.0	987.2	780	952.9	24.9	911.4	3.0
50	7.5	988.4	834	954.7	25.8	913.3	3.1
50	10	989.7	895	956.3	26.8	915.1	3.1
75	0.1	968.0	164	931.9	11.3	889.6	1.9
75	2.5	969.3	171	933.6	11.6	891.7	1.9
75	5.0	970.9	180	935.4	12.0	893.7	1.9
75	7.5	972.3	190	937.1	12.4	895.6	2.0
75	10	973.7	201	938.8	12.7	897.5	2.0
100	0.1	951.1	54.7	-	-	866.8	1.3
100	2.5	952.7	57.6	914.6	6.4	869.5	1.4
100	5	954.3	60.3	916.6	6.6	871.6	1.4
100	7.5	956.0	63.5	918.6	6.8	873.8	1.4
100	10	957.6	66.3	920.5	7.1	876.2	1.5
125	2.5	935.1	25.0	894.8	3.9	845.4	1.0
125	5.0	937.0	26.0	897.1	4.1	847.8	1.0
125	7.5	938.8	26.7	899.3	4.2	850.6	1.1
125	10	940.6	27.8	901.5	4.4	853.3	1.1
150	2.5	916.7	11.8	873.7	2.6	822.5	0.80
150	5.0	918.9	12.2	876.4	2.7	825.9	0.82
150	7.5	920.9	12.6	879.0	2.7	828.8	0.84
150	10	922.9	13.0	881.2	2.8	831.8	0.86
175	2.5	898.1	6.9	853.5	1.9	796.1	0.63
175	5.0	900.5	7.1	856.6	2.0	800.2	0.65
175	7.5	903.0	7.4	859.6	2.0	804.0	0.67
175	10	905.2	7.7	862.5	2.1	807.5	0.68

Table B.11. Density and viscosity of WC-B-B2 bitumen diluted with 1-methylnaphthalene (MN) at 0.1 MPa and measured in the cone and plate viscometer.

Temp. °C	5.0 wt% MN		25 wt% MN		50 wt% MN	
	Density kg/m³	Viscosity mPa·s	Density kg/m³	Viscosity mPa·s	Density kg/m³	Viscosity mPa·s
20	1014.6	41900	1019.4	1380	1022.1	82.8
25	1011.2	20800	1016.0	898	1018.6	64.0
35	1004.4	6290	1009.1	420	1011.5	40.4
45	997.7	2340	1002.2	220	1004.5	27.0
50	994.3	1510	998.7	165	1001.0	22.5

Table B.12. Density and viscosity of WC-B-B2 bitumen diluted with heptol (50 wt% *n*-heptane + 50 wt% toluene) and measured in the capillary viscometer.

Temp. °C	Pressure MPa	5.0 wt% Heptol		25 wt% Heptol		40 wt% Heptol	
		Density kg/m³	Viscosity mPa·s	Density kg/m³	Viscosity mPa·s	Density kg/m³	Viscosity mPa·s
21	0.1	1002.7	13200	946.0	95.7	908.4	16.4
21	2.5	1004.0	14400	947.4	103	910.1	17.0
21	5	1005.3	15800	948.7	108	911.7	17.7
21	7.5	1006.7	17100	950.3	113	913.4	18.4
21	10	1008.3	19900	951.4	117	915.4	18.9
50	0.1	982.7	921	923.8	26.5	884.9	6.9
50	2.5	984.1	995	925.3	27.5	886.8	7.1
50	5	985.6	1060	927.0	28.5	888.6	7.2
50	7.5	987.0	1130	928.7	29.6	890.4	7.4
50	10	988.5	1230	929.7	30.4	892.2	7.6
75	0.1	966.1	196	905.4	12.0	866.1	3.9
75	2.5	967.8	208	907.3	12.3	867.9	4.0
75	5	969.4	220	909.2	12.7	870.1	4.1
75	7.5	970.9	234	911.0	13.1	871.9	4.2
75	10	972.4	249	911.9	13.5	873.9	4.3
100	0.1	949.4	62.5	-	-	-	-
100	2.5	951.2	65.9	889.3	6.7	848.9	2.6
100	5	953.0	69.1	891.2	6.9	851.2	2.7
100	7.5	954.7	72.8	893.3	7.1	853.4	2.8
100	10	956.4	76.3	894.4	7.3	855.9	2.9
125	2.5	934.1	26.9	871.0	4.2	828.8	1.7
125	5	935.9	28.0	873.3	4.3	831.7	1.8
125	7.5	937.8	29.3	875.5	4.4	834.4	1.9
125	10	939.7	30.5	876.8	4.5	837.0	1.9
150	2.5	916.4	13.4	852.0	2.8	808.9	1.4
150	5	918.6	13.9	854.8	2.9	812.2	1.4
150	7.5	920.7	14.5	857.4	3.0	815.2	1.4
150	10	922.6	14.9	858.9	3.0	818.0	1.5
175	2.5	897.5	7.4	832.9	2.0	789.8	1.0
175	5	900.0	7.7	836.2	2.1	793.4	1.1
175	7.5	902.4	8.0	839.2	2.2	796.8	1.1
175	10	904.6	8.3	840.9	2.2	800.1	1.2

Table B.13. Density and viscosity of CO-B-A1 bitumen at 0.1 MPa measured in the cone and plate viscometer.

Temp. °C	Density kg/m³	Viscosity mPa·s
20	1013.5	-
25	1011.0	-
35	1005.1	-
40	-	104853
50	996.2	29793
60	-	11567
75	-	2985
90	972.8	-

Table B.14. Density and viscosity of CO-B-A1 bitumen diluted with toluene at 0.1 MPa and measured in the cone and plate viscometer.

Temp. °C	4.5 wt% Toluene		9.6 wt% Toluene	
	Density kg/m³	Viscosity mPa·s	Density kg/m³	Viscosity mPa·s
15	-	-	1000.8	19795
20	-	-	997.6	12531
25	1003.1	57003	994.5	7872
35	997.0	17992	-	

Table B.15. Density and viscosity of CO-B-A1 bitumen diluted with 14.3 wt% 1-methylnaphthalene at 0.1 MPa and measured in the cone and plate viscometer.

Temp. °C	Density kg/m³	Viscosity mPa·s
25	1013.7	16600
35	1007.2	5550
50	997.4	1540

Table B.16. Density and viscosity of ME-CO-A1 bitumen at 0.1 MPa measured in the cone and plate viscometer.

Temp. °C	Density kg/m³	Viscosity mPa·s
10	876.6	28.0
15	873.0	21.8
20	869.1	18.1
25	865.8	16.1
50	847.9	-

Table B.17. Density and viscosity of ME-CO-A1 bitumen diluted with 10 wt% *n*-pentane and measured in the capillary viscometer.

Pressure MPa	Temp. °C	Density kg/m³	Viscosity mPa·s
0.1	21	836.5	4.85
2.5	21	838.3	5.02
5	21	839.9	5.22
7.5	21	841.7	5.39
10	21	844.0	5.60
2.5	50	816.9	2.66
5	50	818.8	2.75
7.5	50	820.7	2.85
10	50	822.9	2.94
2.5	75	799.5	1.76
5	75	801.8	1.81
7.5	75	803.9	1.87
10	75	806.0	1.93
2.5	100	779.7	1.25
5	100	782.2	1.29
7.5	100	784.5	1.33
10	100	787.1	1.37
2.5	125	761.0	0.95
5	125	764.0	0.98
7.5	125	766.6	1.01
10	125	769.5	1.04
2.5	150	742.1	0.75
5	150	745.6	0.77
7.5	150	748.8	0.80
10	150	751.9	0.82

Table B.18. Density and viscosity of ME-CO-A1 bitumen diluted with toluene at 0.1 MPa and measured in the cone and plate viscometer.

Temp. °C	6.0 wt% Toluene		10 wt% Toluene	
	Density kg/m³	Viscosity mPa·s	Density kg/m³	Viscosity mPa·s
0	886.7	37.0	886.4	26.4
5	882.9	25.8	882.7	18.8
10	879.1	20.5	878.9	15.2
15	875.3	17.4	875.2	13.6

Table B.19. Density and viscosity of bitumen ME-CO-A1 diluted with 1-methylnaphthalene (1-MN) at 0.1 MPa and measured in the cone and plate viscometer.

Temp. °C	2.0 wt% 1-MN		5.0 wt% 1-MN		8.0 wt% 1-MN	
	Density kg/m³	Viscosity mPa·s	Density kg/m³	Viscosity mPa·s	Density kg/m³	Viscosity mPa·s
5	-	-	-	-	889.1	27.9
8	-	-	-	-	886.9	24.3
10	877.4	24.1	881.2	22.3	885.4	20.8
15	873.6	19.0	877.4	17.9	-	-
20	869.9	16.2	873.8	-	-	-
25	866.1	13.6	870.1	12.9	-	-

Table B.20. Density and viscosity of Blend1 (70 wt% WC-B-B2 + 30 wt% ME-CO-A1) at 0.1 MPa and measured in the cone and plate viscometer.

Temp. °C	Density kg/m³	Viscosity mPa·s
10	-	2888.8
25	945.0	754.1
30	-	497.7
35	-	340.3
40	936.8	-
50	930.3	-
60	923.8	-
70	918.3	-

Table B.21. Density and viscosity of Blend1 diluted with *n*-tetradecane at 0.1 MPa and measured in the cone and plate viscometer.

Temp.	2.0 wt% *n*-Tetradecane		5.0 wt% *n*-Tetradecane	
°C	Density kg/m³	Viscosity mPa·s	Density kg/m³	Viscosity mPa·s
0	-	5496	-	3259
10	-	1977	-	1250
20	-	825.3	-	535.8
35	-	298.3	-	194.2
40	932.8	-	926.0	-
50	926.3	-	919.4	-
60	919.8	-	912.9	-

Table B.22. Density and viscosity of Blend1 diluted with 1-methylnaphthalene (MN) at 0.1 MPa and measured in the cone and plate viscometer.

Temp.	5.0 wt% MN		8.3 wt% MN	
°C	Density kg/m³	Viscosity mPa·s	Density kg/m³	Viscosity mPa·s
0	-	4350	-	2887
10	-	1534	-	1079
20	-	673.5	-	454.7
35	-	239.3	-	167.8
40	940.3	-	942.6	-
50	933.7	-	936.0	-
60	926.8	-	929.1	-

Table B.23. Density and viscosity of WC-B-B2-DAO (deasphalted WC-B-B2 bitumen) at 0.1 MPa and measured in a cone and plate viscometer.

Temp.	Density	Viscosity
°C	kg/m³	mPa·s
20	983.2	5455
25	980.0	3193
50	964.3	425.5
90	939.2	-
100	-	32.4

Table B.24. Density and viscosity of WC-B-B2-DAO diluted with 12 wt% *n*-octane at 0.1 MPa and measured in the cone and plate viscometer.

Temp. °C	Density kg/m³	Viscosity mPa·s
20	950.6	497.7
25	947.2	343.5
30	943.8	242.0
35	940.4	173.8
40	937.0	130.0

Table B.25. Density and viscosity of WC-B-B2-DAO diluted with *n*-dodecane at 0.1 MPa and measured in the cone and plate viscometer.

Temp. °C	5.0 wt% *n*-Dodecane		10 wt% *n*-Dodecane		18 wt% *n*-Dodecane	
	Density kg/m³	Viscosity mPa·s	Density kg/m³	Viscosity mPa·s	Density kg/m³	Viscosity mPa·s
25	965.9	1170	950.8	430	930.7	142
35	959.5	520	-	-	-	-
50	949.9	184	934.4	90.1	913.9	38.5
75	933.8	-	918.0	-	897.1	-

Table B.26. Density and viscosity of WC-B-B2-DAO diluted with toluene at 0.1 MPa and measured in the cone and plate viscometer.

Temp. °C	2.0 wt% Toluene		4.5 wt% Toluene		10 wt% Toluene	
	Density kg/m³	Viscosity mPa·s	Density kg/m³	Viscosity mPa·s	Density kg/m³	Viscosity mPa·s
20	980.7	2680	977.4	1420	970.0	415
25	977.5	1660	974.0	916	966.6	299
35	971.1	690	967.6	439	959.9	155
50	961.6	247	957.8	169	949.8	81.0

Table B.27. Expanded Fluid (EF) viscosity model parameters of pure hydrocarbons used in Chapter 5.

Compound	ρ_s^o kg/m^3	c_2	c_3 x10^6 kPa^{-1}
Ethane	724.0	0.1560	0.01
Propane	778.0	0.1740	0.10
Butane	813.0	0.1900	0.15
Pentane	837.0	0.1980	0.18
Heptane	857.8	0.2130	0.17
Octane	862.7	0.2210	0.17
Decane	868.1	0.2360	0.20
Dodecane	871.4	0.2490	0.22
Tridecane	877.8	0.2538	0.23
Tetradecane	875.5	0.2650	0.24
Pentadecane	878.4	0.2698	0.27
Hexadecane	878.6	0.2780	0.28
Eicosane	885.5	0.3060	0.29
Tetracosane	893.2	0.3350	0.29
Cyclohexane	922.1	0.2370	0.16
Methylcyclohexane	937.9	0.2505	0.15
Decaline	1010.0	0.2700	0.09
2,2,4,4,6,8,8-heptamethylnonane	856.8	0.1921	0.25
Toluene	1049.6	0.2155	0.14
P-Xylene	1045.5	0.2260	0.14
O-Xylene	1052.9	0.2320	0.14
Ethylbenzene	1042.4	0.2222	0.14
Hexylbenzene	975.2	0.2159	0.21
1-Methylnaphthalene	1138.0	0.2250	0.14

APPENDIX C: DENSITY AND VISCOSITY DATA OF THE CRUDE OILS, DEASPHALTED OIL, DISTILLATION CUTS, PARTIALLY DEASPHALTED OIL AND ASPHALTENE/TOLUENE MIXTURES USED IN CHAPTER 6

Table C.1. Density and viscosity of WC-B-A2 bitumen measured in the capillary viscometer apparatus.

Temp. °C	Pressure MPa	Density kg/m³	Viscosity mPa·s
49.9	0.1	1004.3	38200
49.9	2.5	1005.6	43400
49.9	5.0	1006.9	48400
49.9	7.5	1008.3	54000
49.9	10.0	1009.6	60700
74.6	0.1	988.6	3140
74.6	2.5	990.1	3470
74.6	5.0	991.6	3800
74.6	7.5	992.9	4140
74.6	10.0	994.3	4560
99.7	0.1	972.6	532
99.7	2.5	974.4	561
99.7	5.0	975.9	608
99.7	7.5	977.6	656
99.7	10.0	979.0	707
124.6	2.5	958.3	152
124.6	5.0	959.9	161
124.6	7.5	961.6	172
124.6	10.0	963.5	183
149.8	2.5	941.5	54.7
149.8	5.0	943.5	57.7
149.8	7.5	945.4	60.9
149.8	10.0	947.3	64.5
174.8	2.5	924.6	25.0
174.8	5.0	926.8	26.2
174.8	7.5	929.1	27.4
174.8	10.0	931.1	28.6

Table C.2. Density and viscosity of WC-B-A3 bitumen measured in the capillary viscometer apparatus.

Temp. °C	Pressure MPa	Density kg/m³	Viscosity mPa·s
49.9	0.1	989.9	5500
49.9	2.5	990.9	5960
49.9	5.0	992.3	6500
49.9	7.5	993.7	7240
49.9	10	995.0	7990
75.2	0.1	973.6	699
75.2	2.5	974.9	746
75.2	5.0	976.4	798
75.2	7.5	977.9	852
75.2	10	979.3	919
100.0	0.1	957.5	161
100.0	2.5	959.0	172
100.0	5.0	960.6	183
100.0	7.5	962.3	195
100.0	10	963.9	209
125.0	2.5	936.3	38.3
125.0	5.0	938.2	40.1
125.0	7.5	940.0	42.1
125.0	10	941.9	44.1
150.0	2.5	919.6	18.5
150.0	5.0	921.8	19.2
150.0	7.5	923.8	20.0
150.0	10	925.8	20.8
175.0	2.5	903.1	10.5
175.0	5.0	905.4	10.8
175.0	7.5	907.8	11.2
175.0	10	909.8	11.6

Table C.3. Density and viscosity of WC-B-B1 bitumen measured in the cone and plate rheometer and density meter at atmospheric pressure.

Temp. °C	Density kg/m³	Viscosity mPa·s
39.3	-	7720
40.0	1000.7	-
50.0	994.3	-
51.1	-	2520
54.7	-	1900
55.0	991.1	-
60.0	987.9	-
68.5	-	634
87.7	-	192
90.0	968.6	-

Table C.4. Density and viscosity of the WC-B-A1, US-HO-A1 and MX-HO-A1 oils measured in the cone and plate rheometer and density meter at atmospheric pressure.

Temp. °C	WC-B-A1 Density kg/m³	WC-B-A1 Viscosity mPa·s	US-HO-A1 Density kg/m³	US-HO-A1 Viscosity mPa·s	MX-HO-A1 Density kg/m³	MX-HO-A1 Viscosity mPa·s
25	992.5	35200	957.3	2160	972.9	
35	-	10800	-	871	-	-
40	983.1	-	-	-	-	-
45	-	-	-	-	959.1	31693
50		2620	941.4	297		
60	970.4	-	934.6	-	948.6	7183
75		433	925.1	77.8	938.2	2147
80	957.8	-	-	-	-	-
90	-	-	915.6	-	927.7	-
100	-	122	-	31.1	-	
125	-	47.1	-	16.0	-	-

Table C.5. Density and viscosity of the CO-B-B1 and EU-HO-A1 oils measured in the cone and plate rheometer and density meter at atmospheric pressure.

Temp. °C	CO-B-B1		EU-HO-A1	
	Density kg/m³	Viscosity mPa·s	Density kg/m³	Viscosity mPa·s
25	994.2	-	-	-
35	-	-	-	1240
40	984.7	-	953.0	-
50	978.3	4023	946.6	383
60	972.0	-	940.4	-
75	-	612	930.9	91.5
80	-	-	927.8	-
90	953.0	-	-	-
100	-	154	-	34.0
125	-	59	-	-

Table C.6. Normal boiling point (T_b), specific gravity (SG), molecular weight (MW), and fitted EF parameters (c_2 and ρ_s^o) of distillation cuts from the WC-B-B1, WC-B-A1, CO-B-A1, CO-B-B1, US-HO-A1, and MX-HO-A1 oils.

Cut	T_b °C	SG	MW g/mol	c_2	ρ_s^o kg/m³
WC-B-B1					
1	335	0.921	247	0.1889	975.8
2	346	0.962	272	0.1416	996.3
3	414	0.973	327	0.2583	1022.5
4	425	0.982	351	0.2555	1019.9
5	427	0.992	424	0.2640	1025.1
6	470	0.999	479	0.2919	1033.9
WC-B-A1					
1	285	0.891	225	-	-
2	313	0.915	259	0.2266	979.6
3	349	0.936	287	0.2486	995.8
4	376	0.952	323	0.2574	1002.6
5	396	0.961	372	0.2641	1005.9
6	412	0.965	451	0.2643	1005.0
7	429	0.968	463	0.2849	1007.0
CO-B-A1					
1	236	0.900	236	0.2424	978.4
2	358	0.924	257	0.2116	979.1
3	389	0.944	301	0.2650	1003.9
4	404	0.961	328	0.2577	1005.1
5	441	0.971	380	0.2663	1008.4
6	487	0.979	397	0.2927	1014.7
7	537	0.988	475	0.3155	1022.6
CO-B-B1					
1	289	0.886	234	0.2405	970.6
2	321	0.923	281	0.2271	980.7
3	338	0.937	306	0.2422	987.8
4	365	0.947	350	0.2416	988.5
5	378	0.958	388	0.2718	998.2
6	395	0.964	432	0.2787	998.9
7	405	0.975	447	0.3005	1008.1
US-HO-A1					
1	290	0.868	227	-	-
2	315	0.900	261	0.2369	967.5
3	342	0.918	295	0.2461	976.6
4	357	0.926	337	0.2558	978.8
5	377	0.936	372	0.2721	984.3
6	406	0.948	411	0.2895	991.1
7	424	0.958	485	0.2915	996.3
MX-HO-A1					
1	298	0.901	265	0.2431	971.4
2	319	0.918	285	0.2397	986.0
3	353	0.930	325	0.2231	978.0
4	372	0.942	345	0.2789	994.2
5	398	0.952	408	0.2569	993.8
6	475	0.968	468	0.3069	1011.7

Table C.7. Viscosity (cone and plate) of distillation cuts from the WC-B-B1 and WC-B-A1 bitumens at 0.1 MPa.

WC-B-B1			WC-B-A1		
Cut	T °C	Viscosity mPa·s	Cut	T °C	Viscosity mPa·s
1	10.6	27.1	1	0.0	14.5
	15.5	19.8	2	0.0	56.8
	20.0	15.6		15.0	23.2
2	10.6	125		25.0	14.5
	20.1	47.3		35.0	9.8
	24.6	29.4	3	15.0	66.9
	34.3	13.7		25.0	36.0
3	25.9	160		35.0	21.8
	41.3	56.4		50.0	12.3
	60.9	20.4	4	15.0	266
	73.4	12.3		25.0	118
	90.9	7.8		35.0	60.4
4	26.0	923		50.0	27.1
	46.9	167		70.0	12.5
	75.2	23.9	5	25.0	342
	82.2	18.5		35.0	152
5	29.0	2910		50.0	57.4
	44.3	581		75.0	18.0
	60.2	155	6	25.0	934
	89.0	28.1		35.0	369
	110.5	12.5		50.0	120
6	29.1	6290		75.0	30.7
	44.5	1310		100.0	12.6
	62.3	285	7	25.0	2110
	85.6	57.0		35.0	767
	120.9	12.9		50.0	223
	-	-		75.0	49.7
	-	-		100.0	17.9
	-	-		110.0	13.2

Table C.8. Viscosity (cone and plate) of distillation cuts from the US-HO-A1 and MX-HO-A1 heavy oils at 0.1 MPa.

US-HO-A1			MX-HO-A1		
Cut	T °C	Viscosity mPa·s	Cut	T °C	Viscosity mPa·s
1	0.0	7.6	1	15	18.9
2	0.0	49.1		17	17.3
	5	36.0		20	14.9
	15	21.2		22	14.1
	30	11.2		25	12.5
3	5	117	2	15	23.8
	15	57.9		20	18.9
	25	32.4		25	15.2
	35	20.0		30	12.6
	50	11.0		35	10.5
4	25	75.6	3	25	57.3
	35	41.7		35	33.1
	50	20.5		45	19.1
	65	11.7		55	13.1
5	25	214	4	25	170
	35	104		35	76.5
	50	43.5		50	34.6
	75	15.5		75	12.9
6	25	895	5	25	433
	35	362.4		35	188
	50	120.5		50	75.6
	75	32.0		75	21.3
	100	13.2		90	13.0
7	25	2920	6	25	2070
	35	984		50	205
	50	281		75	52.4
	75	60.2		100	19.8
	100	21.0		110	14.6
	120	11.6		-	-

Table C.9. Viscosity (cone and plate) of distillation cuts from the CO-B-A1 and CO-B-B1 bitumens.

CO-B-A1			CO-B-B1		
Cut	T °C	Viscosity mPa·s	Cut	T °C	Viscosity mPa·s
1	15	11.7	1	5	10.8
	17	11.0		10	9.1
	20	10.0		15	7.6
2	10	58.5	2	5	89.0
	13	47.7		10	62.0
	20	31.4		20	33.4
	25	24.6		30	20.0
	35	15.5		40	12.6
	42	12.7	3	20	105
3	24	59.8		35	40.0
	37	28.7		50	19.0
	50	16.1		65	10.6
	20	557	4	20	506
4	25	340		35	116
	52	49.9		50	46.1
	75	17.9		75	15.0
5	20	3280	5	20	3630
	25	1780		35	411
	52	148		50	130
	80	32.0		75	32.5
	98	15.5		100	12.5
6	20	17600	6	35	1350
	25	8450		50	308
	53	411		75	61.8
	78	73.2		100	20.8
	105	22.0		115	12.7
7	20	87000	7	35	4620
	25	46900		50	867
	50	1340		75	134
	76	192		100	37.4
	105	38.7		125	15.2
	130	15.9		-	-

Table C.10. Density and viscosity of WC-B-B1-DAO C5-maltenes measured in the capillary viscometer apparatus.

Temp. °C	Pressure MPa	Density kg/m³	Viscosity mPa·s
20.1	0.1	981.3	1280
20.1	2.5	982.5	1390
20.1	5.0	983.7	1540
20.1	7.5	984.9	1650
20.1	10	986.6	1810
50.0	0.1	961.4	145
50.0	2.5	962.8	157
50.0	5.0	964.4	167
50.0	7.5	965.9	177
50.0	10	967.3	187
75.0	0.1	945.1	41.8
75.0	2.5	946.9	44.5
75.0	5.0	948.5	47.2
75.0	7.5	950.0	49.8
75.0	10	951.6	52.6
100.0	0.1	928.2	16.8
100.0	2.5	930.2	17.5
100.0	5.0	931.9	18.3
100.0	7.5	933.6	19.2
100.0	10	935.4	20.1
125.0	0.1	911.5	8.7
125.0	2.5	913.9	9.1
125.0	5.0	915.7	9.4
125.0	7.5	917.6	9.8
125.0	10	919.6	10.2
150.0	2.5	897.2	5.4
150.0	5.0	899.5	5.6
150.0	7.5	901.5	5.8
150.0	10	903.5	6.0
175.0	2.5	880.3	3.5
175.0	5.0	882.8	3.7
175.0	7.5	885.3	3.8
175.0	10	887.5	3.9

Table C.11. Density and viscosity of WC-B-A1-DAO, WC-B-A2-DAO and US-HO-A1-DAO C5-maltenes measured in a cone and plate rheometer and density meter at atmospheric pressure.

	WC-B-A1-DAO		WC-B-A2-DAO		US-HO-A1-DAO	
Temp.	Density	Viscosity	Density	Viscosity	Density	Viscosity
°C	kg/m^3	mPa·s	kg/m^3	mPa·s	kg/m^3	mPa·s
20	972.4	-	-	-	948.9	-
25	-	3670	998.1	43600	-	819
30	966.0	-	-	-	942.2	-
35	-	1420	-	-	-	365
40	959.7	-	-	-	935.7	-
47	-	-	-	2610	-	-
50	953.3	449	982.5	-	929.3	138
60	947.0	-	976.2	-	922.8	-
70	940.7	-	969.9	-	916.4	-
71	-	-	-	358	-	-
75	-	103	966.8			41.5
100	-	36.4		67.9	-	17.8

Table C.12. Density and viscosity of MX-HO-A1-DAO, CO-B-A1-DAO and CO-B-B1-DAO maltenes measured in a cone and plate rheometer and density meter at atmospheric pressure.

	MX-HO-A1-DAO		CO-B-A1-DAO		CO-B-B1-DAO	
Temp.	Density	Viscosity	Density	Viscosity	Density	Viscosity
°C	kg/m^3	mPa·s	kg/m^3	mPa·s	kg/m^3	mPa·s
20	959.3	-	-	-	958.1	-
25	-	856	981.1	32300	-	1400
30	952.4	-	-	-	951.6	-
35	-	-	-	-	-	577
40	945.6	-	-	-	945.1	-
48	-	-	-	1970	-	-
50	939.1	142	965.6	-	938.7	177
60	932.7	-	-	-	932.3	-
70	926.2	-	-	283	925.9	-
75	-	45.6	950.1	-	-	52.8
90	-	-	940.8	-	-	-
100	-	19.4	-	-	-	21.3
104	-	-	-	52.2	-	-

Table C.13. Density and viscosity of partially deasphalted bitumen WC-B-B3 measured in a cone and plate rheometer and density meter at atmospheric pressure. Original asphaltene content of the bitumen is of 22 wt%.

Temp. °C	0 wt% Asphaltenes		3 wt% Asphaltenes		4 wt% Asphaltenes		16 wt% Asphaltenes	
	Density kg/m^3	Viscosity mPa·s	Density kg/m^3	Viscosity mPa·s	Density kg/m^3	Viscosity mPa·s	Density kg/m^3	Viscosity mPa·s
25	992.7	10700	999.1	22300	1000.9	26700	1010.8	161500
35	986.4	3740	992.8	7010	994.7	8970	1005.4	40800
50	976.9	990	983.5	1730	985.4	2150	997.1	7800
75	961.1	188	967.8	295	969.9	354	983.4	1020

Table C.14. Density and viscosity of C5-asphaltenes from samples WC-B-B1 and CO-B-A1. The viscosity was measured at atmospheric pressure using a cone and plate rheometer and the density was indirectly calculated from asphaltene/toluene mixtures assuming regular solution behavior.

Temp. °C	C5-Asphaltenes WC-B-B1		C5-Asphaltenes CO-B-A1	
	Density kg/m^3	Viscosity mPa·s	Density kg/m^3	Viscosity mPa·s
25	1094.5	-	1095.6	-
50	1082.7	-	1083.7	-
75	1070.8	-	1071.9	-
90	1063.7	-	1064.8	-
175	-	1000000	-	979000
178	-	-	-	773000
185	-	454000	-	371000
190	-	271000	-	-
200	-	132000	-	137000

Table C.15. Density and viscosity of 5 wt% WC-B-B1 C5-asphaltenes in toluene measured in the capillary viscometer apparatus.

Temp. °C	Pressure MPa	Density kg/m³	Viscosity mPa·s
20.1	0.1	879.4	0.80
20.1	2.5	881.2	0.82
20.1	5.0	883.1	0.84
20.1	7.5	884.9	0.85
20.1	9.0	886.2	0.86
50.1	2.5	853.7	0.59
50.1	5.0	855.9	0.60
50.1	7.5	857.9	0.61
50.1	9.0	859.3	0.62
74.7	2.5	830.2	0.48
74.7	5.0	832.8	0.48
74.7	7.5	835.1	0.49
74.7	9.0	836.6	0.50
100.0	2.5	806.0	0.39
100.0	5.0	808.8	0.40
100.0	7.5	811.6	0.40
100.0	9.0	813.3	0.41
124.7	5.0	785.4	-
124.7	6.0	786.7	-
124.7	6.5	787.4	-
124.7	7.5	788.7	-
124.7	8.5	790.2	-
124.7	9.0	790.9	-
150.4	5.0	759.8	-
150.4	6.5	762.1	-
150.4	7.5	763.8	-
150.4	9.0	766.1	-
175.1	5.0	733.8	-
175.1	6.0	735.8	-
175.1	7.5	738.9	-
175.1	8.5	740.7	-
175.1	9.0	741.5	-

APPENDIX D: EXPANDED FLUID (EF) VISCOSITY MODEL PARAMETERS FOR PURE HYDROCARBONS IN CHAPTER 6

Table D.1. EF fluid-specific parameters for the *n*-alkanes in the Development Dataset 1 in Chapter 6.

Compound	c_2	ρ_s^o, kg/m³
methane	0.1000	540.0
ethane	0.1560	724.0
propane	0.1740	778.0
n-butane	0.1900	813.0
n-pentane	0.1980	837.0
n-hexane	0.2050	849.1
n-heptane	0.2130	857.8
n-octane	0.2210	862.7
n-nonane	0.2304	865.9
n-decane	0.2360	868.1
n-dodecane	0.2490	871.4
n-tridecane	0.2538	877.8
n-tetradecane	0.2650	875.5
n-pentadecane	0.2698	878.4
n-hexadecane	0.2780	878.6
n-heptadecane	0.2878	881.3
n-octadecane	0.2974	885.1
n-eicosane	0.3060	885.5
n-docosane	0.3100	885.2
n-tricosane	0.3310	891.4
n-tetracosane	0.3350	893.2
n-hexacosane	0.3727	903.9
n-octacosane	0.3788	903.2
n-dotriacontane	0.4082	908.6
n-pentatriacontane	0.4493	919.9
n-hexatriacontane	0.4397	914.9
n-tetratetracontane	0.5071	926.9

Table D.2. EF fluid-specific parameters for the branched alkanes in the Development Dataset 1 in Chapter 6.

Compound	c_2	ρ_s^o, kg/m^3
7-methyltridecane	0.2418	868.1
2,2,3,3,5,6,6-heptamethylheptane	0.2751	899.3
2-methylpentadecane	0.2737	873.8
7-n-propyltridecane	0.2324	866.6
7-n-hexyltridecane	0.2619	874.5
2,6,10,14-tetramethylpentadecane	0.2656	868.1
2,6,11,15-tetramethylhexadecane	0.2813	875.1
8-hexylpentadecane	0.2729	877.2
9-hexylheptadecane	0.2890	881.8
9-octylheptadecane	0.3055	887.2
11-butyldocosane	0.3195	890.0
6,11-dipentylhexadecane	0.3092	887.3
9-ethyl-9-heptyloctadecane	0.3211	891.5
2,2,4,10,12,12-hexamethyl-7-(3,5,5-trimethylhexyl) tridecane	0.3010	868.8
11-n-decyldocosane	0.3575	900.4
13-n-dodecylhexacosane	0.3856	905.0

Table D.3. EF fluid-specific parameters for the mono-aromatics in the Development Dataset 1 in Chapter 6.

Compound	c_2	ρ_s^o, kg/m³
benzene	0.2260	1066.4
toluene	0.2155	1049.6
o-xylene	0.2320	1052.9
p-xylene	0.2260	1045.5
ethylbenzene	0.2222	1042.4
propylbenzene	0.2214	1017.8
n-butylbenzene	0.2247	1005.8
n-pentylbenzene	0.2026	976.5
n-hexylbenzene	0.2159	975.2
n-heptylbenzene	0.2270	968.7
n-octylbenzene	0.2437	967.7
n-nonylbenzene	0.2505	963.6
n-decylbenzene	0.2661	963.4
n-undecylbenzene	0.2857	965.0
n-dodecylbenzene	0.2973	963.8
n-tridecylbenzene	0.3068	962.0
n-tetradecylbenzene	0.3164	960.7
n-pentadecylbenzene	0.3258	959.5
n-hexadecylbenzene	0.3361	958.8

Table D.4. Fitted EF fluid-specific parameters for the cyclics in the Development Dataset 1 in Chapter 6.

Compound	c_2	ρ_s^o, kg/m^3
cyclohexane	0.2370	922.1
cycloheptane	0.2310	933.7
cyclooctane	0.2541	950.7
methylcyclopentane	0.2464	944.5
ethylcyclopentane	0.2630	966.8
propylcyclopentane	0.2483	950.5
n-butylcyclopentane	0.2440	939.0
n-pentylcyclopentane	0.2550	937.2
n-hexylcyclopentane	0.2700	937.7
n-heptylcyclopentane	0.2858	938.9
n-octylcyclopentane	0.3002	939.6
n-nonylcyclopentane	0.3145	940.7
n-decylcyclopentane	0.3309	942.8
n-undecylcyclopentane	0.3293	937.5
n-dodecylcyclopentane	0.3276	932.7
n-tridecylcyclopentane	0.3314	930.4
n-tetradecylcyclopentane	0.3424	931.4
n-pentadecylcyclopentane	0.3443	929.0
n-hexadecylcyclopentane	0.3461	926.7
methylcyclohexane	0.2505	937.9
ethylcyclohexane	0.2495	950.1
propylcyclohexane	0.2472	941.7
n-butylcyclohexane	0.2447	933.7
n-pentylcyclohexane	0.2345	920.6
n-hexylcyclohexane	0.2464	920.7
n-heptylcyclohexane	0.2574	920.8
n-octylcyclohexane	0.2660	921.0
n-nonylcyclohexane	0.2794	921.9
n-decylcyclohexane	0.2783	917.8
n-undecylcyclohexane	0.2852	917.0
n-dodecylcyclohexane	0.2867	914.6
n-tridecylcyclohexane	0.2916	913.6
n-tetradecylcyclohexane	0.3005	914.6
n-pentadecylcyclohexane	0.3095	915.4
n-hexadecylcyclohexane	0.3060	911.7

Table D.5. Fitted EF fluid-specific parameters for the aromatics in Development Dataset 1 in Chapter 6.

Compound	c_2	ρ_s^o, kg/m^3
Non-Fused Aromatics		
Diphenyl methane	0.2485	1132.6
1,1-diphenylethane	0.2359	1106.2
1-phenyl-2-cyclohexilethane	0.2418	1027.8
1-phenyl-3-cyclopentylpropane	0.2564	1031.1
1-cyclohexyl-1-phenylethane	0.2300	1022.5
1,3-diphenylbenzene	0.2464	1155.6
1,2-diphenylbenzene	0.2219	1120.6
1,1-diphenylheptane	0.2389	1024.4
1,5-diphenyl-3-(2-phenylethyl)pentane	0.2569	1072.2
1-phenyl-3-(2-phenylethyl)hendecane	0.2717	997.3
1,1diphenyltetradecane	0.2957	994.6
Fused Aromatics		
naphthalene	0.3054	1212.5
1-methylnaphthalene	0.2250	1138
2-n-butylnaphtalene	0.2204	1060.2
1-tert-butylnaphtalene	0.2086	1061.8
4,5-dimethylphenantrene	0.2366	1154.1
4,5-dimethyl-9,10-dihydrophenantrene	0.2447	1121.3
1,2,3,4,4a,7,8,9,10,11,12,12a-Dodecahydrochrysene	0.2392	1024.2
1,4-dimethyl-5-octylnaphthalene	0.2532	1020.6
2-butyl-3-hexylnaphthalene	0.2656	1008.5
7-butyl-1-hexylnaphthalene	0.2724	1007.4
2-octyltriphenylene	0.2757	1107.0

Table D.6. Fitted EF fluid-specific parameters for the naphthenes in Development Dataset 1 in Chapter 6.

Compound	c_2	ρ_s^o, kg/m³
Non-Fused Naphthenes		
bicyclopentyl	0.2640	1015.3
bicyclohexyl	0.2527	990.8
1,1-dicyclopentylethane	0.2611	1005.3
1,1-dicyclohexylethane	0.2608	982.2
1-cyclohexyl-3-cyclopentylpropane	0.2637	967.6
tricyclopentyl methane	0.2444	1020.6
1,2-dicyclohexyl cyclohexane	0.2345	987.7
7-cyclopentylmethyl tridecane	0.2608	908.8
7-cyclohexyltridecane	0.2612	909.1
1-cyclopentyl-4-(3-cyclopentylpropyl) dodecane	0.3196	939.4
1-cyclohexyl-3-(2-cyclohexylethyl) undecane	0.3239	936.6
9-(3-cyclopentylpropyl) heptadecane	0.3142	913.4
9-(2-cyclohexylethyl)heptadecane	0.3163	913.0
Fused Naphthenes		
decalin	0.2700	1010.0
2-n-butyldecalin	0.2486	969.5
2-butyl-1-hexylhexahydroindan	0.2535	937.6
5-butyl-6-hexylhexahydroindan	0.2597	944.7
1,4-dimethyl-5-octyldecalin	0.2703	951.2
7-butyl-1-hexyldecalin	0.2772	945.1
perhydrodibenzo[a,i]fluorene	0.2345	1033.2
1-alpha-decalylhendecane	0.2948	953.0
1,2-bis(decahydro-1-naphthyl)ethane	0.2742	1006.8
1-n-hexadecylindan	0.3315	973.6
6-n-octylperhydrobenz[de]anthracene	0.3004	1000.5
phenanthrene, 2-dodecyl-9,10-dihydro-	0.3089	1027.4
2-decylperhydroindeno-(2,1-a)indene	0.3513	989.9
3-decylperhydropyrene	0.2916	991.6
2-n-dodecylperhydrophenanthrene	0.3377	976.6
9-n-Dodecylperhydrophenanthrene	0.3116	972.7
7-Hexadecylspiro[4.5]decane	0.3528	948.0
cholestane	0.2784	982.5
9(4-as-perhydroindacenyl)heptadecane	0.3449	991.6

APPENDIX E: DETAILS ON MALTENE CHARACTERIZATION FOR CHAPTERS 6, 7 AND 8

Table E.1. Maltene characterization of WC-B-B1 oil.

i	Wt	T_b, K	SG	T_c, K	P_c, kPa	Z_{RA}	H/C	$\rho_{37.7°C}$ kg/m³	$\mu_{37.7°C}$ mPa·s	c_2	ρ_s^o, kg/m³	c_3 x10⁷, kPa-1
1	0.1608	557.9	0.914	759.1	2223.7	0.3437	1.673	913.9	6.8	0.2220	996.2	2.72
2	0.0577	606.4	0.937	804.4	1934.4	0.3373	1.627	937.3	17.0	0.2370	1010.0	2.77
3	0.0692	635.2	0.950	830.3	1776.8	0.3322	1.603	949.7	32.2	0.2485	1017.7	2.78
4	0.0797	664.1	0.961	855.8	1630.7	0.3265	1.581	961.5	67.6	0.2621	1025.3	2.79
5	0.0883	692.9	0.973	880.8	1495.3	0.3204	1.559	972.7	161.6	0.2784	1032.6	2.80
6	0.0939	721.8	0.983	905.3	1369.8	0.3138	1.538	983.3	457.1	0.2978	1039.7	2.80
7	0.0960	750.6	0.994	929.5	1253.6	0.3066	1.519	993.6	1597.9	0.3209	1046.6	2.80
8	0.0943	779.5	1.003	953.4	1146.0	0.2991	1.499	1003.4	7290.7	0.3482	1053.3	2.80
9	0.0890	808.3	1.013	977.1	1046.4	0.2911	1.481	1013.0	46497.6	0.3806	1059.9	2.80
10	0.0807	837.2	1.022	1000.5	954.5	0.2827	1.463	1022.3	452690.1	0.4192	1066.5	2.80
11	0.0703	866.0	1.031	1023.7	869.6	0.2740	1.445	1031.4	7551110.5	0.4649	1073.0	2.80
12	0.0202	885.4	1.038	1039.2	816.2	0.2680	1.434	1037.5	73445427.1	0.5004	1077.4	2.80

Table E.2. Maltene characterization of CO-B-A1 oil.

i	Wt	T_b, K	SG	T_c, K	P_c, kPa	Z_{RA}	H/C	$\rho_{37.7°C}$ kg/m³	$\mu_{37.7°C}$ mPa·s	c_2	ρ_s^o, kg/m³	c_3 x10⁷, kPa-1
1	0.1493	546.4	0.880	738.8	2120.4	0.3453	1.739	614.7	4.1	0.2220	970.4	2.49
2	0.0515	597.8	0.904	786.2	1820.5	0.3377	1.691	631.7	8.9	0.2380	985.5	2.64
3	0.0623	638.2	0.921	822.0	1610.6	0.3302	1.659	643.6	17.9	0.2545	996.9	2.71
4	0.0730	678.6	0.937	856.8	1422.6	0.3219	1.628	654.6	41.3	0.2753	1007.8	2.75
5	0.0827	719.0	0.951	890.8	1254.2	0.3126	1.600	664.8	115.5	0.3015	1018.1	2.78
6	0.0908	759.4	0.965	924.1	1103.4	0.3024	1.573	674.5	424.0	0.3346	1028.0	2.79
7	0.0965	799.8	0.978	956.8	968.7	0.2914	1.548	683.7	2258.7	0.3765	1037.4	2.79
8	0.0994	840.1	0.991	989.1	848.5	0.2797	1.523	692.5	19991.3	0.4295	1046.6	2.80
9	0.0990	880.5	1.003	1021.0	741.5	0.2673	1.499	701.2	356604.0	0.4968	1055.6	2.80
10	0.0955	920.9	1.016	1052.7	646.7	0.2544	1.476	709.7	17083281.4	0.5822	1064.7	2.80
11	0.0892	961.3	1.028	1084.4	563.4	0.2413	1.452	718.4	3.4628E+09	0.6905	1073.8	2.80
12	0.0107	984.3	1.036	1102.5	520.7	0.2338	1.437	723.6	1.7823E+11	0.7648	1079.2	2.80

Table E.3. Maltene characterization of US-HO-A1 oil.

i	Wt	T_b, K	SG	T_c, K	P_c, kPa	Z_{RA}	H/C	$\rho_{37.7°C}$ kg/m^3	$\mu_{37.7°C}$ mPa·s	c_2	ρ_s^o, kg/m^3	c_3 x10^7, kPa-1
1	0.0048	319.7	0.739	498.6	4266.4	0.4095	2.011	738.9	0.3	0.2018	937.3	1.86
2	0.0086	378.0	0.795	569.9	3656.7	0.4114	1.903	794.7	0.5	0.1999	956.4	2.29
3	0.0198	427.2	0.833	625.5	3190.8	0.4047	1.829	832.7	1.0	0.2014	962.4	2.53
4	0.0397	476.4	0.865	677.6	2777.1	0.3965	1.767	865.0	1.9	0.2062	971.7	2.68
5	0.0695	525.7	0.893	726.8	2412.3	0.3884	1.713	893.1	3.9	0.2146	984.1	2.75
6	0.1062	574.9	0.918	773.6	2091.5	0.3800	1.665	917.9	8.6	0.2271	997.6	2.78
7	0.1418	624.1	0.940	818.6	1809.6	0.3707	1.622	940.0	22.3	0.2443	1011.1	2.79
8	0.1653	673.4	0.960	861.9	1562.2	0.3600	1.583	960.1	74.3	0.2677	1024.1	2.80
9	0.1684	722.6	0.978	903.9	1344.9	0.3477	1.548	978.4	366.3	0.2991	1036.4	2.80
10	0.1498	771.8	0.996	945.0	1154.4	0.3339	1.515	995.5	3239.6	0.3412	1048.0	2.80
11	0.1163	821.0	1.012	985.1	987.7	0.3187	1.483	1011.7	6.7893E+04	0.3975	1059.2	2.80
12	0.0103	849.9	1.021	1008.5	900.0	0.3094	1.466	1021.0	7.1483E+05	0.4391	1065.9	2.80

Table E.4. Maltene characterization of CO-B-B1 oil.

i	Wt	T_b, K	SG	T_c, K	P_c, kPa	Z_{RA}	H/C	$\rho_{37.7°C}$ kg/m^3	$\mu_{37.7°C}$ mPa·s	c_2	ρ_s^o, kg/m^3	c_3 x10^7, kPa-1
1	0.0049	340.6	0.771	526.9	4153.0	0.3775	1.949	770.9	0.4	0.2028	956.1	1.43
2	0.0079	391.8	0.817	588.6	3623.3	0.3757	1.860	817.1	0.7	0.2015	971.0	1.72
3	0.0173	434.6	0.849	636.7	3221.2	0.3700	1.797	849.4	1.1	0.2028	974.6	1.95
4	0.0339	477.4	0.878	682.1	2858.6	0.3637	1.743	877.6	2.1	0.2067	982.5	2.17
5	0.0590	520.2	0.902	725.3	2533.2	0.3574	1.695	902.4	4.0	0.2134	992.8	2.37
6	0.0918	563.0	0.925	766.7	2241.7	0.3511	1.652	924.7	8.3	0.2230	1004.1	2.53
7	0.1272	605.8	0.945	806.6	1980.9	0.3441	1.613	944.8	19.7	0.2363	1015.7	2.64
8	0.1573	648.6	0.963	845.1	1747.5	0.3362	1.577	963.2	56.4	0.2538	1027.0	2.71
9	0.1734	691.4	0.980	882.6	1538.8	0.3272	1.544	980.2	214.3	0.2767	1037.9	2.75
10	0.1705	734.2	0.996	919.1	1352.1	0.3171	1.514	996.0	1223.8	0.3064	1048.3	2.78
11	0.1495	777.0	1.011	954.9	1185.4	0.3059	1.485	1011.0	1.2459E+04	0.3447	1058.4	2.79
12	0.0074	800.4	1.019	974.2	1102.0	0.2995	1.470	1018.9	6.1817E+04	0.3703	1063.8	2.79

Table E.5. Maltene characterization of MX-HO-A1 oil.

i	wt	T_b, K	SG	T_c, K	P_c, kPa	Z_{RA}	H/C	$\rho_{37.7°C}$ kg/m³	$\mu_{37.7°C}$ mPa·s	c_2	ρ_s^o, kg/m³	c_3 x10⁷, kPa-1
1	0.0172	293.8	0.717	465.6	4641.4	0.3933	2.054	716.6	0.3	0.2056	918.1	1.57
2	0.0184	364.7	0.791	556.1	3872.4	0.3986	1.909	791.4	0.5	0.2014	961.5	2.12
3	0.0325	421.7	0.838	621.8	3315.5	0.3924	1.820	837.5	1.0	0.2019	970.3	2.44
4	0.0525	478.7	0.876	682.7	2828.2	0.3836	1.746	875.7	2.1	0.2068	980.4	2.64
5	0.0776	535.7	0.908	739.6	2406.2	0.3748	1.684	908.0	5.0	0.2165	994.6	2.74
6	0.1048	592.7	0.936	793.5	2041.9	0.3654	1.630	936.0	14.1	0.2319	1010.0	2.78
7	0.1295	649.7	0.961	845.0	1727.9	0.3545	1.582	960.8	53.3	0.2545	1025.2	2.80
8	0.1463	706.7	0.983	894.6	1457.3	0.3416	1.539	983.1	329.1	0.2867	1039.6	2.80
9	0.1512	763.6	1.003	942.6	1224.4	0.3266	1.499	1003.4	4497.5	0.3320	1053.2	2.80
10	0.1429	820.6	1.023	989.4	1024.3	0.3097	1.463	1022.5	216238.0	0.3957	1066.4	2.80
11	0.1235	877.6	1.041	1035.5	853.1	0.2913	1.427	1040.7	7.7616E+07	0.4850	1079.4	2.80
12	0.0035	908.1	1.050	1059.9	772.4	0.2812	1.409	1050.3	6.3176E+09	0.5468	1086.4	2.80

Table E.6. Maltene characterization of WC-B-A1 oil.

i	wt	T_b, K	SG	T_c, K	P_c, kPa	Z_{RA}	H/C	$\rho_{37.7°C}$ kg/m³	$\mu_{37.7°C}$ mPa·s	c_2	ρ_s^o, kg/m³	c_3 x10⁷, kPa-1
1	0.0166	429.8	0.839	629.6	3207.4	0.3593	1.817	839.3	1.0	0.2019	967.4	2.31
2	0.0185	480.7	0.873	683.4	2781.1	0.3520	1.752	872.6	2.1	0.2069	977.1	2.53
3	0.0330	521.7	0.896	724.6	2474.2	0.3461	1.707	896.1	3.8	0.2137	987.3	2.65
4	0.0537	562.8	0.917	764.1	2198.3	0.3400	1.666	917.3	7.5	0.2233	998.3	2.72
5	0.0793	603.9	0.937	802.2	1950.6	0.3335	1.629	936.5	16.3	0.2361	1009.6	2.76
6	0.1066	645.0	0.954	839.1	1728.1	0.3261	1.595	954.1	41.2	0.2528	1020.6	2.78
7	0.1302	686.0	0.970	875.0	1528.5	0.3178	1.563	970.4	131.2	0.2742	1031.1	2.79
8	0.1445	727.1	0.986	910.0	1349.3	0.3085	1.534	985.7	577.6	0.3017	1041.2	2.80
9	0.1459	768.2	1.000	944.3	1188.6	0.2983	1.506	1000.0	3996.9	0.3369	1050.9	2.80
10	0.1338	809.3	1.014	978.0	1044.7	0.2872	1.480	1013.7	51781.8	0.3817	1060.4	2.80
11	0.1116	850.3	1.027	1011.3	916.1	0.2753	1.454	1026.9	1.6083E+06	0.4390	1069.7	2.80
12	0.0263	877.5	1.035	1033.1	838.9	0.2671	1.438	1035.5	3.0001E+07	0.4853	1075.9	2.80

APPENDIX F: WALTHER MODEL PARAMETERS *A* AND *B* FOR PURE HYDROCARBONS IN CHAPTER 7

Table F.1. Walther model parameters for n-alkanes in Development Dataset 1 in Chapter 7.

Compound	*A*	*B*
methane	3.610	2.398
ethane	3.660	2.140
propane	5.466	2.795
n-butane	5.392	2.641
n-pentane	5.800	2.775
n-hexane	5.890	2.760
n-heptane	6.750	3.065
n-octane	6.903	3.086
n-nonane	6.892	3.084
n-decane	6.975	3.052
n-undecane	7.216	3.116
n-dodecane	7.442	3.189
n-tridecane	7.902	3.339
n-tetradecane	8.101	3.401
n-pentadecane	8.401	3.501
n-hexadecane	8.607	3.566
n-eicosane	7.731	3.162
n-tetracosane	8.706	3.506

Table F.2. Walther model parameters for branched alkanes in Development Dataset 1, Chapter 7.

Compound	*A*	*B*
isopentane	4.987	2.407
2,3-dimethylpentane	6.316	2.895
7-methyltridecane	8.730	3.658
2,2,3,3,5,6,6-heptamethylheptane	8.887	3.653
2-methylpentadecane	8.846	3.661
7-n-propyltridecane	9.812	4.059
7-n-hexyltridecane	9.476	3.872
2,6,10,14-tetramethylpentadecane	10.010	4.083
2,6,11,15-tetramethylhexadecane	9.974	4.054
8-hexylpentadecane	9.977	4.053
9-hexylheptadecane	9.795	3.962
9-octylheptadecane	9.630	3.880
11-butyldocosane	9.257	3.715
6,11-dipentylhexadecane	10.314	4.135
9-ethyl-9-heptyloctadecane	9.850	3.929
11-n-decyldocosane	9.095	3.624
13-n-dodecylhexacosane	8.742	3.457

Table F.3. Walther model parameters for monoaromatics in Development Dataset 1, Chapter 7.

Compound	*A*	*B*
benzene	7.169	3.176
toluene	8.214	3.600
p-xylene	6.023	2.712
o-xylene	6.588	2.909
ethylbenzene	6.069	2.724
propylbenzene	9.966	4.262
butylbenzene	7.056	3.065
pentylbenzene	7.096	3.048
hexylbenzene	7.764	3.297
heptylbenzene	7.965	3.354
octylbenzene	8.412	3.513
nonylbenzene	9.354	3.877
decylbenzene	8.696	3.591
undecylbenzene	9.078	3.731
dodecylbenzene	8.154	3.347
tridecylbenzene	9.004	3.674
tetradecylbenzene	9.056	3.680
pentadecylbenzene	9.032	3.658
hexadecylbenzene	8.980	3.626

Table F.4. Walther model parameters for fused aromatics in Development Dataset 1, Chapter 7.

Compound	*A*	*B*
naphthalene	10.149	4.203
1-methylnapthalene	7.971	3.317
2-n-butylnaphtalene	9.519	3.906
1-tert-butylnaphtalene	11.861	4.772
4,5-dimethylphenantrene	10.676	4.193
4,5-dimethyl-9,10-dihydrophenantrene	11.822	4.647
1,4-dimethyl-5-octylnaphthalene	10.832	4.317
2-butyl-3-hexylnaphthalene	10.708	4.279
7-butyl-1-hexylnaphthalene	10.362	4.146
2-octyltriphenylene	11.205	4.348

Table F.5. Walther model parameters for non-fused aromatics in Development Dataset 1, Chapter 7.

Compound	*A*	*B*
diphenyl methane	7.796	3.247
1,1-diphenylethane	9.236	3.794
1-phenyl-2-cyclohexilethane	9.149	3.757
1-phenyl-3-cyclopentylpropane	8.340	3.452
1-cyclohexyl-1-phenylethane	10.188	4.147
1,3-diphenylbenzene	8.636	3.276
1,2-diphenylbenzene	14.356	5.633
1,1-diphenylheptane	10.864	4.366
1,5-diphenyl-3-(2-phenylethyl)pentane	11.694	4.627
1-phenyl-3-(2-phenylethyl)hendecane	10.214	4.080
1,1diphenyltetradecane	9.937	3.947

Table F.6. Walther model parameters for cyclic and alkyl cycloalkanes in Development Dataset 1, Chapter 7.

Compound	*A*	*B*
cyclohexane	8.726	3.752
cycloheptane	8.681	3.684
cyclooctane	9.420	3.925
bicyclopentyl	6.589	2.839
methylcyclopentane	6.235	2.832
ethylcyclopentane	5.603	2.559
propylcyclopentane	5.857	2.634
n-butylcyclopentane	6.143	2.718
pentylcyclopentane	7.619	3.284
n-hexylcyclopentane	7.771	3.315
heptylcyclopentane	7.820	3.310
octylcyclopentane	7.900	3.318
nonylcyclopentane	7.911	3.302
decylcyclopentane	8.473	3.506
undecylcyclopentane	8.170	3.369
dodecylcyclopentane	8.394	3.443
tridecylcyclopentane	8.525	3.481
tetradecylcyclopentane	8.497	3.457
pentadecylcyclopentane	8.581	3.480
hexadecylcyclopentane	8.731	3.526
methylcyclohexane	6.575	2.918
ethylcyclohexane	6.523	2.877
propylcyclohexane	7.904	3.412
butylcyclohexane	8.191	3.502
pentylcyclohexane	8.881	3.749
hexylcyclohexane	9.020	3.778
heptylcyclohexane	8.542	3.560
octylcyclohexane	8.845	3.658
nonylcyclohexane	9.157	3.772
decylcyclohexane	8.990	3.682
undecylcyclohexane	9.508	3.880
dodecylcyclohexane	9.706	3.944
tridecylcyclohexane	9.823	3.977
tetradecylcyclohexane	9.724	3.927
pentadecylcyclohexane	9.640	3.884
hexadecylcyclohexane	9.958	3.996

Table F.7. Walther model parameters for fused and non-fused naphthenics in Development Dataset 1, Chapter 7.

Compound	*A*	*B*
decaline	7.856	3.288
2-n-butyldecalin	9.408	3.849
2-butyl-1-hexylhexahydroindan	9.879	3.979
5-butyl-6-hexylhexahydroindan	10.770	4.329
1,4-dimethyl-5-octyldecalin	10.181	4.080
7-butyl-1-hexyldecalin	10.503	4.198
perhydrodibenzo[a,i]fluorene	14.049	5.469
1-alpha-decalylhendecane	10.722	4.295
1,2-bis(decahydro-1-naphthyl)ethane	12.980	5.040
1-n-hexadecylindan	10.222	4.045
6-n-octylperhydrobenz[de]anthracene	12.895	5.069
phenanthrene, 2-dodecyl-9,10-dihydro-	10.006	3.928
2-decylperhydroindeno-(2,1-a)indene	9.652	3.781
3-decylperhydropyrene	9.825	3.857
2-n-dodecylperhydrophenanthrene	9.289	3.652
9-n-Dodecylperhydrophenanthrene	10.188	4.005
7-Hexadecylspiro[4.5]decane	8.739	3.473
cholestane	11.812	4.551
4-(9-Heptadecanyl)dodecahydro-as-indacene	9.975	3.911
non-Fused Naphthenics		
bicyclopentyl	6.585	2.836
bicyclohexyl	8.899	3.669
1,1-dicyclopentylethane	7.468	3.141
1,1-dicyclohexylethane	9.696	3.933
1-cyclohexyl-3-cyclopentyl propane	8.779	3.601
tricyclopentyl methane	9.814	3.969
1,2-dicyclohexyl cyclohexane	13.846	5.461
7-cyclopentylmethyl tridecane	10.099	4.103
7-cyclohexyltridecane	10.645	4.298
1-cyclopentyl-4-(3-cyclopentylpropyl) dodecane	9.569	3.813
1-Cyclohexyl-3-(2-cyclohexylethyl)undecane	10.257	4.048
9-(3-cyclopentylpropyl) heptadecane	9.577	3.839
9-(2-cyclohexylethyl)heptadecane	9.840	3.928

Table G.1. Thermal conductivity and density data of oil WC-B-B3.

Temp. °C	Pressure MPa	Density kg m^{-3}	Thermal Cond. mW m^{-1} K^{-1}
21.7	0.1	1022.0	137.0
49.6	0.1	1003.1	133.5
75	0.1	985.9	130.4
100.1	0.1	969.0	127.5
21.8	2.5	1023.2	137.4
49.9	2.5	1004.3	134.0
75.3	2.5	987.1	130.9
100.1	2.5	970.4	128.2
125.5	2.5	953.3	125.2
22	5	1024.3	137.9
50	5	1005.6	134.5
75.3	5	988.7	131.4
100.1	5	972.1	128.8
125.5	5	955.2	125.8
22.1	7.5	1025.6	138.5
50.1	7.5	1007.1	135.0
75.5	7.5	990.3	132.0
100.1	7.5	973.9	129.3
125.5	7.5	957.1	126.4
22.1	10	1027.2	139.1
50.2	10	1008.3	135.6
75.5	10	991.3	132.7
100.1	10	974.8	129.8
125.5	10	958.0	127.0

Table G.2. Thermal conductivity and density data of deasphalted oil WC-B-B3.

Temp. °C	Pressure MPa	Density kg m^{-3}	Thermal Cond. mW m^{-1} K^{-1}
22	0.1	987.4	133.1
50	0.1	968.7	129.2
75.1	0.1	952.1	126.1
22.4	2.5	988.3	133.4
50.2	2.5	970.1	129.7
75.3	2.5	953.7	126.5
22.4	5	989.5	134.0
50.4	5	971.4	130.2
75.4	5	955.3	127.0
22.2	7.5	991.0	134.5
50.4	7.5	972.8	130.8
75.5	7.5	956.5	127.6
22.5	10	992.4	135.1
50.4	10	974.4	131.3
75.6	10	958.2	128.2

Table G.3. Thermal conductivity and density data of oil WC-B-A3(1).

Temp. °C	Pressure MPa	Density kg m^{-3}	Thermal Cond. mW m^{-1} K^{-1}
22	0.1	1007.9	138.4
50	0.1	990.0	134.4
75.1	0.1	974.2	131.3
22.4	2.5	1008.6	138.8
50.2	2.5	990.9	134.9
75.3	2.5	975.3	131.8
22.4	5	1009.7	139.3
50.4	5	992.0	135.5
75.4	5	976.2	132.4
22.2	7.5	1011.0	139.9
50.4	7.5	993.7	136.1
75.5	7.5	978.2	133.1
22.5	10	1012.1	140.4
50.4	10	994.9	136.7
75.6	10	979.7	133.7

Table G.4. Thermal conductivity and density data of oil WC-B-A3(2).

Temp. °C	Pressure MPa	Density kg m^{-3}	Thermal Cond. mW m^{-1} K^{-1}
23	0.1	1009.2	139.1
50	0.1	991.7	135.5
75	0.1	975.5	132.7
23	2.5	1010.5	139.6
50.1	2.5	993.3	136.0
75.4	2.5	977.1	133.3
99.5	2.5	961.8	130.4
124.9	2.5	945.6	127.5
23.2	5	1011.5	140.1
50.2	5	994.5	136.4
75.5	5	978.6	133.8
99.7	5	963.4	130.9
125	5	947.5	128.1
23.5	7.5	1012.8	140.5
50.2	7.5	996.0	137.0
75.4	7.5	980.2	134.5
99.8	7.5	964.8	131.5
125.1	7.5	948.9	128.9
23.5	10	1013.9	141.0
50.3	10	997.2	137.4
75.4	10	981.6	135.0
99.9	10	966.4	132.3
125.2	10	950.7	129.6

Table G.5. Thermal conductivity and density data of oil EU-HO-A1.

Temp. °C	Pressure MPa	Density kg m^{-3}	Thermal Cond. mW m^{-1} K^{-1}
22	0.1	960.4	133.0
50	0.1	942.4	129.2
75.1	0.1	927.0	126.3
22.4	2.5	962.6	133.4
50.2	2.5	944.0	129.8
75.3	2.5	927.8	126.9
22.4	5	963.8	134.0
50.4	5	945.1	130.3
75.4	5	929.3	127.5
22.2	7.5	965.1	134.5
50.4	7.5	946.6	130.9
75.5	7.5	930.8	128.2
22.5	10	966.6	135.1
50.4	10	948.1	131.4
75.6	10	932.3	128.8

Table G.6. Thermal conductivity and density data of oil CO-B-B1.

Temp. °C	Pressure MPa	Density kg m^{-3}	Thermal Cond. mW m^{-1} K^{-1}
18.5	0.1	998.3	136.1
50	0.1	978.3	133.0

Table G.7. Thermal conductivity and density data of oil WC-B-A1.

Temp. °C	Pressure MPa	Density kg m^{-3}	Thermal Cond. mW m^{-1} K^{-1}
22.5	0.1	994.1	132.5
50	0.1	976.7	129.5

Table G.8. Thermal conductivity and density data of oil ME-CV-A1.

Temp. °C	Pressure MPa	Density kg m^{-3}	Thermal Cond mW m^{-1} K^{-1}
19	0.1	870.1	130.0
50	0.1	847.9	126.5

Table G.9. Thermal conductivity and density data of oil WC-B-A3(2) diluted with pentane.

		5.1 wt% *n*-pentane	
Temp. °C	Pressure MPa	Density kg m^{-3}	Thermal Cond. mW m^{-1} K^{-1}
21	0.1	980.9	136.3
21	2.5		136.8
21	5		137.4
21	7.5		138.0
21	10		138.5
50	0.1	961.4	132.4
50	2.5		132.9
50	5		133.6
50	7.5		133.9
50	10		134.5
75	0.1	944.5	129.1
75	2.5		129.6
75	5		130.2
75	7.5		130.8
75	10		131.4
100	2.5		126.1
100	5		126.8
100	7.5		127.4
100	10		128.0

Table G.10. Thermal conductivity and density data of oil WC-B-A3(2) diluted with heptane.

Temp. °C	Pressure MPa	10.3 wt% *n*-heptane	
		Density kg m^{-3}	Thermal Cond. mW m^{-1} K^{-1}
22	0.1	959.0	133.5

Table G.11. Thermal conductivity and density data of oil WC-B-A3(2) diluted with tetradecane.

Temp. °C	Pressure MPa	9.8 wt% tetradecane		19.6 wt% tetradecane	
		Density kg m^{-3}	Thermal Cond. mW m^{-1} K^{-1}	Density kg m^{-3}	Thermal Cond. mW m^{-1} K^{-1}
21.4	0.1	977.2	138.5		
24	0.1			946.3	137.1

Table G.12. Thermal conductivity and density data of oil WC-B-A3(2) diluted with toluene.

Temp. °C	Pressure MPa	8.9 wt% toluene		37.7 wt% toluene	
		Density kg m^{-3}	Thermal Cond. mW m^{-1} K^{-1}	Density kg m^{-3}	Thermal Cond. mW m^{-1} K^{-1}
21	0.1	991.7	137.5	950.9	135.9
21	2.5		138.1		136.5
21	5		138.5		137.3
21	7.5		139.0		137.7
21	10		139.6		138.4
50	0.1	972.8	133.9	927.5	129.6
50	2.5		134.5		130.3
50	5		135.0		131.0
50	7.5		135.7		131.7
50	10		136.2		132.3
75	0.1	955.8	131.2	907.4	124.7
75	2.5		131.9		125.5
75	5		132.4		126.2
75	7.5		133.1		127.1
75	10		133.8		127.9
100	2.5		128.4		
100	5		129.1		
100	7.5		129.8		
100	10		130.5		
124	2.5		125.1		
124	5		125.9		
124	7.5		126.7		
124	10		127.4		

Table G.13. Thermal conductivity and density data of oil WC-B-A3(2) diluted with cyclohexane.

Temp. °C	Pressure MPa	4.6 wt% Cyclohexane		28.2 wt% Cyclohexane	
		Density kg m^{-3}	Thermal Cond. mW m^{-1} K^{-1}	Density kg m^{-3}	Thermal Cond. mW m^{-1} K^{-1}
23/21	0.1	995.4	137.0	931.9	128.9
23/21	2.5		137.5		129.5
23/21	5		138.1		130.0
23/21	7.5		138.5		130.5
23/21	10		139.1		131.1
50	0.1	977.6	133.5	909.6	125.0
50	2.5		134.1		124.8
50	5		134.7		126.7
50	7.5		135.3		127.4
50	10		135.9		128.1
75	0.1	961.2	131.1	889.5	121.1
75	2.5		131.7		121.7
75	5		132.3		122.4
75	7.5		132.8		123.0
75	10		133.5		123.7
100	2.5		128.2		116.6
100	5		128.9		117.4
100	7.5		129.4		118.1
100	10		130.2		119.0
124.5	2.5		125.5		
124.5	5		126.1		
124.5	7.5		126.9		
124.5	10		127.6		

Table G.14. Thermal conductivity and density of Asphaltene/toluene mixtures collected in this study. The asphaltenes were precipitated from oil WC-B-A3(1) using *n*-pentane.

Temp. °C	Pressure MPa	1.2 wt% asphaltene		8.7 wt% asphaltene	
		Density kg m^{-3}	Thermal Cond. mW m^{-1} K^{-1}	Density kg m^{-3}	Thermal Cond. mW m^{-1} K^{-1}
23/22	0.1	867.2	132.1	883.4	135.7
23/22	2.5		132.9		136.4
23/22	5		133.8		137.2
23/22	7.5		134.7		138.2
23/22	10		135.5		138.9
26	0.1	864.2	130.9	879.1	134.1
26	2.5		132.0		135.2
26	5		133.0		135.9
26	7.5		133.8		136.7
26	10		134.9		137.6
30	0.1	860.1	129.6	875.5	132.8
30	2.5		130.9		133.7
30	5		131.9		134.5
30	7.5		133.2		135.2
30	10		133.9		136.4
35	0.1			870.0	131.0
35	2.5				132.0
35	5				133.1
35	7.5				133.7
35	10				135.0

APPENDIX H: FITTING PARAMETERS IN EQUATION 8.4 FOR PURE HYDROCARBONS

$$\rho = (a_1 + a_2 T)\exp\left\{a_3\left[1 - \exp\left[-(a_4 T + a_5)P\right]\right]\right\}$$

The value of the parameter a_3 was fixed to 0.21 for all hydrocarbons.

Table H1. Fitting parameters for hydrocarbons in Equation 8.4.

component	a_1 kg m^{-3}	a_2 kg m^{-3} °C^{-1}	a_4 x 10^8 °C^{-1} kPa^{-1}	a_5 x 10^6 kPa^{-1}
n-pentane	643.5	0.9446	10.0789	5.4661
n-hexane	677.9	0.9274	8.7096	4.7917
n-heptane	700.9	0.8577	6.8859	3.7822
n-octane	718.8	0.8060	5.4634	3.6370
n-decane	746.1	0.7980	5.5643	2.9854
n-dodecane	762.9	0.7015	3.6782	2.6579
n-tetradecane	776.9	0.6840	3.3817	2.2241
toluene	885.9	0.9601	3.2135	3.0404
cyclohexane	798.4	0.9847	6.5015	2.3198

APPENDIX I: EXPANDED FLUID THERMAL CONDUCTVITY MODEL FITTED PARAMETERS FOR PURE HYDROCARBONS

Table I.1. Expanded Fluid thermal conductivity model parameters for n-alkanes in Development Dataset 1, Chapter 8.

compound	ρ_s^o, kg m^{-3}	$c_{2\lambda}$	λ_s^o, mW m^{-1} K^{-1}
methane	540.0	12.285	341.2
ethane	724.0	11.927	331.4
propane	778.0	10.411	241.8
butane	813.0	12.569	249.5
n-pentane	837.0	11.996	221.4
n-hexane	849.1	11.720	209.5
n-heptane	857.8	11.517	202.8
n-octane	862.7	11.846	201.6
n-nonane	865.9	11.718	196.6
n-decane	868.1	10.483	189.7
n-dodecane	871.4	10.250	182.7
n-tridecane	877.8	8.955	174.8
n-tetradecane	875.5	8.648	178.7
n-pentadecane	878.4	9.683	179.2
n-hexadecane	878.6	11.670	186.4
n-heptadecane	881.3	8.324	177.7
n-octadecane	885.1	7.617	176.9
n-eicosane	885.5	10.422	195.0
n-docosane	885.2	10.512	198.3
n-tricosane	891.4	9.947	197.5
n-tretracosane	893.2	10.344	203.5

Table I.2. Expanded Fluid thermal conductivity model parameters for branched alkanes in Development Dataset 1, Chapter 8.

compound	ρ_s^o, kg m^{-3}	$c_{2\lambda}$	λ_s^o, mW m^{-1} K^{-1}
2,2-dimethylhexane	911.5	11.744	189.9
3-ethylhexane	892.1	11.883	174.2
3-methyl-3-ethylpentane	876.5	11.625	161.1
4-methylheptane	904.6	10.774	201.7
2,2-dimethylpentane	857.9	14.049	184.6
2-methylhexane	861.2	12.486	194.0
3-methylpentane	858.5	13.368	203.7
2,2,4-trimethylpentane	859.4	13.357	163.2

Table I.3. Expanded Fluid thermal conductivity model parameters for cyclics in Development Dataset 1, Chapter 8.

compound	ρ_s^o, kg m^{-3}	$c_{2\lambda}$	λ_s^o, mW m^{-1} K^{-1}
cyclopentane	933.0	11.344	216.9
methylcyclopentane	944.5	11.858	200.7
cyclohexane	922.1	7.646	155.4
cis-1,2-dimethylcyclohexane	926.5	10.419	162.5
trans-1,2-dimethylcyclohexane	911.5	4.839	149.4
cis-1,3-dimethylcyclohexane	921.2	10.765	164.7
trans-1,3-dimethylcyclohexane	922.7	10.483	165.8
ethylcyclohexane	950.1	10.478	173.3
n-propylcyclopentane	950.5	10.726	175.4
n-butylcyclohexane	933.7	10.204	153.1
bicyclohexyl	990.8	9.723	157.9
n-decylcyclohexane	917.8	16.455	153.2

Table I.4. Expanded Fluid thermal conductivity model parameters for aromatics in Development Dataset 1, Chapter 8.

compound	ρ_s^o, kg m^{-3}	$c_{2\lambda}$	λ_s^o, mW m^{-1} K^{-1}
benzene	1066.4	10.384	212.0
ethylbenzene	1052.0	9.343	182.5
o-xylene	1052.9	10.139	182.1
p-xylene	1045.5	11.637	196.8
toluene	1049.6	11.542	203.6
n-propylbenzene	1017.8	12.172	178.0
styrene	1058.0	9.519	182.7
indene	1230.2	11.055	188.1
indane	1076.3	10.021	171.1
D-limonene	991.5	10.610	164.1
cis-decahydronaphthalene	1029.4	4.809	128.8
trans-decahydronaphthalene	996.5	5.416	129.8
1-methylnaphthalene	1138.0	9.204	176.2
2-methylnaphthalene	1130.0	9.389	176.3
n-pentylbenzene	976.5	9.922	153.0
biphenyl	1154.6	5.936	160.8
1-ethylnaphthalene	1105.0	9.365	165.5
diphenylmethane	1132.6	6.630	159.1
n-heptylbenzene	968.7	9.499	144.0
anthracene	1373.0	4.331	151.0
phenanthrene	1301.2	1.363	133.1
1,1-diphenylethane	1106.2	9.835	164.0
n-octylbenzene	967.7	9.586	146.0
n-decylbenzene	963.4	9.255	137.5

APPENDIX J: EF THERMAL CONDUCTVITY BINARY INTERACTION PARAMETERS FOR THE BINARIES AND THE PSEUDO-BINARIES IN THE DEVELOPMENT DATASET 2 IN CHAPTER 8

Table J1. Fitted and Correlated interaction parameters for the pure hydrocarbon binaries in the Development Dataset 2 in Chapter 8.

component i	component j	ΔSG_{norm}	θ_{ij} Fitted	θ_{ij} Correlated
alkane/alkane				
heptane	hexane	0.037	0.0000	0
heptane	octane	0.024	-0.0029	0
hexane	octane	0.061	-0.0053	0
heptane	decane	0.116	0.0152	0
heptane	hexadecane	0.113	0.0167	0
undecane	hexadecane	0.044	0.0000	0
heptane	undecane	0.070	0.0086	0
2,3-dimethylbutane	2,2,4-trimethylpentane	0.060	-0.0112	0
alkane/aromatic				
toluene	2,2,4-trimethylpentane	0.211	0.0124	0
heptane	2,2,4-trimethylpentane	0.024	-0.0089	0
heptane	benzene	0.245	-0.0146	-0.0170
heptane	toluene	0.235	0.0029	-0.0102
2,2,4-trimethylpentane	o-xylene	0.221	-0.0004	-0.0009
cyclic/alkane				
cyclopentane	heptane	0.083	0.0013	0
methylcyclohexane	2,2,4-trimethylpentane	0.092	0.0085	0
cyclic/cyclic				
cyclopentane	methylcyclohexane	0.033	-0.0124	0
aromatic/aromatic				
toluene	*o*-xylene	0.010	0.0064	0
toluene	benzene	0.010	-0.0513	0
benzene	*p*-xylene	0.020	-0.0450	0

Table J2. Fitted and Correlated interaction parameters for the bitumen/solvent pseudo-binaries in the Development Dataset 2 in Chapter 8.

component i	component j	ΔSG_{norm}	θ_{ij} Fitted	θ{ij} Correlated
WC-B-A3(2)	pentane	0.541	-0.2060	-0.2148
WC-B-A3(2)	heptane	0.459	-0.1750	-0.1598
WC-B-A3(2)	tetradecane	0.358	-0.0686	-0.0920
WC-B-A3(2)	toluene	0.229	-0.0192	-0.0060
WC-B-A3(2)	cyclohexane	0.3463	-0.0711	-0.0844